Molecular and Genetic Basis of Inherited Optic Neuropathies

Padraig James Flannery

BA MSc

Thesis submitted to Newcastle University in candidature for the degree of

Doctor of Philosophy

Institute of Genetic Medicine

Faculty of Medical Sciences

Newcastle University

To Mum, Dad and Ciara

Abstract

Inherited optic neuropathies represent an important cause of chronic visual morbidity among children and young adults. This group of disorders is genetically heterogeneous and it can be caused by pathogenic mutations within both the mitochondrial and nuclear genomes. The unifying pathophysiological theme is mitochondrial dysfunction, but the specific disease mechanisms that ultimately precipitate neuronal loss, particularly retinal ganglion cell (RGC) degeneration, still remain unclear. The work presented in this thesis provides further insight into the molecular and genetic basis of two classical forms of inherited optic neuropathy, namely autosomal dominant optic atrophy (DOA) and Wolfram syndrome.

Dominant optic atrophy (DOA) secondary to pathogenic *OPA1* mutations is the most common inherited optic neuropathy diagnosed in clinical practice. The pathology is characterised by the preferential loss of RGCs within the inner retina and optic nerve degeneration. Although most *OPA1* mutation carriers will only develop isolated optic atrophy, a subgroup of patients, referred to as DOA plus (DOA+), will develop more severe neuromuscular complications in addition to visual failure. The complexity of these clinical presentations may be due in part, to the various roles of OPA1 in the mitochondrial compartment such as regulating mitochondrial fusion and cristae structure,sequesterisation of pro-apoptotic molecules, mitochondrial DNA (mtDNA) maintenance,proper functioning of the oxidative phosphorylation system and calcium homoeostasis.

To investigate the disease mechanisms that could explain the varying clinical manifestations and severity of *OPA1* mutations, I made use of a cohort of eight fibroblast cell lines established from four patients with pure optic atrophy (OA) and four patients with DOA+ phenotypes. *OPA1* expression and mitochondrial fragmentation patterns were compared between these two groups. There was no significant disruption in *OPA1* transcription, mitochondrial OXPHOS and mtDNA maintenance. DOA primary fibroblasts showed increased fragmentation of the mitochondrial network and cell lines established from patients with DOA+ phenotypes were found to be particularly susceptible to fragmentation under basal conditions, which had not been reported previously.

To further explore the findings obtained in *OPA1* mutant fibroblasts, I made use of a cohort of nine myoblast cell lines that had previously been established from patient muscle biopsies. Interestingly, a similar mitochondrial fragmentation pattern was observed in *OPA1* mutant primary myotubes and this was associated with decreased mitochondrial DNA molecule number in DOA+ myotubes.

I also investigated two sisters from a consanguineous Arab Muslim family who developed a fatal form of juvenile-encephalopathy complicated by optic atrophy and cardiomyopathy. Exome sequencing identified a putative homozygous *OPA1* mutation, which was confirmed by both functional studies and *in silico* modelling.

Whole-exome analysis was carried out on a cohort of fourteen patients with optic atrophy that had previously been found to be *OPA1*-negative. Pathogenic mutations in the Wolframin (*WFS1*) gene, which is known to cause Wolfram syndrome, were identified in 3/14 (21%) patients. Based on our results, *WFS1* mutations are an important cause of inherited optic atrophy and genetic testing should be considered in *OPA1*-negative patients.

In conclusion, the body of work presented in my PhD thesis has provided further insight into the expanding genotypic and phenotypic spectrum of inherited optic neuropathies, which is highly relevant for clinical diagnosis and patient management.

Author's Declaration

This thesis is submitted to Newcastle University for the degree of Doctor of Philosophy. Research described within was conducted between the years 2012-2016 and was supervised by Dr. Patrick Yu-Wai-Man and Professor Patrick Chinnery. I certify that none of the material contained within this thesis has been previously submitted by me for a degree or other qualification at this or any other university.

Acknowledgements

First and foremost, I would like to thank my supervisors Dr. Patrick Yu-Wai-Man and Professor Patrick Chinnery for giving me the opportunity to work on an excellent project. Their outstanding mentorship and guidance over the past few years were invaluable and it was a privilege to work with them.

I would also like to offer my special thanks to both Kamil Sitarz and Florence Burte who provided patience, continual support and guidance over the course of my PhD. They helped to mould the scientist I am today.

Of course, I must also mention Dr. Aurora Gomez-Duran who provided valuable insight and expertise and was always available anytime I had a 'quick question'. Her scientific guidance will serve me in years to come over the course of my scientific career.

A special mention is also deserved for Drs. Gavin Hudson, Angela Pyle and Glyn Nelson who were more than willing to share their technical knowledge and experience which helped shape the course of my PhD project.

Moreover, I must also thank my other colleagues within the PFC lab group for providing a friendly and enjoyable work environment. They supported my scientific endeavours and I had a great experience, both working and socialising, with a fantastic group of scientists these past few years.

Finally, I would like to thank the UK Medical Research Council and Newcastle University for providing me with a PhD studentship to advance my scientific career and making all of this possible.

List of Contents

Table of Contents

LIST OF TABLES

TABLE OF FIGURES

List Of Publications

1. **Flannery, P.,** Sitarz, K.S., Burte, F., Gomez-Duran, A., Taylor, R.W., Chinnery, P., Yu-Wai-Man, P., OPA1 mutations affect mitochondrial morphology and mitochondrial DNA repopulation in pure and syndromic dominant optic atrophy. [Manuscript under preparation]
2. Spiegel, R. Saada, A., **Flannery, P.J.**, Burté, F., Soiferman, S., Khayat, M., Eisner Sagüés, V., Vladovski, E., Taylor, R.W., Bindoff, L.A., Shaag, A., Mandel, H., Furman, O., Shalev, S.A., Elpeleg, O., Yu-Wai-Man, P. Fatal infantile mitochondrial encephalomyopathy and hypertrophic cardiomyopathy associated with homozygous *OPA1* mutations. J Med Genet. 2016;53(2):127-31.
3. Liao, C., Ashley, N., Diot, A., Morten, K., Phadwal, K., Williams, A., Fearnley, I., Rosser, L., Lowndes, J., Fratter, C., Ferguson D.J.P., Vay, L., Quaghebeur, G., Moroni, I., Bianchi, S., Lamperti, C., Downes, S.M., Sitarz, K.S., **Flannery P.J.**, Carver, J., Dombi, E., East, D., Laura, M., Reilly, M.M., Mortiboys, H., Prevo, R., Campanella, M., Daniels, M.J., Zeviani, M., Yu-Wai-Man P., Simon, A.K., Votruba, M., Poulton, J. Dysregulated mitophagy and mitochondrial organisation in optic atrophy due to *OPA1*mutations. [Under peer review -Neurology]

Abbreviations

µl	Microlitre
AARS2	Alanyl-tRNA synthetase 2
AAV	Associated Viral Vector
ADOA	Autosomal Dominant Optic Atrophy
ADOAC	Autosomal Dominant Optic Atrophy with premature Cateracts
ADP	Adenosine Diphosphate
AFG3L2	AFG3-like AAA Atpase 2
APEX1	AP-endonuclease 1
ARS	Aminoacyl-tRNA synthases
ASD	assymetric strand displacement model
ATAD3	ATpase family, AAA Domain containing 3
ATP	Adenosine Triphosphate
B2M	Beta-2-microglobulin
BAK	BCL2-Antagonist Killer
BAX	BCL2-Associated X-protein
BCL-2	b-Cell Lymphoma 2
BER	Base Excision Repair
bp	base pair
CASPASE	Cysteine Aspartic protease
CBC	Cap Binding Complex
CC	Coiled Coil
CC_1	Coiled Coil Domain
COX	Cytochrome C Oxidase
COX	Cytochome C oxidase
C_t	Threshold Cycle
DARS	Aspartyl-tRNA synthetase
DIDMOAD	Diabetes Insipidus, Diabetes Mellitus, Optic Atrophy and Deafness
D-loop	Displacement loop
DMSO	DiMethylSulphOxide
DNA	Deoxyribonucleic Acid
dNTP	DeoxyriboNucleotide TriPhosphate
DRP1	Dynamin Related Protein 1
EARS2	Glutamyl-tRNA synthetase 2

ECL	Enhanced Chemoluminescence
EDTA	EthyleneDiamineTetracetic Acid
EJC	Exon Junction Complex
EJC	Exon Junction Complex
ER	Endoplasmic Reticulum
ERMES	The ER-mitochondria Encounter Structure
ESP6500	Exome Sequencing Project 6500
EtBr	Ethidium Bromide
Exo1	Exonuclease 1
FAD	Flavin Adenine Dinucleotide
$FADH_2$	Reduced Flavin Adenine Dinucleotide
FAP	FASTAP Thermosensitive Alkaline Phosphatase
FARS2	Phenylalanine-tRNA synthetase 2
FBS	Foetal Bovine Serum
Fe^{2+}	Iron Ion
FMV	Flavin Mononucleotide
GAPDH	GlycerAldehyde-3-Phosphate DeHydrogenase
GARS	Glycl-tRNA synthase
GED	Guanosine Triphosphate Effector Domain
GTPase	Guanosine Triphosphate
H_2O	Water
H_2O_2	Hydrogen Peroxide
HARS2	Histidyl-tRNA synthetase 2
HFIS1	Human mitochondrial FISsion 1
HSP1	Heavy Strand Promotor 1
HSP2	Heavy Strand Promotor 2
HSP60	Heat Shock Protein 60
H-Strand	Heavy-Strand
IF	Initiation Factor
IMM	Inner Mitochondrial Membrane
IMS	Intermembrane Space
IVF	In-Vitro Fertilisation
KARS	Lysyl-tRNA synthase
kb	kilobase
kb	Kilobase
KCl	Potssium Chloride
Kda	KiloDaltan
KH_2PO_4	MonoPotassium Phosphate
LARS2	Leucyl-tRNA synthetase 2
LCR	Low Complexity Region
LHON	Leber's Hereditary Optic Neuropathy

LogMar	Logarithm of the minimm angle of resolution
l-opa1	Long isoforms of OPA1
Lp-BER	Long patch Base Excision Repair
L-Strand	Light-Strand
MARS2	methionyl-tRNA synthetase 2
MCU	Mitochondrial Calcium Uniporter
MEF	Mouse Embryonic Fibroblast
MELAS	Mitochondrial encephalomyopathy, lactic acidosis and stroke like symptoms
MeM	Minimum Essential Media
MERRF	Myoclonic epilepsy and ragged red fibres
MFF	Mitochondrial Fission Factor
MFN	MitoFusiN
Mg^{2+}	Magnesium Ion
$MgSO_4$	Magnesium Sulphate
MIRO-1	Mitochondrial Rho GTPase 1
MIS	Mitochondrial Importer Sequence
ml	Millilitre
mls	millilitres
mm	millimetres
mM	Millimolar
MPP	Mitochondral Processing Pepsidase
mRNA	Messenger RNA
mtDNA	mitochondrial DNA
mtEFtu	Mitochondrial Elongation factor Tu
mtIF	Mitochondrial Translational Inititation Factor
mtRF	Mitochondrial Translational Release Factor
MTS	Mitochondrial Targeting Sequence
mtSSB	MiTochondrial Single Stranded Binding Protein
mt-tRNA	Mitochondrial tRNA
NaCl	Sodium Chloride
NAD^+	Nicotinamide Adenine Dinucleotide +
NADH	Nicotinamide Adenine Dinucleotide
ND1	NADH Dehydrogenase 1
nm	nanometre
nM	nanoMolar
NMD	Nonsense Mediated mRNA Decay
NMD	Nonsense Mediated mRNA Decay
OH	Heavy-strand Origin of replication
OL	Light-strand Origin of replication
OMM	Outer Mitochondrial Membrane

OPA	Optic Atrophy
OXPHOS	oxidative phosphorylation
p0	Rho 0
PABPN1	Poly(A) Binding Protein, Nuclear 1
PALM	PhotoActivated Localisation Microscopy
PARL	Presenilin Associated, Rhomboid like
PBS	Phosphate Buffer Saline
PCR	Polymerase Chain Reaction
PHB	Prohibitin
Pi	Inorganic Phosphate
PINK1	pta-INduced putative Kinase 1
PNKP	Polynucleotide Kinase 3' Phosphatase
POLG	Polymerase Gamma
POLRMT	Polymerase R Mitochondrial
PTC	Premature Termination Codons
QT-PCR	Quantitative Real-Time Polymerase Chain Reaction
RARS2	Arginyl-tRNA synthetase 2
RGC	retinal ganglion cells
RITOLS	RNA Incorporation ThroughOut the Lagging Strand
ROS	Reactive Oxygen Species
RPM	Revolutions per Minute
rRNA	Ribosomal RNA
RT-PCR	Reverse Transcription Polymerase Chain Reaction
SARS2	Seryl-tRNA synthetase 2
SDH	Succinate Dehydrogenase
SIMH	Stress Induced Mitochondrial Hyperfusion
SLP-2	Sloppy paired 2
SMAC/ Diablo	Second mitochondria-derived activator of caspase /direct inhibitor of apoptosis-binding protein with low pI
SNP	Single Nucleotide Polymorphism
S-OPA1	Short isoforms of OPA1
Sp-BER	Short patch Base Excision Repair
SPG7	Spastic Paraplegia 7
SSB	Single Stranded Break
SSCB	Synchronous Strand Coupled Bidirectional
STED	STimulaed Emission Depletion
SURF2	Surfeit 2
TAE	Tris-Acetate Ethylenediaminetratracetic acid
TARS2	Threonyl-tRNA synthetase 2
TFAM	Transcription Factor A
TFB2M	Transcription Factor B2 Mitochondrial

TM	Transmembrane domain
TM_1	Transmembrane Domain
TOM20	Translocase of Outer Membrane 20
tRNA	Transfer RNA
tRNA	Transfer RNA
TTBS	Tris-Buffered Saline and Tween
VARS2	Valyl-tRNA synthetase 2
VDAC	Voltage Dependent Ion Channel
WS	Wolfram Syndrome
YARS2	Tyrosyl-tRNA synthetase
YME1L	YME-like 1

Chapter 1

Introduction

1.1 Inherited Optic Neuropathies

1.1.1 Epidemiology

Mitochondrial diseases are now recognised as a major cause of chronic morbidity and the minimum prevalence has been estimated at 1 in 5,000 in the United Kingdom (Gorman et al., 2015). Reflecting the ubiquitous nature of mitochondria and their fundamental roles in energy production, patients with mitochondrial genetic disorders often manifest a heterogeneous combination of tissue and organ involvement, which can lead to significant diagnostic delays. Optic nerve involvement is a major manifestation of mitochondrial diseases and it is an important cause of significant visual impairment. As a group, these inherited optic neuropathies affect approximately 1 in 10,000 individuals in the general population and there are currently limited treatment options (Yu-Wai-Man, 2010a; Newman and Biousse, 2004, Man et al., 2003). The pathological hallmark is the preferential loss of retinal ganglion cells (RGCs) within the inner retina, leading to progressive degeneration of the optic nerve and the onset of visual loss (**Figure 1-1**). Inherited optic neuropathies encompass a number of distinct clinical entities, but typically, the visual deterioration is bilateral and symmetrical with the development of a dense central or caecocentral scotoma (Yu-Wai-Man, 2009).

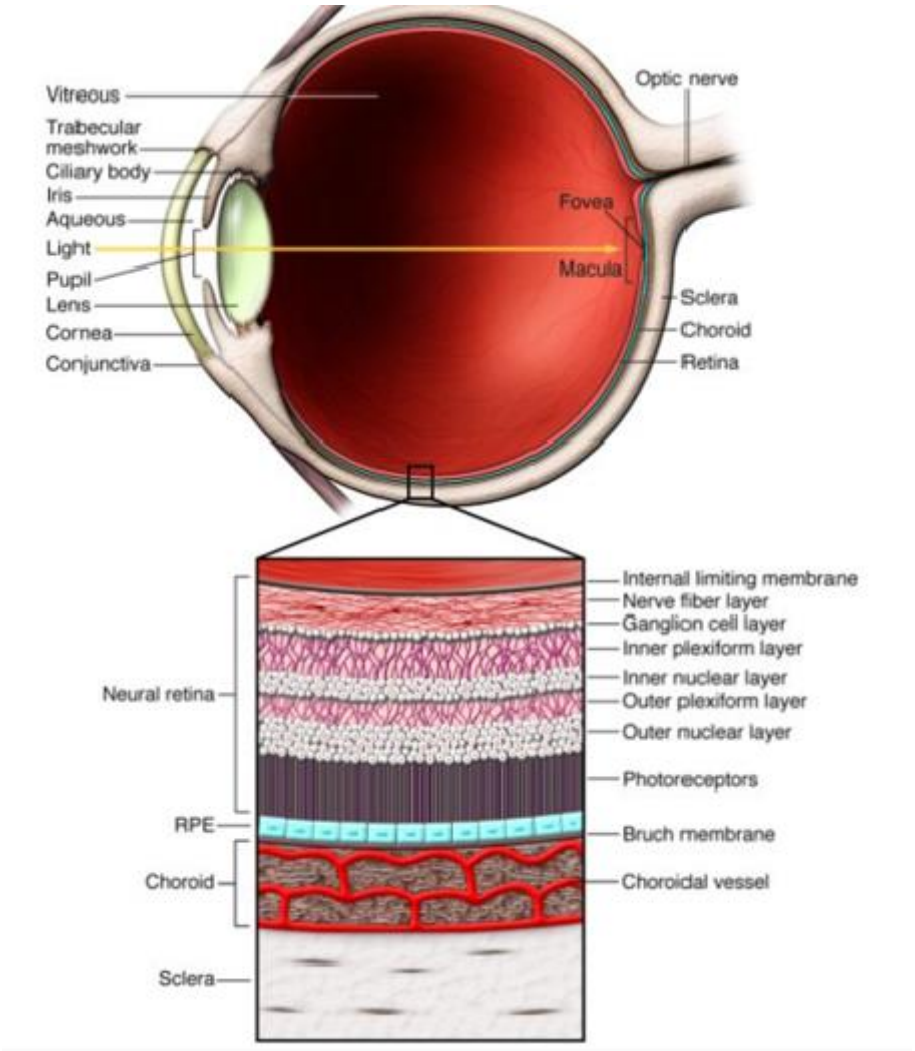

Figure 1-1 Anatomical structure of the human eye with a cross-section detailing the different retinal layers.

Reproduced from Caspi, 2010.

1.1.2 Classification

Historically, inherited optic neuropathies have been classified either based on their mode of inheritance, or on whether the optic atrophy was isolated or part of a more complicated syndromic presentation (Newman and Biousse, 2004). Mutations within the mitochondrial genome are maternally inherited whereas nuclear genetic defects are inherited either in a recessive or a dominant fashion **(Table 1-1**). However, with greater access to genetic testing and more careful phenotyping of affected patients with inherited forms of optic atrophy, these categorical distinctions have become more blurred. With the advent of next-generation exome and whole genome sequencing, the list of nuclear genes that cause inherited optic atrophy has also expanded markedly over the past few years. Three important groups have emerged, namely Leber hereditary optic neuropathy (LHON), autosomal dominant optic atrophy (DOA), and Wolfram syndrome (Yu-Wai-Man *et al.*, 2011). These specific disorders will be described in more detail to highlight some of the key clinical and pathological manifestations, as well as the gaps in our current knowledge.

Inheritance	Locus	Gene	OMIM	Phenotype
Dominant	1p36.2	MFN2	601152	Hereditary motor and sensory neuropathy type 6 (HMSN-6,CMT2A)
	3q28-q29	OPA1	165500	Isolated optic atrophy (OA) and syndromal dominant optic atrophy (DOA+)
	4p16.1	WFS1	600965	Wolfram syndrome spectrum disorders
	16q24.3	SPG7	607259	Hereditary spastic paraplegia type 7 (HSP-7)
	18p11.21	AFG3L2	610246	Spinocerebellar ataxia
	19q13.2-q13.3	OPA3	165300	Autosomal dominant optic atrophy and early-onset cataracts (ADOAC)
	22q13.2	ACO2	614559	Infantile-cerebellar retinal degeneration
Recessive	1q23.3	NDUFS2	252010	Optic atrophy-dystonia-deafness (Mohr-Tranbjaerg syndrome)
	4p16.1	WFS1	222300	Wolfram syndrome 1
	4q24	CISD2/WFS2	604928	Optic atrophy,neuropathy, deafness, diabetes mellitus, ulcer bleeding
	5q.22.1	SLC25A46	616505	Optic atrophy, peripheral neuropathy
	6q21	RTN4IP1	616732	Optic atrophy, seizures, mental retardation +/- ataxia
	9q13-q21.1	FXN	229300	Friedreich's ataxia (FRDA)
	9q22.31	AUH	250950	Type I-III methylglutaconic aciduria
	10p11.23	MTPAP	613672	Optic atrophy, dysarthria,spastic paraparesis, cerebellar ataxia +/-nystagmus
	11q14.1-q21	TMEM126A	612989	Optic atrophy +/- auditory neuropathy
	12p11.21	DRP1	614388	Optic atrophy, lactic acidemia, hypotonia, microcephaly
	12q24.31	C12ORF65	615035	Optic atrophy, peripheral neuropathy,spasticity+/- intellectual disability
	19q13.2-q13.3	OPA3	258501	Type III 3-methylglutaconic aciduria (Costeff syndrome)

Table 1-1 Nuclear mitochondrial/ ER disorders with prominent optic nerve involvement

1.2 Leber Hereditary Optic Neuropathy (LHON)

1.2.1 Epidemiology

Leber hereditary optic neuropathy (LHON) is a primary mitochondrial DNA (mtDNA) disorder that predominantly affects young adults with a peak age of onset in the second and third decades of life. The minimum prevalence of LHON has been estimated at about 1 in 31,000 of the population with a much higher prevalence in men at about 1 in 14,000 (Man *et al.,* 2003; Mascialino *et al.,* 2012).

1.2.2 Molecular genetics

Three point mutations within the mitochondrial genome (m.3460G>A, m.11778G>A and m.14484T>C) account for about 90% of cases (**Figure 1-2**) with the m.11778G>A mutation being the most prevalent (60-80%) cause of LHON worldwide. Two peculiarities of this mitochondrial optic neuropathy are the marked incomplete penetrance and the male bias for visual loss (Johns *et al.,* 1993; Nikoskelainen, 1994). Although there can be wide intra- and inter-familial variability, the lifetime risk of visual loss is about 50% for male carriers and about 10% for female carriers (Yu-Wai-Man *et al.,* 2011).

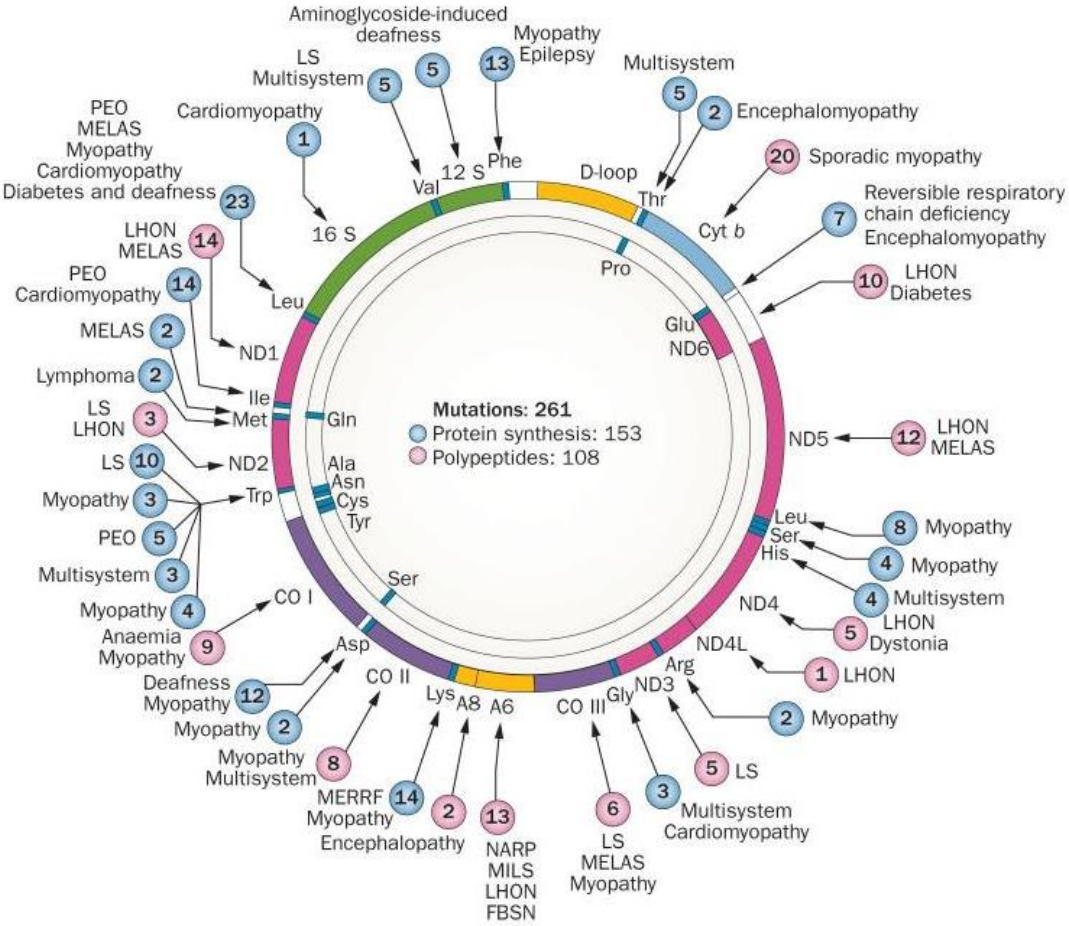

Figure 1-2 Schematic illustrating the three common pathogenic mitochondrial DNA mutations found in LHON.

Schematic illustrating the mitochondrial genome and the location of the three most common mtDNA LHON mutations, which all affect critical subunits of complex I. Reproduced from DiMauro *et al.*, 2013.

1.2.3 Clinical manifestations

Patients with LHON classically present wth subacute, painless, central visual loss in one eye, which is followed 2-4 months later by the fellow eye. Unilateral optic nerve involvement in LHON is exceptionally rare and another underlying pathological process should be actively excluded in these atypical cases. Bilateral simultaneous onset probably occurs in about 25% of patients and it is unusual for LHON carriers to experience visual loss beyond 50 years of age. The visual loss in LHON is severe and it usually plateaus over the next six months with most patients achieving visual acuities of 6/60 or worse (**Figure 1-3**).

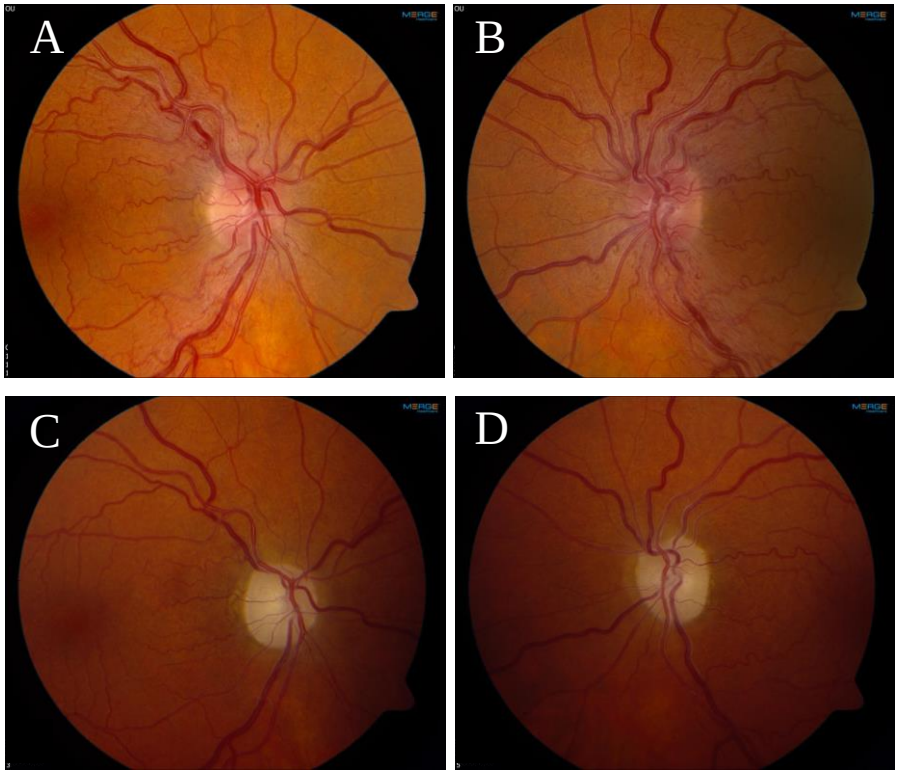

Figure 1-3 Acute and chronic stages of LHON

A and **B**. Classical fundoscopic appearance in acute LHON with optic disc hyperaemia, swelling of the peripapillary retinal nerve fiber layer, prominent vascular tortuosity and fine telangiectatic vessels. **C** and **D**. Marked pallor of the neuroretinal rim in chronic LHON.

1.2.4 LHON plus phenotypes

LHON is monosymptomatic in the majority of patients with pure optic nerve involvement. However, a minority of LHON carriers can develop a more severe syndromic phenotype, known as LHON plus (LHON+), where the optic atrophy is associated with cardiac arrhythmias, peripheral neuropathies, myoclonus, juvenile-onset encephalopathy, ataxia and spastic dystonia (Yu-Wai-Man et al. 2011; Gropman et al., 2004; Howel et al., 1991). There is also a well-reported association between the three primary mtDNA LHON mutations (m.3460G>A, m.11778G>A and m.14484T>C) and a multiple sclerosis-like illness, especially among female carriers (Harding's disease) (Pfeffer *et al.*, 2013a).

1.2.5 Pathophysiology

The mechanisms that underpin the preferential loss of RGCs in LHON have not yet been fully elucidated and the pathological triggers are likely to be multifactorial. The axons of RGCs are unmyelinated until they reach the lamina cribosa and to sustain efficient neuronal conduction, there is a relatively high concentration of mitochondria in the prelaminar segment. Furthermore, the axons with the papillomacular bundle, which subserve the central vision, are relatively small and this anatomical characteristic is thought to result in a reduced mitochondrial reserve, which would put them at increased risk under pathological conditions that impair mitochondrial function (Pan *et al*., 2012). The two main pathological factors that have been put forward is impaired mitochondrial oxidative phosphorylation (OXPHOS) precipitating a bioenergetics crisis and the increased chronic release of reactive oxygen species (ROS) (Carelli *et al.*, 2004). These are not mutually exlusive and once a threshold is reached, which exceeds the cell's innate compensatory mechanisms, an irreversible cascade of events is initiated that precipitate apoptotic cell death. The incomplete penetrance observed in LHON reflects this precarious balancing act and the likelihood of a carrier losing vision is likely to be influenced by secondary genetic factors, both mitochondrial and nuclear, and environmental exposures. There is mounting evidence that smoking significantly increases the risk of disease conversion by further exacerbating the underlying mitochondrial bioenergetic deficit and unaffected carriers should, therefore, be strongly advised not to smoke (Kirkman *et al.*, 2009). An attractive explanation that has been put forward to explain the marked male predominance observed in LHON is the neuroprotective influence of oestrogen hormones on

RGCs when under conditons of heightened mitochondrial stress (Giordano *et al*., 2011; Pisano *et al*., 2015)

1.2.6 Other mtDNA mutations causing optic neuropathies

Optic nerve involvement is also seen with other pathogenic mtDNA mutations, but visual loss is frequently a secondary disease manifestation overshadowed by more severe neurological deficits. An important category is the mitochondrial encephalomyopathies, which encompass several distinct phenotypes such as mitochondrial encephalomyopathy, lactic acidosis, and stroke-like episodes (MELAS), myoclonic epilepsy and ragged-red fibers (MERRF), maternally inherited Leigh syndrome (MILS), and mitochondrial neurogastrointestinal encephalomyopathy (MNGIE) (**Figure 1-4**). Although variable and not a disease-defining feature, the occurrence of optic atrophy is well described in this group of patients (Man *et al.*, 2002; Sitarz *et al.*, 2012).

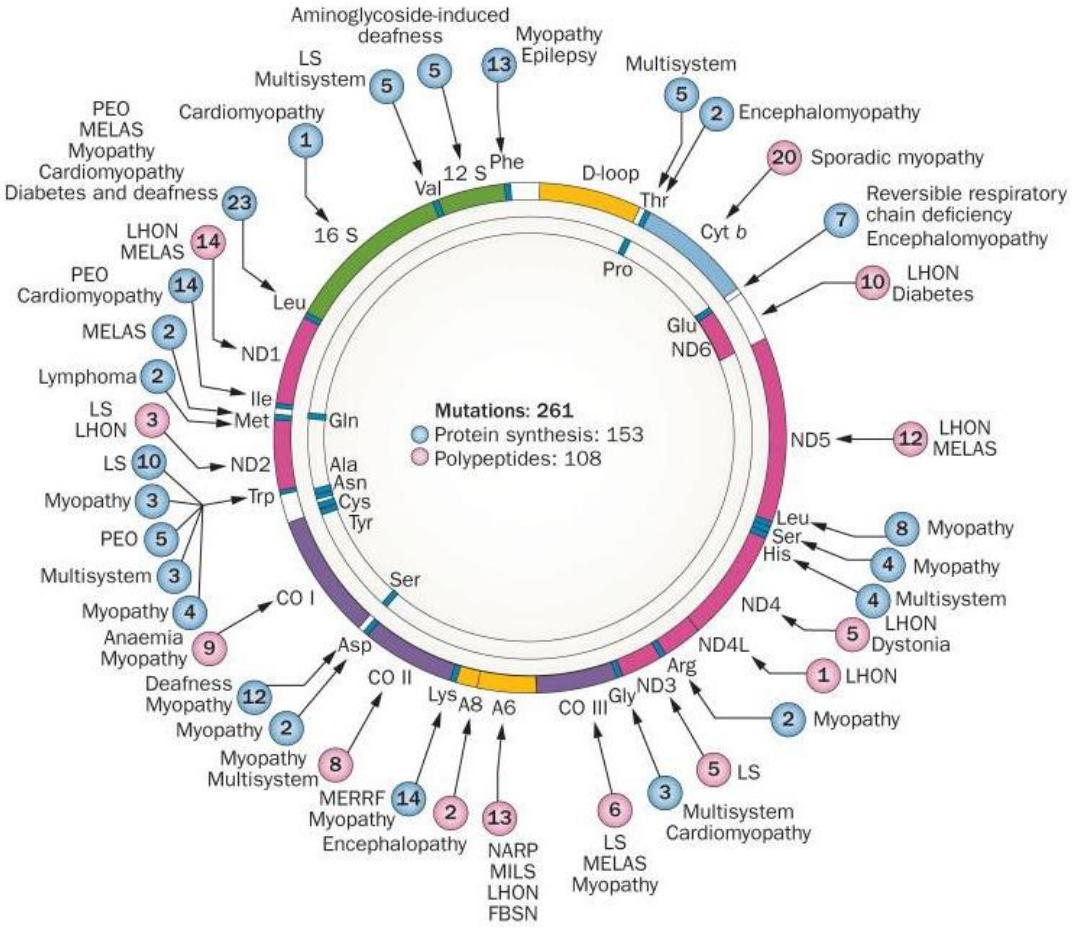

Figure 1-4 Mitochondrial genome illustrating the marked phenotypic heterogeneity observed in patients with primary mitochondrial disease.

Colour-coded sections: pink – complex I (ND) subunits; light blue – complex III (cyt b) subunits; purple – complex IV (CO) subunits; yellow – complex V (A6,A8) subunits; green – 12S and 16S rRNA; blue – 22 tRNA with corresponding 3-letter amino acid code. Circles: blue – mutations that impair protein synthesis; pink – mutations in OXPHOS subunit proteins. The number within the circle indicated the location of the pathogenic mutation wthin the mitochondrial genome. Reproduced from DiMauro *et al.*, 2013.

Abbreviations: Cyt b – Cytochome b; FBSN – familial bilateral striatal necrosis; LHON – Leber hereditary optic neuropathy; LS – Leigh syndrome; MELAS – mitochondrial encephalomyopathy, lactic acidosis, stroke-like episodes; MERRF – myoclonus epilepsy and ragged red fibers; MILS – maternally inherited Leigh syndrome; NARP – neuropathy, ataxia and retinitis pigmentosa; ND – NADH – dehydrogenase; PEO – progressive external ophthalmoplegia.

1.3 Autosomal Dominant Optic Atrophy

1.3.1 Epidemiology

DOA is the most common inherited optic neuropathy in the general population and the prevalence has been estimated at 1 in 25,000 in the north east of England (**Figure 1-5**) (Yu-Wai-Man *et al.*, 2010a; Yu-Wai-Man *et al.*, 2013). An even higher prevalence of 1 in 10,000 has been reported in the Danish population, which is likely due to a founder event (Thiselton *et al.*, 2002).

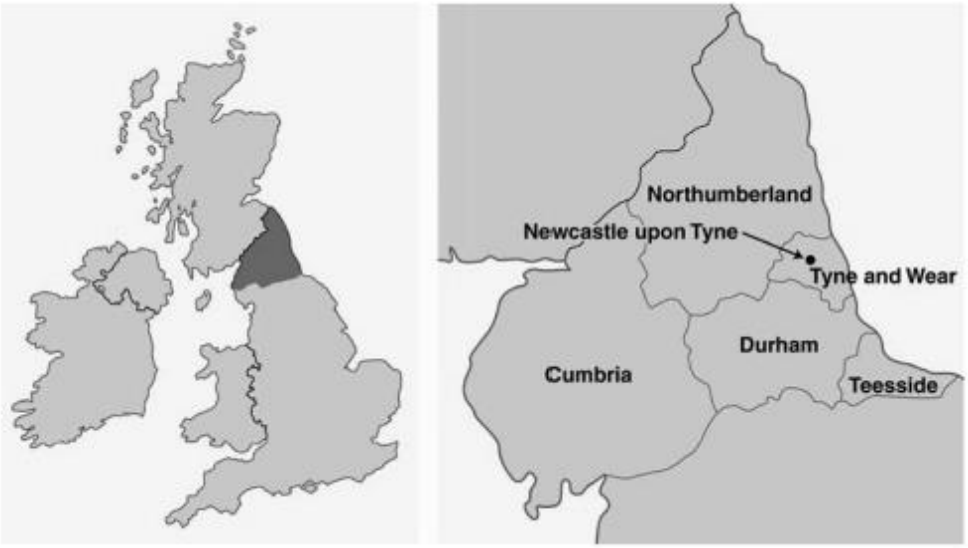

Figure 1-5 Epidemiological study of DOA in the North East of England.

Reproduced from Yu-Wai-Man *et al.*, 2014.

1.3.2 Molecular genetics

OPA1 is the primary causative gene accounting for ~ 60% of cases of DOA (Delettre *et al.*, 2000; Cohn *et al.*, 2007). There are 30 exons spanning over 100 kb of genomic DNA and it codes for a 960-amino acid, dynamin-related GTPase protein that localises to the inner mitochondrial membrane. Disease penetrance is high with 80-90%, of mutation carriers developing optic atrophy and visual failure (Thiselton *et al.*, 2002; Toomes *et al.*, 2001; Cohn *et al.*, 2007) Over 200 *OPA1* pathogenic mutations have been reported and these cluster in two specific regions: the GTPase domain (exons 8-15) and the C-terminus, which is the proposed site of the GTPase effector domain (GED) (**Figure 1-6**). The majority of *OPA1* mutations (~ 50%) lead to premature termination codons (PTCs) as a result of nonsense mutations, frameshifts from small insertions or deletions, or splice-site mutations. The resulting truncated mRNAs are unstable and they are degraded by nonsense mediated mRNA decay (NMD), which are in-built protective cellular mechanisms against mutant proteins with possible dominant negative or gain-of-function effects. The role of haploinsufficiency in DOA is further substantiated by reports of patients with large-scale *OPA1* rearrangements, including the complete loss of one copy of *OPA1* in one family (Marchbank *et al.*, 2002). The functional roles of OPA1 are discussed from **Sections 1.7.2-1.7.7.**

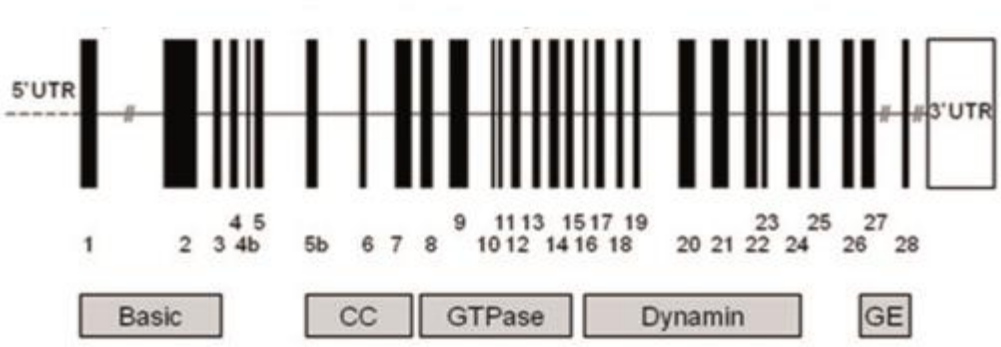

Figure 1-6 Schematic representation of the *OPA1* gene.

Basic domain = exons 1-3; coiled coil domain = exons 5b-7; GTPase domain = exons 7-15; middle domain = exons 16-25; GTPase effector domain = exons 27-28. Adapted from Yu-Wai-Man *et al.*, 2010b.

1.3.3 Clinical manifestations

Visual decline in DOA usually starts in early childhood and the majority of patients are symptomatic before the age of 20 years old (Cohn *et al.*, 2008; Yu-Wai-Man *et al*., 2010a). The average visual acuity is between 20/80 and 20/120, but there is wide intra- and interfamilial variability with disease severity ranging from 6/6 to light perception (Cohn *et al.*, 2007; Kjer *et al.*, 1996; Votruba *et al.*, 1998a). In a study of 21 DOA pedigrees, 80% of individuals maintained a stable visual acuity of 20/200 or better (Votruba *et al.*, 1998a). The reasons for these phenotypic variations are not fully understood, but secondary genetic, epigenetic and/or environmental factors have been implicated. Although the rate of visual loss is usually slow, the majority of patients are eventually registered legally blind and the prognosis is guarded. Patients with DOA will also manifest other features pointing towards optic nerve dysfunction, including dyschromatopsia and central or centrocaecal scotomas due to the primary involvement of the papillomacular bundle (Lenears *et al*., 2012; Smith, 1972; Puomila *et al.,* 2005). The optic disc pallor in DOA falls into two main categories: diffuse pallor involving the entire neuro-retinal rim in about half of all cases or a temporal wedge of pallor in the remainder (**Figure 1-7**). Excavation of the optic nerve head in DOA can sometimes lead to a clinical misdiagnosis of normal tension glaucoma (Fournier *et al.*, 2001; Buono *et al.*, 2002).

Figure 1-7 Optic disc appearance in a patient carrying a confirmed pathogenic *OPA1* mutation.

There is bilateral global optic disc pallor, which is more marked in the temporal quadrant consistent with the more severe involvement of papillomacular bundle (RE- Right eye, LE- Left eye).

1.3.4 DOA plus phenotypes

DOA can present either with isolated optic nerve involvement (pure DOA) or with additional neuromuscular features which include visual failure, sensorineural deafness, ataxia/myopathy/neuropathy and PEO (DOA plus, DOA+) (**Figure 1-8**). Previous work from our group have shown that ~ 20% of patients harbouring pathogenic *OPA1* mutations develop the more severe DOA+ phenotype (Yu-Wai-Man *et al.*, 2010b). These neuromuscular complications cause major functional disability in patients who are already severely visually impaired (Amati-Bonneau *et al.*, 2005; Bailie *et al*., 2013).

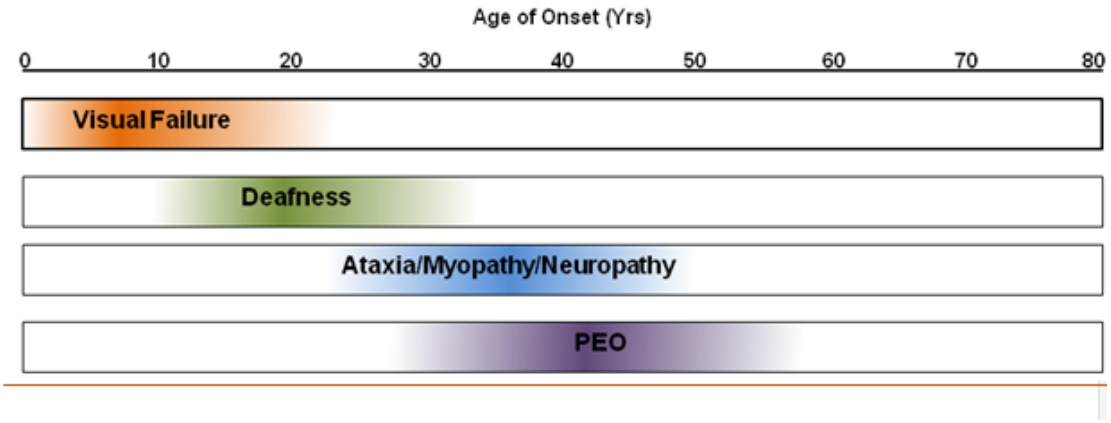

Figure 1-8 Age of onset for clinical features associated with DOA plus phenotypes.

PEO: progressive external opthalmoplegia. Reproduced from Yu-Wai-Man et al., 2010b.

These syndromic variants of DOA have been linked with the secondary accumulation of multiple mtDNA deletions and with the presence of cytochrome *c* oxidase (COX)-deficient fibres in skeletal muscle biopsies obtained from affected mutation carriers (Amati-Bonneau *et al.*, 2008; Hudson *et al.*, 2008). There is a threefold increased risk of developing the more severe DOA+ phenotype with missense *OPA1* mutations involving the GTPase domain compared with other mutational subgroups (Yu-Wai-Man *et al.*, 2010b). The deleterious consequences of this specific group of *OPA1* mutations on RGC survival is therefore clearly linked to the development of multisystem organ involvement in DOA+, suggesting a possible dominant negative effect. However the fundamental question still remains – ***why does a subgroup of patients with OPA1 mutations develop DOA+ features, leading to an increased neurological disability in addition to a worse visual prognosis?***

1.3.5 Recessive *OPA1* mutations

Recently the clinical spectrum of DOA+ was further expanded with the description of Behr syndrome (Marelli *et al.*, 2011). Behr syndrome is an autosomal recessive disorder originally classified by the German ophthalmologist Carl Behr, and describes an infantile form of optic atrophy compounded with mental retardation, ataxia, spasticity and peripheral neuropathy.

Most known cases of DOA are due to dominant inheritance which can either lead to an isolated optic nerve involvement or a syndromic optic atrophy. However, in rare instances, patients with compound heterozygous *OPA1* variants with either recessive or semi dominant inheritance have been identified with severe visual loss and/ or ataxia, cortocospinal tract involvement, peripheral neuropathy and myopathy (Pesch *et al.,* 2001; Marelli *et al.,* 2011; Schaaf *et al.,* 2011; Carelli *et al.,* 2015a, Bonneau *et al.,* 2014; Bonifert *et al.,* 2014). Although both heterozygous and compound heterozygous *OPA1* mutations have been detected in patients presenting with Behr syndrome, pathological homozygous variants have yet to be clinically identified. Three *OPA1* mouse models have been developed with truncative OPA1 variants located in exons 8 (c.1051C>T) (Davies *et al.,* 2007), intron 10 (c.1065+5 G> A) (Alavi *et al.,* 2007) and exon 27 (c.2708-2711delTTAG) (Sarzi *et al.,* 2012). These heterozygous models faithfully replicate the visual deterioration found in DOA. However, strikingly, homozygous models died *in utero* suggesting that *OPA1* is highly relevant for early development. Based on this observation of embryonic lethality, it is therefore not surprising that compound heterozygous or homozygous pathogenic deletions or duplications have yet to be found in DOA affected individuals.

1.3.6 Other DOA genes

Additional prominant genes associated to a dominant form of congenital optic neuropathy include *MFN2*, *OPA3*, *AFG3L2*, *SPG7* and *ACO2* (**Table 1-1**). These are translated and dispatched to the mitochondrial compartment where they are primarily involved in mitochondrial fission/fusion dynamics and/or disparate functions of mitochondrial metabolism and quality control. Pathological mutations in these genes can lead to a syndromal form of optic atropy similar to the DOA+ phenotype which includes visual loss, spastic paraplegia and ataxia among other unique neuropathological presentations.

1.3.7 OPA3

About 40% of clinically diagnosed DOA patients do not harbour pathogenic variants in *OPA1* (Yu-Wai-Man *et al.,* 2011). The causative nuclear defects in a small number of families have been mapped to other chromosomal loci; *OPA3, OPA4, OPA5, OPA8,OPA9 and OPA10* of which only the *OPA3* gene has been characterised (**Section 1.5; Table 1-3**) (Garcin *et al.,*

1961; Reynier *et al.*, 2004; Kerrison *et al.*, 1999; Barbet at al., 2005; Carelli *et al.*, 2007; 2011b;Angebault *et al*., 2015).

OPA3 was originally identified in 8 Iraqi Jewish families with an autosomal recessive form of optic atrophy, associated with neuro-cognitive deficits, elevated urinary excretion of 3-methyl glutaconic acid and increased plasma 3-methylglutaric acid levels (Type III 3-methylglutaconic aciduria or Costeff syndrome) (Anikster *et al.*,2001). Subsequent case series also identified heterozygous mutations in *OPA3* which can be responsible for dominant cases of either isolated or complex multi-systemic bilateral optic atrophy (Grau *et al.*, 2013; Reynier *et al.*, 2004; Sergouniotis *et al.*, 2015). Patients typically present with optic atrophy and infantile-onset cataracts but may display other visual and ocular abnormalities such as dyschromatopsia and temporal optic disk pallor. Additional neurological features may also include sensorineural deafness, spasticity and extrapyramidal dysfunction.

Functional investigation of OPA3 has shown that it is expressed as two different isoforms (A and B) of which isoform *OPA3-A* has a greater level of expression than its counterpart (Huizing *et al.*, 2010) (**Figure 1-9**). A recent homozygous (c.365T>C; p.Leu122Pro) *OPA3* mouse line has been developed modelling the type 3-methylglutaconic aciduria condition found in humans and will be invaluable in dissecting the molecular mechanisms of recessive and complex OPA3- related optic disorders (Davies *et al.*, 2008; Wells *et al.*, 2012).

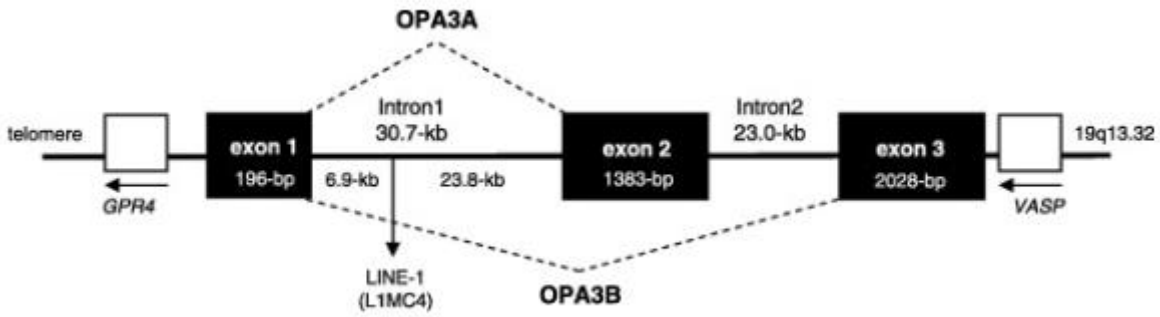

Figure 1-9 Schematic diagram of *OPA3* illustrating the two alternative isoforms OPA3A and OPA3B.

Adapted from Huizing *et al.*, 2010.

1.3.8 MFN2

MFN2 is a GTPase known to be involved in OMM fusion, ER-mitochondrial interaction, mitochondrial axonal transport and mitophagy. Mutations found in the gene encoding this GTPase are responsible for an optic neuropathy known as Charcot Marie Tooth 2A(CMT2A). It is the most common axonal CMT disorder responsible for at least 20% of known cases. Similar to DOA, CMT2A has a complex presentation, most notably with foot deformities, walking difficulty, areflexia, sensory loss, physical weakness and in some cases sensorineural hearing loss and optic atrophy. The inheritance of CMT with optic atrophy can be due to both dominant and recessive inheritance of defective MFN2.

1.3.9 SPG7

SPG7 encodes for paraplegin, a primary constituent of the m-AAA (mitochondrial-AAA) protease responsible for both degrading aberrant mitochondrial proteins and maturation of specific polypeptide substrates such as OPA1. In rare cases, mutations in *SPG7* are associated with a dominant form of OA which can either present as an isolated OA or OA complicated with cerebellar atrophy and peripheral neuropathy (Klebe *et al.,* 2012).

1.4 Wolfram Syndrome

1.4.1 Epidemiology

In some conditions with optic neuropathy, the optic degeneration is not the primary symptom and is associated with other primary manifestations as is the case in Wolfram syndrome. Wolfram syndrome, also described as DIDMOAD or diabetes insipidus, diabetes mellitus, optic atrophy and deafness (Bessahraoui *et al.,* 2014), has a prevalence of 1 in 770,000 individuals in the United Kingdom with most cases described as recessive or sporadic (Barrett *et al.,* 1995). Some cases with dominant inheritance have also been identified (Bai *et al.,* 2014; Bonnycastle *et al.,* 2013).

1.4.2 Molecular genetics

The genetic component of Wolfram syndrome, *WFS1* was first identified in 1998 through genetic mapping and a candidate gene approach. Mutations within *WFS1* have been found in most recorded cases of Wolfram syndrome (Inoue *et al.*, 1998; Strom *et al.*, 1998; de Heredia *et al.*, 2013). A wide variety of mutations have been detected in *WFS1* which include splice-site, stop and frameshift mutations. However no mutational hotspot has been located in the *WFS1* gene (De Heredia *et al.*, 2013). Currently most pathogenic variants described in patients diagnosed with Wolfram Syndrome are loss of function (90%). There are <200 total variants reported (www.euro-wabb.org -June 2015) in *WFS1* with 51.8% substitutions, 37% deletions, 9.1% duplications, 1.6% insertions and 0.4% insertion/deletion.

Another manifestation of Wolfram Syndrome was reported in a Jordanian family and the genetic component designated *WFS2* (El-Shanti *et al.*, 2000). The locus for *WFS2* was mapped to chromosome 4q22-24. Clinical presentation involved the classical symptoms of Wolfram syndrome which included optic atrophy and diabetes mellitus. There was however, no incidence of diabetes insipidus and a few patients were bleeding and had upper gastrointestinal ulceration with/without sensorineural hearing loss (Rigoli *et al.*, 2011; El-Shanti *et al.*, 2000; Amr *et al.*, 2007). Linkage analysis identified *CISD2* as the causative genetic factor. Similar to *WFS1*, *CISD2* encode for a protein located within the ER compartment.

1.4.3 Clinical manifestations

The progression of Wolfram syndrome is variable with, in most cases, onset occurring in the first or second decade of life. Either a loss in visual acuity and optic atrophy may precede other syndromic features, or a mild dyschromatopsia or optic atrophy may occur initially followed by visual loss (Barrett *et al.*, 1997). In the latter stages of the condition, visual loss is extreme and there is an obstruction of visual fields with a pathological cupping of the optic disc. Although the 'minimum ascertainment' of wolfram syndrome was initially optic atrophy and juvenile diabetes mellitus (<16 years) (**Table 1-2**), investigation into the underlying genetic aetiology of this condition has highlighted cases of Wolfram syndrome without characteristic diabetes insipidus or diabetes mellitus (Barrett *et al.*, 1995; Khanim *et al.*, 2001; Chaussenot *et al.*, 2015; Marshall *et al.*, 2013; Kytovuori *et al.*, 2013).

Major criteria	Minor criteria	Minimum required	Other variable suggestive evidence:
-Diabetes mellitus <16 yrs *(87%)* -Optic atrophy <16 yrs *(80%)*	- Diabetes insipidus *(42%)* - Diabetes mellitus >16yrs*(4%)* -Optic atrophy >16 yrs *(7%)* -Sensorineural deafness *(48%)* -Neurological signs (ataxia, epilepsy, cognitive impairment) *(29%)* -Renal tract abnormalities (structural or functional) *(33%)* -1 loss of function mutation in *WFS1/CISD2* AND/OR family history of Wolfram syndrome	-2 major OR -1 major plus 2 minor criteria OR -2 pathological *WFS1* or *CISD2* mutations are identified	- Hypogonadism (males) *(6%)* - Absence of type 1 diabetes auto-antibodies -Bilateral cataracts *(1%)* -Psychiatric disorder *(26%)* -Gastrointestinal disorders *(5%)*

Table 1-2 Minimum ascertainment parameters for the diagnosis of Wolfram syndrome.

Reproduced from http://www.orpha.net/national/data/IE-EN/www/uploads/Wolfram2014.pdf

1.4.4 Pathophysiology

WFS1 is localised to the ER where it is involved in polypeptide quality control in the unfolded protein response (UPR) (Hofmann *et al.*, 2003; Takeda *et al.*, 2001). The UPR consists of post translational modifications (PTMs), folding and assembly of functional cellular proteins. WFS1 is a component of the UPR negative feedback loop and interacts with the transcription factor ATF6α which is responsible for the upregulation of chaperones, the

mediators of protein folding (Osman *et al.,* 2003). Disturbed ER mechanics can culminate in ER stress due to the accumulation of malformed polypeptides and ultimately upregulate the apoptotic response. Pancreatic β cells, retinal ganglion cells and cochlear cells have all shown to have a greater susceptibility to this stress response than other tissue types (Example of human retinal layers from Wolfram syndrome diagnosed patients in **Figure 1-10**). Additional functions of WFS1 include protein trafficking, calcium homoeostasis and cell signalling pathways (Zatyka *et al.,* 2008; Yamaguchi *et al.,* 2004; Fonseca *et al.,* 2005; Yamada *et al.,* 2006; Hofmann and Bauer, 2006)

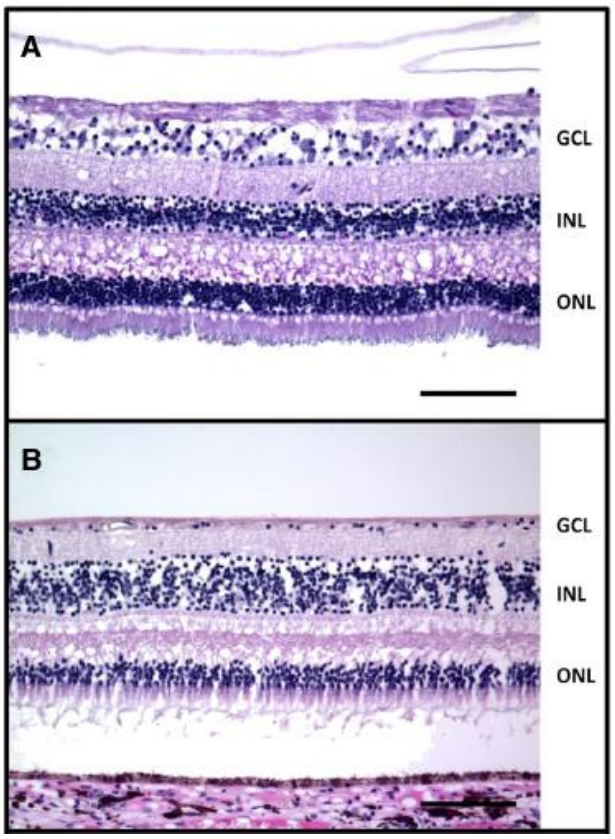

Figure 1-10 Light micrographs derived from paraffin-embedded sections of human retina from a patient with Wolfram syndrome.

Haematoxylin and eosin stained Cross-sections taken 3.5mm from optic nerbe centre from (**A**) Control human macula and (**B**) Macula from patient suffering from Wolfram Syndrome. Control (**A**) shows normal staining of human retinal layers while retinal layers from patient with Wolfram Syndrome (**B**) displays loss of retinal ganglion cell layer. Figure adapted from Ross-Cisneros *et al.,* 2013.

1.5 Other Inherited Optic Neuropathies

Other genetic loci have been identified in patients with dominant and recessive inherited optic neuropathies (**Table 1-1**). Intriguingly, the pathophysiology of these disorders typically involves either mitochondrial or ER function suggesting a unifying biochemical theme for this clinically heterogenous group of disorders. As for *OPA1* mutation carriers, the reported cases are either characterised by isolated optic atrophy or more severe syndromc manifestations complicated by varying combinations of sensorineural deafness, peripheral neuropathy, cognitive decline, seizures, hypotonia, ataxia and spasticity. About half of all patients with suspected inherited optic neuropathies do not yet have a confirmed molecular diagnosis and the hope is that more of these cases will be resolved in the next few years with the greater availability of next-generation exome and whole genome sequencing (Allen *et al.*, 2015) (**Table 1-3**). Case series of isolated optic nerve involvement have also been described, such as autosomal recessive chiasmal optic neuropathy (Pomeranz *et al.*, 1999) and apparent sex-linked optic atrophy (Went *et al.*, 1975; Assink *et al.*, 1997), but the genetic basis still remains unknown.

Locus	Chromosome	Gene	Inheritance Pattern	References
OPA1	3q28-29	*OPA1*	Dominant	Delettre *et al.*, 2000 Alexander *et al.*, 2000
OPA2	Xp11.4-p11.21	-	X-linked recessive	Assink *et al.*, 1997
OPA3	19q13.2-q13.3	*OPA3*	Dominant / Recessive	Reynier *et al.*, 2004; Anikster *et al.*,2001
OPA4	18q12.2-q12.3	-	Dominant	Kerrison *et al.*, 1999
OPA5	22q12.1-q13.1	-	Dominant	Barbet, 2005
OPA6	8q21-q22	-	Recessive	Barbet, 2003
OPA7	11q14.1-q21	*TMEM126A*	Recessive	Hanein *et al.*, 2009
OPA8	16q21-22	-	Dominant	Carelli *et al.*, 2011
OPA9	6q21	*RTN4IP1*	Recessive	Angebault *et al.*, 2015

Table 1-3 Mapped genetic loci and nuclear genes identified in patients with inherited optic neuropathies.

Adapted from Wiggs, 2015

1.6 Mitochondria in Health and Disease

Mitochondria are cellular organelles, which primary function is to produce chemical energy in the form of adenosine triphosphate (ATP) in the process of aerobic respiration. These organelles exist in an intricate interconnected dynamic network known as the mitochondrial reticulum (Chen and Chan *et al.*, 2005). Mitochondria do not exist as discrete organelles but instead are in a constant state of dynamic fission or fusion with other members of the reticulum. They are found in the cytoplasm of most eukaryotic cells and their number varies from a few hundred to several thousand depending on the cell's energy requirements. **(Figure 1-11**).

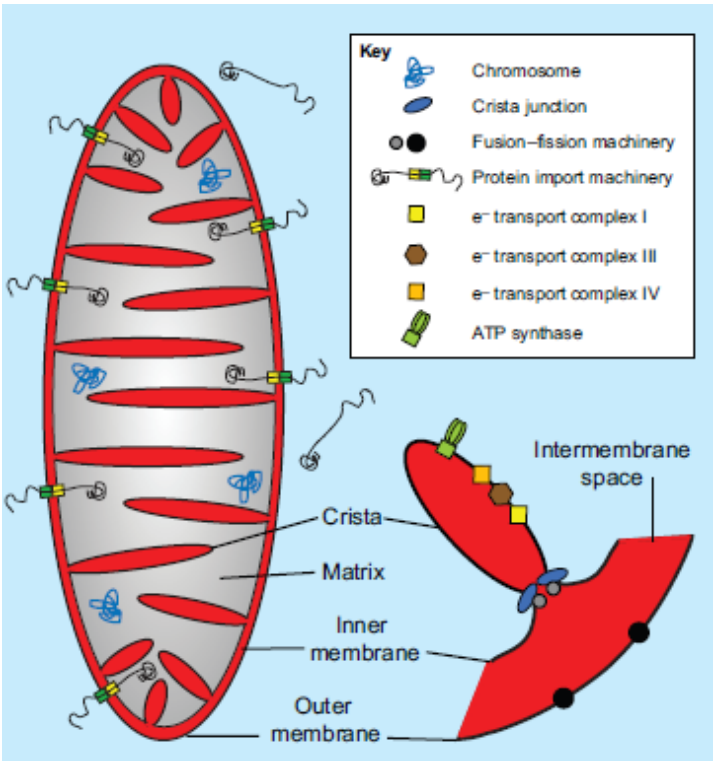

Figure 1-11 Structure of the mitochondrion. Depiction of the structure of mitochondrial cristae and the position of the mitochondrial respiratory chain supercomplexes. Reproduced from Saxton and Hollenbeck, 2012.

1.6.1 Origin

The current hypothesis known as endosymbiotic theory, suggests that mitochondria arose from aerobic α-proteobacteria which were gradually assimilated by primitive glycolytic eubacteria (Lang *et al.,* 1997). Over the course of evolution, much of the genetic material from these aerobic α-proteobacteria were transferred to the genome of the eubacterion which formed a symbiotic relationship. This is evidenced by phylogenetic study of *Alphaprobacteria – Rickettsia prowazekii* and mitochondria which lends support to a common evolutionary origin (Lang *et al.,* 1997; Gray *et al.,* 1999; Margulis *et al.,* 1971).

1.6.2 Structure

Each mitochondrion is bounded by an outer and an inner membrane, and these are separated by an intermembrane space (Frey and Mannella, 2000). The outer mitochondrial membrane allows the free diffusion of molecules of ≤ 5 kDa. These molecules cross through membranous channels which are either formed by integral proteins known as porins or voltage dependent anion channels (VDACs). The inner membrane lacks porins and is rich in cardiolipin, which makes it highly impermeable. Molecules therefore need to be actively transported via specific active transport channels from the intermembrane space (IMS) into the matrix compartment. This allows the establishment of an electrochemical gradient. The inner membrane is compartmentalized into structures called cristae which increase the effective surface area for ATP production by the respiratory chain complexes (Perkins et al,1997). The mitochondrial matrix contains soluble enzymes involved in the β-oxidation of fatty acids,the citric acid cycle and the intricate machinery required for the replication and transcription of mtDNA which are packaged into structures known as nucleoids *(Alberts et al*., 2002). Mitochondria also play an important role in calcium handling (Herrington *et al.*, 1996), apoptosis (Green, 1998), and the metabolism of amino acids, lipids, cholesterol and nucleotides (McBride *et al.*, 2006).

1.6.3 Mitochondrial genetics

The mitochondrial genome is a circular double stranded DNA molecule of 16,569 base pairs (bp) (Anderson *et al.,* 1981). Originally it was thought that these genomic molecules were naked DNA backbones with a protective coat in the form of histone proteins similar to nuclear DNA (Nass *et al.,* 1969, Iborra *et al.,*2004). It is now known that mtDNA molecules are instead contained within nucleoprotein structures known as nucleoids which are approximately 100 nm (Kukat *et al.,* 2011). A recent investigation has suggested that each nucleoid contains a single mtDNA genome. There are approximately 1-10 mtDNA copies in each mitochondrion. Thousands of mtDNA molecules can exist in a cell depending on its metabolic requirements (Kukat *et al.,* 2011).

The structure of the mitochondrial genome consists of a purine-rich heavy chain (H-strand) and a pyrimidine-rich light chain (L-strand) (Anderson *et al.,* 1981). Unlike nuclear DNA, this genome contains no introns but instead has a 1.1kb region known as the displacement loop (D-loop) (**Figure 1-12**). This is a non-coding triple-stranded region which is involved in processes such as transcription and replication (Sbisa *et al.,* 1997; Roberti *et al.,* 1998). This region has numerous regulatory elements such as binding sites for transcription factor A (TFAM-A), a termination associated sequence (TAS) and conserved sequence blocks (CSB1, CSB2 and CSB3) (Suissa *et al.,* 2009; Sbisa *et al.,* 1997). The origin of the H-strand is located within the D-loop. Most of the genes encoded by mtDNA are found on the H-strand and include two ribosomal RNAs (12S and 16S rRNA), 14 transfer RNAs (tRNAs) and 12 subunits of the oxidative phosphorylation (OXPHOS) complexes. There are additional genes on the L-strand which include ND6 and eight tRNA genes. Other mitochondrial proteins are encoded by the cell's nuclear genome and are targeted to the mitochondrial organelles. Due to the relatively small size of the mtDNA molecule and the lack of intronic sequences, many of these genes are overlapping and produce polycistronic transcripts. The tRNA genes found on both the H- and L-strand regulate this polycistronic transcriptional processing (Ojala *et al.,* 1980). Other unique features of the mitochondrial genome include the presence of only two stop codons (AGA and AGG) while the nuclear genome contains three (UAA, UGA, UAG) (Barrell *et al.,* 1979. In addition the nuclear stop codon UGA instead transcribes for tryptophan in mtDNA (Barrell *et al.,* 1979).

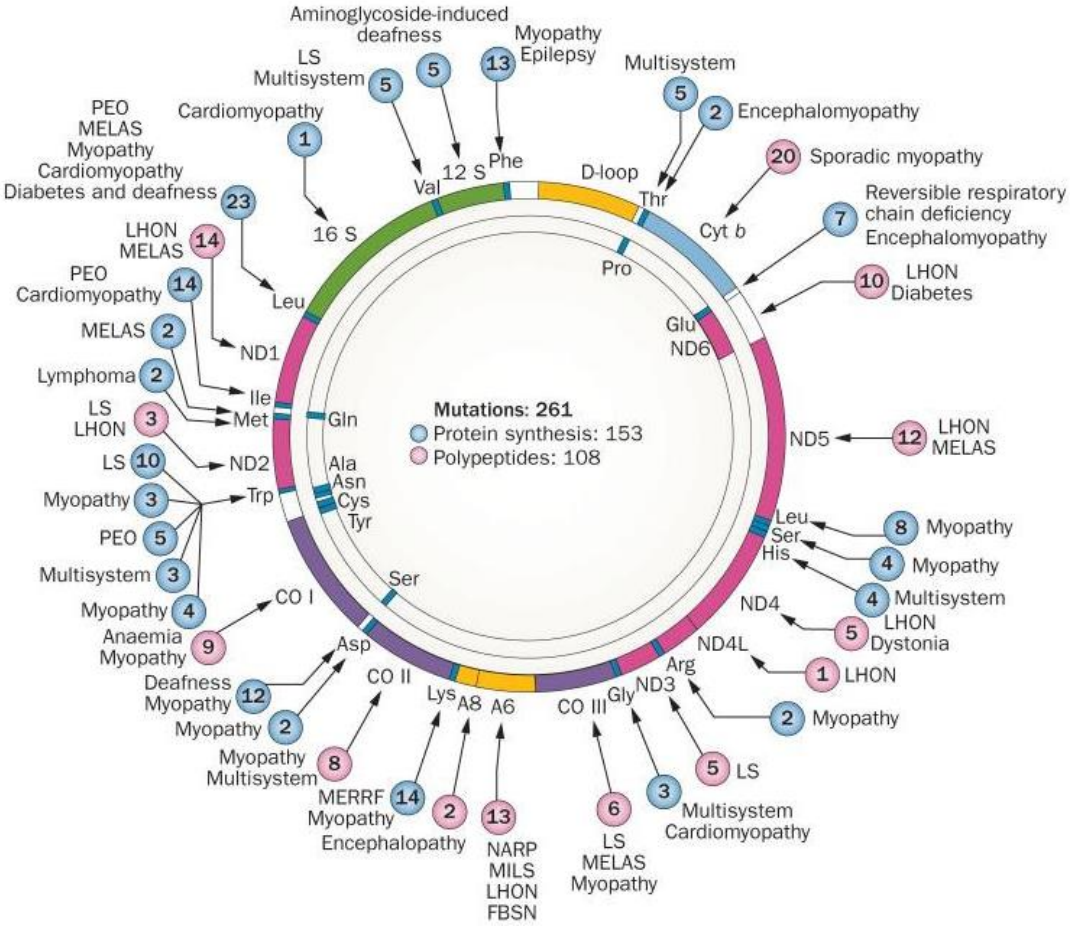

Figure 1-12 Schematic illustration of the human mitochondrial genome.

MtDNA contains of 16,569 bps and is composed of two strands known as the heavy and light strand. Two promoters known as I_{H1} and I_{H2} are found on the heavy strand while one promoter I_L on the light strand and these promoters are responsible for mtDNA replication. Promoters and other elements required for mtDNA replication are all found in the D-loop in an untranslated region of mtDNA mtDNA transcription occurs on both strands to encode required OXPHOS, ribosomal and t-RNA mRNAs. Reproduced from DiMauro *et al.*, 2013.

1.6.4 Mitochondrial nucleoids

The mitochondrial nucleoid is a nucleoprotein structure which encapsulates the mtDNA molecule (Spelbrink *et al.,* 2010). Analysis of nucleoid aggregates with stimulated emission depletion microscopy (STED) has revealed that these structures are relatively uniform in size, however there is controversy as to the number of mtDNA per nucleoid. STED microscopy suggests that each nucleoid only contain a single mtDNA genome (Kukat *et al.,* 2011), but another study using super resolution photoactivated localisation microscopy (PALM) found at least three mtDNA molecules per nucleoid (Brown *et al.,* 2011). The latter study also found that the size of these nucleoids was dependent on the number of mtDNA molecules that they contained. Recent observation also demonstrates that nucleoids retain and regulate their own mtDNA and do not freely distribute it amongst other nucleoids (Gilkerson *et al.,* 2008).

Transcription factor-A (TFAM) is the primary protein which comprises the nucleoid and is involved in compartmentalising and organising mtDNA. Other subsidiary proteins contained within this structure include T7-like helicase (Twinkle, PEO1), mtSSB protein, Lon, DEAD-box protein 28 (DDX28), suv3-like helicase, POLRMT, and mtDNA polymerase γ (POLG) (**Figure 1-13**) (Y.Wang and Bogenhagen, 2006).

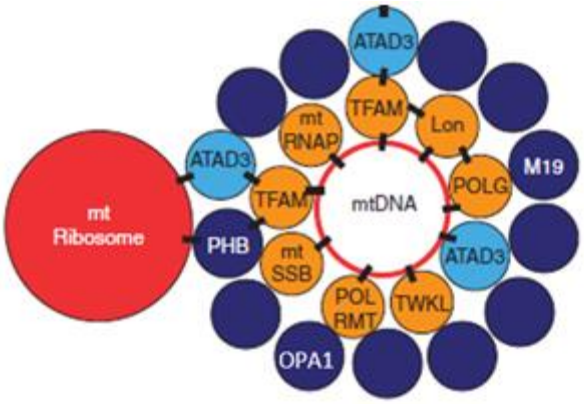

Figure 1-13 Mitochondrial nucleoid illustrating both the core (gold) and peripheral (blue) constituents.

Core constituents (POLG, POLRMT, mtSSB, TFAM, TWINKLE, Lon) are capable of binding to mtDNA molecules and regulating transcription, translation and replication. Peripheral components (ATAD3, M19, PHB, and OPA1) are associated with integrating mtDNA and the nucleoid with global cellular signalling. Black rectangles indicate known protein and DNA interactions. Adapted from Gilkerson *et al.*, 2013

An additional group of proteins are transiently associated with a subset of mitochondrial nucleoids at any given time in order to perform a necessary function. An example of this are the mtDNA repair proteins and others involved on the process of mtDNA replication such as ATAD3. Although the mechanism of mtDNA copy number maintenance has still to be elicited, preliminary findings suggest that ATAD3 and POLG2 are some of the primary regulators involved. ATAD3 knockdown has also demonstrated an association with nucleoid formation (He *et al.*, 2007; Holt *et al.*, 2007.)

These nucleoids are functionally diverse and promote mtDNA transcription and replication at the nucleoid core, while translation of mtDNA occurs on the outer periphery of these structures. The nucleoid is also believed to be involved in the organisation and distribution of mtDNA in dividing mitochondria by localizing to a tethered ER-mitochondrial complex, the ERMES complex as observed in a yeast model (Murley *et al.*, 2013). These relocalised nucleoids are primarily the ones which are in the process of replicating new mtDNA. This allows mitochondrial nucleoids to segregate evenly following mitochondrial

division within each daughter mitochondria and allows maintenance of functioning newly developed organelles. The exact mechanism of how actively replicating nucleoids associate with these mitochondrial division sites is an active area of research. The ERMES complex has not been found in mammalian cells but present research suggests that a similar structure may exist. Genetic knockdown of DRP1, a regulator of mitochondrial fission, promotes the aggregation of nucleoids (Ban-Ishihara *et al.,* 2013). MIRO-1 has also been observed to co-localise to ER-mitochondrial contacts where mitochondrial fission takes place. (Kornmann *et al.,* 2011). MIRO-1 is a homologue of gem1 in yeast which is a RHO-like small GTPase responsible for releasing the mitochondrial –ER contacts.

There is evidence from studies in yeast that the nucleoid also undergo remodelling under different metabolic conditions. Nucleoids may play a similar role to histones, which are protein structures binding to nuclear DNA and providing an additional level of complex regulation. *Kucej and colleagues* studied the yeast protein Abf2, which is an homolog of Human mTF1 and similar in function to human TFAM s using a Chip-on -chip assay (Kucej *et al*., 2008). They demonstrated that Abf2 was not as tightly bound and concentrated along mtDNA and formed a less compact nucleoid structure under conditions of respiration and growth which may potentially promote transcription of mtDNA. Greater accessibility of mtDNA may also promote regulation and binding of other factors but this remains to be elicited. Under conditions of glucose or amino acid starvation, factors such as hsp60 and ilv5 are recruited to nucleoids (Kucej *et al.,* 2008). These factors are believed to be involved in nucleoid/mtDNA maintenance. This preliminary research in yeast would suggest that the nucleoid is a dynamic structure which regulates mtDNA in response to metabolic homeostasis. These observations have yet to be extended into the human model but because of the high degree of functional conservation between yeast and higher order organisms, it is conceivable that such mechanisms may play a role in human health and disease states.

1.6.5 Mitochondrial heteroplasmy

The mitochondrial genome has a greater susceptibility to acquire genetic variants than the nuclear genome due to a number of factors. The close proximity of mtDNA to high levels of reactive oxygen species (ROS) produced as a byproduct of the OXPHOS system, the lack of

protective histones and the high replication rate of mtDNA molecules which promote replication error all contribute to polymorphism generation. The primary source of ROS is derived from the OXPHOS system, particularly from H_2O_2 species generation which together with redox-active metals such as Fe^{2+} undergo Fenton chemistry to create free radicals which effectively damage mtDNA (Thomas *et al.*, 2009; Droge, 2002).

As a cell comprises hundreds to several thousand mitochondria and each organelle contains between 2-10 mitochondrial genomes, mtDNA molecule are present in high copy number in individual cells. As a result of mutations caused by ROS, mtDNA population can be described as either homoplasmic or heteroplasmic. A homoplasmic mtDNA population is composed of mtDNA molecules with an identical genetic sequence. A heteroplasmic population comprises mtDNA molecules with different variants in the mtDNA genetic code (Wallace and Chalkia, 2013). Pathogenic mtDNA mutations are due to deleterious variants in a heteroplasmic population of mtDNA. In heteroplasmic populations, a minimum critical threshold of pathogenic mutated mtDNA molecules compared to wild-type (approximately 60-80%) is necessary before biochemical defects and tissue dysfunction become apparent (**Figure 1-14**) (Wallace and Chalkia, 2013; Stewart and Chinnery. 2015). This threshold level varies depending on the mutation and differs amongst tissues, depending on their level of reliance on OXPHOS metabolism.

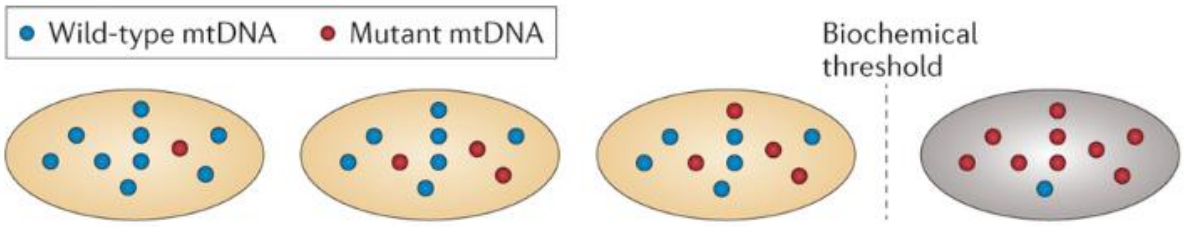

Figure 1-14 Biochemical threshold of mutant mtDNA species.

Reproduced from Stewart and Chinnery, 2015.

1.6.6 Mitochondrial DNA maintenance

To combat genetic damage, the mitochondrial genome employs a number of DNA repair strategies which include mismatch repair and base excision repair of the mtDNA molecule. Base excision repair (BER) is the predominant and most well characterised mtDNA repair pathway (Alexeyev *et al.,* 2013). This pathway is divided into two generalised mechanisms of BER, SP-BER (short-patch base excision repair) and LP-BER (long-patch base excision repair) (Svilar *et al.,* 2011). The factors influencing the initiation of SP-BER or LP-BER are still being investigated but may be associated with the specific type of lesion, whether the cell is actively dividing or senescent and what stage of the cell cycle the lesion occurs. BER is achieved by (i) detection of the DNA lesion (ii) Strand scission/ gap tailoring and (iii) DNA synthesis/ligation (**Figure 1-15**). (Alexeyev *et al.,* 2013)

In SP-BER, detection of the genetic lesion is facilitated by monofunctional or bifunctional glycosylases which introduce a single stranded break (SSB) (Anderson and Friedberg, 1980; Ohtsubo *et al.,* 2000; Dodson and Lloyd, 2002). This SSB is further processed by AP-endonuclease-1 (APE1) or polynucleotide kinase 3'-phosphatase (PNKP) and ligated by the activity of POLG (**Figure 1-15**).

LP-BER is the most common repair strategy for oxidative damage. It differs from SP-BER because the DNA polymerase forms a 'flap' which is 6-9 nucleotides long from the point of excision. This 'flap' is processed by two nucleases FEN1 and DNA2 which create a DNA duplex which is ligated by LIG3 (**Figure 1-15**) (Alexeyev *et al.,* 2013).

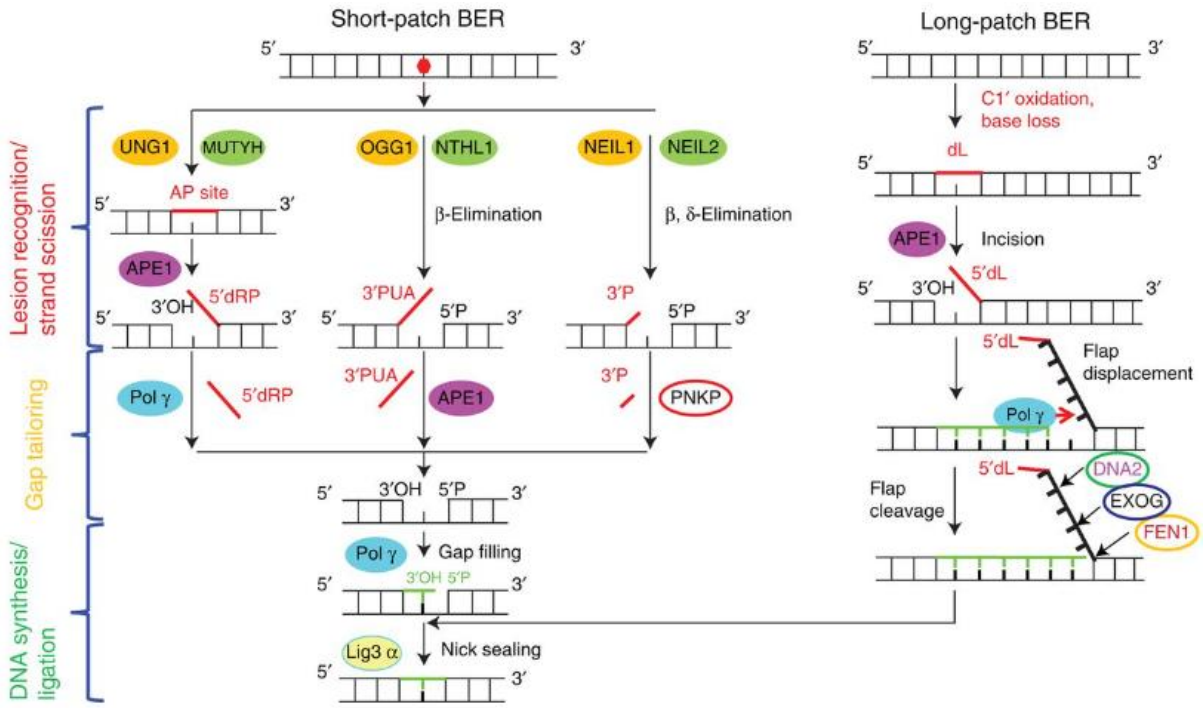

Figure 1-15 Mechanisms protecting against genetic damage to mtDNA.

Reproduced from Alexeyev *et al.*, 2013**.**

1.6.7 Mitochondrial haplogroups

The mitochondrial genome has a greater susceptibility to acquire genetic variants than the nuclear genome (Howell *et al.*, 1996; Jazin *et al.*, 1998). This is due to a number of factors. The close proximity of mtDNA to high levels of ROS, a byproduct of the OXPHOS system, the lack of histones which protect against genetic damage and the high replication rate of mtDNA molecules which promote replication error all contribute to polymorphism generation (Raha and Robinson, 2000, Alexeyev *et al.*, 2013). MtDNA is inherited through a maternal lineage and it is through these genetic lines that different mtDNA polymorphisms have been acquired and fixed by distinct human populations (Cann, 2001). These fixed polymorphisms follow the pattern of human migration from Africa some 150,000 years ago into each of the different continents. Eighteen major phylogenetic haplogroups have been categorised in the

human species which comprise 497 unique haplogroup polymorphisms. Within Europe there are nine distinct haplogroups defined as H,I,J,K,T,U,V,W and X. H is the most common European haplogroup accounting for over half the population (Torroni and Wallace,1994; Herrnstadt and Howell, 2004, Herrnstadt *et al.*, 2002).

1.6.8 Mitochondrial DNA replication

MtDNA replication is a process controlled by proteins encoded by the nuclear genome but is asynchronous to the cell cycle in mitotic and post-mitotic cells (Bogenhagen and Clayton, 1977). It is regulated by the mitochondrial replisome, which is a complex composed of four different proteins which include POLG, mtSSB, TFAM and TWINKLE HELICASE (Wanrooij *et al.*, 2010) and replication occurs at differential rates dependent on tissue type.

The model which describes mtDNA replication is currently a controversial issue with three distinct mechanisms proposed. These three mechanisms are (i) asymmetric strand displacement (ASD) model (Clayton, 1982), (ii) synchronous strand coupled bidirectional (SSCB) model (Holt *et al.*, 2000; Bowmaker *et al.*, 2003) and (iii) asymmetric strand displacement model combined with the incorporation of RNA at the lagging strand of replication (RITOLS model) (**Figure 1-16**) (Yasukawa *et al.*, 2006).

The ASD model, originally described by Clayton (1982), suggests that replication commences at the origin of replication (O_H) on the leading\heavy strand (H-strand) and proceeds in a clockwise manner. This clockwise replication expands the D-region and exposes a second origin of replication ($O_{L)}$ on the inner lagging\light strand (L-strand). When H-strand clockwise replication has successfully replicated two thirds of the circular leading strand, anti-clockwise replication of the inner L-strand begins. This form of replication generates two daughter mtDNA molecules but due to the asynchronous timings of the H and L strand, one daughter mtDNA is fully generated while the second daughter mtDNA is still replicating its L-strand.

The synchronous strand coupled bidirectional (SSCB) model of mtDNA replication by *Holt and colleagues* is one that describes synchronous replication of both the H- and L-strands (Holt *et al.*, 2000). This conclusion resulted from the examination of replicative intermediates of mammalian mtDNA found in 2D agarose gel electrophoresis. Their proposed

model suggests that replication begins on both the H and L strand simultaneously at a region known as O_Z, a single origin of replication where commences coupled strand replication. This generates two replication forks which expand and create two daughter mtDNA molecules simultaneously. *Holt and colleagues* propose that this model may occur independent or concurrent with the original strand displacement model (Holt *et al*., 2000)

The RITOLS model of replication is mechanistically similar to the original ASD model which describes differential replicative timing of the leading and lagging mtDNA strand. However the RITOLS model proposes that mtDNA is first transcribed to RNA and subsequently reverse transcribed to the newly formed DNA strand (Yasukawa *et al.,* 2006).

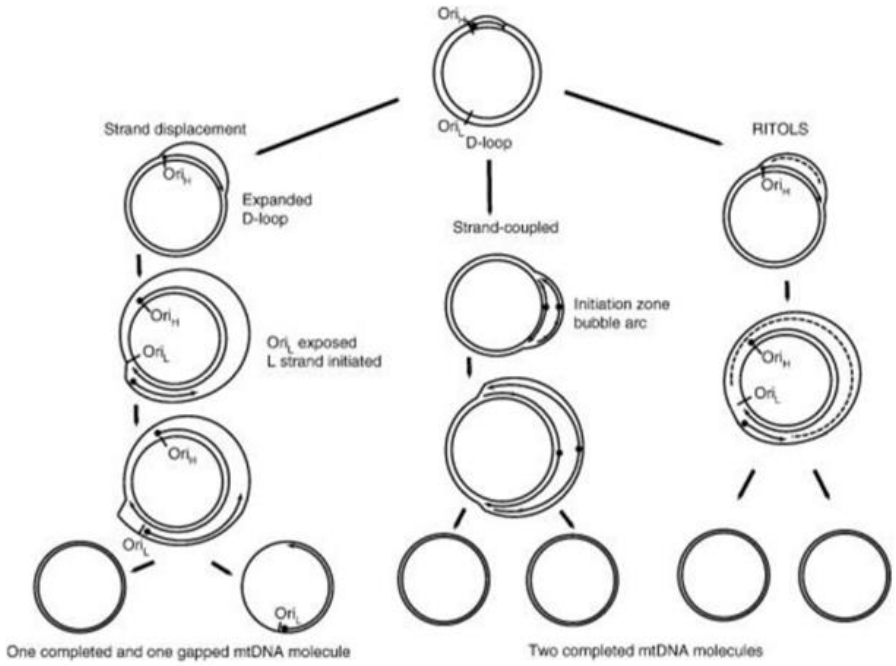

Figure 1-16 Alternative proposed models of mtDNA replication

(i) Assymetric Strand displacement model: (Left panel) Replication begins at O_H and replicates clockwise until O_L is revealed on the light strand. A second replication event commenses on the light strand at O_L in an anti-clockwise manner to generate two daughter mtDNA molecules. (ii) Synchronous Strand coupled bidirectional model: (middle panel) Replication on the heavy and light strand commenses simultaneously at O_Z producing two coupled replication forks and generates two daughter mtDNA molecules. (iii) RITOLS model: (Right panel) Similar to the assymetric strand displacement model, replication on heavy and light strands occurs in an asynchronous manner however mtDNA is instead transcribed to RNA before being transcribed into two mtDNA daughter molecules. Reproduced from Kasiviswanathan *et al.*, 2011.

1.6.9 Mitochondrial transcription

Transcription of mtDNA can be initiated independently on the H and L strands. H-strand transcription can occur on two separate promotor sites, 150bp apart (**Figure 1-17**) These initiation sites are known as HSP1 and HSP2 and are differentially regulated (Litonin *et al.*, 2010; Lodeiro *et al.,* 2012). Most often, the HSP1 promoter is initiated to create two tRNAs and two mitochondrial rRNAs. The HSP2 promoter alternatively produces a large polycistronic transcript which is punctuated by tRNA sequences, necessary to define rRNA and mRNA transcripts. The H-strand is responsible for transcribing twelve mRNA, fourteen tRNA and two rRNA species. The L-strand has only a single promoter initiation site designated LSP. It is responsible for transcribing a single mRNA and eight tRNA species. All three transcription initiation promoters are contained within the mitochondrial D-loop and each contains a 15bp consensus sequence (Cantatore *et al.,* 1980; Montoya *et al.,* 1982; Martin *et al.,* 2005)

The intricate mitochondrial transcription machinery is composed of POLRMT (mitochondrial RNA polymerase) and two initiation factors designated transcription factor A (TFAM) and transcription factor B2 (TFB2M) (Morozov *et al.,* 2014). This model for mitochondrial transcription involves a simple mechanism where TFAM binds to a recognition site upstream of the D-loop transcriptional promoter. TFAM is required for transcription specificity at the transcription promoter sites. This TFAM bends the mtDNA and permits recruitment and interaction of POLRMT to form the pre-initiation complex (Morozov *et al.*, 2014). This pre-initiation complex in turn recruits TFB2M to form the initiation complex which is required for melting of the mtDNA and commencement of transcription.

The concentration of TFAM is also believed to have a relationship on transcription promoter regulation. There are currently two models which describe this process, the cooperative looping monomer-dimer model and the cooperative spreading dimer model. These models describe how the binding of TFAM, initially at the LSP promoter site and subsequently at the inter- promoter region, drive structural changes of the mtDNA molecule and as a consequence adjust activation of the mitochondrial transcriptional promoter (Wong *et al.,* 2009; Gangelhoff *et al.,* 2009; Campbell *et al.,* 2012).

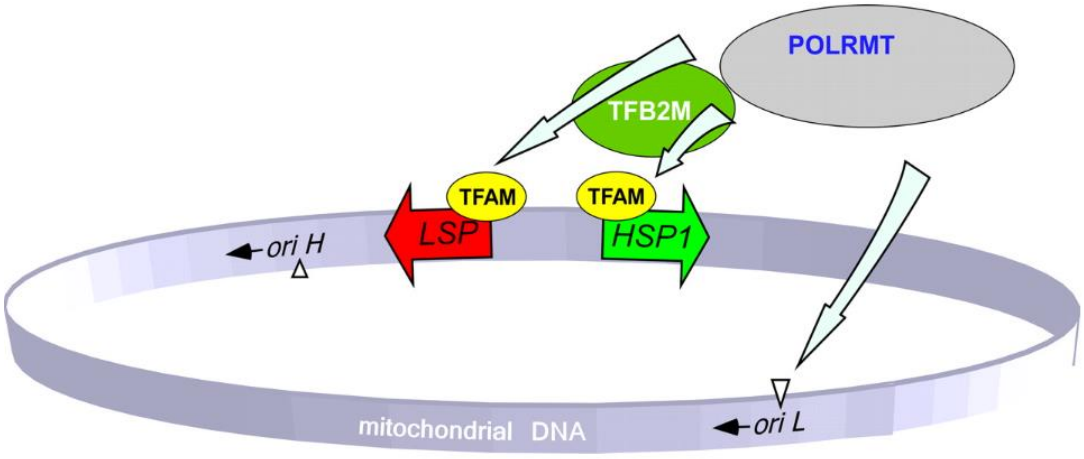

Figure 1-17 Schematic of the mechanism of mtDNA transcription

The intricate mitochondrial transcription machinery is composed of POLRMT (mitochondrial RNA polymerase) and two initiation factors designated transcription factor A (TFAM) and transcription factor B2 (TFB2M). Reproduced from Litonin *et al.*, 2010.

1.6.10 Mitochondrial translation

The mitochondrion possess over 1000 different proteins, most of which are encoded by the eukaryotic translation machinery found in the cytoplasm (Endo *et al.*, 2011). However a subset of these proteins are synthesised by a distinct mitochondrial translation system encoded by the mitochondrial genome. These proteins include 22 tRNAs, 2 rRNAs and 13 OXPHOS complex subunits.

The mitochondrial translation system is not well characterised but close parallels have been noted between mitochondrial and prokaryotic translation machineries. This is primarily due to the lack of a proper *in vitro* model of mitochondrial protein synthesis. The subunits of the mitochondrial ribosome are mostly encoded by the nuclear genome. Recent efforts have defined the structure of the mitochondrial ribosome at a resolution of 3.5 angstrom (Amunts *et al.*, 2015). This analysis has determined that this ribosome is a complex of approximately 80 proteins including three ribosomal RNA proteins, 12S, 16S and mt-tRNA^{Val}.

Protein translation involves three steps, initiation, elongation and termination (**Figure 1-18)**. The initiation step is catalysed by initiation factors mtIF2 and mtIF3 which are orthologous to the IF1 and IF2 initiation factors in prokaryotes (Myasnikov *et al.*, 2009). The

initiation factor mtIF3, dissociates the 55S ribosomal subunit into two smaller subunits 39S and 28S to facilitate formation of the initiation complex. The mtIF2 factor is responsible for initiating an interaction between fMet-tRNA (tRNA carrying the first amino acid for protein synthesis) and the 28S subunit to form this initiation complex (Myasnikov *et al.*, 2009). Elongation involves three elongation factors similar to prokaryotes, mtEFTu, mtEFTs and mtEFG which promote mRNA read-through by coding-anticoding interaction, amino acid peptide bond formation and peptide elongation (Hammarsund *et al.*, 2001; Ling *et al.*, 1997; Xin *et al.*, 1995). Termination of mitochondrial translation is regulated by two release factors $_{Mt}$RF1 and $_{M}$tRF2 and a recycling factor $_{mt}$RRF. This process begins at a mitochondrial stop codon (UAA, UAG, AGA or AGG). When this stop codon is recognised, the peptide is released from the tRNA (Smits *et al.*, 2010).

Interestingly, over 200 pathogenic mutations which affect tRNA processing enzymes and aminoacyl-tRNA synthases (ARS) of mitochondrial translation have been implicated in complex clinical diseases (Abbott *et al*., 2014). Mutations in tRNA enzymes typically disrupt aminoacylation and can impact the expression of OXPHOS complex subunits in these mitochondrial disorders.

Two classical and most well characterised cases associated with mitochondrial translational defects include mitochondrial encephalomyopathy, lactic acidosis and strike like symptoms (MELAS) and myoclonic epilepsy and ragged red fibres (MERRF) (Kobayashi *et al*., 1990; Shoffner *et al*., 1990). Intrigingly, presentation of these two diseases is predominantly due to defects at a tRNA anticodon wobble position (mt-tRNA^{LEU}- MELAS; mt-tRNA^{LYS}- MERRF). In addition to these phenotypes, other more rare tissue specific presentations with alternative mutations can afflict the auditory or visual system, similar to optic neuropathies (Yan *et al*., 2011a; Crimi *et al*., 2003)

.Mutations in mitochondrial tRNA modifying factors like glycl-tRNA synthase (GARS) and lysyl-tRNA synthase (KARS), which are encoded solely by mtDNA, can lead to diseases of the peripheral nervous system such as Charcot-Marie-Tooth. Other mitochondrial nuclear encoded modifying factors such as HARS2 (histidyl-tRNA synthetase 2), LARS2 (leucyl-tRNA synthetase 2), DARS (aspartyl-tRNA synthetase), RARS2 (arginyl-tRNA synthetase 2), YARS2 (tyrosyl-tRNA synthetase 2), SARS2 (seryl-tRNA synthetase 2), AARS2 (alanyl-tRNA synthetase 2), MARS2 (methionyl-tRNA synthetase 2), FARS2 (phenylalanine-tRNA

synthetase 2), EARS2 (glutamyl-tRNA synthetase 2), VARS2 (valyl-tRNA synthetase 2) and TARS2 (threonyl-tRNA synthetase 2) have also all been implicated in other mitochondrial related disorders demonstrating the complexity of mitochondrial translation in disease (Abbott *et al*., 2014).

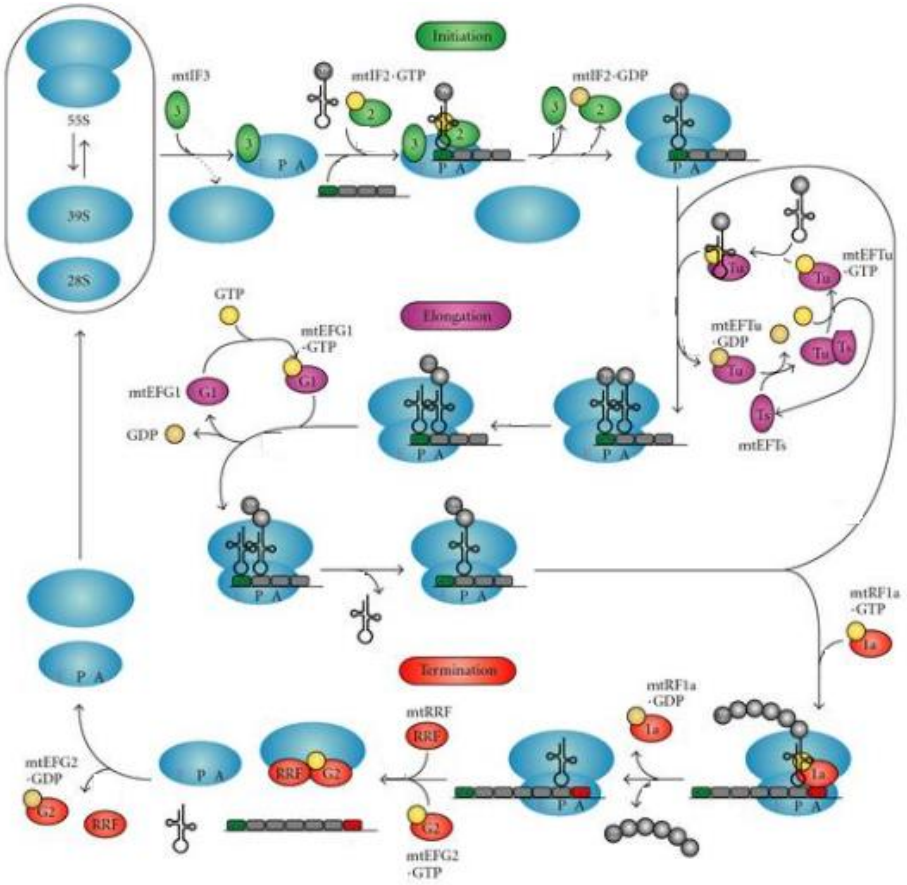

Figure 1-18 Schematic of the three stages (initiation, elongation and termination) involved in mitochondrial translation.

Adapted from Smits *et al.*, 2010.

1.6.11 Mitochondrial oxidative phosphorylation

The majority of the cells energy requirement in the form of ATP is provided by the mitochondrial respiratory chain. OXPHOS is regulated by five protein transmembrane complexes bound to the matrix side of the IMM (Inner Mitochondrial Membrane) (Bellance *et al.*, 2009). These complexes are NADH ubiquinone oxidoreductase (complex I), succinate ubiquinone oxidoreductase (complex II), ubiquinol cytochrome c reductase (complex III), cytochrome c oxidase (complex IV) and ATP synthase (complex V). Each complex is composed of multiple subunits which are encoded by either the mtDNA or the nuclear genome. The only exception to this is complex II, whose subunits are entirely transcribed from the nuclear genome. This chemical energy 'production line' is intrinsically linked to the Krebs cycle located within the mitochondrial matrix. The Krebs cycle produces cofactors known as Reduced Nicotinamide Adenine Dinucleotide ($NADH_2+H^+$) and Reduced Flavin

Adenine Dinucleotide ($FADH_2$) and these molecules are oxidised when they interact with complexes I and II, respectively. The donated electrons are transported along the mitochondrial OXPHOS chain by coenzyme Q_{10} and cytochrome c and protons are pumped across the intermembrane space to generate an electrochemical gradient. This proton gradient is employed by ATP synthase (complex V) to generate ATP from the constituents' adenosine diphosphate ADP and inorganic phosphate P_i (**Figure 1-19**).

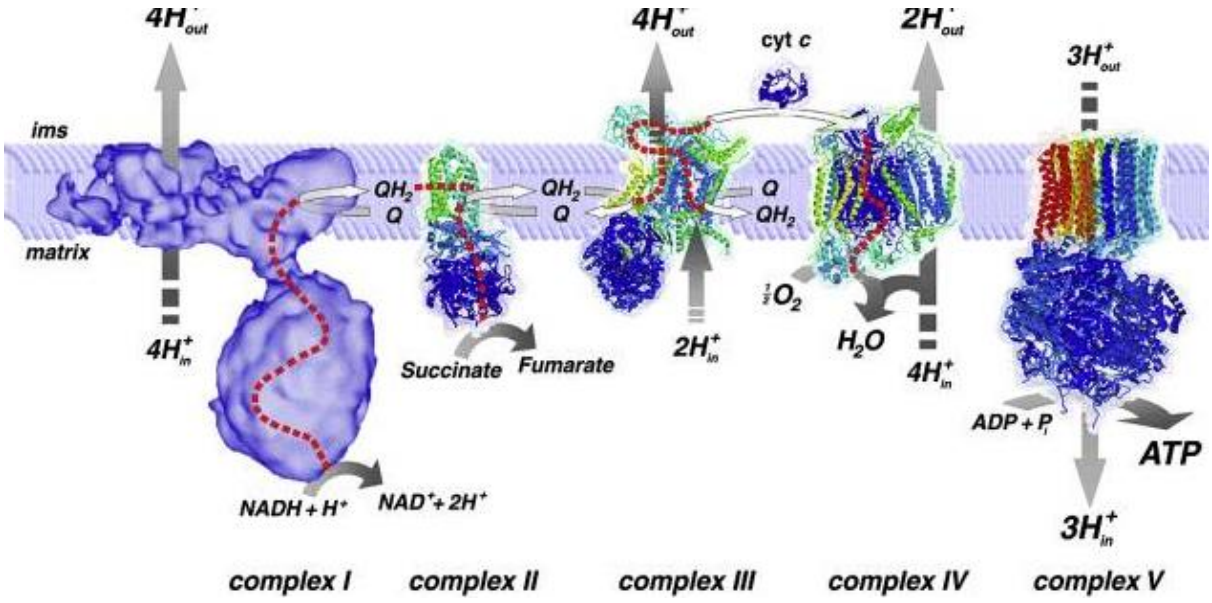

Figure 1-19 The mitochondrial respiratory chain complexes.

Reproduced from Nijtmans *et al.*, 2004

1.6.12 Complex I: NADH ubiquinone oxidoreductase

Complex I is an L-shaped multiprotein structure composed of 47 subunits and is the largest complex of the OXPHOS system with a molecular weight of 980kDa. The hydrophobic components of this complex are embedded in the IMM while the hydrophilic arm extends into the mitochondrial matrix (Grigorieff, 1999). The subunits which compose this structure are composed of 7 mitochondrial and 40 nuclear encoded proteins which are shuttled and imported into the mitochondrion. The complex contains the co-enzyme Flavin mononucleotide (FMN) and up to nine iron sulphur clusters (Hinchliffe and Sazanov, 2005; Koopman *et al.*, 2007). NADH is oxidised to NAD^+ at complex I and two electrons are transferred to coenzyme Q_{10} (ubiquinone). Ubiquinone is reduced to ubiquinol and diffused within the IMM. Each molecule of NAD^+ is then used to pump four protons across the IMM to form an electrochemical gradient (Raha and Robinson, 2000).

1.6.13 Complex II: succinate ubiquinone oxidoreductase

Complex II (succinate-ubiquinone oxidoreductase or succinate dehydrogenase; SDH) is unique because it is the only complex to be completely composed of nuclear encoded subunits. Structurally, it is the smallest complex and is constructed of only four subunits. Subunits A (73KDa) and B (27KDa) are hydrophilic with subunit A containing a covalently-bound flavin adenine dinucleotide coenzyme and subunit B with three iron-sulphur clusters (Hatefi and Galante, 1980; Lancaster and Kroger, 2000). The remaining subunits C and D contain heme groups. Similar to complex I, it produces electrons through the process of oxidation to reduce ubiquinone to ubiquinol. These electrons are derived from succinate which is oxidised to fumarate at the FAD coenzyme and transferred by the iron-sulphur clusters to ubiquinone. However unlike complex I, this oxidation process in not accompanied by proton transfer.

1.6.14 Complex III: ubiquinol cytochrome c reductase

Complex III has a dimeric structure and is composed of eleven subunits. Ten are nuclear encoded while a single subunit, cytochrome b, is mitochondrial. Three subunits of this complex, cytochrome b (which contains two haem groups), cytochrome c_1 (with a covalently bound haem c) and an iron-sulphur protein (Rieske protein) are components of a functional catalytic core known as the cytochrome bc_1 complex (Yu *et al.,* 1999). The primary function of complex III is to transfer electrons to cytochrome c through a series of oxidation/reduction reactions of ubiquinol and ubiquione in a mechanism known as the Q cycle (Mitchell *et al.,* 1976). This occurs in conjunction with protein pumping across the IMM which establishes an electrochemical gradient (Acin-Perez *et al.,* 2004).

1.6.15 Complex IV: cytochrome c oxidase

Complex IV (cytochrome c oxidase; COX) is composed of thirteen subunits and is a soluble haemoprotein structure with a molecular weight of 204kDa. Ten subunits are nuclear encoded while the remaining three are mitochondrial (COX1, COXII and COXIII). It is the terminal electron acceptor of the OXPHOS system (Kadenbach *et al.,* 1983). The complex spans the

inner membrane facing both the mitochondrial matrix and the IMS. It contains two copper centres (CU_A and CU_B) and two heme groups (cytochrome a and a3). Cytochome a3 and CU_B create a binuclear centre required for the reduction of molecular oxygen to water. This process occurs by the transfer of electrons from cytochrome c to this binuclear centre which reduces oxygen. Two protons are transferred to this reduced oxygen molecule to form water. In conjunction with this process, four additional protons are translocated across the IMM forming an electrochemical gradient (Saraste *et al.,* 1999).

1.6.16 Complex V: ATP synthase

Complex V (F_0F_1-ATP synthase) is composed of seventeen different subunits and has an approximate molecular weight of 500kDa (Von Ballmoos *et al.,* 2009) Fifteen of these subunits are nuclear encoded while two are mitochondrial (ATP6 and ATP8) (Boyer, 1997) The ATP synthase complex is composed of two primary structures, the F_0 motor which is located in the IMM and the F_1 motor, a structure with a catalytic domain located in the mitochondrial matrix. F_1 is a cylindrical structure derived from α, β, γ ,δ and ε subunits in an $\alpha_3\beta_3\gamma\varepsilon$ stoichiometry (Abrahams *et al.,* 1994; Yoshida *et al.,* 2001). Alternative α and β subunits form a cylinder bounding the γ subunit. The F_0 motor has an $a_1b_2c_{12}$ stoichiometry with c subunits forming a cylindrical structure and bounded by a and b subunits. The F_0 and F_1 motors are connected by a ring of subunit c which links the γ subunit through mutual contacts with ε subunit. Together these F_0 and F_1 moieties of ATP synthase form a rotor-stator model where protons are translocated along the cylindrical F_0 structure which acts as a channel through the mitochondrial membrane and turns this F_0 motor (Gibbons *et al.,* 2000; Ko *et al.,* 2000). These protons are generated through the electrochemical gradient established by complexes I, III and IV. Rotation of the F_0 motor subsequently rotates the catalytic F_1 motor which binds ADP and P_i and generates ATP (Kayalar *et al.,* 1977).

1.7 Mitochondrial dynamics

Mitochondrial dynamics is a term describing the fusion and fission processes which occur between intracellular mitochondrial organelles. These dynamic processes mediate a broad variety of cellular functions. These functions include the maintenance of the mitochondrial genome, adaptation to extracellular stress, localizing mitochondria in areas of high energy demand, regulation of programmed cell death and calcium buffering between the endoplasmic reticulum and the mitochondrial compartments. (Ferree and Shirihai, 2012; Mcbride *et al.*, 2006).

1.7.1 Mitochondrial fusion

Fusion of adjacent mitochondria involves the coordinated fusion of the OMM and IMM (Meeusen et al, 2006; Song *et al.*, 2007). Although these two fusional steps occur independently, OMM and IMM fusion usually occur in a synchronous manner through the tightly regulated interactions of OPA1 on the IMM, and the mitofusin complex (MFN1 and MFN2) on the OMM. OPA1, MFN1 and MFN2 regulate both transient and complete fusion of the mitochondrial network. Transient fusion is defined as an event in which only the OMM is fused while complete fusion involves both the outer and inner mitochondrial membranes. Transient or 'kiss and run' fusion is used to distribute mRNAs, small solutes and proteins between two mitochondria while complete fusion allows the distribution of both soluble and essential components required for mitochondrial survival.

1.7.2 OPA1

OPA1 is a nuclear encoded gene of approximately 100kb (30 exons) which lies on chromosome 3. Early linkage association studies mapped OPA1 to a locus at chromosomal position 3q28 (Eiberg *et al.*, 1994) and subsequenct studies performed by both Delettre *et al.* and Alexander *et al.* (2000) identified the *OPA1* gene. OPA1 belongs to the dynamin protein family and contains a putative conserved GTPase, a middle and GTPase effector domain. It is transcribed into eight different mRNA species which are alternatively spliced at exons 4, 4b

and 5b and translated by cytosolic ribosomes into OPA1 precursor (**Figure 1-20**). These *OPA1* transcripts are constitutively expressed in all human tissues but are mostly abundant in heart, brain, testis, retina and muscle (Alexander *et al.,* 2000).

Downregulation of OPA1 protein levels caused by mutations or RNAi knockdown can result in mitochondrial network fragmentation (Griparic *et al.,* 2004; Olichon *et al.,* 2003) Knockdown of OPA1 to suboptimal levels (i.e. haploinsufficiency) can disrupt the formation of a stable fusion complex with MFN1 and MFN2, an essential step necessary for both transient and complete mitochondrial fusion (Cipolat *et al.,* 2004). More recently, experimental data has emerged showing that OPA1 level is a critical factor in the formation and stability of mitochondrial respiratory chain complexes I, II and III. Reduced OPA1 levels or aberrant mutant proteins can therefore disrupt OXPHOS, leading to protein leakage as well as loss of mitochondrial membrane potential (Zanna *et al.,* 2008).

1.7.3 Proteolytic processing of OPA1

The OPA1 precursor is targeted to the mitochondrial compartment by a mitochondrial targeting sequence (MTS) at the N-terminus which is cleaved upon import by the matrix metalloprotease mitochondrial processing pepsidase (MPP) to produce the long isoform of OPA1 (L-OPA1) (Olichon *et al.,* 2002; Satoh *et al.,* 2003). L-OPA1 is embedded in the IMM and it is further processed by three additional proteases to produce OPA1 protein isoforms (**Figure 1-20**). These proteases target conserved S1 and S2 cleavage sites located at exons 5 and 5b, respectively (**Figure 1-21**). The rhomboid protease PARL and the (matrix-AAA protease) mAAA-protease paraplegin cleave OPA1 at S1 (Cipolat *et al.,*2006; Ishihara *et al.,* 2006) and the (intermembrane-AAA protease) i-AAA protease YME1L cleaves OPA1 at S2 site (Song *et al.,* 2007) to produce short isoforms of OPA1 (S-OPA1). OMA1 also cleaves OPA1 at the S1 site under basal conditions but as it is an inducible protease, it can upregulate cleavage at this site and promote mitochondrial fission. Both long and short isoforms of OPA1 are localised to the IMS and are required for proper mitochondrial fusion to take place. It is thought that L-OPA1 is anchored to the IMM while the S-OPA1 is only peripherally associated with the IMM and can diffuse through the IMS to the OMM (Olichon *et al.,* 2002; Satoh *et al.,* 2003; Griparic *et al.,* 2004; Ishihara *et al.,* 2006; Ciplolat *et al.,* 2006).

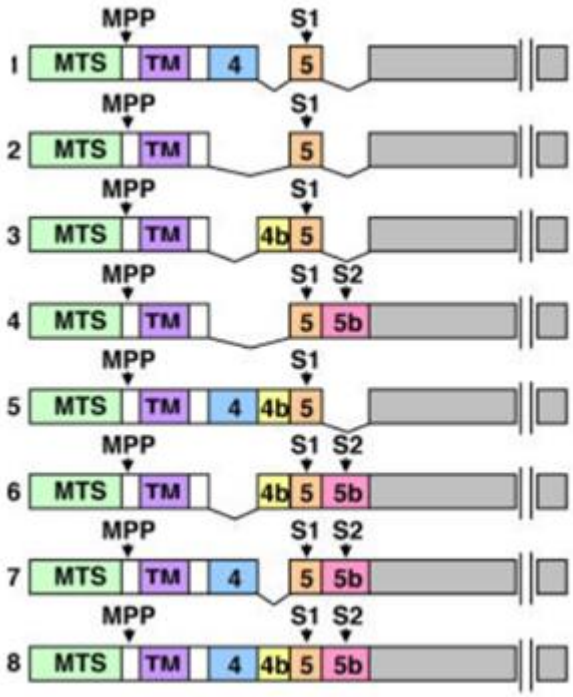

Figure 1-20 Eight isoforms of OPA1 generated through alternative splicing at S1 and S2.

Reproduced from Song *et al.*, 2007

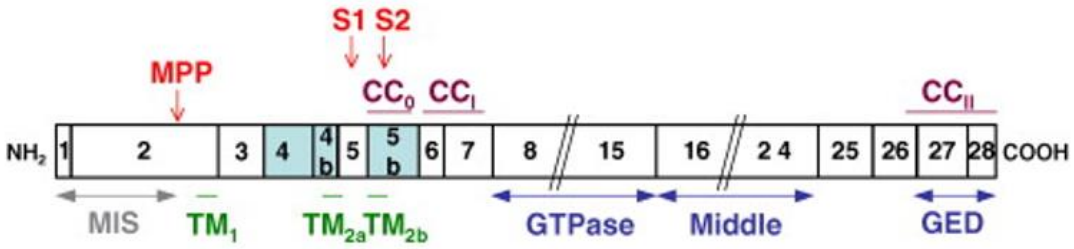

Figure 1-21 Schematic of the structure of the *Opa1* gene containing exons 1-30 inclusive of exons 4b and 5b.

The structure of Opa1 is similar to other dynamins and contains a GTPase domain (exons 7-15), middle domain (exons 16-25) and a GTPase Effector domain (exons 27-28). S1 and S2 are proteolytic cleavage sites for paraplegin, OMA1 and YME1L required to produce mature *Opa1* mRNA transcripts. OPA1 also contains a mitochondrial importer sequence (MIS), a carboxy-terminal coiled coil domain (C_c), a transmembrane domain (TM_1) and an amino-terminal C_C which is present on all eight isoforms of OPA1. Reproduced from Landes *et al.*, 2010.

1.7.4 - OPA1 processing and OXPHOS

The balance between mitochondrial fusion and fission is tightly regulated by these long and short OPA1 isoforms. The metalloproteases YME1L and OMA1 alter the cleavage pattern of OPA1 depending on the efficiency and rate of ATP production through the OXPHOS system (Mishra *et al.,* 2014; Anand *et al.,* 2014).

OMA1 is a metalloprotease responsible for cleaving OPA1 at the S1 site to produce short isoforms of OPA1 (S-OPA1). It is tuned to the electrochemical gradient produced through proton pumping of complexes I, III and IV. If this electrochemical potential is significantly decreased which may occur due to a defect in the rate of ATP production along OXPHOS, OMA1 is upregulated to enhance cleavage of OPA1 at the S1 site. This proteolytic processing of OPA1 produces an abundance of S-OPA1 isoforms which is thought to promote mitochondrial fragmentation (Anand *et al.,* 2014).

In a study to examine of the mechanism of OPA1 cleavage by YME1L, *Mishra and colleagues* (2014) demonstrated that cleavage of OPA1 at the S2 site was tuned to OXPHOS activity. This cleavage mediates IMM fusion and proposes a mechanism in which metabolic signals may trigger differential cleavage of OPA1 and regulate IMM fusion. OMM fusion was not found to be triggered through cleavage of OPA1 by YME1L. The short (S2-OPA1) isoforms generated by YME1L may work in concert with long isoforms of OPA1 (L-OPA1) to promote this fusion, however this requires further investigation (Mishra *et al.,* 2014). Interestingly, inhibition of ATPase activity to hyperpolarise the IMM demonstrated that YME1L activity is not tuned to the electrochemical gradient of OXPHOS as a measure of OXPHOS activity. Preliminary evidence indicates that YME1L may instead directly interact with subunits of ATPase (Stiburek *et al.,* 2012).

Additional studies also found that cells with primary defects of the OXPHOS system had a lower capacity to upregulate YME1L and promote IMM fusion (Mishra *et al.,* 2014).The mechanism of how these metalloproteases mediate metabolic signalling and mitochondrial dynamics is still under intense investigation.

1.7.5 OPA1 processing and mitochondrial fragmentation

Studies investigating the role of OMA1 and YME1L found no morphological difference in mitochondria between wild type and $OMA1^{-/-}$ primary mouse embryonic fibroblasts (Anand *et al.,* 2014). However, investigation of $YME1L^{-/-}$ primary mouse fibroblasts produced excessive fragmentation of the mitochondrial network. Similar levels of L-OPA1 were detected in wild-type and YME1L $^{-/-}$ cells. This would suggest that upregulation of OMA1 cleavage at the S1 site promotes mitochondrial fragmentation which is supported by *in vitro* localisation studies. These studies suggest that S-OPA1 and L-OPA may form punctuate structures which colocalise with fission machinery and mitochondrial-ER contact sites (Anand *et al.,* 2014).

OMA1 may respond to both a transient decrease of IMM potential to cleave OPA1 during the rapid depolarisation of a mitochondrial fission/fusion event and it may respond to a more chronic decrease in IMM potential due to impaired OXPHOS. This cleavage of OPA1 serves to inhibit fusion and isolate damaged mitochondria from the network. These mitochondria are then targeted for destruction by the mitophagic quality control mechanism.

1.7.6 OPA1 and apoptosis

The majority of OPA1 protein (~90%) localises to the cristae junctions on the IMM and is thought to play a structural role in maintaining the shape and organisation of these cristae folds (Perkins *et al.,* 2009). OPA1 isoforms containing exon 5b are likely involved in the sequestering of cytochrome c in these specialised IMM folds. OPA1 is proposed to form an oligomeric complex at cristae junctions which may act as a dam and prevent the passage of large proteins and macromolecules (Perkins *et al.,* 2009). Disruption of these oligomeric OPA1 complexes facilitates the widening of cristae junctions. But electrostatic interaction between cardiolipin and cytochrome C within the IMM prevents cytochrome C's release (Rytomaa and Kinnunen, 1995; Rytomaa *et al.,* 1992; Tuominen *et al.,* 2002). tBID has been observed to associate with cardiolipin on the IMM to produce condensed mitochondria, reversing the curvature of cristae membranes at contant sites which may facilitate cytochrome C release (Gonzalves *et al.,* 2005; Kuwana *et al.,* 2002; Lutter *et al.,* 2000). Disruption of these regulatory mechanisms unsurprisingly leads to increased rates of apoptotic cell death (Olichon *et al.,* 2007) (**Figure 1-22**).

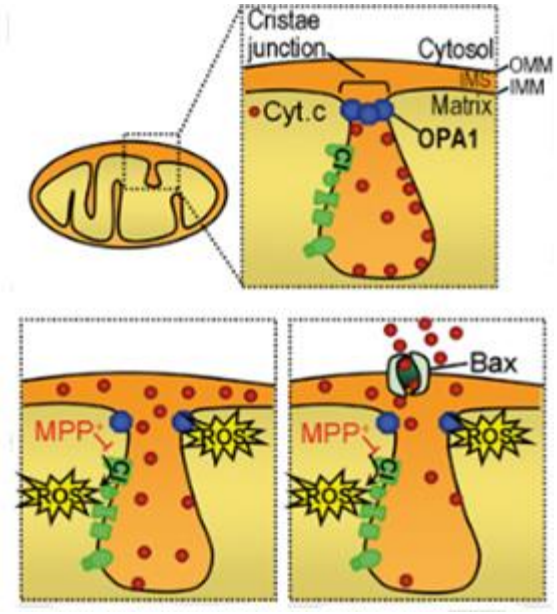

Figure 1-22 Maintenance of cristae junctions on the IMM is facilitated by OPA1 which aids in sequestering cytochrome c.

Reproduced from Ramonet *et al.,* 2013.

1.7.7 OPA1 and mtDNA maintenance

OPA1 is classified as a nuclear gene associated with mtDNA stability. Pathogenic variants in OPA1 have been shown to disrupt the stead-state of mtDNA through either a depletion of mtDNA as seen in an OPA1 mouse model with late-onset cardiomyopathy (Chen *et al.,* 2012), proliferation of mtDNA (Sitarz *et al.,* 2012; Yu-Wai-Man *et al.,* 201b) or multiple mtDNA deletions (Hudson *et al.,* 2008) in human patients. Recent studies investigating the mechanistic link between OPA1 and mtDNA maintenance has found that OPA1 isoforms which contain exon 4b are involved in anchoring the mitochondrial nucleoid to the IMM (Elachouri *et al.,* 2011). Anchoring the nucleoid is required to replicate mtDNA and is reminiscent of the chromosome replication mechanism found in bacteria (Thanbichler and Shapiro, 2006). Interestingly, YME1L which is linked to IMM fusion and OXPHOS by cleaving OPA1 is also responsible for producing the mature OPA1 exon 4b-containing isoform to facilitate mtDNA replication (Elachouri *et al.,* 2011; Anand *et al.,* 2014; Mishra *et al.,* 2014; Kukat et al, 2011).

1.7.8 Mitofusins

MFN1 and MFN2 both contain GTPase functional domains required for the fusion of the OMM. These proteins share approximately 60% homology and their structure is also highly complementary with that of OPA1 (**Figure 1-23**). Both MFN1 and MFN2 form multimeric complexes with OPA1 to regulate complete fusion (Chen *et al.*, 2003). MFN2 regulates other cellular functions in addition to mitochondrial fusion. More recently MFN2 was observed to also be localised to the endoplasmic reticulum (ER) where it regulates ER morphology. Since MFN2 is located on both the ER and the mitochondrion, it is involved in the tethering of these two structures with each other. MFN2 plays a fundamental role in calcium homeostasis and is also involved in the maintenance of cellular glucose levels. Other functions of MFN2 include regulation of the OXPHOS system by influencing the expression of the respiratory chain subunits and maintenance of the mitochondrial genome (Sitarz *et al.*, 2012; Rouzier *et al.*, 2012).

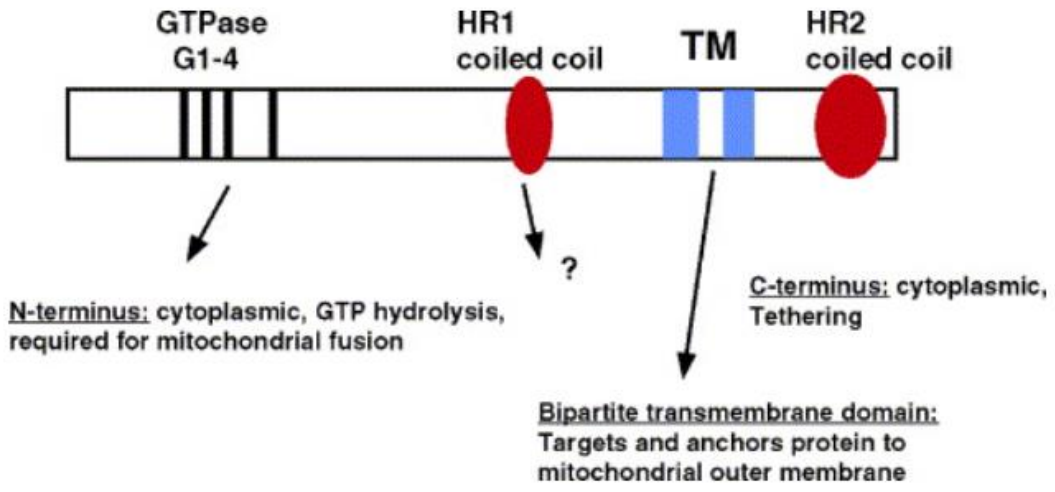

Figure 1-23 Depiction of the conserved structures found in MFN proteins and their respective functions.

Reproduced from Santel, 2006.

1.7.9 Mitochondrial fission

Mitochondrial fission is regulated by Dynamin related protein 1 (DRP1) and this key protein is recruited from the cytosol by human Fission 1 protein (hFIS1) and mitochondrial fission factor (MFF). hFIS1, which is located on the outer mitochondrial membrane, forms a complex with DRP1 at sites of mitochondrial fission (Loson *et al.,* 2013). A spiral of DRP1-hFIS1 complexes wrap around these sites to trigger mitochondrial fission. To ensure complete mitochondrial fission, fusion must be downregulated at the same time and this is achieved by cleavage of the long form of OPA1 (Olichon *et al.,* 2007).

1.7.10 Mitochondrial quality control

The mitochondrial quality control system employs a number of different and sophisticated strategies to maintain cellular homeostasis in the reticulum. These strategies include local quality control mechanisms such as regulating mitochondrial protein stability through proteases such as AFG3L2 and paraplegin which remove unstable N-terminal residues, effectively stabilising mitochondrial proteins and other more global mechanisms which regulate the mitochondrial dynamic machinery to identify and remove dysfunctional mitochondria from the cellular network (Rugarli and Langer, 2012).

OPA1 is involved in many mitochondrial processes such as mitochondrial dynamics, replication of the mitochondrial genome, OXPHOS, maintenance of cristae structure and sequestering of cytochrome c (Olichon *et al.,* 2003; Elachouri *et al.,* 2011; Zanna *et al.,* 2008; Cogliati *et al.,* 2013; Ramonet *et al.,* 2013). Its role in many of these processes make it a prime candidate for involvement in mitochondrial quality control. OPA1 has been shown to be regulated by a sophisticated cascade of proteases such as paraplegin, AFG3L2, PARL, OMA1 and YME1L (**Section 1.7.3-1.7.5**), which can alter the ratio of long and short isoforms and as a consequence, bias the mitochondrial network toward increased fission or fusion.

The role of mitochondrial dynamics in cellular quality control and homeostasis is highlighted through pathological conditions such as Parkinson and Alzheimer diseases which display increased fragmentation of the mitochondrial network promoting mitochondrial autophagy (mitophagy) and apoptosis (Rugarli and Langer, 2012). Furthermore, events such as mitochondrial fission are tightly coupled with mitosis to maintain an adequate number of

mitochondria for cellular functioning in daughter cells. These observations suggest that regulators of mitochondrial dynamics are themselves maintained by cellular homeostatic pathways.

1.7.11 Mitochondrial autophagy

Mitophagy and apoptosis serve as additional quality control mechanisms under a persistent stress. Selective mitophagy is a mechanism which specifically isolates and targets damaged mitochondria for degradation in cellular lysosomes (Ding and Yin, 2012). Depolarisation of the mitochondrial membrane is an important trigger for the detection of dysfunctional mitochondria (Rodriquez-Enriquez *et al.,* 2006). In healthy mitochondria, membrane potential is maintained by an active OXPHOS system which produces cellular ATP. Pathogenic variants in mtDNA can compromise the OXPHOS system by disrupting the production of OXPHOS protein subunits. This can lead to decreased activity of the OXPHOS system and reduced membrane potential Gilkerson *et al*., 2012.

Reduced potential can trigger a mechanism of selective mitochondrial degradation which involves both the regulators of mitochondrial fission and fusion dynamics. As mentioned in **Section 1.7.4**, OPA1 can be selectively cleaved at the S1 position by OMA1, a protease recruited through reduced mitochondrial membrane potential. This cleaves L-OPA1 and helps to inhibit mitochondrial fusion. In this manner, the damaged organelle is isolated from the mitochondrial network (Anand *et al*., 2014; Twig and Shirihai, 2011).

Concurrently, a second mechanism specifically targets these dysfunctional mitochondria for degradation. PTEN-induced putative kinase 1 (PINK1) and PARKIN are mediators of targeted mitochondrial degradation (**Figure 1-24**). PINK1 normally is sequestered to the mitochondrial outer membrane where it is degraded by PARL (Jin *et al.*, 2010). Upon collapse of membrane potential, this degradation is obstructed and PINK1 accumulates on the outer mitochondrial membrane where it phosphorylates OMM proteins. Phosphorylated MFN2 acts as a receptor for an E3-ubiquitin ligase known as PARKIN, which is recruited to the outer membrane and proceeds to ubiquinate outer mitochondrial membrane proteins in a non-selective manner (Jin *et al.,* 2010). Ubiquinated proteins on the outer membrane attract autophagosomes which begin the process of mitophagy. Dysfunctional

mitochondria are consumed by autophagosomes and transported to lysosomes where they are degraded and their constituent components recycled.

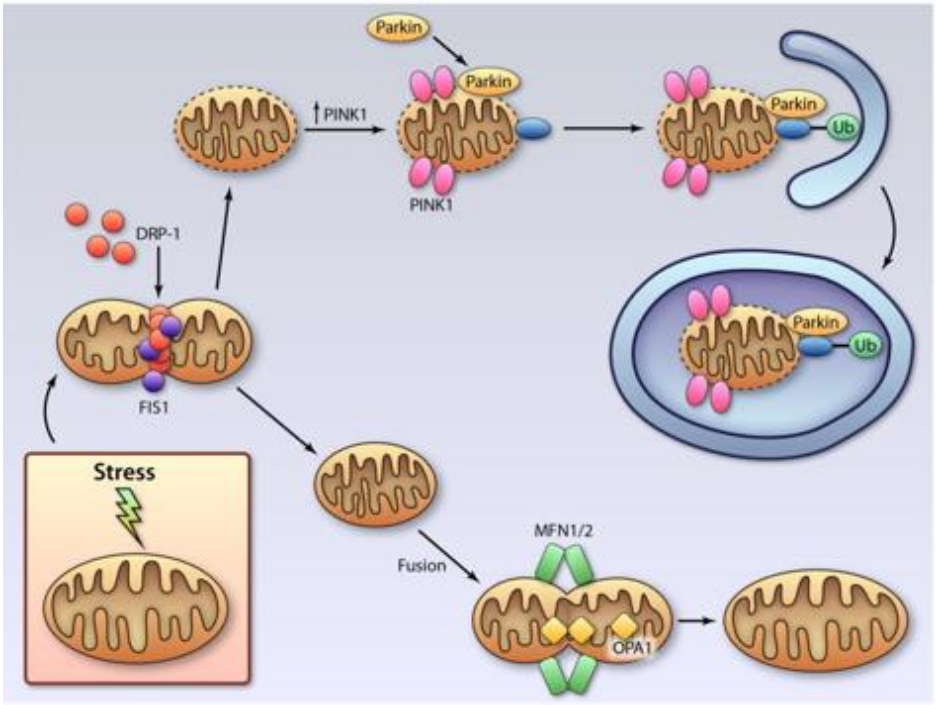

Figure 1-24 Schematic illustrating the mechanism of PINK1/PARKIN in mitophagy

After membrane fission, daughter mitochondria both maintain an optimal membrane potential subsequent to depolarisation and can fuse with other organelles of the mitochondrial reticulum or there is membrane potential collapse due to a defective OXPHOS system. This triggers the sequesterisation of OMA1 into the IMM to cleave L-OPA1 and inhibits further mitochondrial fusion. Concurrently PINK1 is allowed to accumulate on the OMM and phosphorylate MFN2 which acts as a receptor for PARKIN, a protein ubiquitinator. Ubiquitination of OMM proteins signals for organelle degradation through autophagy and mitochondria are transported to and degraded by cellular lysosomes. Reproduced from Kubli and Gustafsson, 2012.

1.7.12 Mitochondrial dynamics and apoptosis

Mitochondrial fission plays a significant role in cell death pathways. It occurs in concordance with disrupted cristae structure along the IMM, release of numerous pro-apoptotic factors: cytochrome c, SMAC/DIABLO HtrA2/omi and permeabilisation of the mitochondrial membrane. These events evoke a response from the CASPASE family to trigger apoptotic cell death. The mitochondrial apoptotic pathway involves both anti (BCL-2) and pro apoptotic (Bax, Bak) mediators which have roles in regulating mitochondrial morphology (**Figure 1-25**). Pro-apoptotic proteins Bax and Bak inhibit MFN2 leading to a bias towards mitochondrial fragmentation (Karbowski *et al*., 2006) These mediators have also been found to colocalise with DRP1 on the OMM at sites of mitochondrial fragmentation (Karbowski *et al*., 2002).

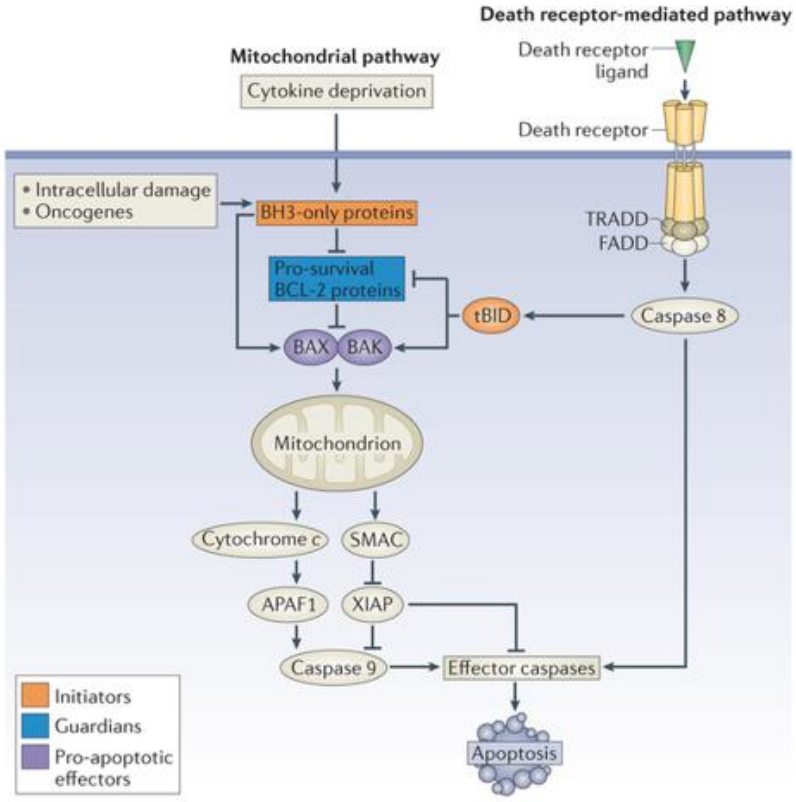

Figure 1-25 Mechanism of apoptotic cell death triggered by mitochondrial dysfunction.

Reproduced from Czabotar *et al.*, 2014.

1.7.13 Stress induced mitochondrial hyperfusion

The current mitochondrial dynamic model for adapting cellular homeostasis to metabolic demand suggests that under acute stress or nutrient deprivation, the mitochondrial network will undergo stress induced mitochondrial hyperfusion (SIMH). This process increases mitochondrial fusion through inactivation of DRP1 by protein kinase A which phosphorylates DRP1 at residue Ser637 and acts to inhibit GTPase activity. This serves to downregulate mitochondrial fission. Concurrently the prohibitin-related protein SLP-2 interacts with OPA1 to prevent stress-induced cleavage of OPA1 long isoforms. (Tondera *et al.*,2009). The involvement of SLP-2 appears to be a requisite for SIMH and the mechanism of how it prevents stress-induced cleavage by OMA1 is under current investigation. It is hypothesised that the mitochondrial dynamic fusion machinery is upregulated, however the mechanism of this upregulation is currently unknown.

Increased SIMH is believed to act as a transient cellular protective mechanism and current research is focused on the relationship between apoptosis, mitophagy and mitochondrial fusion (Tondera *et al.*, 2009). Several mechanisms have been put forward to explain the protective effects of SIMH, namely:

(i) Fusion of the mitochondrial network to inhibit mitophagy.

Increasing fusion between mitochondria in the network serves to block their engulfment by autophagosomes and their subsequent delivery to lysosomes for degradation and recycling of constituent components.

(ii) Increased fusion to promote mitochondrial content-mixing.

Increasing the fusion between mitochondrial organelles results in the distribution of proteins, RNA, lipids and mtDNA within the reticulum. This may help to ‘buffer’ mitochondrial organelles which have damaged components which may otherwise ultimately lead to dysfunctional ATP production through OXPHOS.

(iii) Increased fusion as a response to other cellular protective pathways

Recent research also suggests that mitochondrial dynamics and anti-oxidant gene expression are coupled. This idea is exemplified through the stabilisation of nrf2 under conditions of oxidative stress (Ma, 2013) Nrf2 is a transcription factor which upregulates anti-oxidant

defences such as superoxide dismutase and glutathione associated protective enzymes. This may serve to decrease cellular damage and return the morphology of the mitochondrial network from a hyperfused state to more normal homoeostatic fission/fusion dynamics.

Chronic stress of the mitochondrial network would ultimately lead to a loss of SIMH and increased fragmentation due to the accumulation of damaged organelles or depolarisation of the mitochondrial membrane. Whether this fragmentation would lead to mitochondrial clearance through mitophagy or cellular apoptosis would depend on the nature and duration of the stress.

1.8 Mechanism of Nonsense-Mediated Decay

Eukaryote cells contain a tightly regulated control quality system against error-prone DNA expression to limit the effects of misfolded proteins due to pathogenic mutations. During transcription, pre-mRNA is first transcribed by polymerase II to form a messenger ribonucleoprotein complex. This pre-mRNA is processed into mature mRNA through a series of steps. A 5'-m^7GpppN cap and a poly(A) tail are attached to protect the mRNA from degradation. Other factors also contribute to protect mRNA from degradation such as the CBC (CBP80-CBP20) complex at the 5' cap and PABPN1 and PABPC1 at the poly(A) tail. Pre-mRNA is composed of both exons and introns and these introns must be spliced out by the exon junction complex (EJC) to form alternative isoforms. Splicing factors play an important role in isoform specific nonsense-mediated decay (NMD). Intron-less isoforms are invulnerable to NMD.

Translation begins when one or more ribosomes bind to these ribonucleoprotein complexes and the CBC is replaced by a translation initiation factor. Degradation of mRNA by the NMD mechanism occurs at the first round of translation during ribosome stalling. This stalling occurs if there is a truncation 50-55 nucelotides upstream of an exon junction complex (EJC) bound region. The truncated site is positioned at the ribosomal 'A' site where it is bound by the NMD SURF (SMG1-UPF1-Erf1-Erf3) complex (Schweingruber *et al.*, 2013). This triggers a process to detach the ribonucleoprotein complex from the ribosome and

prevent further translation (**Figure 1-26**). The ribonucleoprotein complex is subsequently degraded by SMG5-7, XRN1 and the exosome complex.

One of the factors that contribute to clinical variability is the position dependent mechanism of NMD. If a frameshift or nonsense variant occurs 5' of the NMD detection boundary, the ribonuceoprotein complex is subsequently degraded preventing the expression of the mutated allele. In the case of heterozygous mutations, haploinsufficiency could result in a milder clinical phenotype. However, if a pathological variant lies 3' to this detection boundary, it is not recognised by the NMD machinery, resulting in a possible dominant-negative effect and a more severe clinical phenotype.

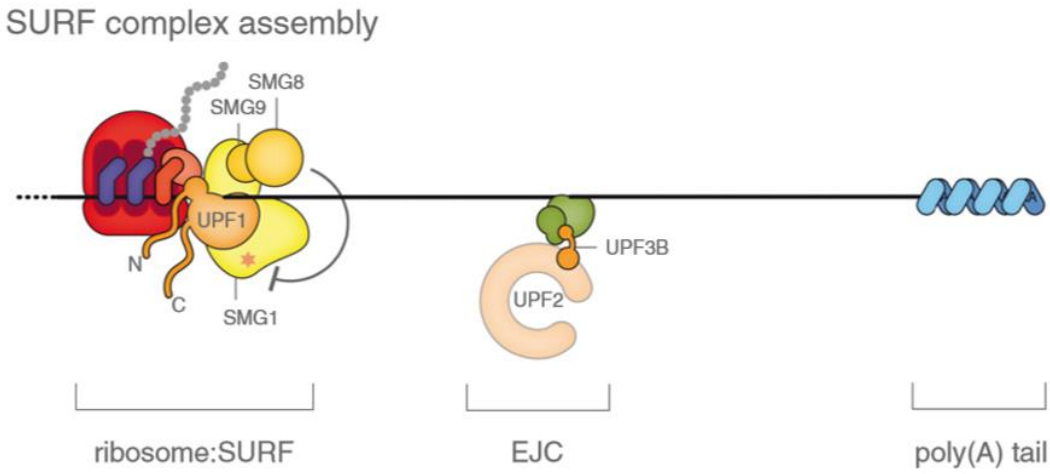

Figure 1-26 Schematic diagram of SURF complex assembly upsteam of the exon junction complex (EJC).

The EJC inhibits translation of the faulty mRNA and subsequently leads to its degradation by the exosome complex. Reproduced from Schweingruber *et al.*, 2013.

1.9 Mitochondrial Disease Mechanisms in *OPA1*-related DOA

1.9.1 Disturbance of the mitochondrial network

As described in **Section 1.7** *OPA1*, *MFN1* and *MFN2* are primary regulators of mitochondrial fusion in the reticulum. Therefore, it is not surprising that pathogenic mutations in these genes can give rise to disturbed mitochondrial dynamics. In patient tissue, the pathological hallmark of *OPA1* and *MFN2* mutations is a striking fragmentation of the mitochondrial reticulum. Pathological variants in *OPA1* also result in disrupted cristae along the IMM and proapoptotic calcium and cytochrome c release.

1.9.2 Bioenergetic dysfunction

OXPHOS is tightly regulated by mitochondria in the production of ATP which produces most *in vivo* energetic requirements (Yu-Wai-Man, 2009). *OPA1* pathological variants have been described in the context of OXPHOS dysfunction. OPA1 has been shown to directly interact with OXPHOS complexes (Zanna *et al.,* 2008; Cogliati *et al.,* 2013). This interaction was hypothesised to facilitate structural stability of the OXPHOS system. It may be possible that deleterious mutations which affect the stabilisation of these OXPHOS complexes, such as those found in DOA may cause exasperated proliferation of mtDNA to account for this structural instability. Although proliferation of mtDNA has been noted in DOA, the precise sensing mechanisms responsible for mtDNA steady state remain to be investigated.

Studies have identified impairment of complex activity although conflicting reports point to either a complex I or COX deficiency (Amati-Bonneau *et al.,* 2005; Chevrollier at al., 2008). This decrease in activity has been observed in conjunction with a decrease in membrane potential due to proton leakage and increased fragmentation of the mitochondrial reticulum (Amati-Bonneau *et al.,* 2005). This deficit in OXPHOS appears to disrupt the rate of ATP synthesis but does not culminate in a significant decline of gross ATP level in patient fibroblasts (Zanna *et al.,* 2008; Amati-Bonneau *et al.,* 2005). Compensatory mechanisms may contribute to maintaining a steady state of ATP such as mtDNA proliferation.

Severe bioenergetic defect culminating in apoptotic cell death may be tissue specific. RGCs require a higher level of ATP synthesis and may be more susceptible to this deficit in

ATP production contributing to optic nerve degeneration. However dysfunction of the OXPHOS system alone cannot explain the increased susceptibility of the optic nerve. Preliminary evidence suggests that OPA1 isoforms directly interact with complexes of this pathway. Dysregulation of OPA1 may alter complex assembly and stability although further research is required (Zanna *et al.,* 2008).

1.9.3 Oxidative stress

Elevated ROS production secondary to pathogenic variants in OPA1 and dysfunction of the OXPHOS system may further contribute to apoptotic cell death of RGCs. Investigation of pathogenic homozygous *OPA1* generated through somatic mutagenesis in a drosophila model (dOPA1), demonstrated a significant rise in ROS which may have deleterious consequences for mitochondrial components and contribute to an already compromised subcellular environment (Tang *et al.,* 2009). Enhanced mitochondrial fragmentation and an ommatidial phenotype was also noted in this model. Other models of OPA1 dysfunction have also noted an increase in ROS production, most noticeably in a OPA1 mouse model with late onset cardiomyopathy and primary lymphoblast lines (Chen *et al.*, 2012; Kao *et al.*, 2015).

1.9.4 MtDNA instability

The mitochondrial genome is packaged into nucleoids contained within the mitochondrial matrix. These nucleoids are associated with several proteins involved in mitochondrial DNA replication which include POLG, TWINKLE, the mtSSB, ligase proteins and topoisomerases (Gilkerson *et al.,* 2013). Under mtDNA maintenance dysregulation conditions, mtDNA can either be depleted (Kim *et al.,* 2005; Chen *et al.,* 2012) or proliferated due to clonal expansion of deleterious mtDNA molecules; both states have a detrimental effect on the OXPHOS system (Hudson *et al.,* 2008; Amati-Bonneau *et al.,* 2005). This biochemical defect can be demonstrated diagnostically through the use of COX-SDH staining of patient muscle tissue. COX/SDH (cytochrome c oxidase)-negative muscle fibres which harbour high levels of mtDNA deletions are stained blue as opposed to the characteristic brown stain of non-OXPHOS compromised tissue.

Patients with DOA have a marked increase in deleterious mtDNA molecules which have been identified in skeletal muscle biopsies (Yu-Wai-Man *et al.,* 2010b). This observation may indicate that these mutations contribute to the clinical phenotype of DOA. Strikingly, the number of COX negative fibres in DOA+ patients was over four times higher than in pure optic atrophy which may indicate the importance of deleterious mtDNA proliferation in multi-systemic disease (Yu-Wai-Man *et al.,* 2010b).

1.9.5 Calcium homeostasis

Interaction between the endoplasmic reticulum and the mitochondrion has been a recent hot topic of interest. Recent investigation has highlighted signalling pathways at these interfaces. Most of the intracellular calcium is buffered either within the ER or the mitochondrion (Romagnoli *et al.,* 2007). Mitochondria-associated membranes (MAMs) are sub-domains of the ER which are responsible for creating microenvironments for lipid and calcium flux between these two cellular compartments (Giorgi *et al.,* 2015). This process is regulated by the mitochondrial calcium uniporter (MCU) and mitochondrial calcium uptake protein 1 (MICU1). Calcium performs a variety of functions which include intracellular signalling, engagement and facilitation of apoptosis and a response to neurotransmitter excitotoxicity.

Deleterious mutations in *OPA1* and *MFN2* have been shown to disrupt the machinery within these MAMs which highlight the importance of mitochondrial profusion regulators in calcium homeostasis and lipid biosynthesis (Dayanithi *et al.,* 2010; Singaravelu *et al.,* 2011; Kushnareva *et al.,* 2013). Both calcium flux and storage within the ER and mitochondrion buffer the cell against calcium spiking which may promote apoptotic cell death. Disruption of this process, especially in the optic nerve which is also susceptible to glutamate excitotoxicity may sensitise RGCs to degeneration (Kushnareva *et al.,* 2013). Mutations in mtDNA associated with complex I or COX are also known to disrupt this calcium homeostasis and may possibly contribute to DOA pathogenesis through dysfunction of OXPHOS (Trevelyan *et al.,* 2010) in RGCs.

1.10 Overlapping Disease Mechanisms Leading to RGC Loss

The optic nerve is composed of 1.2 million retinal ganglion fibres and is a susceptible target of degeneration due to pathological primary or secondary mitochondrial variants present in optic neuropathy. Both structural and biochemical parameters contribute to this predilection for RGC death (Maresca *et al.,* 2013). The distribution and structure of RGCs are not homogenous throughout the retina. Smaller RGCs containing shorter axons and dendritic fields are located near the fovea and the papillomacular bundle (PMB) consists of densely packed parvocellular (P) and magnocellular (M) RGC subtypes. The density of RGCs decreases peripherally and there is a concomitant increase in axonal size. Both the density and the anatomical structure of RGCs might be relevant to the high prevalence of optic neuropathy in patients with mitochondrial disease. A relatively small axon could impose physical constraint on mitochondrial motility, which is a vital mechanism for transporting these organelles from the RGC soma where they undergo biogenesis, to more energetically dependent areas of the axon. RGCs are typically sheathed with myelin posterior to the lamina cribosa which have efficient saltatory conduction. Unmyelinated axons require a greater concentration of mitochondrial organelles to facilitate conduction velocities and as a consequence may present a structural vulnerability, particularly for mitochondrial dysfunction (Carelli *et al.,* 2004; Andrews *et al.,* 1999; Bristow *et al.,* 2002). These smaller RGCs within the PMB are also preferentially lost due to the limited mitochondria energy reserve of these smaller axons (Pan *et al.,* 2012; Ross-Cisneros *et al.,* 2013). However these reasons alone do not completely explain RGC susceptibility to apoptotic cell death.

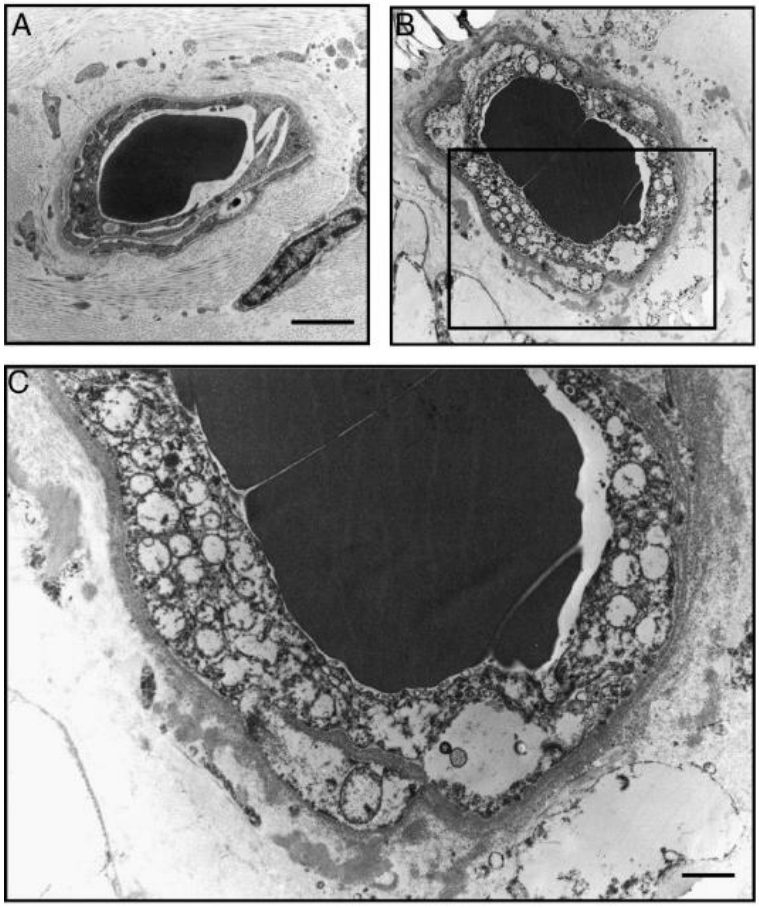

Figure 1-27 Depiction of capillaries and mitochondrial abnormalities present in a LHON patient with the m.11778G>A mtDNA mutation.

(A) Optic nerve head capillaries in a healthy control**;** (B) Disruption of optic nerve head capillaries and mitochondrial proliferation; (C) Swollen cristae indicative of a metabolic mitochondrial defect. Reproduced from Carelli *et al.,* 2009.

Additional observed structural abnormalities include edematous appearance of surrounding nerve fibres and tortuous and often enlarged vessels (Nikoskelainen *et al.,* 1982). Upon examination of the visual field, there is usually a caecocentral scotoma and limited but variable peripheral vision (Carelli *et al.,* 2004; Yu-Wai-Man *et al.,* 2011). This finding is highlighted through histopathological investigation showing a severe loss of central RGCs with cell sparing in the ocular periphery. Other common structural features highlight axon

degeneration, differential myelin thickness, proliferation and build-up of swollen mitochondria in the post-laminar ocular area (**Figure 1-27**). Cytoskeletal condensation and debris are also observed. These characteristics are suggestive of a progressive low-grade optic degeneration. Unusually, histopathological investigation also demonstrated sparing of melanopsin RGCs in both classical paradigms of optic neuropathy, LHON and DOA, however the reason for this has yet to be investigated (Sitarz *et al.,* 2012).

The precise biochemical mechanisms that lead to optic degeneration have not yet been clarified. Unfortunately, research in this area has been limited by the lack of human tissues and the inability to study the optic nerve directly. The investigation of factors leading to RGC loss has primarily been limited to the use of both cell and animal models. Typical biochemical parameters that contribute to classical models of optic neuropathy include a dysfunction of OXPHOS-driven ATP synthesis, enhanced ROS production and sensitivity to excitotoxic stimuli. Investigation of OXPHOS dysfunction and how it may lead to degeneration of the optic nerve is still an active area of research (Yu-Wai-Man *et al.,* 2011; Barbiroli *et al.,* 1995; Loiseau *et al.,* 2007; Amati-Bonneau *et al.,* 2005; Chevrollier *et al.,* 2008). Current hypotheses include a prolonged decrease of ATP synthesis which may compromise high-intensive energy dependent tissue such as RGCs in the optic nerve (Zanna *et al.,* 2008). This hypothesis is partially supported by *in vitro* investigations of DOA showing a consistent defect in the rate of ATP synthesis due to either decreased activity of complex I or IV (Zanna *et al.,* 2008; Chevrollier *et al.,* 2008). However, this again, does not fully explain why RGCs are particularly susceptible to degeneration, especially considering other tissue with high energy demand which remain unaffected (Zanna *et al.,* 2008; Lodi *et al.,* 2004).

A partial explanation may involve the anterograde-retrograde transport of mitochondria from the soma to unmyelinated axonic regions of the RGC (**Figure 1-28**). It is possible that a depletion in OXPHOS ATP could affect this process and interfere with the efficiency of synaptic transmission. This point may be particularly important in cells with relatively high rate of synaptic firing as seen in RGCs. This is supported by mitochondrial clumping, debris and loss of microtubules in spared RGCs shown through histochemical staining of LHON tissue (Sadun *et al.,* 1994; Carelli *et al.,* 1999). This suggests that dysfunction of axonal transport may be another common biochemical feature of optic neuropathy.

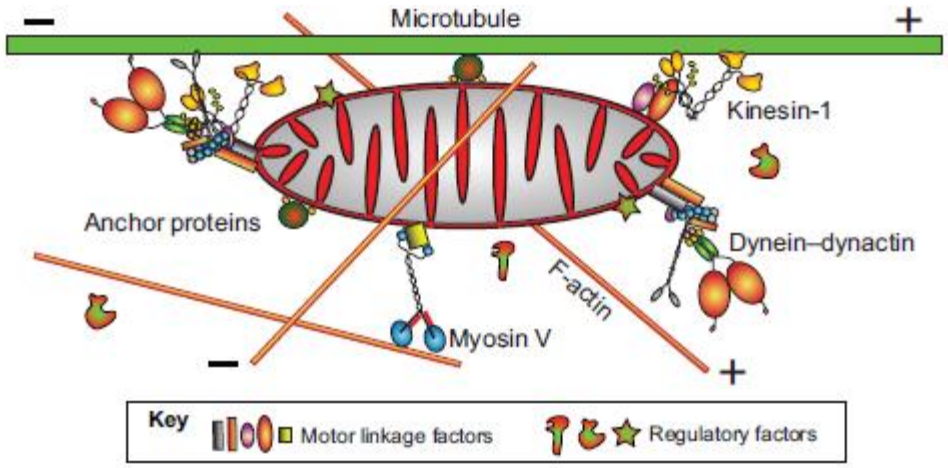

Figure 1-28 Schematic of mitochondrial anterograde/retrograde signalling mechanism required for synaptic transmission in retinal ganglion cells.

(+) and **(-)** symbols illustrate the direction of mitochondrila transport along the microtubule with kinesin-1 and dyenin motors driving mitochondrial movement along these tubules from the RGC Soma alon the axons to regions of high energy demand required for synaptic transmission. Ancillary proteins linking kinesin-1 include Milton, Miro and syntabulin which are required for kinesin-1 recruitment and local mitochondrial fusion. Reproduced from Saxton and Hollenbeck, 2012.

Other common themes associated with OXPHOS dysfunction involve a chronic increase in ROS production (ROS). Increased ROS levels contribute to activation of cell death pathways and also affect the myelin sheath, specifically the retrolaminar myelinated region of the optic nerve. Such effects would culminate in an enhanced susceptibility to pathological dysfunction in the papillomacular bundle (PMB).

A recent LHON mouse model developed by *Lin and colleagues* successfully recapitulated the severe visual deficit of LHON due to a dysfunction of complex I (Lin *et al.*, 2012). An excess of ROS production, disrupted cristae, mitochondrial proliferation and axon swelling were noted. However ATP homeostasis was maintained leading to the conclusion that ROS production and oxidative damage was more pertinent to visual failure than a defect in ATP synthesis rate, at least for this ND6 P25L model. This observation is contrasted with other biochemical assays which demonstrate an impairment of complex I-driven ATP synthesis in LHON (Parker *et al.*, 1989; Majander *et al.*, 1991; Carelli *et al.*, 1997; Baracca *et*

al., 2005). Further research is required to clarify these secondary mechanisms and establish their contribution to RGC death '*in vivo*'.

1.11 Animal models of inherited optic neuropathies

Both *in vitro* modelling of disease pathology and limited access to post mortem patient tissue may only provide partial insight into the pathomechanisms for this group of diseases. The use of transgenic or pharmacologically treated animal models in tangent with these other paradigms can therefore provide a more robust picture of the presentation and progression of optic neuropathies. Different animal models have been generated for both LHON and DOA.

In order to mimic the selectivity of RGC degeneration found in LHON, rotenone, an inhibitor of OXPHOS complex I, was injected through the murine vitreous and more recently, the use of rotenone loaded microspheres which are uptaken into murine RGCs have both been used as pharmacological options which recapitulate the selective degeneration of the optic nerve (Zhang *et al*., 2002; Marela *et al*., 2010). In parallel, a transgenic LHON mouse, discussed briefly in **Section1.10,** with the G14600A mutation, equivalent to the human ND6 P25L, has also been generated and presents with common hallmarks of LHON. These hallmarks include demyelinating axons, mitochondrial proliferation and degeneration, axonal swelling and loss and increased ROS (Lin *et al*., 2012).

In DOA, as mentiond in **Section 1.3.5**, three different truncative OPA1 models have been developed which include exons 8 (c.1051C>T) (Davies *et al.,* 2007), intron 10 (c.1065+5 G> A) (Alavi *et al.,* 2007) and exon 27 (c.2708-2711delTTAG) (Sarzi *et al.,* 2012). These models mimic both many of the ocular and extraocular clinical features found in DOA patients which include an age –dependent severe ocular nerve degeneration, visual loss, deafness, encephalomyopathy, peripheral neuropathy, cardiomyopathy, demylination of the optic nerve and mitochondrial ultrastructural abnormalities. Increased mitophagy was also noted. In conjunction, drosophila melanogaster has also been used to model the role of abnormal ROS production in *OPA1* DOA disease progression (Tang *et al*., 2009).

Finally, both a DOA murine mouse model (c.365T>C) and zebrafish model (engineered with 5.2kb DNA insertion downseam of the mitochondrial leader sequence) has also been developed for OPA3,a paradigm for Costeff syndrome (Davies et al., 2008; Pei *et al*., 2010) . A significant loss of RGCs as well as impaired swimming behaviour due to ataxia, los of buonancy and hypokinesia have been determined in OPA3 zebrafish mutants while 3-methylglutaconic aciduria type III, impaired visual acuity, optic nerve degeneration, cardiomyopathy, neuromuscular defects,extrapyramidal dysfunction amd elevated serum lactate have been noted in the murine model . Currently, the role of OPA3 is still unknown and these models will prove invaluably in delinating its precise mitochondrial function.

1.12 Therapeutic strategies for inherited optic neuropathies

Effective therapeutic strategies directed against optic neuropathy are still within the early stages of development. To combat degeneration of the optic nerve, a number of different avenues are being explored. These include pharmacological treatment, genetic therapy and the therapeutic potential of stem cells (Yu-Wai-Man *et al.,* 2014; Sadun *et al.,* 2012; Newman *et al.,* 2012; Guy *et al.,* 2002). Patients who present with optic neuropathy represent an excellent cohort for clinical studies due to both the localised dysfunction of many of these disorders within the eye and the organs ease of accessibility for assessment and treatment.

1.12.1 Pharmacological options

Current drug use designed to improve the clinical phenotype of optic neuropathies has been met with limited success. Such drugs include mitochondrial vitamin cocktails (B_2,B_3,B_{12},C,E and folic acid), the use of ubiquinone analogues like coenzyme Q_{10}, Idebenone, EP1-743, the use of steroids and immuno-suppressants (Pfeffer *et al.,* 2013; 2012; Newman *et al.,* 2012; Porcelli *et al.,* 2009) and finally the use of both compounds and molecules to activate mitochondrial biogenesis such as bezafibrate, rogsiglitazone, AICAR (5-aminoimidazone-4-carboxamide ribonucleoside) and resveratrol (La Morgia *et al*., 2014). Some of these therapeutic compounds have been clinically tested but were investigated on a small,

statistically underpowered cohort of patients with no objectively significant benefit that improved visual function.

Idebenone is an antioxidant that has shown limited success in visual recovery if treatment commenced at an early stage and patients receive a prolonged treatment (greater than 24 weeks) (Carelli *et al.,* 2011a). Similarly, EPI-743 is another anti-oxidant which is similar in structure to Co-enzyme Q_{10}. Although it has been tested on only a small cohort (5 patients) with mitochondrial dysfunction, it shows promising results with noted improvement in field, colour vision and acuity (Sadun *et al.,* 2012). More rigorous testing is required to determine the most effective, dose and time-course for treatment.

Increased mitochondrial biogenesis is assocated with unaffected LHON carriers and is proposed to act as a compensatory mechanism through hightened OXPHOS capacity (La Morgia *et al.,* 2014). Pharmacological stimulators of biogenesis such as AICAR, bezafibrate, rogsiglitazone and resveratrol may act to improve the clinical presentation of various optic neuropathies.

1.12.2 Gene therapy paradigms

Gene therapy is a potential strategy to halt optic nerve degeneration in inherited optic neuropathies because the RGC layer is easily accessible to manipulation (Yu-Wai-Man *et al.,* 2014). However, the fact that many optic neuropathy-related genes are encoded by the mitochondrial genome presents a technical hurdle. To overcome this obstacle, an associated viral vector (AAV) is being devised to transfect functional mitochondrial genes efficiently into the nuclear compartment to compensate for defective genetic material found in the mtDNA population. Such a strategy would be particularly effective for conditions such as LHON where pathogenic variants lie on mtDNA (Guy *et al.,* 2002).

The most recent research has successfully imported mitochondrial proteins in this manner in plants (Pineau *et al.,* 2005), yeast (Roucou *et al.,* 1999) and cultured mammalian cells (Guy *et al.,* 2002; Oca-Cossio *et al.,* 2003). Current research has also successfully imported the ND4 protein to compensate for a mtDNA defect G11778A in a rodent model of LHON (Guy *et al.,* 2009; Ellouze *et al.,* 2008; Qi *et al.,* 2007a). However before this technique can be used in a clinical setting, further research is needed to demonstrate that this

allotopically expressed protein is fully integrated into complex IV of the OXPHOS system. Dr Patrick Yu-Wai-Man is currently involved in clinical trials to assess this mt-ND4 construct in patients presenting with LHON (> 1 year).

Additionally, control of allotopic gene expression is required before it could be used as a feasible strategy for LHON patients with a G11778A mtDNA defect. Clinical trials are currently underway to assess patient safety and efficacy using this approach. A similar alternative strategy to replace the defective mitochondrial gene includes transfection of the ROS scavenger gene *SOD2*, which would mop up excess ROS and promote cell survival. Qi and colleagues (2007b) successfully demonstrated this in LHON cybrid cell lines.

1.12.3 Stem cells and regenerative medicine

Current research into stem cell therapeutics is divided into two different strategies. One consists in both differentiating and transplanting RGCs to directly replace damaged cells of the optic nerve. The alternative is to grow lines of differentiated RGCs which would produce trophic factors. These trophic factors would then be used to promote RGC survival within the optic nerve (Marchetti *et al.*, 2010; Dahlmann-Noor *et al.*, 2010). Currently, development of effective clinical stem cell therapeutics is still in its infancy. Obstacles include the efficient generation of mature RGCs and their introduction *in vivo* to promote the appropriate topographical connections. The most likely use of these human-derived RGCs is as a tool to explore RGC physiology through drug screening and biochemical analysis in the near future. This may help to both understand how RGCs are affected in different disease states and also refine RGC development and incorporation into the optic nerve.

1.12.4 Genome editing and mitochondrial donation

Unlike LHON which tends to be monosymptomatic with no impact on life expectancy, a subset of patients harbouring more deleterious mtDNA mutations or nuclear genetic defects that result in severe mtDNA depletion can develop an aggressive disease course, frequently starting in early childhood, and characterised by irreversible encephalopathy, intractable epilepsy, liver failure and multisystem organ failure. The outcome of these mitochondrial

syndromes is invariably fatal and in the absence of effective treatments, significant effort has been invested in developing tractable means of selectively eliminating these pathogenic mutations through germline genome editing, or in preventing the maternal transmission of pathogenic mtDNA mutations from mother to child.

Several research groups worldwide are working on mitochondrial-targeted nucleases that have been engineered to selectively eliminate mutated mtDNA molecules. Zinc finger nucleases (ZFNs) and transcription activator-like effector nucleases (TALENs) are able to recognise these altered DNA sequences and they create double-strand breaks that effectively eliminate the mutated mtDNA molecules (Minczuk *et al.,* 2008; Bacman *et al.,* 2010, 2013).The ability to shift the level of heteroplasmy could be used to reduce the overall mutant load in the oocyte of a woman carrying a known pathogenic mtDNA mutation to subthreshold level, thereby eliminating the risk of her child developing overt mitochondrial disease. The use of ZFNs or TALENs as a reproductive tool for manipulating levels of heteroplasmy is still in early stages of development and a number of technical difficulties need to be resolved. Germline genome editing, namely with the CRISPR/Cas9 system, could also be used to correct for pathogenic mutations within the nuclear genome (Jinek *et al.,* 2012; Yin *et al.,* 2014).

The elimination of mutated mtDNA molecules to shift the level of heteroplasmy to subthreshold level is an attractive strategy to prevent a biochemical deficit and rescue the cellular phenotype. However, in some mitochondrial diseases, such as LHON, the majority of carriers harbour homoplasmic mtDNA mutations and a different experimental strategy is needed to prevent the transmission of a pathogenic mtDNA mutation from mother to child. Two related in vitro fertilisation (IVF) techniques have been developed that involves transferring the parental nuclear genetic material into a donor cytoplast containing a normal wild-type mtDNA population (Tachibana *et al.,* 2009; Craven *et al.,* 2010). Although encouraging, further work is needed to explore the safety implications of these IVF techniques for embryo development, including the concerns that have been raised about epigenetic abnormalities and the possibility of nuclear-mitochondrial genetic mismatch leading to unforeseen negative consequences (Chinnery *et al.,* 2014). The Nuffield Council on Bioethics has concluded that mitochondrial replacement might be appropriate within a strictly regulated research environment, and with the prospective parents being fully informed about

the potential risks, both real and theoretical. In February 2015, both Houses of Parliament in the UK have voted strongly in favour of mitochondrial donation to prevent the maternal transmission of mitochondrial disease paving the way for future clinical implementation (http://www.parliament.uk/business/news/2015/february/lords-mitochondrial-donation-si/, accessed on 28 December 2015).

Chapter 2

Research Aims

The central aim of my PhD project was to investigate the disease mechanisms that contribute to RGC loss and optic nerve neurodegeneration in inherited optic neuropathies. To achieve this goal, I performed a series of studies that made use of tissue samples collected from patients carrying confirmed pathogenic *OPA1* mutations. I also made use of whole-exome sequencing (WES) to investigate a cohort of patients with a suspected genetic basis for their optic atrophy, but who do not have a confirmed molecular diagnosis.

Study Aims:

1. To explore the biochemical differences that might explain disease severity in *OPA1* disease by comparing primary fibroblasts established from patients with DOA+ and OA phenotypes.
2. To quantify the morphology of the mitochondrial network and the distribution of nucleoids in differentiated myotubes established from primary myoblasts of patients with DOA+ and OA phenotypes.
3. To confirm the pathogenic nature of a novel homozygous *OPA1* variant identified in two affected sisters presenting with lethal infantile encephalopathy, hypertrophic cardiomyopathy and optic atrophy.
4. To identify potentially pathogenic disease variants in a cohort of patients with suspected inherited optic atrophy by using WES analysis.
5. To further investigate the pathogenic nature of *WFS1* variants identified with WES.

Chapter 3

Materials and Methods

3.1 Fibroblast Cell Line

3.1.1 Fibroblast line maintenance

Fibroblasts were grown as a monolayer until 70-80% confluence. The cells were grown in glucose (5mM) MeM media (Gibco, Life Technologies,Paisley, UK) with 10% Foetal Bovine Serum (FBS) (Gibco, Life Technologies, Paisley, UK). The media was supplemented with 1% L-glutamine, 1% sodium pyruvate, 1% non-essential amino acids , 1% Penicillin-streptomycin and 1% Vitamins (All obtained from Gibco, Life Technologies, Paisley, UK). These cells were grown in a T25 flask until 70% confluence was reached then seeded in a T75 flask for further growth. These flasks were stored at 37°C in 5% CO_2 humidified air. Media in these flasks was changed every fourth day to allow an increased concentration of growth factors.

3.1.2 Subculture of fibroblast cells

When the cells in each respective flask reached 80% confluence, they were harvested in 1x trypsin (Gibco, Life Technologies, Paisley, UK) and PBS (Oxoid). They were then centrifuged at 1200 rpm for five minutes in 10 ml media. This media was aspirated, fresh media was added to the cellular pellet and these cells were homogenised and re-seeded into new T75 flasks.

3.1.3 Fibroblast cryostorage

For longer term storage, the cells in a T75 flask were harvested and re-suspended in 1 ml FBS (Gibco, Life Technologies, Paisley, UK) with 10% DMSO (Freezing solution- Sigma Aldrich). These cells were stored in cryovials and transferred to a larger cryostorage container containing isopropanol (Greiner) in a -80 freezer. Freezing solution was added dropwise to the cryovials to prevent bubble formation. The isopropanol container allowed for the gradual decrease in temperature to prevent excessive cell death. After 24 hours storage at -80°C, the cells were then transferred to liquid nitrogen storage.

3.1.4 Thawing of cryo-preserved fibroblasts

When these cells were retrieved, they were thawed as fast as possible in a water bath at 37°C. Once the freezing media with fibroblasts was defrosted, it was added dropwise to 10 mls (millilitres) pre-warmed media and centrifuged for 5 minutes at 1200 rpm to pellet these cells. The supernatant was aspirated to remove DMSO (Sigma-Aldrich) and cells were suspended in fresh media. They were then transferred to a T25 flask. This flask was left at 37°C in 5% CO2 humidified air overnight. The media in this T25 was removed to discard cell debris from this defrosting process. When cell confluence in this flask reached 70-80%, cells were trypsinised and transferred to a T75 flask for further growth.

3.1.5 Mycoplasma detection

All primary cell lines were routinely checked for the presence of mycoplasma using a luminescent detection kit (Lonza, UK) according to the manufacturer's instructions. All incubation steps took place at room temperature. Approximately100ul of cell line media taken from primary line flasks (<48 hours) was transferred to a 1.5ml eppendorf tube. One volume of re-constituted MycoAlert^{TM} reagent was added and the sample was allowed to incubate for 5 minutes. A Fluoroskan Ascent (Thermo Scientific, Paisley, U.K.) was then used to detect luminescent signal denoted 'reading A'.

In the second stage, 100µl of MycoAlert^{TM} substrate was added to the sample and allowed to incubate for 10 minutes. A second luminescent reading was detected and denoted 'reading B'. To determine if the sample was contaminated with mycoplasma, a ratio between reading B and reading A is calculated. If this ratio >1, the sample is deemed mycoplasma negative. A sample ratio of 1 is deemed borderline and a re-test is taken of the sample. If the ratio is <1, the sample is deemed mycoplasma positive and the primary lines are destroyed using 2% (w/v) Virkon® (Du Point, Hertfordshire, UK).

3.1.6 Cell seeding

All cell counting and seeding was achieved using a haemocytometer chamber (AC1000 Improved Neubauer; Hawksley, Lancing, UK). Briefly, primary cell lines were harvested as described in **Section 3.1.2**. Cell pellets were resuspended in 1 ml media. This media was homogenised and 100µl of sample was transferred to a fresh eppendorf tube where it was mixed with 100µl Trypan Blue (Sigma-Aldrich), a stain which is absorbed by apoptotic or necrotic cells. 10µl of this mixture was then added to a haemocytometer chamber complete with coverslip. The number of viable cells was counted in four squares of the haemocytometer chamber grid and averaged. This average value was then multiplied by 2 to account for the dilution of sample with Trypan Blue (Sigma-Aldrich) and then multiplied by a factor of $1x10^4$ to determine the number of viable cells per ml of media.

3.2 Protein Extraction

3.2.1 Protein extraction from muscle tissue

Muscle tissue was thawed on dry ice before it was cut and weighed in an eppendorf tube. This cut muscle tissue was resuspended in ripa buffer (Sigma-Aldrich) with complete mini, EDTA-free protease inhibitor cocktail (Roche Diagnostics) on ice. Tissue homogenisation and performed with a motor-driven Teflon pestle at 600 rpm at 4˚C. The sample was transferred to an eppendorf tube where it underwent centrifugation at 13,000 rpm at 4˚C. Supernatant containing the protein extract was transferred to a fresh eppendorf tube and kept on ice. Protein samples were aliquoted and stored at -80˚C.

3.2.2 Protein extraction from fibroblast line

Cells were grown in T75 flasks until 70-80% confluence was reached. These cells were then tripsinised and transferred to 10 ml of media. The cells were centrifuged at 1200 rpm for 5 minutes. The media was aspirated and 1 ml of PBS (Oxoid) was added to the cell pellet in the container. The pellet was homogenised, transferred to a sterile eppendorf tube and centrifuged for a second time at 300g for 5 minutes. The PBS (Oxoid) was aspirated and the cell pellet was transferred to cold storage at -80 degrees for future experiments.

These cell pellets were lysed to extract protein using lyses buffer. This lyses buffer is composed of 500 µl Tris PH 7.5, 260 ul 5M NaCl (BDH AnalaR), 20 ul 1M MgCl2 (BDH AnalaR), 1 ml Triton (10%) (All obtained from Sigma-Aldrich), 8.2 ml dH2O and 1 tablet of Roche protease inhibitor (Roche Diagnostics).

50 µl of this lyses buffer was added to the cell pellets of each respective line. These pellets were vortexed for 30 seconds and incubated on ice for 30 minutes to allow for the chemical lyses of the cellular membrane. This homogenate was then spun down at 4 degrees for 2 minutes and the pellet discarded.

3.3 Western Blotting

3.3.1 Bradford assay

The protein concentration from these cell pellets was measured using a Bradford assay. A 1:30 dilution of each of these cell pellets was prepared by adding 3 µl of lyses buffer/ protein homogenate with 87 µl nanopure water in eppendorf tubes. This solution was vortexed and 10 µl per well of each sample was transferred to a 96 well plate. Each cell line was repeated in triplicate. A calibration curve was used to provide a standard baseline against which to measure protein concentration. This calibration curve was created using defined dilutions of BSA (Bovine Serum Albumin- Sigma-Aldrich). This calibration curve was plated in duplicate.

200 µl of Bradford solution (BioRad) was added to each well using a multichannel. Protein concentration was measured by using absorbance of each protein sample and the BSA calibration curve. These absorbencies were measured using a spectrophotometer microplate reader at 595 nm. The absorbencies were calculated using the Beer- Lambert law $A = \varepsilon lc$**.**

3.3.2 SDS-PAGE electrophoresis

The level of protein expression was measured using a western blotting technique. Once the protein concentration of each of the samples was determined, the amount of loading due and lyses buffer to be loaded into each of the wells of a precast agarose gel (mini-protean 4-15%

precast gels, Biorad) was determined. Each sample to be loaded was prepared with protein sample, lyses buffer, 6x loading dye, and benzonase with Mg^{2+} (Sigma-Aldrich) .

Lysis buffer was used to equalise the volumes in each well of the precast dye. This mixture was heated at 37 degrees for 30 minutes on a heating block to prevent aggregation of COX I. The samples were then boiled at 95 degrees to alter the conformation of protein and allow passage through the porous agarose gel (BioRad). These protein samples were then flash spun and left on ice prior to well loading of the precast gels.

Ten-well precast gel electrophoresis was used to separate protein based on size and molecular weight. These gels were also loaded with 10 µl seablue coloured protein ladder (Life Technologiesnologies) and 5µl biotinylated ladder (New England Biolabs). This biotinylated ladder was boiled for 5 minutes at 95 degrees prior to loading. Gel electrophoresis was conducted in 1x running buffer (10x running buffer is composed of 30.3g Trizma base , 144g Glycine and 10g SDS (all obtained from Sigma-Aldrich) made up to 1 litre with nanopure water. A 1:10 dilution in nanopure water of this 10x running buffer is used in gel electrophoresis at 150 V for approximately 1 hour.

3.3.3 Protein transfer to PVDF membrane

Once gel electrophoresis was complete, protein was transferred from this gel to a PVDF membrane (Thermofisher Scientific) for detection. The gel was equilibrated in 1x transfer buffer for approximately 10 minutes. (10 x transfer buffer is composed of 30.3g of Trizma base, 144g of glysine and 2g of SDS (All obtained as powder form from Sigma-Aldrich). This is made up to 1 litre with nanopure water. 1x transfer buffer is created by diluting 150 ml 10x transfer buffer in 225 ml of methanol (Sigma-Aldrich) making this up to 1.5L with nanopure water.

The PVDF membrane (ThermoFisher Scientific) is activated with absolute methanol and washed in 1x transfer buffer. The gel and membrane are then assembled in a cassette with blotting paper and sponges soaked in transfer buffer. Protein transfer was conducted in 1x transfer buffer at 4 degrees Celsius with 400 mA for 1.5 hours. An ice block was added to the transfer buffer of this apparatus to reduce heat produced by the transfer process and increase the efficiency of transfer.

3.3.4 Densitometry and statistical analysis

Analysis of all Western blot membranes was conducted with VisionworksLS Version 7.0.2, ImageJ statistical software and Microsoft windows excel 2007. Each western blot membrane was visualised through chemiluminescense by using an ECL kit (Biorad) to treat each membrane according to the manufacturer's instructions. Each membrane was left for five minutes in the dark room to allow the ECL solution to be absorbed by the membrane. These membranes were then exposes to UV light for a set period by using the 500 biospectrum imaging system to detect the relevant protein bands. Once detected these images were digitalised by using the VisionworksSL software which allow adjustments of these images for brightness and contrast. The files were converted to .tiff and .mpeg files. The files were analysed using ImageJ. ImageJ quantified these bands through densitometry by detecting the relative intensity of each band. To normalise each of these bands, the housekeeping gene GAPDH was used in each protein and control sample.

3.4 ATP Levels from cultured DOA Fibroblasts

3.4.1 Fibroblast seeding and drug treatment

Primary fibroblast lines were harvested from two T75 flasks as described in **Section 3.1.2.** These cells were then counted as described in **Section 3.1.6** and 30,000 cells were seeded into each well of a 96-well cell line plate (Greiner). These cells were left to incubate in 200µl cell line media for 24 hours. On the second day, media was aspirated from each well and washed 2x with 200µl PBS (Oxoid) before being treated with the drug of interest. Each primary line was treated under four different drug conditions measured in ATP measuring buffer (156mM NaCl, 3mM KCl, 2mM $MgSO_4$, 1.25Mm KH_2PO_4, 2mM $CaCl_2$ and 20mM Hepes- All obtained from Sigma-Aldrich). These conditions include 1) 5mM Glucose with 1% pyruvate, 2) 5mM D-deoxyglucose with 1% pyruvate, 3) 5mM glucose, 1% pyruvate and 20uM oligomycin and 4) 5mM d-deoxyglucose, 1% pyruvate and 20uM oligomycin (All obtained from Sigma-Aldrich).

3.4.2 Quantification of ATP levels

Primary cell lines were left to incubate at 37˚C and 5% CO_2. After 1.5 hours, 90µl of media was aspirated from each well and 100µl of CellTiter-Glo substrate solution (Cell Titer-Glo® Luminescent Cell Viability Assay, Promega) was added to each well. The plate was left to incubate in the dark at room temperature for 15 minutes before the luminescent signal from each well was detected and quantified using a Fluroskan Ascent (Thermo Scientific, Paisley, U.K.). Each experiment was quantified in triplicate and further statistical analysis was conducted with excel (Microsoft, Reading, UK) and Graphpad™ V. 5 (Graphpad software).

3.5 DNA Extraction

3.5.1 Genomic DNA extraction from blood

DNA was extracted from blood using Whole Blood Genomic Extraction kit (Nucleon) according to the manufacters protocol. All centrifugation steps were performed at room temperature. 5 mL of patient blood was added to a 50mL polypeptide centrifuge tube (Scientific Laboratory Supplies, Life Science). 4 volumes of reagent A were added and each sample was inverted and centrifuged at 3500g for 5 minutes to generate a cell pellet.

The supernatant was discarded and a further 5mL of reagent A was added to suspend this pellet. The sample was vortexed and allowed to stand for 1 minute. The samples were centrifuged again at 3500g for five minutes and the supernatant discarded. 1mL Reagent B was added to lyse this cell pellet. 350uL of reagent C and 300µl Nucleon Resin were then added to each sample to achieve protein degradation and this sample was centrifuged at 3500g for 4 minutes.

The DNA was then precipitated by transferring the supernatant to a clean polypropylene centrifuge tube (Scientific Laboratory Supplies, Life Science) and adding 1 volume of absolute propan-2-ol. The tube was inverted several times and centrifuged at 4000g to pellet the precipitated DNA. Supernatant was removed and the DNA washed by adding 1mL of 70% ethanol. The DNA was repelleted by centrifuging at 4000g and allowed to air dry for 10 minutes. The DNA was finally resuspended in TE buffer. These DNA samples

were measured using a NanoDropTM ND-1000 (NanoDrop Technologies, Wilmington, USA) .DNA samples were stored at -20˚C.

3.5.2 Genomic DNA extraction from tissue

To extract DNA from patient muscle, approximately 10-20 µg of muscle tissue from each patient was added to a glass test-tube and each sample was homogenised and treated with reagents from a blood and tissue kit (Qiagen) according to the manufacterers instructions. Briefy, 180µls of buffer ATL was added to each sample and the muscle was homogenised with tissueruptor (Qiagen). Once homogenised, each sample was transferred to a 1.5ml Eppendorf tube and 20 uls of proteinase K (Life Technologies) was added. The samples were heated to 56ºC overnight on a thermomixer (Sigma-Aldrich) to ensure maximum lysis of tissue. The following day, 200µls of buffer AL and 200µls of absolute ethanol (Sigma-Aldrich) were added to each sample after brief vortexing and the samples were transferred to a 2ml collection tube within a DNeasy spin-column. The samples were centrifuged at 6000g for 1 minute, flo-through was discarded and the filter was placed in a new collection tube. 500µls buffer AW1 was added to this new spin-column. After an additional centrifugation at 6000g for 1 minute, flo-through was again discarded and 500µls of buffer AW2 was added. The samples were then centrifuged at 20,000g for 3 minutes and the filters of each spin column added to a 1.5ml Eppendorf tube. 100uls elution buffer was added to each filter and left at room temperature for 1 minute. The tubes were then centrifuged again at 6000g for 1 minute to obtain purified DNA from each sample.

3.5.3 Genomic DNA extraction from fibroblast line

DNA was extracted from patient cell lines using the DNeasy® blood and tissue extraction kit (Quigen). Centrifugation steps for this protocol were performed at 21-25°C at 10,000 rpm. A cell pellet from each patient line (maximum 5 x 10^6) cells was homogenised in 200µl PBS (Oxoid). Protinase K (20 µl) (Life Technologies(and Buffer AL (200ul) were used to lyse the cells at 56°C for 10 minutes. Subsequently absolute ethanol (200 µl)(Sigma-Aldrich) was added to each of the patient samples to precipitate the DNA from the pellet. Each sample was

vortexed and transferred to a DNeasy® Mini spin-column which was placed in a 2ml collection tube. Each sample was centrifuged for 1 minute and then each sample spin column was transferred to a new collection tube. The previous tube containing sample supernatant was discarded. 500 µl of buffer AW1 was added to each spin column and these columns were centrifuged for one minute to wash the sample. The flow through was collected and discarded with the collection tube. A fresh tube was added to each spin column and 500 µl of buffer AW2 was used in the last washing stage of the protocol. These columns were centrifuged for 3 minutes at 14,000 rpm to dry the DNeasy® membrane containing the DNA. This DNA was then eluted into a 1.5ml eppendorf tube by adding 100ul of elution buffer which was allowed to incubate on the membrane for 1 minute at room temperature. The spin column was centrifuged for 1 minute and the eluted DNA was collected in the eppendorf tube. The concentration of this DNA was determined by using a NanoDropTM ND-1000 (NanoDrop Technologies, Wilmington, USA) and these DNA samples were transferred to -20 for short term storage.

3.6 Polymerase chain reaction

A polymerase chain reaction (PCR) was achieved with a Veriti® 96-well thermal cycler (Applied Biosystems, Life Technologies, Paisley, UK) in 0.2 ml PCR strip-tubes (STARLAB, Hanburg Germany). Approximately 50ng of DNA from each sample was amplified in a 25µl mastermix reaction containing 5µls GoTaq buffer (Promega, Southhampton, UK)., 2.5uls dNTPs (dATP,dTTP,dCTP,dGTP (VH Bio, Gateshead, UK), 0.13 uls G_2Taq polymerase (Promega, Southhampton, UK), 14.4 uls dH_2O and 0.5uls 10uM forward and reverse primers (Integrated DNA Technologies, Interleuvenlaan, Belgium). DNA amplification was achieved under the following thermal cycler parameters: 95˚C for 7 minutes (denaturation); x30-x35 cycles further denaturation with 95˚C for 1 minute, 58˚C for 1 minute and 72˚C for 1 minute; an extension step at 72˚C for 10 minutes and cooling to 4˚C for sample storage and prevent degradation. The amplicons genereated from these PCR reactions were stored at -20˚C.

3.7 Gel extraction of DNA amplicons

To assess the efficiency and accuracy of mtDNA copy number quantification, three different templates were created using standard PCR protocols described in **Section 3.6.** These amplicons were run through and separated on a 1% (w/v) TAE agarose gel (BioRad) (**Figures 3-1 and 3-2**). Once separated, these templates were cut from the gel and placed into separate 2 ml eppendorf tubes (Cell Star). The tubes were weighed and each tube was allowed to hold a maximum of 200mg of gel fragment.

The DNA from these gels was extracted using the QIAquick® Gel Extraction Kit (Qiagen). All centrifuge steps in this protocol were performed at 20-25°C at 13,000 rpm. The gel fragments were treated with Buffer QG (600ul) and incubated for 10 minutes at 50°C. The tubes were vortexed every two minutes to dissolve the agarose gel. 200 ul of isopropanol was added to precipitate the DNA. This solution was added to a QIAquick® spin column placed in a 2ml collection tube and centrifuged for 1 minute. The supernatant in the collection tube was discarded. 750 µl of buffer PE was added to the spin column and the tube was centrifuged again for 1 minute. The spin column was then transferred to a fresh 2ml Eppendorf tube and centrifuged for 1 minute to dry the spin column membrane. This was then placed in a 1.5ml Eppendorf tube and 30µl of elution buffer applied to the membrane. 1 minute after the addition of the elution buffer, the column was centrifuged for 1 minute and the supernatant containing the DNA collected in the eppendorf tube. The concentration of DNA was quantified using a nanodrop ND-1000 (NanoDrop Technologies) and these tubes were stored at -20 °C.

The number of mtDNA copies per ul of control DNA template were calculated by using the following equation where C = template concentration, Mw is the molecular weight (bp Product length x 2 x 330) and A is Avogadro's constant (6.02 x 1023mol^{-1}).

$$\text{Copies/µl} = \frac{C}{Mw} \cdot A$$

A standard curve was generated from ctDNA template. The number of mtDNA copies in these templates was determined by measuring DNA concentration and using the mtDNA copy number calculation mentioned previously to quantify copy number in each of the control

templates. Each of these templates was then tested for efficiency before the experiment by performing a serial dilution and quantifying the PCR amplification as described in **Section 3.10.2**.

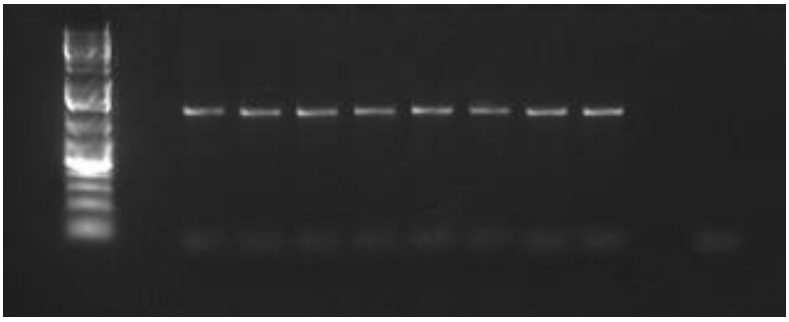

Figure 3-1 Representative image of ND1 amplicons generated through PCR and separated using a TAE agarose gel.

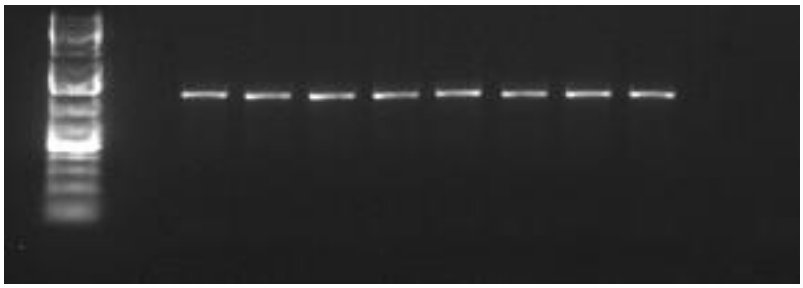

Figure 3-2 Representative image of B2M amplicons generated through PCR and separated using a TAE agarose gel.

3.8 RNA Extraction

3.8.1 RNA extraction from fibroblast lines

RNA was isolated from patient and control cell pellets by following the manufacturer's instructions (RNeasy minikit, Qiagen). All centrifugation was performed at room temperature. RNA concentration from each sample was quantified using NanoDropTM ND-1000 (NanoDrop Technologies, USA). These samples were then stored at -80 degrees in cold storage.

3.9 Reverse Transcription PCR of RNA Isolates

3.9.1 cDNA synthesis

To prepare the samples for quantitative PCR analysis, a superscript III first strand synthesis system (Invitrogen) was used to create cDNA from patient and control RNA isolates. This cDNA was created with a reverse transcription PCR method as outlined in the manufacturer's instructions using the random hexamer protocol.

The first stage was to prepare the RNA/Primer mix for the reverse-transcription PCR (RT-PCR) reaction. The RNA of interest was mixed with 1 µl 10mm dNTPs, 1 ul random hexamers AND DEPC water to a final volume of 10 µl. Each sample was then incubated at 65˚C for five minutes and placed on ice for a minimum time of 1 minute.

A 10 µl synthesis mix was added which contained 2 ul 10x RT buffer, 4 ul 25 mM MgCl2, 2 ul 0.1M DTT, 1 ul RNaseOUT recombinant nuclease inhibitor and 1 ul Supercript III RT. This 20 ul mixture was then run with the following PCR protocol: 10 minutes at 25ºC, 50 minutes at 50ºC, 5 minutes at 85ºC and cool to 4ºC. This PCR protocol results in the generation of cDNA. Each sample is then briefly centrifuged and 1 µl of RNase H is added. The sample is heated to 37ºC for 20 minutes to degrade any contaminating RNA. It can then be stored at -20ºC for future PCR reactions.

3.10 Real-Time PCR

3.10.1 Principles of real-time PCR

Real time quantitative PCR (RTqPCR) is a reliable method which has greater sensitivity than standard PCR reactions at detecting product produced from amplification of sample DNA. The principle of RTqPCR involves the non-specific fluorescent dye iQ™ SYBR® green (BioRad) which is designed to integrate into the DNA structure and provide a fluorescent signal. This signal is detected and quantified by a detector within the IQ5 thermocycler.

During the DNA amplification process by the iTaq polymerase, the iQ5™ optical system software v.2.0 (BioRad) detects the level of sybergreen fluorescence which exceeds the background fluorescence and leads to a linear increase in the amplification curve. This linear increase should directly correspond to the amount of DNA being amplified exponentially during each cycle. The number of cycles in which fluorescence exceeds background noise is known as the threshold cycle (Ct). Preparations of reagents for RTqPCR analysis were performed in a UV-sterilised Aura PCR workstation (Bioair Instruments, Milan, Italy) to prevent contamination.

3.10.2 Quantification of mtDNA copy number

RTqPCR was used to quantify the levels of mtDNA copy number in each of the templates and patient lines. The real-time PCR analysis was performed on a 96 well plate (BioRad). The mtDNA copy number was assessed by amplifying two reference genes in each patient sample, the mitochondrial *ND1* gene and the nuclear *B2M* gene (**Figures 3-3 to 3-6**). The relative number of ND1 copies amplified in each patient with respect to B2M is an indication of mtDNA copy number. These samples were analysed in biological triplicates. The protocol for RTqPCR amplification included denaturation at 95°C for 3 minutes**,** denaturation for 40, 10 second cycles at 95 °C and annealing/extension for 1 minute at 62.5°C. The samples then underwent denaturation at 95 °C for 1 minute to ensure contamination did not take place.

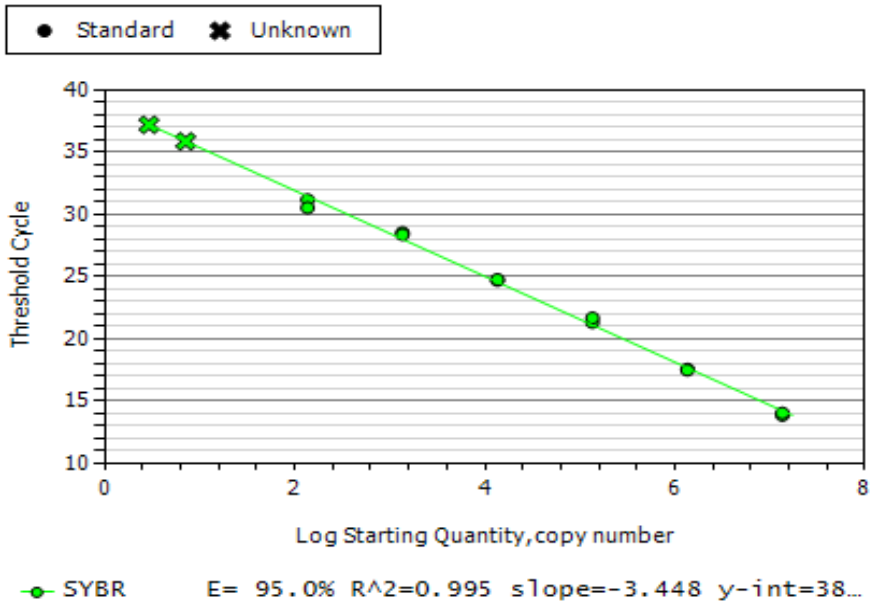

Figure 3-3 Example of a ND1 amplicon serial dilution standard curve demonstrating efficiency (E), linearity (R^2) and slope.

Generated by Bio-Rad IQ5^{TM} software V.2.0.

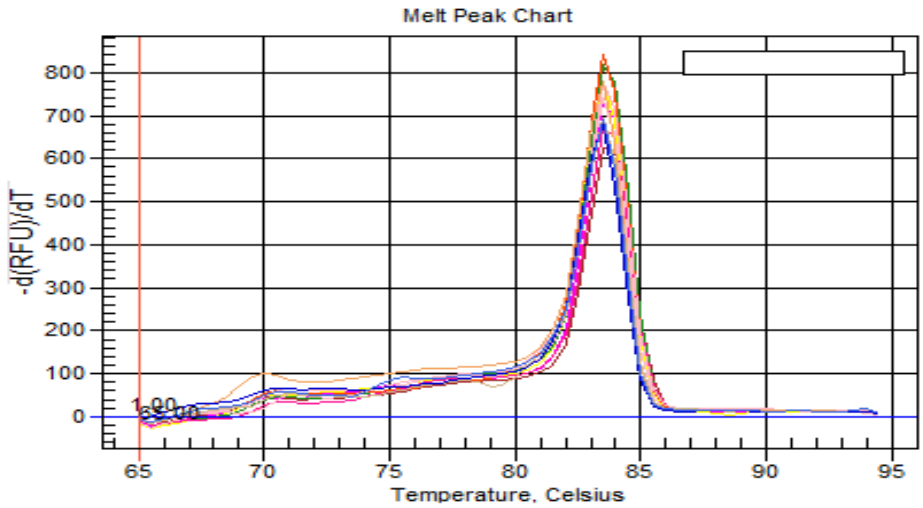

Figure 3-4 ND1 melt-curve.

This was generated through serial dilution of the ND1 amplicon and by measurement of the SYBRgreen fluorescent signal at each respective PCR amplication step.

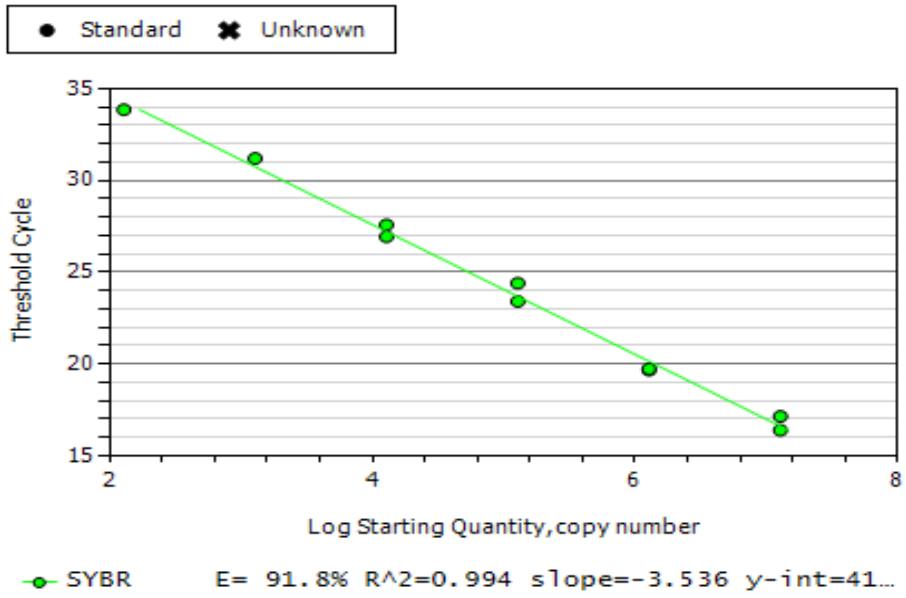

Figure 3-5 Example of a B2M amplicon serial dilution standard curve demonstrating efficiency (E), linearity (R^2) and slope.

Generated by Bio-Rad IQ5™ software V.2.0.

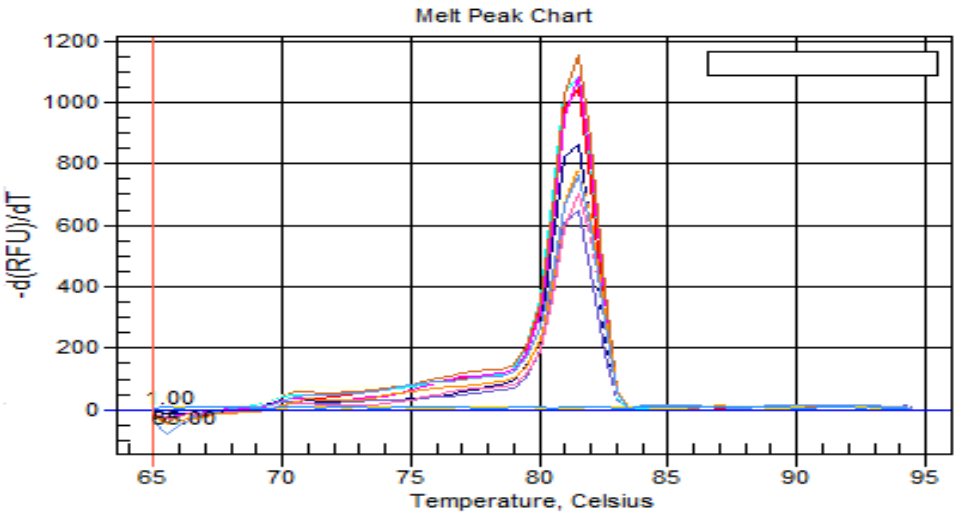

Figure 3-6 B2M melt curve.

This was generated through serial dilution of the B2M amplicon and by measurement of the fluorescent signal at each respective PCR amplification step.

3.10.3 Quantification of gene expression using real-time PCR

Similar to the quantification of mtDNA copy number using RTqPCR in **Section 3.10.2**, the relative mRNA expression of a specified gene was quantified by measuring the levels of cDNA in each patient and control line relative to a standard amplification curve. cDNA levels in each sample were also internally corrected against 2 reference genes *B2M* and *B-Actin* as described in **Table 4-4**. The protocol for RTqPCR includes denaturation at 95°C for 3 minutes**,** denaturation for 40 10 second cycles at 95 °C and annealing/extension for 1 minute at 62.5°C. The samples then underwent denaturation at 95 °C for 1 minute to ensure contamination did not take place.

3.11 Statistical Analysis of real-time PCR Data

Analysis of gene expression was assessed using the ΔΔCt method. Following the amplification of DNA using the IQ5 thermocycler, a Ct value was generated for each of the patient samples. The fluorescent threshold for these samples was set at 500 RFU for mtDNA copy number and 200 RFU for relative gene expression. Each patient sample for each gene was repeated in triplicate per plate. The experiment was repeated three times to ensure accuracy of the results. The final value used in the analysis of mRNA expression levels in each patient was calculated by using the equation 2^-ΔΔct.

3.12 Long-Range PCR

Determination of multiple mtDNA deletions in patient sample was determined using the TaKara LA Taq^{TM} PCR system (Takara Bio, Otsu, Japan). This system is capable of amplifying a DNA fragment thousands of bps long. The mitochondrial genome is approximately 16 kbs in length which makes it an ideal candidate for targeted long range PCR amplification. All long range PCR reactions were performed in a Veriti® thermal cycler (Applied Biosystems, Life Technologies) in 0.2ml strip tubes (STARLAB, Hamburg, Germany). DNA extracted from patient muscle was used in a 25 µl long-range PCR mastermix used to amplify a 11kb DNA region. This mastermix contained 2.5µls 10x LA Taq

buffer (Takara, Bio), 4µls dNTPs (VH Bio), 0.25 µls TaKara LA Taq polymerase (Takara, Bio), 16.75 µls dH_2O, 0.25 µls of 20µM forward and reverse primers and 1µl of patient DNA template per sample. Each sample was to amplify approximately 1-2ng of DNA. Amplification was carried out under the following conditions: denaturation occurred at 94˚C for 1 minute, x28 cycles of 94˚C for 30 seconds (further denaturation), 58˚C for 45 seconds (annealing step) and 68˚C for 11 minutes (extension step). The final step post-cycle is 72˚C for 12 minutes.

After the successful amplification of the targeted 11kb region of mtDNA, these amplicons underwent gel electrophoresis on a 0.7% (w/v) TAE agarose gel (BioRad) as described in **Section 3.13.1.** 6 µl PCR amplicon was added to 6ul of Orange G (Sigma-Aldrich) ((**Section 3.13.2**) and 10ul of sample was added to each well of the agarose gel (BioRad). Gel electrophoresis was conducted with 1x TAE running buffer (Sigma-Aldrich) at a constant voltage of 30V for 4 hours. To confirm that the amplified PCR product was approximately 11kbs, Generuler^{TM} 1kb Plus DNA ladder (75-20,000 bps) (Fermentas, St Leon-Rot Germany) was run in parallel. The ladder and the PCR amplicons were visualised using a UV light source from an AlphaImager® 2200 system (Aalpha Innotech).

3.13 Sanger Sequencing of Nuclear Genes

3.13.1 Agarose gel electrophoresis

Amplicons of genomic DNA generated through PCR were observed by running these PCR products through a 2% (w/v) 1x TAE agarose gel (BioRad) using electrophoresis. Agarose gel was created using 1x TAE buffer (0.04M Tris-acetate, 0.001M EDTA, pH: 8.3 (Helena Biosciences)) which was added to a conical flask and heated in a microwave for 2-5 minutes. This mixture was allowed to cool and EtBr was added (0.4ug/ml (Sigma-Aldrich)) to intercalate DNA. This mixture was then added to an electrophoresis tray with gel combs and allowed to polymerise.

3.13.2 PCR Amplification

PCR amplification was achieved using 50ng genomic DNA as described in **Section 3.6.** The approximate concentration of these amplicons was compared by first mixing 6µl of each PCR product with 6µl of Orange G solution (Sigma-Aldrich), 70% nanopure dH_2o (v/v) and 30% glyverol (Sigma-Aldrich). 10 µl of this mixture was then added to wells in a 2% w/v agarose gel with ethidium bromide as previously described in **Section 3.13.1.** Hyperladder IV was also added (5ul) to a well of the agarose gel to visualise PCR product size. These samples then underwent gel electrophoresis using 1xTAE as running buffer and a constant voltage of 80V for approximately 40 minutes-1 hour. PCR amplicon bands were visualised under UV light generated by an AlphaImager ® 2200 system (Alpha Innotech, Kasendorf, Germany).

3.13.3 ExoFap methodology

The ExoFap reaction is a fast and efficient PCR clean-up step which degrades unwanted deoxynucleotides and primers left over from genomic amplification. ExoFap consists of FastAP Thermosensitive Alkaline Phsophatase (FAP) (Thermo Scientific) and Exonuclease 1 (Exo 1) (Thermo Scientific). Volumes of 0.5 µl of Exo 1 and 1 ul of FAP were added to each 3/5µl PCR reaction in a 96-well sequence reation plate (Greiner) on ice. The plate was sealed with a rubber met and pulse spun in a centrifuge before the mixture was incubated at 37°C for 15 minutes. These enzymes was subsequenctly inactivated by incubating the mixture at 80°C for a further 15 minutes.

3.13.4 Big-Dye™ sequencing

BigDye™ Terminator v3.1 Cycle Sequencing Kit (Applied Biosystems, Life Technologies) is used for preparing a fluorescent-based cycle sequencing reaction in a standard PCR thermocycler. A mixture of 2µl BigDye Terminator v3.1 Sequencing Buffer (x5), 11µl nanopure water, 1µl Primer and 1 µl Big Dye was added to the 3/5 µl PCR reactant. This mixture was then run using the Big Dye thermocycler protocol which includes 1 minute at 96°C, x25 cycles of 96°C for 10 seconds, 50°C for 5 seconds and 60°C for 4 minutes.

3.13.5 Ethanol precipitation

In order to remove non-incorporated nucleotides and excess salts, each sample underwent an ethanol precipitation step. 2 µls of 125mM EDTA, 2 uls of sodium acetate (3M) and 70 µls of absolute ethanol were added to each sample well in a 96 well sequencing reaction plate (All obtained from Sigma-Aldrich). These samples were incubated at room temperature for 15 minutes before they were centrifuged at 2000g for 30 minutes. The supernatant was removed and 70 µls of 70% ethanol (Sigma-Aldrich) was added to each sample. The plate was centrifuged at 1650g for a further 15 minutes before this supernatant was also removed and the plate was allowed to air dry for 10 minutes. Samples were suspended in 10uls Hi-Di (Applied Biosystems, Life Technologies).

3.13.6 Genomic sequencing

After resuspension of samples in Hi-Di, samples were denatured at 95˚C for 2 minutes before loading onto the ABI 3130xl genetic analyser (Applied Biosystems, Life Technologies). Sequence chromatograms generated which were compared against reference sequence reproduced from Genbank (http://www.ncbi.nlm.nih.gov/RefSeq/) by using Seqscape v. 2.6 (Applied Biosystems).

3.14 Live Cell Imaging with Confocal Microscopy

3.14.1 Cell seeding

Primary fibroblasts were seeded on a glass bottomed confocal dish (Wilco) at a density of 100-150,000 cells and incubated with Minimum Essential growth media (as described in **Section 3.1.6**) at 37˚C for 24 hours. Primary fibroblasts which were incubated in an oxidative media (galactose) containing MeM glucose-free media with 5mM galactose (Sigma-Aldrich) and supplemented with 1% L-glutamine, 1% sodium pyruvate, 1% non-essential amino acids , 1% Penicillin-streptomycin and 1% Vitamins for 48 hours (All obtained from Gibco, Life Technologies, Paisley, UK).

Primary myotubes were seeded at a density of 70,000 cells in a glass bottomed confocal dish (Wilco) and incubated in Skeletal Muscle Cell Differention Media (Promocell) with 2% FBS and 1% Penecillin-Streptomycin (All obtained fro, Gibco, Life Technologies, Paisley, UK) for 24 hours at 37˚C.

3.14.2 MitoTracker® Red CMXRos incubation

On the day of imaging, growth media was aspirated from each dish and primary cells were incubated with fresh media containing 75nM MitoTracker® CMXRos (Life Technologies) for 30 minutes. These cells were then washed twice with PBS (Oxoid) and incubated in fresh media without phenol red and containing 25mM Hepes (Sigma-Aldrich). A similar protocol was used for the dual-staining of patient primary myotubes with MitoTracker® Red CMXROS and Quant-iT™ PicoGreen® (Life Technologies). This protocol can be found in **Section 5.2.4.**

3.14.3 Mitochondrial fragmentation in fibroblasts

Images of the primary fibroblast and myotube mitochondrial network were captured with an A1r inverted confocal microscope (Nikon) using a 63x 1.4 NA objective unless otherwise stated.

3.14.4 Image analysis

The excitation wavelength for MitoTracker® Red CMXRos (Life Technologies) was 561nm, respectively. Primary fibroblasts were z-stacked with section interval at 0.1µm for 69 slices. Approximately 50 cells were captured for each primary fibroblast cell line.

3.14.5 Statistical analysis

Quantitative Analysis was analysed using excel (Microsoft, Reading, UK) and Graphpad™ V.5 (Graphpad software)

Chapter 4

Genotype-Phenotype Characterisation in Autosomal Dominant Optic Atrophy

4.1 Introduction

Autosomal dominant optic atrophy (DOA) is the most common congenital optic neuropathy with a global prevalence of 3 in 100,000 individuals (Thiselton *et al.*, 2002). It is characterised by the selective degeneration of the retinal ganglion cell layer leading to the deterioration of the optic nerve. The syndrome presents as a gradual and severe visual deficit until virtually all patients diagnosed with this condition fulfill the requirements for registered legal blindness (Lenaers *et al.*, 2012). It was originally clinically identified by Batten in 1896 but adopted the name Kjer's Optic Neuropathy due to additional studies performed by Poul Kjer in 1959 who described 19 families with the condition (Kjer, 1959). Most patients present with isolated optic atrophy (OA), although, some patients with similar age of onset of progressive visual loss also develop with extra-ocular multi-systemic symptoms, a subgroup often refered as DOA 'plus' (DOA+). In some instances, members of the same family carrying the same pathogenic *Opa1* mutation may present with different severity of the disease (Yu-Wai-Man *et al.*, 2010b). Transmission of DOA+ to succeeding generations is, however, typically more severe with incomplete penetrance (Yu-Wai-Man *et al.*, 2010b; Amamti-Bonneau *et al.*, 2008; Hudson *et al.*, 2008).

Until the last few decades, clinical research on DOA was hampered by the lack of longitudinal and follow-up studies of patients due in part to the lack of knowledge of the underlying genetic aetiology of the disease. In clinical practice, patients were phenotypically categorised which may have excluded individuals with underlying *OPA1* mutations (Votruba *et al*.1998b).

Genetic and biochemical analyses have frequently treated DOA as a single clinical manifestation grouping both OA and DOA+ together in order to determine common threads between DOA and other mitochondrial related optic neuropathies (Zanna *et al.*, 2008; Agier *et al.*, 2012), in part due to the lack of sufficient biobank material from either DOA+ or OA patients. A rigorous investigation of the underlying complex biochemical parameters which are distinct between these two groups has yet to be investigated. Preliminary investigation suggests that OA usually results from deletions, nonsense mutations and splice site defects which normally result in OPA1 haploinsufficency (Olichon *et al.*, 2003; Marchbank *et al.*, 2002). On the other hand, missense mutations found in the *OPA1* GTPase domain tend to be

more associated with a dominant-negative effect which may have a role in the increased severity of the disease (Olichon *et al.*, 2007).

Previous investigations of the molecular mechanisms governed by OPA1 have been carried out in a range of *in vivo* and *in vitro* models which include Drosophila *melanogaster*, Rattus *norvegicus*, Danio *rerio* and primary human tissues (Zanna *et al.*, 2008; Chen *et al.*, 2007; Yarosh *et al.*, 2008; Rahn *et al.*, 2013). Fibroblasts are easily accessible from skin tissue derived from patients which can be obtained through non-invasive means. In the present project, primary human fibroblasts were then selected as a model to investigate the biochemical mechanisms which underpin DOA pathogenesis.

The aim of this study was then to investigate and compare biochemical parameters between OA and the more severe DOA+ syndromes to identify both common and divergent factors which may explain why a subgroup of patients diagnosed with DOA develops a more severe visual deficit in addition to secondary multi-systemic features.

4.2 Materials and Methods

4.2.1 OPA1 patient cohort

The investigation of the disease mechanisms between DOA+ and OA was conducted in primary fibroblasts derived from eight patients described in **Table 4-1.** Four of these patients harbour missense mutations found in the GTPase domain of OPA1 (exons 8-15) and were diagnosed with an optic atrophy with additional multi-systemic symptoms. The remaining four patients presented with an isolated optic nerve involvement and harboured either deletions or splice-site *OPA1* mutations. This study had the relevant institutional approval and written informed consent was obtained from all patients.

Pedigree	Age (Years)	Gender	Optic atrophy	Deafness	Ataxia	Myopathy	Neuropathy	PEO	Others	*OPA1* mutations	Exon / Intron
DOA+(1)	69	M	+		+	+			Spasticity	c.768C>G, c.854A>G	5b ,8
DOA+(2)	50	M	+	+				+		c.1198C>T	12
DOA+(3)	57	M	+	+		+		+		c.1334G>A	14
DOA+(4)	57	M	+		+	+	+	+		c.34521294A>G	13
OA(1)	44	M	+							c.1516+1G>T	Intron 15
OA(2)	64	M	+							Exon 1-5 del.	1-5 del.
OA(3)	48	M	+							c.2708_2711 del(TTAG)	27
OA(4)	46	M	+							c.876-878 del (TGT)	9

Table 4-1. Clinical features and *OPA1* mutations of the patients included in this study.

4.2.2 Cell culture

Cell lines were maintained according to the protocol mentioned in **Section 3.1.** Each line was routinely checked for the presence of mycoplasma and all lines were found to be consistently mycoplasma negative for all experimental investigations.

4.2.3 MitoTracker® Red CMXRos staining

Cell seeding and MitoTracker® Red CMXRos (Life Technologies) staining of the mitochondrial network was performed according to the protocol in **Section 3.14.** Two glass-bottomed confocal dishes (Wilco) containing primary *Opa1* primary fibroblasts were stained simultaneously and washed twice with PBS (Oxoid) and left to incubate in imaging media containing 25mM HEPES (Sigma-Aldrich). One dish was used for imaging while the second dish was kept at 37ºC in an incubator without a CO_2 regulator one hour prior to imaging on each day. A total of 24 glass bottomed dishes were prepared (4 control and 8 primary patient fibroblast lines).

4.2.4 Mitochondrial network image capture and quantification

Mitochondrial network image capture was performed using an A1r confocal microscope (Nikon) with a x63 oil-based objective lens. Imaging was performed at 3% laser power at 561nm with a 512x512 voxel frame. A total of 69 slices (8µm) was captured along the z-axis for each fibroblast analysed. Approximately 50 cells were captured (25 cells per confocal dish) for each patient and control primary line analysed.

Five parameters were measured under each condition: (1) Total Mitochondrial Length; (2) Total Mitochondrial Volume; (3) Total Number of Fragments; (4) Average Mitochondrial Length (5) Average Mitochondrial Volume; Average Mitochondrial Length and Volume were quantified by determining the Total Mitochondrial Length and Volume respectively and dividing by the number of mitochondrial fragments in each fibroblast to determine the 'total length' of each mitochondrial structure.

4.2.5 Protein expression in cultured fibroblasts

Protein expression levels were analysed using western blot analysis to measure the expression in both OPA1 and individual constituent subunits of the respiratory complexes in DOA+ and OA primary fibroblasts. Protein levels were corrected to GAPDH protein levels and investigated using the method described in **Section 3.3.** Primary antibodies used to detect these proteins can be found in **Table 4-2.**

4.2.6 *OPA1* and mtDNA maintenance gene expression

Quantification of mtDNA copy number in primary *Opa1* fibroblasts was conducted with an iQ^{TM} SYBR® Green (Bio-Rad) methodology and a RTqPCR detection system (Bio-Rad). The relative number of mtDNA copies was determined by quantifying the number of mtND1 copies relative to the number of nuclear B2M copies using the ΔΔCT method (described in **Section 3.10.2**). MtDNA copy number was quantified in four primary controls and eight primary DOA patient fibroblasts.

Investigation of mtDNA copy number maintenance was also conducted by quantifying the mRNA expression level of TFAM using a reverse transcription qPCR protocol as described in **Section 3.10.3**. Details of RTqPCR primers used have been provided in **Table 4-3 and 4-4.**

4.2.7 Cell Titer-Glo luminescent cellular ATP assay

Investigation of ATP levels was achieved by seeding primary fibroblasts onto 96-well cell line plates (Greiner) and treating them with drugs to inhibit either the glycolytic or the OXPHOS ATP synthesis as described in **Section 3.4**. The levels of ATP were quantified using a CellTiter-Glo Bioluminescent Cell Viability Assay (Promega) according to the manufacters protocol.

Primary antibody target	Product number	Concentration used	Protein molecular weight	Species	Incubation period/time
OPA1	ab119685	1:1000	80-100 kDa	mouse monoclonal	1h room temperature
NDUFB8	ab110242	1:4000	17kDa	mouse mo noclonal	1h room temperature
SDHA	ab14715	1:1000	70kDa	mouse monoclonal	1h room temperature
COXII	ab110258	1:1000	24kDa	mouse monoclonal	1h room temperature
ATP5A	ab14748	1:4000	55kDa	mouse monoclonal	1h room temperature
GAPDH	sc-25778	1:1000	37kDa	rabbit polyconal	1h room temperature

Table 4-2 List of primary antibodies and dilutions used to perform western blot analysis of OPA1 and mitochondrial repiratory subunits.

OPA1: Optic atrophy 1 protein; NDUFB8: Nuclear encoded complex I subunit; SDHA: Nuclear encoded complex II subunit; COXII: mitochondria encoded complex IV subunit; ATPA5: nuclear encoded complex V subunit; GAPDH: glyceraldehyde-3-phosphate.

Template	Base Pairs	Forward Primer (5'-3')	Reverse Primer (3'-5')
B2M	1092	CGCAATCTCCAGTGACAGAA	GCAGAATAGGCTGCTGTTCC
MTND1	1041	AGGAACTCGGCAAATCTTACC	GTCATGTGAGAAGAAGCAGG
RTqPCR			
B2M	231	CACTGAAAAAGATGAGTATGCC	AACATTCCCTGACAATCCC
MTND1	111	ACGCCATAAAACTCTTCACCAAAG	GGGTTCATAGTAGAAGAGCGATGG

Table 4-3 List of primers for mtDNA copy number quantification.

Templates were designed to produce standard curves with known DNA copy number. qPCR primers were used for the real-time PCR assay.Genbank accession numbers: *B2M*: NM_004048.2; *mtND1*: NC_012920.1. RTqPCR conditions used to quantify mtDNA copy number is described in **Section 3.10.2**.

Template	Base Pairs	Forward Primer (5'-3')	Reverse Primer (3'-5')
TFAM	139	GCTCCCCTTCAGTTTTGTGT	TTTTGCATCTGGGTTCTGAGCT
OPA1	117	GTTCAACTGGCGGAAGACC	TGCAGAGCTGATTATGAGTACGA
Reference Genes	bp		
B2M	231	CACTGAAAAAGATGAGTATGCC	AACATTCCCTGACAATCCC
B-ACTIN	131	GATGCAGAAGGAGATCACTGC	ACATCTGCTGGAAGGTGGAC

Table 4-4 List of primers for relative mRNA gene expression of mitochondrial maintenance markers.

TFAM: transcription factor A, mitochondrial*;OPA1: Optic atrophy 1*; *B2M*: beta-2-microglobulin.

Gen bank accession numbers: *TFAM:* NM_003201.2; *OPA1*: NM_015560.2; *B2M*: NM_004048.2; *B-Actin*: NM_001199954.1. The RTqPCR conditions used to quantify gene expression are described in **Section 3.10.3**.

4.3 Results

4.3.1 OPA1 protein and gene expression in fibroblasts from DOA patients

OPA1 protein levels were assessed in fibroblasts from the cohort of patients described in **Table 4-1** using western blot analysis. Fibroblasts from DOA+ and OA patients were directly compared with fibroblasts from healthy donors.

Overall, DOA+ primary fibroblasts had similar OPA1 protein levels compared with healthy controls **(Figure 4-1)**. However, when studying patients separately, the four different patients showed varying levels **(Appendix Figure A-1)**. Interestingly, DOA+(1) fibroblasts, presenting as a compound heterozygote **(Table 4-1)** had significant lower OPA1 protein levels, probably a direct result of two mutated versions of the protein.

OA primary fibroblasts consistently had lower OPA1 protein levels compared with controls **(Appendix Figure A-1; A-2)**. Overall, OPA1 levels were statistically decreased by less than 50% **(Figure 4-1)**, consistent with the expression of one wild-type (WT) allele and a deleted one.

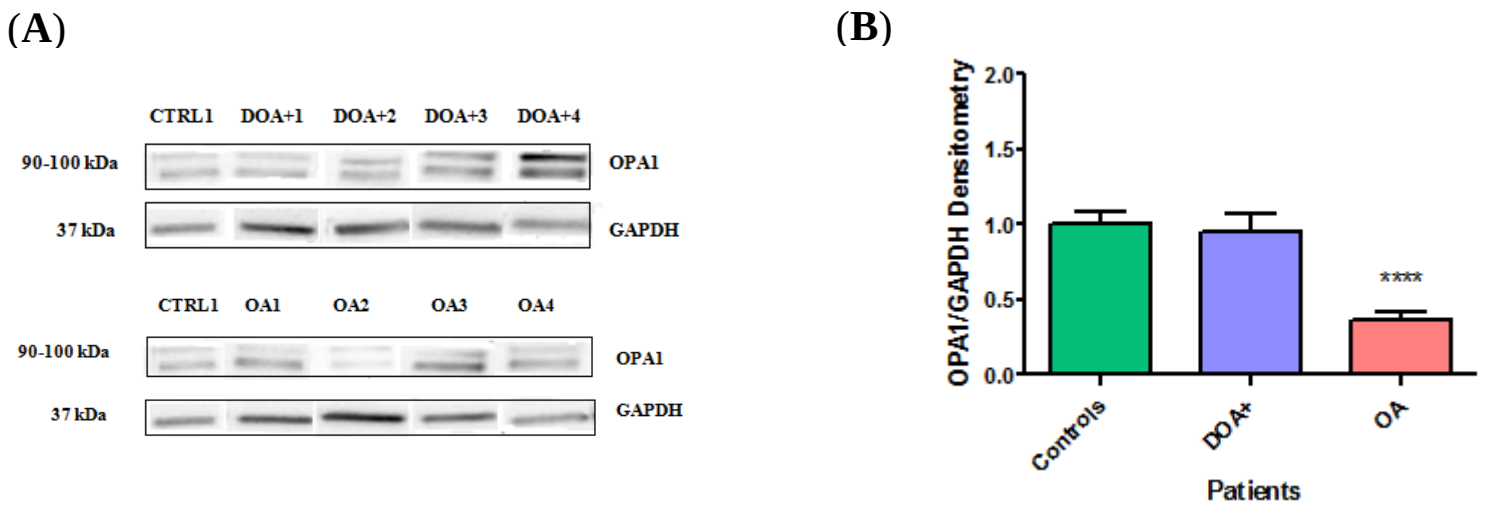

Figure 4-1 OPA1 protein densitometric analysis from primary fibroblasts from DOA+ and OA patients

Representative images of western blots measuring OPA1 and GAPDH levels from controls, DOA+ and OA patient fibroblast **(A)**. Densitometric analysis was performed using ImageJ and OPA1 densitometry normalised to GAPDH. OPA1/GAPDH ratios were expressed compared to mean of three different control cell lines (n=4) **(B)**. Error bars represent standard error of the mean (SEM) **** $p \leq 0.0001$ using a Student's unpaired t-test against controls. Refer to appendix A for representative raw images of immunoblots.

OPA1 mRNA expression was also assessed in fibroblasts from the cohort of patients described in **Table 4-1** using real-time PCR anaysis. Fibroblasts from DOA+ and OA patients were directly compared with fibroblasts from healthy donors.

Overall, DOA+ primary fibroblasts showed a statistically significant decrease in *OPA1* gene expression by ~50% compared with controls **(Figure 4-2)**.

The OA group also showed a similar low trend, however, this was not significant (Figure 4-2). This is due to the variability in gene expression in individual patients. Indeed OA(1) and OA(3) had decreased OPA1 gene expression, whilst OA(4) did not (**Appendix Figure B-1**), suggesting different mechanisms regulating the gene expression of the different mutated *OPA1* alleles in the different patients.

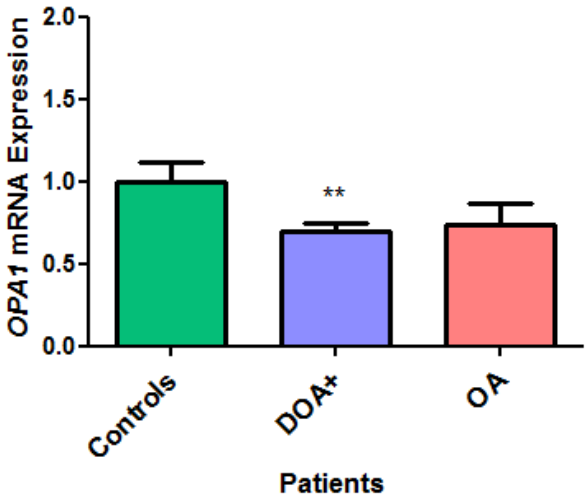

Figure 4-2 *OPA1* gene expression of primary fibroblasts from DOA+ and OA patients.

Relative *OPA1* gene expression was measured using real-time PCR and standardised against mean *B-actin* and *B2M* gene expression. *OPA1*/mean housekeeping genes was expressed compared to mean of three different control cell lines (n=3). Error bars represent Standard Error of the Mean (SEM). * $p \leq 0.05$ using a Student's unpaired t-test against controls.

4.3.2 Mitochondrial network in primary fibroblasts from DOA+ and OA patients

Mitochondrial networks from fibroblast cell lines were visualised using the mitochondrial-specific MitoTracker® Red CMXRos stain. Images were capture along the z-axis for each fibroblast analysed allowing 3D-representation for further analysis. Images were then processed and filtered using the Huygens deconvolution algorithm (part of Huygens Essential software) **(Figure 4-3)**. The Object analyser wizard (Hugens Essential) allowed detection and measurement of mitochondrial fragments in each cell.

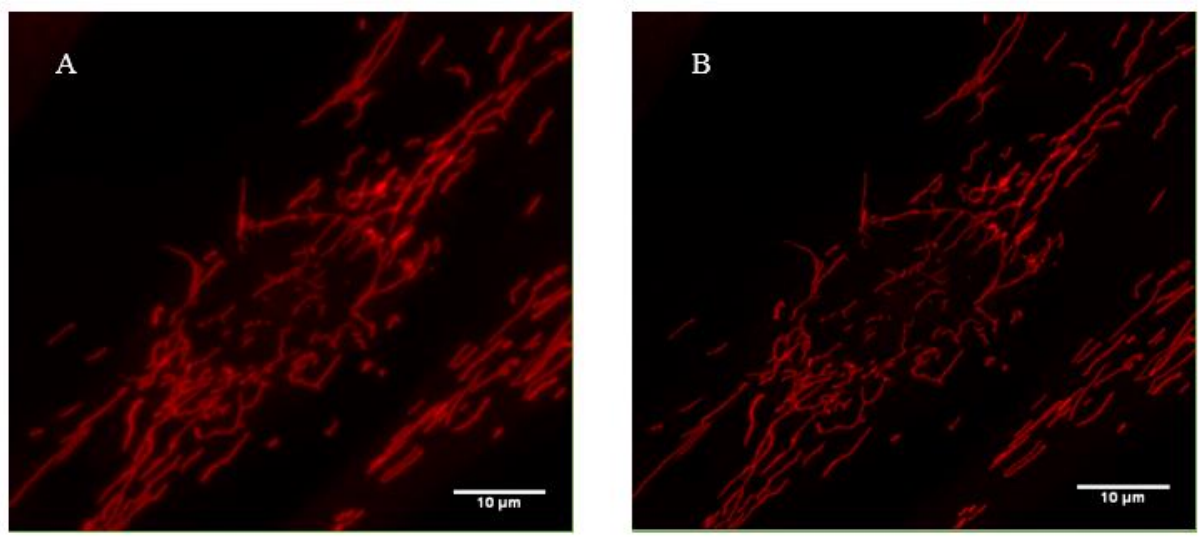

Figure 4-3 Mitochondrial staining of fibroblast cells and image processing

Staining of the mitochondrial network was performed with MitoTracker® Red CMXRos (Molecular Probes, Life technologies). Raw image of control primary fibroblast was captured using Nikon T_i confocal microscope objective x63 assisted with Nyquist sampling **(A)**. Computerised Image deconvolution of the same control primary fibroblast obtained using Huygens Essential deconvolution wizard **(B)**. Scale bars represent 10µm.

Fibroblast mitochondrial network was visualised under two different bioenergetics conditions. Cell lines were grown in basal condition consisting of glucose suplemented medium, favorising glycolytic-driven energy production alongside basal OXPHOS-driven energy production. Fibroblast mitochondrial network was also visualised following specific OXPHOS-driven energy production, consisting of a medium supplemented with galactose but lacking glucose. Fibroblasts from all patients in the study cohort were then visualised and mitochondrial network quantified.**(Figure 4-4)**.

Total mitochondrial network length was expanded in all DOA+ patients and half of the OA patients (**Appendix Figure C-1**). Consequently, total mitochondrial length was statistically increased in both DOA+ and OA patients but with an exagerated effect in DOA+ **(Figure 4-5A)**. Total volume was also increased in most patients of the two groups (**Appendix Figure C-1**) leading to a mild significant increased average of total volume in both DOA+ and OA patient groups **(Figure 4-5B)**.

Following galactose treatment in control fibroblasts, total mitochondrial network length was retracted alongside with an increased total volume, suggesting a swollen total mitochondrial network. A similar effect was observed in both DOA+ and OA groups, although more intense in the OA group **(Figure 4-5)**.

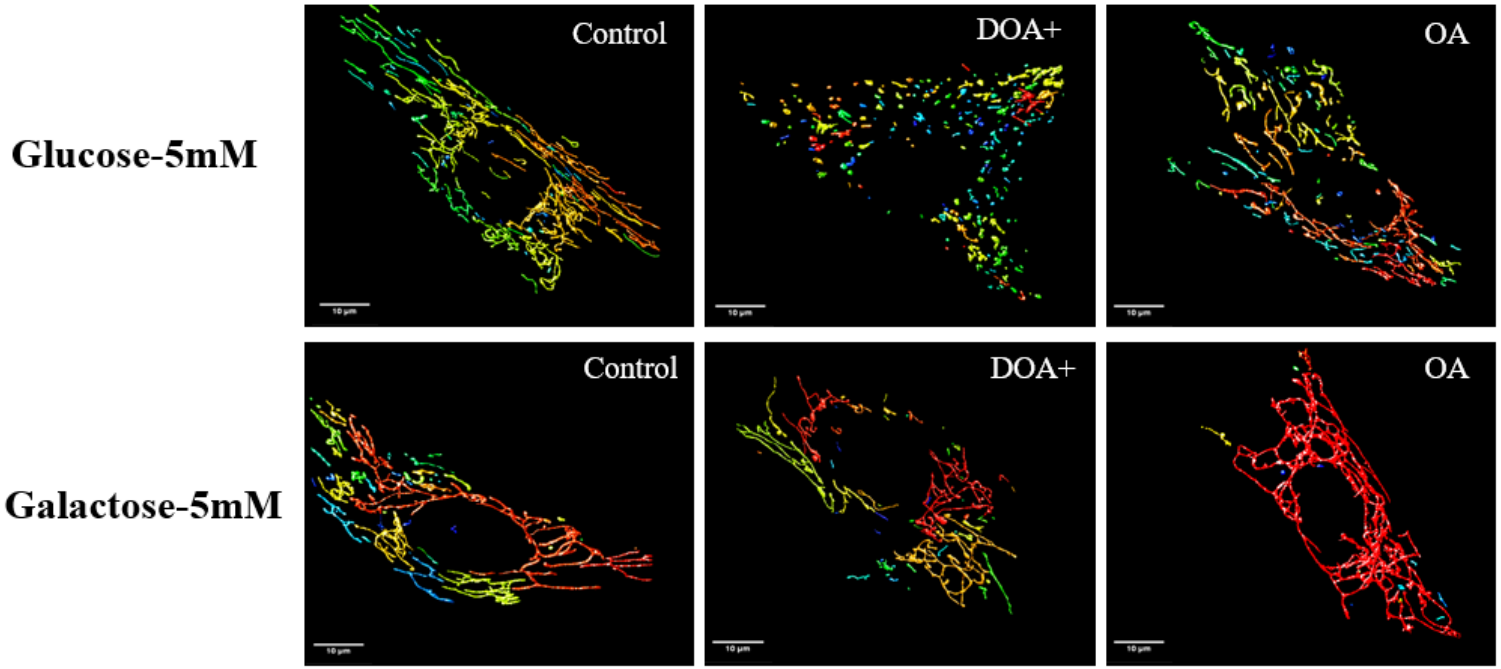

Figure 4-4 Mitochondrial network staining in fibroblast patients and controls under different bioenergetics conditions

Staining of the mitochondrial network was performed with MitoTracker® Red CMXRos (Molecular Probes, Life technologies). Images of primary fibroblasts were captured using Nikon Ti confocal microscope objective x63 assisted with Nyquist sampling followed by Computerised Image deconvolution using Huygens Essential deconvolution wizard. Representative images of Fibroblast controls (A,D), Fibroblasts from DOA+ (B,E) and OA patients (C,F). All fibroblasts were treated to two different bioenergetics conditions: glucose treatment for 24 hours (A-C) or galactose treatment for 48 hours (D-F). Scale bars represent 10μm. .

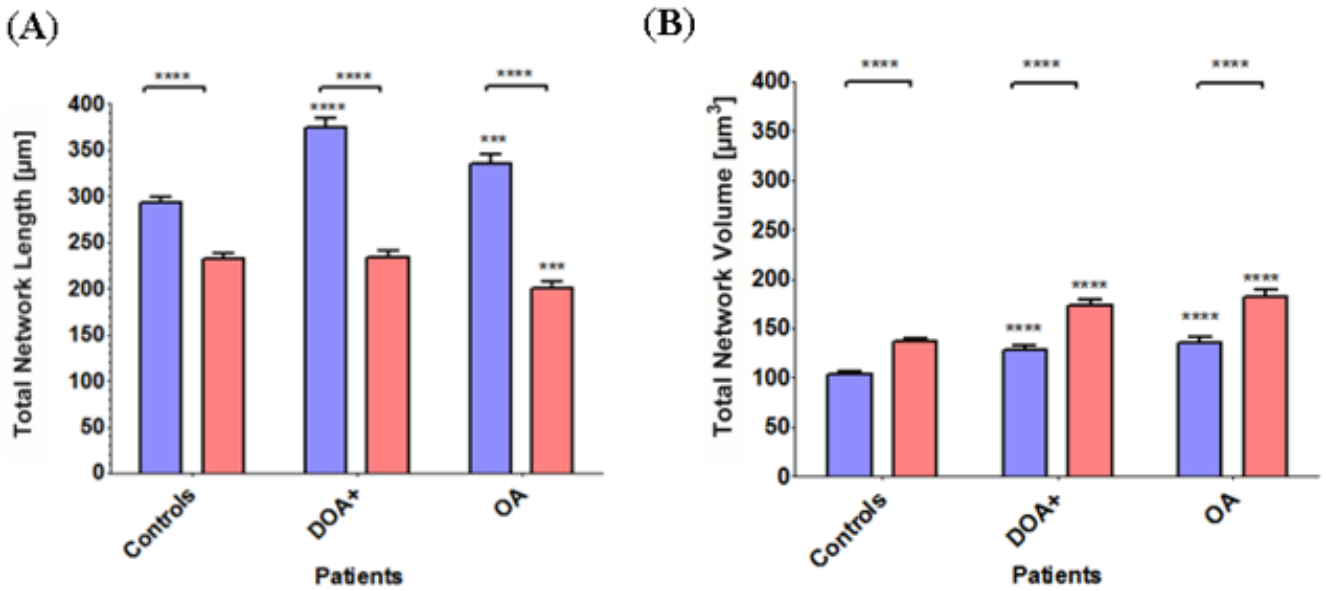

Figure 4-5 Total length and Volume measurements of the Mitochondrial Network patient and control Primary Fibroblasts

Total mitochondrial length **(A)** and total volume **(B)** were measured using Huygens Object analyser module in fibroblasts imaged following either 24 hour incubation with 5mM glucose (blue) or 48 hour incubation with 5mM galactose (red). Error bars represent the standard error of the mean (SEM). *** $p \leq 0.001$ and **** $p \leq 0.0001$ using a Student unpaired t-test against controls (n=200).

Under glucose conditions, the total number of mitochondrial fragments was significantly increased virtually in all patient fibroblasts (**Appendix Figure C-2**), with higher numbers in the DOA+ group (**Figure 4-6A**). Average length of mitochondrial fragments was also significantly decreased in both groups with shorter fragments measured in DOA+ patients **(Figure 4-6B, Appendix Figure C-3A)**. Both these obsevations suggest a higher level of fragmentation in DOA+ patient fibroblasts under basal conditions than in OA patient fibroblasts, both groups showing fragmentation compared with controls. In parallel, the average volume was only midly decreased in DOA+ patients but not in OA patients compared with controls **(Figure 4-6C, Appendix Figure C3B)**.

Galactose treatment had the overall effect of decreasing the number of mitochondrial fragments, increasing the average fragment length and increasing the average fragment volume, consistent with mitochondrial elongation and mitochondrial swelling. A similar trend was observed in patient fibroblasts in both groups. However, this elongation effect (represented by a decreased mitochondrial fragment number and an increased fragment length) was exagerated in OA patient fibroblasts **(Figure 4-6A-B and Appendix Figure C2C C3B and C5A)**. Strikingly, fibroblasts from OA patients had bigger fragment average volumes than from DOA+ patients, suggesting a high level of swelling. However, both DOA+ and OA groups had swollen mitochondria compared to control fibroblasts.

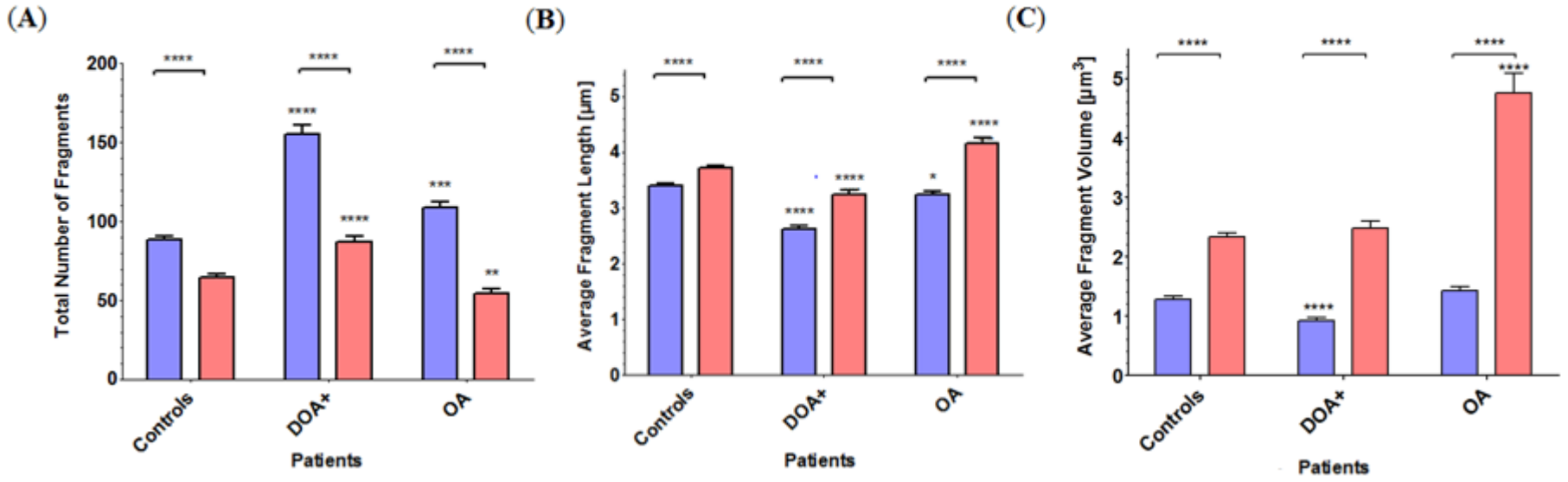

Figure 4-6 Mitochondrial fragmentation of the Network in patient and control primary fibroblasts

Average number of mitochondrial fragments **(A)** were measured using Hugens Object analyser software in fibroblasts imaged following either 24 hour incubation with 5mM glucose (blue) or 48 hour incubation with 5mM galactose (red). Average fragment length **(B)** and average fragment volume **(C)** were calculated as described in section **4.2.4.** Error bars represent the standard error of the mean (SEM). * $p \leq 0.05$, ** $p \leq 0.01$, *** $p \leq 0.001$, and **** $p \leq 0.0001$ using a Student's unpaired t-test against controls (n=200).

4.3.3 MtDNA maintenance

Mitochondrial DNA (mtDNA) copy number was measured using a RTqPCR assay designed to compare the relative levels of mitochondrial gene ND1 with respect to nuclear-encoded β-2-microglobulin (B2M) in fibroblasts from healthy controls, DOA+ and OA patients. Compared with fibroblast from controls, fibroblasts from patients, whether from DOA+ or OA groups, did not reveal major variations in mtDNA copy number **(Figure 4-7A, Appendix Figure D-1A)**.

Mitochondrial transcription factor A (TFAM) mRNA expression was also measured using RTqPCR. TFAM mRNA levels seemed slightly decreased in most DOA+ and OA patient fibroblasts **(Figure 4-7B, Appendix Figure D-1B)**. Due to high variability between patients, this decrease was only significant in the DOA+ group but not in the OA group.

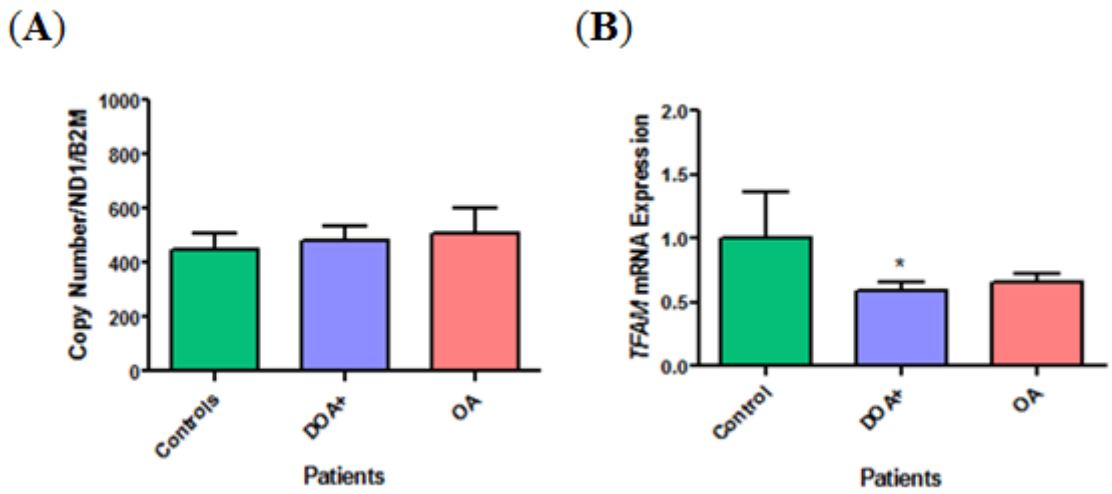

Figure 4-7 MtDNA maintenance markers in primary fibroblasts from DOA+ and OA patients.

MtDNA copy number was measured using real-time PCR and normalised to nuclear encoded *B2M* copy number (A). TFAM was measured using real-time PCR and standardised against mean *B-actin* and *B2M* gene expression (B). Both mitochondrial maintenance markers were expressed compared to mean of three different control cell lines (n=3). Error bars represent Standard Error of the Mean (SEM). * $p \leq 0.05$ using a Student's unpaired t-test against controls.

4.3.4 OXPHOS protein levels and ATP levels

Several OXPHOS complex subunit protein levels were assessed using western blot analysis in fibroblasts from DOA+ and OA patients and compared with fibroblasts from healthy donors **(Figure 4-8)**. Overall, subunit protein levels were variable between the different DOA patients **(Appendix Figures E-1; E-2;E-3;E-4)**.

Complex I subunit NDUFB8 had overall increased levels in both DOA+ and OA groups (**Figure 4-9A**). The nuclear-encoded complex II SDHA had significant increased levels in the DOA+ group, mainly due to one patient DOA+(1), whilst OA patients had consistently similar levels to controls (**Figure 4-9B and Appendix Figure E-1B**). The mitochondria-encoded complex IV subunit COXII had similar levels in DOA+ patient fibroblasts compared with controls. The OA group showed a mild increase mainly due to one of the patients (**Figure 4-9C and Appendix E2-C**). Overall, complex V subunit ATP5A showed no gross variation in protein level in both DOA+ and OA groups compared with controls (**Figure 4-9D**).

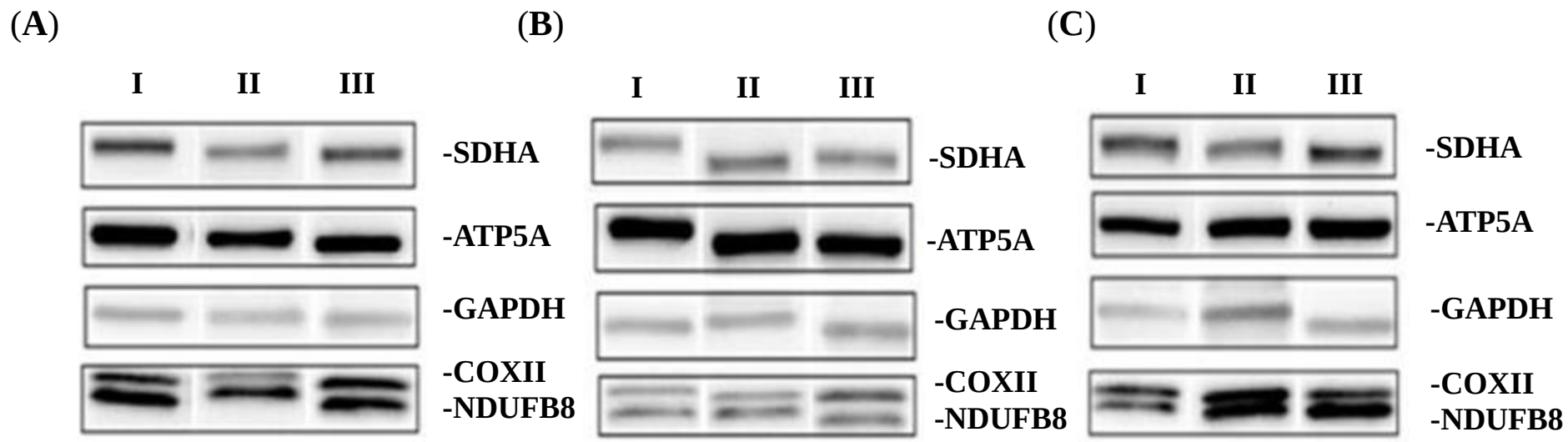

Figure 4-8 Montage of OXPHOS complex subunits western blot images from primary fibroblasts from DOA+ and OA patients.

Representative images of western blots measuring OXPHOS complex subunits and GAPDH levels from controls **(A)**, DOA+ **(B)** and OA **(C)** patient fibroblasts. COX II: mitochondria encoded complex IV subunit (17kDa); SDHA: Nuclear encoded complex II subunit (70kDa); NDUFB8: Nuclear encoded complex I subunit(14kDa); ATP5A: nuclear encoded complex V subunit (55kDa) and GAPDH: housekeeping protein (37kDa). Refer to Appendix E for representative raw images of immunoblots.

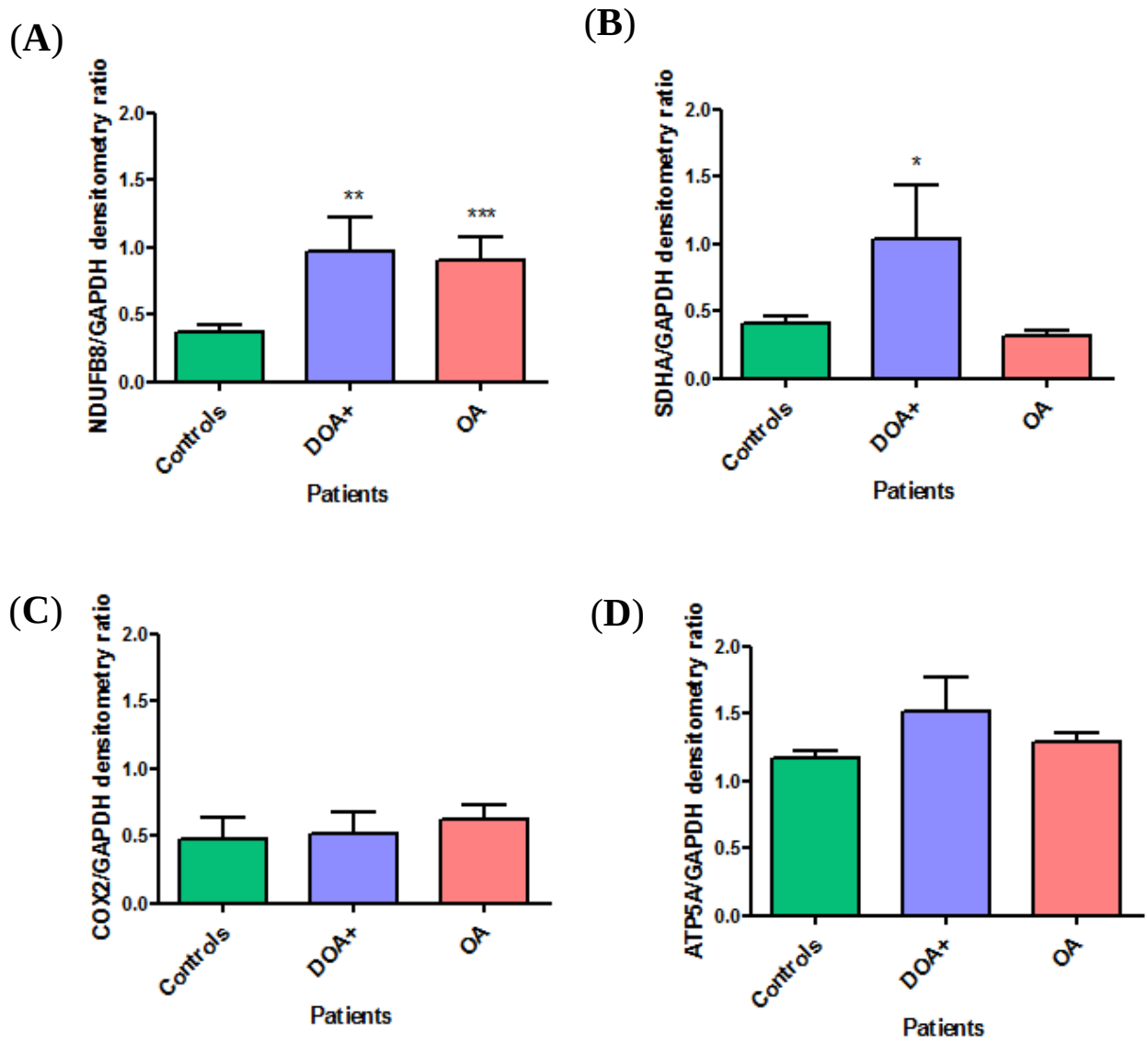

Figure 4-9 OXPHOS complex subunits protein levels from primary fibroblasts from DOA+ and OA patients

Densitometric analysis of NDUFB8 **(A)**, SDHA **(B)**, COXII **(C)** and ATP5A **(D).** OXPHOS subunit immunoblots was performed using ImageJ and each subunit densitometry normalised to GAPDH. Ratios were expressed compared to mean of three different control cell lines (n=3). Error bars represent standard error of the mean (SEM). * $p \leq 0.05$, ** $p \leq 0.01$ and *** $p \leq 0.001$ using a Student's unpaired t-test against controls.

Following the observed disturbances in OXPHOS subunit levels, ATP levels were measured using a luminescent assay under different biogenesis conditions **(Figure 4-11 and Appendix Figure E-4)**.

Under basal glucose conditions, total ATP levels were not statistically different between the DOA+, OA and control groups. Under glycolysis-driven conditions, with oligomycin treatment, ATP levels were lower than under glucose conditions in all groups. Similarly, under basal conditions, ATP levels in the DOA+ group were slightly lower than the other two groups, although not significant.

Under OXPHOS-driven conditions, with D-deoxyglucose treatment, ATP levels were approximately three times lower than in glucose conditions and twice lower than under oligomycin treatment in all groups. There was no difference in ATP levels in both DOA+ and OA groups compared with controls.

Under minimal bioenergesis, treated with a combination of oligomycin and D-deoxyglucose, ATP levels were very low showing minimal ATP production.

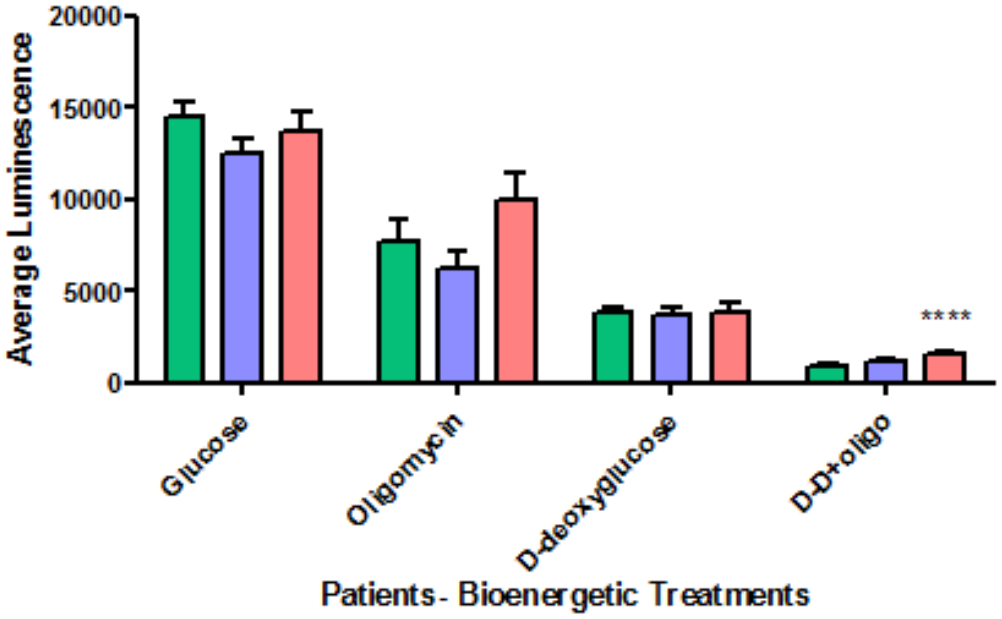

Figure 4-10 ATP levels measured in primary fibroblasts from DOA+ and OA patients

Fibroblasts from patients and controls were treated with a range of bioenergetics conditions: glucose **(Glucose)**, glucose and oligomycin **(oligomycin)**, glucose and d-deoxyglucose **(D-Deoxyglucose)** and glucose with d-deoxyglucose and oligomycin **(D-D+oligo)**. Error bars represent standard error of the mean (SEM). **** $p \leq 0.0001$ using a Student's unpaired t-test against controls (n=3).

4.4 Discussion

4.4.1 Different mechanisms of *OPA1* allelic expression in OA and DOA+ patients

The effects of different types of mutations on OPA1 expression at the mRNA and protein levels were very different and potentially pinpoint different types of pathogenetic mechanisms within the same disease, DOA.

OA syndrome is characterised with isolated optic nerve involvement and accounts for approximately 80% of all DOA cases (Lenears *et al.*, 2012). Except for OA(4) patient, all other OA patients had lower protein levels, due to a decrease in gene expression as shown by the RTqPCR assay. Of note, gene expression was not statistically significant and as low as for protein levels in the OA group compared with controls because it was missing OA(2) patient in the group analysis, however all three remaining patients showed consistency between protein and gene expression. A decrease of 50% in gene expression is consistent with the expression of only one WT allele and silencing of the mutant allele. This effect is described as loss of function also refered as haploinsufficiency. Haploinsufficiency in DOA was first hypothesised by *Alexander and colleagues* (2000) and the first evidence in different types of *OPA1* mutations was described soon afterwards (Pesch *et al.,* 2001; Marchbank *et al.,* 2002). For *OPA1* mutations leading to loss of transcription of the mutated allele, *Schimpf and colleagues* (2008) were able to demonstrate a nonsense-mediated decay mechanism. However, they also observed that for some of the mutations, particularly those not leading to premature termination codon, such as missense and in-frame mutations, a nonsense-mediated decay did not occur and OPA1 mRNA and protein levels were normal.

OA(4) patient harbours an 876-878 (TGT) deletion in exon 9 which results in an in-frame deletion of a single amino acid at the C-terminus of the protein (termination at codon 960) which may go undetected by nonsense-mediated decay quality control. Gene and protein levels in OA(4) were found to be consistently normal, which may indicate that OA(4) is not subject to nonsense mediated quality control.

One limitation of quantifying OPA1 OA protein level in this study is that the commercial antibody used in the western blot analysis to determine protein level is

targeted to an epitope on the C-terminus of the OPA1 protein. If the mutated *OPA1* allele were to express a truncated protein in a dominant negative fashion as hypothesised by *Kushnareva and colleagues,* 2016, it would be undetectable by this assay because the truncation is upsteam of the antibody epitope. However Kunshnareva's study which used an N-terminus targeted antibody reaffirmed a model of haploinsufficiency and it is likely that the same mechanism is operating in primary fibroblasts.

On the other hand, DOA+ subgroup, presenting with extra-ocular symptoms in addition to the optic neurodegeneration defining DOA, account for approximately 20% of all cases (Lenaers *et al.,* 2012; Yu-Wai-Man *et al.,* 2010b). Most of these patients harbour pathological missense variants in the GTPase domain of *OPA1* (Yu-Wai Man*et al.,* 2010b).

OPA1 expression analysis showed higher variability within DOA+ patients. In the case of missense or in-frame mutations, as the resultant transcript would not be truncated but instead modified, such mutation would not be detected by non-sense mediated decay (Schimpf *et al.,* 2008). However, mutated proteins could post-transcriptionally be degraded or, if not detected by a cellular chaperone system (Kriegenburg *et al*., 2012), result in the production of misfolded protein in the cell. In the case of DOA+(2), DOA+(3) and DOA+(4), OPA1 protein levels were not decreased indicating that both alleles should be expressed. The resulting overexpressed or normal levels of OPA1 protein suggest a potential dominant-negative effect in the DOA+ group, as previously hypothesised (Olichon *et al.,* 2007).

Decreased OPA1 protein levels with normal gene expression in DOA+(1) patient could be explained by the presence of the two heterozygous missense mutations (c.768 C>G (exon 5b) and c.854A>G (exon 8) in trans). It is very likely that one or the two alleles are fully expressed but the two resulting mutated proteins have a dominant-negative effect resulting in destabilsation of the protein and a lower level than expected. Further study of allelic expression and OPA1 complex structure would be required. Interestingly, this patient presents with one of the most clinically severe cases of DOA in this cohort with optic atrophy, ataxia, myopathy and spasticity.

OA and DOA+ syndromes are characterised by two different types of mutations leading to two very different pathogenetic mechanisms: haploinsufficiency in most OA patients and dominant-negative mechanism in most DOA+ patients with mutations in the GTPase domain. These two different mechanisms could result in the involvement of different cellular and mitochondrial pathways between the two groups, potentially explaining different levels of severity between the two syndromes. Due to the multifunctional roles of OPA1 protein in mitochondrial dynamics, mitochondrial cristae structure, apoptosis, calcium signalling, OXPHOS complex stabilisation and mtDNA maintenance (Chevrollier *et al.,* 2012; Zanna *et al.,* 2008; Hudson *et al.,* 2008; Amati-Bonneau *et al.,* 2008; Agier *et al.,* 2012; Fueloep *et al.,* 2011), it is difficult to predict how the different types of mutations can affect mitochondrial and cellular function.

4.4.2 Mitochondrial network fragmentation and morphological differences in DOA+ and OA patients

Analysis of mitochondrial fragmentation patterns was performed by confocal microscopy followed by semi-quantitative 3D image analysis allowing the measurement of three separate parameters: total mitochondrial length, total mitochondrial volume and number of total fragments per cell. These three parameters were then used to calculate two further metrics: average mitochondrial length and average mitochondrial volume. This image analysis method has great quantitative sensitivity in detecting mitochondrial morphological differences compared to previous qualitative (Zanna *et al*., 2008; Olichon *et al.,* 2007; Chevrollier *et al.,*2008) and semi-quantitative (Agier *et al.*,2012; Chevrollier *et al.,* 2012) analyses some of which are described below.

Investigating morphological differences between DOA+ and OA primary fibroblasts under basal conditions in which cells use both OXPHOS and primarily glycolytic systems to derive chemical energy, highlighted two relevant observations. The first was a significant increase in total length in all DOA+ and half OA fibroblast lines (**Table 4-5**) and there are a number of possible reasons for this observation. The simplest explanation was that the total number of mitochondrial fragments found in DOA primary lines was significantly greater than control. This appears to correlate with a significant increase in total mitochondrial length (**Appendix C1 and C2**). So therefore this significant

increase in total length is a cumulative effect of the length of a much greater number of mitochondrial fragments. *Agier and colleagues* who observed a similar increase in total length of *OPA1* primary lines also found a significant decrease in DRP1 steady-state which occurred at the post-transcriptional level (Agier *et al.,* 2012). This may also indicate that DRP1 may have a role in modulating total length although further evidence is required to make this assertion. The second observation was an increased fragmentation of average length and volume in DOA primary fibroblasts. This was reported in previous reports by Zanna *et al.* (2008); Olichon *et al.* (2007) and Chevrollier *et al.* (2008). However, DOA+ was found to be particularly susceptible to fragmentation under these basal conditions which has not been reported previously. This observation was reinforced by quantification of average volume which also demonstrated significant fragmentation in DOA+ compared with control. Severe fragmentation in DOA+ with milder fragmentation in OA would appear to be a basic pathophysiological observation.

Investigation of morphological differences under forced oxidative conditions (5mM galactose) in which chemical energy is reliant on the OXPHOS system rather than glycolytic ATP (Rossignol *et al.,* 2004; Bustamante and Pedersen, 1977), highlighted three relevant observations. The first was a general increase in both average length and volume of mitochondria in control, DOA+ and OA primary fibroblasts. This is reminiscent of *Tondera and colleagues* (2009) stress-induced mitochondrial hyperfusion (SIMH). SIMH is a normal acute physiological adaptation to a stress to promote cell survival through mitochondrial morphology modulation (Tondera *et al*., 2009). However, this increase in average length and volume was particularly intensified for OA primary fibroblasts with both excessive length and disproportionate swelling observed.

Variations in mitochondrial morphology between both OA and DOA+ groups might be a direct consequence of *OPA1* allelic expression.*OPA1* is expressed as different spliced isoforms that form oligomeric complexes to direct its fusion and cristae remodelling roles (Frezza *et al.,* 2006; Ramonet *et al.,* 2012). The presence of mutated OPA1 protein due to missense mutations in the GTPase domain detected in DOA+ patients may interfere with oligomeric complex stabilisation, in turn impinging on OPA1 functional and structural roles under basal conditions and lead to excessive fragmentation of mitochondrial network.

Under SIMH conditions induced by galactose treatment, ATP is specifically produced via OXPHOS and mitochondrial production is increased. The exaggerated SIMH and disproportionate swelling found in OA may be directly linked to OPA1 haploinsufficiency. Deletions found in OA *OPA1* lead to the degradation of truncated *OPA1* mRNA and the translation of only wild-type OPA1 isoforms. With the absence of a modified protein, the resulting oligomerisation would lead to the formation of wild-type stable complexes and normal function, explaining the lesser impact on mitochondrial network morphology observed under normal conditions compared to DOA+ cases. However, the severe defect mainly observed under SIMH induced by OXPHOS-driven conditions might be more associated by the low levels of OPA1 protein available suggesting a higher demand of the protein during intense cristae remodelling required to maintain the mitochondrial network. This phenomenon implies a threshold of OPA1 molecules needed beyond which disturbance of mitochondrial morphology can be detected. The mechanism of this mitochondrial swelling merits further investigation but one could hypothesize that this increase in mitochondrial volume may be due to a dysregulation of calcium/ potassium flux, resulting in the efflux of calcium and subsequenct swelling of the mitochondrial network due to a loss in cristae structure (Kushnareva *et al.*, 2013).

The different morphologies found in DOA+ and OA primary fibroblasts under basal and oxidative conditions imply alternative biochemical dysfunctions within mitochondria of OA and DOA+ patients. Variations in morphological parameters which occur within DOA+ and OA groups are likely reflective of either the underlying *OPA1* mutation or relative number of passages on each line. However, similar fragmentation patterns were also quantified in **Chapter 5** reaffirming the different morphologies between these two groups. Further understanding the nature of these alternative dysfunctions may explain clinical differences observed between these two groups in future studies. This is particularly pertinent given that optic and auditory systems, the central and peripheral nervous system, heart, muscle, pancreas, kidney and liver are all susceptible to mitochondrial dysfunction (Chinnery *et al*., 2015).

4.4.3 mtDNA maintenance is mildly dysregulated in DOA+ patients with no steady-state consequence on mtDNA copy number

To assess the effects of *OPA1* mutations on mtDNA maintenance, mtDNA copy number was measured using a real-time PCR. No variation in mtDNA copy number between controls, DOA+ and OA primary fibroblasts were detected. This observation is consistent with a previous report by *Agier and colleagues* who also demonstrated no significant difference in their cohort of four DOA patients implying that at least in these primary fibroblasts, pathological mutations in *OPA1* do not appear to impact on gross mtDNA maintenance (Agier *et al*., 2012). However, this observation was contradicting *Zanna and colleagues* work who demonstrated a significant increase in mtDNA copy number in primary fibroblasts derived from a cohort of ten patients (Zanna *et al.*, 2008).

The maintenance of mtDNA was further assessed by analysing the relative gene expression of *TFAM*, a component of the mitochondrial nucleoid involved in mtDNA coiling and transcription. *TFAM* gene expression was significantly decreased in DOA+ but not in OA when compared against control.A slight decrease in TFAM levels with normal mtDNA copy number suggests a mild impairment in mtDNA maintenance with no overall effect in steady-state mtDNA copy number in normal conditions. This is consistent with previous in-house analyses which demonstrate a defect in mtDNA replication rate under stress conditions (driven repopulation of mtDNA after treatment with ethidium bromide).

Currently there is much controversy in the field as to how pathological *OPA1* mutations may impact mtDNA maintenance. In addition to mtDNA levels quantified in primary fibroblasts, investigation of primary leukocytes using RTqPCR have indicated both a slight mtDNA depletion or a significant mtDNA proliferation in different studies (Kim *et al.*, 2005; Sitarz *et al.*, 2012). Additional investigation in single skeletal muscle fibres also demonstrates a mechanism of significant mtDNA proliferation, especially in COX-negative tissue (Yu-Wai-Man *et al.*, 2010b). This may indicate that pathological disruption of OPA1 may result in a gross disruption of mtDNA maintenance although there may not be a different level of susceptibility of mtDNA maintenance in the different tissues.

4.4.4 OXPHOS subunit protein level variations in DOA do not have direct effect on overall ATP cellular levels

OPA1 performs a variety of functions, which include maintance of cristae morphology, regulation of the IMM fusion and stabilisation of OXPHOS complex assembly (Zanna *et al.,* 2008). Given these functions, it is plausible that *OPA1* mutations may disturb OXPHOS function. Relative protein expression levels of individual subunits of OXPHOS complexes I, II, IV and V were semi-quantitatively analysed using western blot. Previous reports have found an abnormal steady-state of subunits associated with complex I (Zanna et al., 2008) which was potentially associated with an OXPHOS enzymatic defect. Analysis of these OXPHOS subunits corrected against GAPDH demonstrated a significant increase in NDUFB8 in both DOA+ and OA. However a significant increase of nuclear encoded SDHA was also detected in DOA+ which may indicate an excess of mitochondrial organelles. Further investigation is needed to detect a potential OXPHOS complex assembly defect (using blue-native gel electrophoresis) and analysis of enzymatic activity of complexes I. Abnormal steady-state levels of complex I subunits in OA may be preliminarily indicative of an underlying OXPHOS system defect.

To further investigate the effects of varying OXPHOS subunit protein levels, cellular ATP production was measured. Total cellular, glycolysis-driven and OXPHOS-driven ATP production were independently analysed and compared. No major ATP production disturbances were observed in any conditions between the three groups. This observation in consistent with previous measurements of ATP performed by *Zanna and colleagues* who also reported no gross differences in ATP level in DMEM glucose (Zanna *et al.,* 2008).

D-deoxyglucose specifically inhibits the glycolytic pathway by competitive inhibition. D-deoxyglucose contains a hydrogen in place of two hydroxyl groups which prevents glucose molecules from being further processed to glucose-6-phosphate. This inhibition decreases the efficiency of glycolysis to generate ATP and increases the reliance of the primary fibroblasts to generate ATP through the OXPHOS system. In contrast, instead of inhibiting the glycolytic pathway, galactose is broken down to generate ATP via glycolysis but with a much lower ATP net yield. As the medium is supplemented by

glutamine, the cell mainly relies on the OXPHOS system for ATP generation via amino acid metabloism.

The alternative mechanisms which these drugs use to enhance ATP production through OXPHOS may partially explain why there is no significant defect detected in DOA+ and OA groups under d-deoxyglucose treatment while primary fibroblasts treated under galactose exhibit abnormal mitochondrial morphology. Furthermore, mitochondrial morphology was quantified after 48 hours incubation with galactose while ATP generation was quantified under 1.5 hours incubation with d-deoxyglucose. It could be that any defect in OXPHOS may not be detectable until a later time point when mitochondrial morphology remodelling may exacerberate a defect in OXPHOS. Evidence for altered mitochondrial bioenergetics was demonstrated in Zanna *et al.,* (2008) in which they observed increased mitochondrial ATP following 24 hour galactose treatment in both control and DOA primary fibroblasts, pointing to an underlying biochemical defect. Further investigation of how mitochondrial morphology in DOA under galactose treatment is linked to OXPHOS is required, particularly in OA patients.

4.4.5 Conclusion

The present study presented two very distinct syndromes of DOA with two different mutational effects. On one hand, primary fibroblast lines from DOA+ patients with missense muations showed normal levels of *OPA1* gene and protein, with propensity to escape cellular quality control mechanisms such as nonsense-mediated decay. Such mutations led to a clear fragmentation of the mitochondrial network suggesting an impairment of OPA1 mediated maintenance of the mitochondrial structure and potentially an impairment of fusion under normal conditions. Pathological missense variants may then impact on normal OPA1 function, indicative of dominant–negative effect. Mitochondrial respiration and mtDNA copy number did not seem to be directly affected; however, the decrease in TFAM gene expression implicated a wider effect on mtDNA maintenance. In conclusion, dysfunction in DOA+ primary fibroblasts may be due to impaired mitochondrial fusion/structure and mtDNA replication rate (**Table 4-5**).

On the other hand, investigation of OA primary fibroblasts showed a significant decrease in OPA1 steady state which occurred at the post transcriptional level probably

due to nonsense mediated decay. Haploinsufficiency led to a mildly significant fragmentation of the mitochondrial network under basal conditions. There was also no gross defect in mitochondrial respiration and mtDNA maintenance detected. Under oxidative conditions, OA primary fibroblasts showed a clear effect on mitochondrial morphology, represented by excessive SIMH and excessive swelling of mitochondria. This may indicate that under oxidative conditions, where a greater threshold of OPA1 is required for adaptation to stress, OPA1 function is severely compromised. In conclusion, as a consequence of OPA1 haploinsufficiency, OA primary fibroblasts may have a greater impact under stressful conditions and this defect may be due to a dysregulation of mitochondrial structure (**Table 4-5**).

	DOA+	OA
OPA1 levels	**Normal levels**	**< 50% lower levels**
Mitochondrial Network under basal conditions	**Expansion of total mitochondrial network** **Acute fragmentation**	Mild expansion of total mitochondrial network Mild fragmentation
Mitochondrial Network under OXPHOS-driven conditions	Normal retraction of total mitochondrial network SIMH	Intensisfied retraction of total mitochondrial network **Exagerated SIMH accompanied by intensified swelling**
mtDNA maintenance and replication	Normal mtDNA copy number **lower TFAM levels**	Normal mtDNA copy number but 40% lower TFAM levels
OXPHOS function	Increased protein levels of CI subunit No overall significant ATP production changes	Increased CI subunit protein level No overall significant ATP production changes
	Dominant negative effect	**Haploinsufficiency**

Table 4-5 Summary of data obtained from analysis of DOA+ and OA primary fibroblasts.

SIMH: Stress-induced Mitochondrial Hyperfusion; CI: complex I from the OXPHOS system, represented by NDUFB8A subunit; CII: complex II from the OXPHOS system represented by SDHA subunit

Chapter 5

Mitochondrial Network and Nucleoid Distribution in *OPA1*-Mutant Myotubes

5.1 Introduction

Mitochondrial nucleoids are essential structures that play numerous roles including regulating mtDNA maintenance and copy number, segregation of mtDNA in daughter mitochondria following fission, manipulating mtDNA transcription and acting as an interface between mtDNA function and global cellular signalling pathways (Alam *et al.*, 2003; Moraes *et al.*, 2001; Tyynismaa and Suomalainen, 2009).

Case series investigating key pathological mechanisms underpinning *OPA1* mutations and mitochondrial dysfunction originally identified a disruption of mtDNA maintenance illustrated by the presense of multiple mtDNA deletions in patients diagnosed with optic atrophy and mitochondrial myopathy using histopathological staining (Amati-Bonneau *et al*., 2008).

This observation was also confirmed in a pedigree of optic atrophy with progressive external ophthalmoplegia, ataxia, deafness, visual failure and sensory-motor neuropathy due to a pathological missense variant identified in *Opa1* (Hudson *et al.*, 2008). *Hudson and colleagues* then proposed that OPA1 may be a component of the mitochondrial nucleoid which may explain its involvement in mtDNA instability (Hudson *et al.*, 2008).

This initial set of observations combined with more recent investigations suggesting a relationship between *OPA1* dysfunction and mtDNA proliferation (Sitarz *et al*., 2012; Yu-Wai-Man *et al*., 2010b), led to an investigation by *Elachouri and colleagues* to identify this mechanistic link between OPA1 and mtDNA maintenance (Elachouri *et al*., 2011). Their work highlighted a physical interaction of a 10kDa N-terminus OPA1 isoform with mtDNA, implicating OPA1 protein in mtDNA maintenance within HeLa cells. Similar to ATAD3, this 10kDa isoform was responsible for anchoring the mitochondrial nucleoid to the IMM, a necessary step for mtDNA replication, fidelity and nucleoid distribution within the mitochondrial network (**Figure 5-1**).

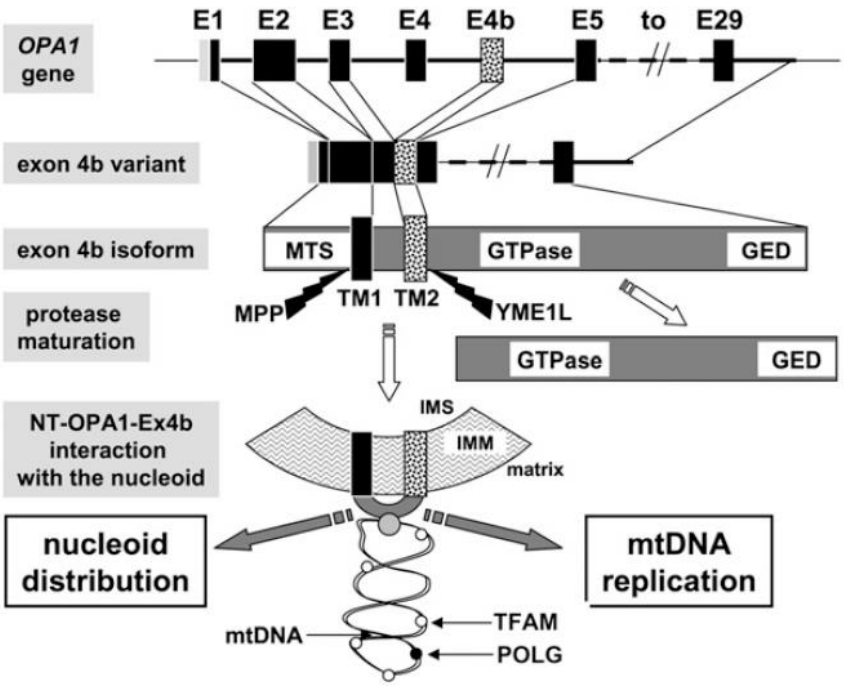

Figure 5-1 Mitochondrial nucleoid anchoring to the inner mitochondrial membrane via binding with OPA1

OPA1 is alternatively spliced to produce pre-mature isoforms containing exon 4b. These isoforms are further processed by OPA1 protease YME1L and the mature protein isoform acts to bind mitochondrial nucleoids to the IMM to facilitate mtDNA replication and nucleoid distribution (Reproduced from Elachouri *et al.*, 2011)

In addition, disruption of mitochondrial dynamics has been identified as a common hallmark of neurodegenerative disorders (Santel *et al.*, 2006; Kijima *et al.*, 2005; Zuchner *et al.*, 2004; Waterham *et al.*, 2007; Olichon *et al.*, 2003). This is particularly pertinent for DOA because mutations in *Opa1* may lead to a generalised disruption of mitochondrial fusion and increased fragmentation of the mitochondrial network (Zanna *et al.*, 2008). This disruption may impinge on quality control, inhibiting both mitochondrial content mixing and the distribution of nucleoids (Meeusen *et al.*, 2006; Detmer and Chan, 2007; Chen *et al.*, 2007). This hypothesis is based upon experimental observation that mitochondrial fusion results in the repopulation of ρ^0 cells through the slow migration of mtDNA/nucleoids in these fusion events (Legros *et al.*, 2004). Moreover, mitochondrial networks with excessive fragmentation have been found to contain at least one mtDNA/nucleoid per mitochondrial fragment. These observations imply that mtDNA/nucleoid

distribution may be a regulated process and that potential disruption of this process, perhaps through excessive mitochondrial fragmentation, may impact mtDNA number and distribution (Margineantu *et al.*, 2002). Strikingly, MFN2 dysfunction was shown to inhibit outer membrane fusion and lead to a decrease in mtDNA copy number further validating this hypothesis (Chen *et al.*, 2010; Vielhaber *et al.*, 2013). These observations imply a relationship between mitochondrial dynamics and mtDNA/ nucleoid maintenance, number and distribution which has yet to be investigated in primary DOA patient tissue.

To investigate this mechanistic relationship, we employed both Quant-iT™ PicoGreen® cytochemical and MitoTracker® Red CMXRos staining. The use of Quant-iT™ PicoGreen® has been used previously by Ashley *et al.* (2008) and Ylikallio *et al.* (2010) to determine both the relative number and size distribution of mtDNA/nucleoid molecules in primary cell models of mtDNA depletion due to pathological *POLG1* mutations in Alpers syndrome and a bitransgenic Twinkle/TFAM mouse model, respectively. Both studies presented a detrimental decrease in mtDNA molecule number, respectively.

Although Quant-iT™ PicoGreen® staining of live cells is less sensitive than anti-dsDNA antibodies, its advantages include a greater accuracy in quantifying nucleoid/mtDNA level (Ashley *et al.*, 2008). Live cell cytochemical staining also provides additional data on the distribution and morphology of these mtDNA molecules and bypass the necessity to fix the cells. The use of mitotracker to analyse the fragmentation of the mitochondrial network in DOA primary tissue is also a well validated technique and ideal for *in vitro* analysis (Zanna *et al.*, 2008; Agier *et al.*, 2012; Chevrollier *et al*., 2012).

The development of these confocal fluorescent assays has led us to investigate both mitochondrial fragmentation and the relative number and distribution of mitochondrial nucleoids. These parameters were measured in primary myotubes which are a tractable model system derived from quiescent satellite cells from patient muscle tissue. Advantages of this model include the ability to culture these satellite cells before myotube differentiation and to retain many of the biochemical traits of donor cells and mirror phenotypic traits which can be found in DOA+ and OA primary tissue (Thompson *et al.*, 1996; Bell *et al.*, 2010; Spinazzi *et al.*, 2008). These differentiated myotubes are also more biochemically related to patient muscle fiber than primary fibroblasts and myoblasts. This is particularly pertinent given the observation of COX deficiency and bioenergetic

failure revealed through histochemical staining of DOA+ patient muscle biopsies as a consequence of the clonal proliferation of mtDNA molecules with multiple deletions (Hudson *et al*., 2008; Amati-Bonneau *et al*, 2008.)

In parallel, primary differentiated myotubes with a pathological *WFS1* mutations were also quantified using this *in vitro* live cell assay. The presentation of a pathological phenotype due to mutations of *WFS1* is reminiscent of the many multi-systemic optic disorders normally associated with mitochondrial dysfunction such as DOA. However *WFS1* is housed within the endoplasmic reticulum and is not primarily a mitochondrial disorder.

The aim of this study was to quantify fragmentation of the mitochondrial reticulum in primary myotubes of patients diagnosed with DOA+ and OA and correlate these findings with the distribution of mtDNA molecules to detect a potential disturbed nucleoid distribution maintenance and number, which may play a role in the pathogenesis of DOA.

5.2 Materials and Methods

5.2.1 Patient cohort

Mitochondrial nucleoid distribution within the mitochondrial network was investigated using primary differentiated myoblasts, myotubes, derived from nine patients and three controls as described in **Table 5-1.** This study was supported by institutional approval and written informed consent was obtained from all patients.

Control Group	**Age**	**Gender**	**OA**	**Spastic Paraplegia**	**Myopathy**	**Deafness**	**Ataxia**	
MyoControl(1)	47	M	-	-	-	-	-	
MyoControl(2)	21	F	-	-	-	-	-	
MyoControl(3)	29	F	-	-	-	-	-	
DOA+ Group								***OPA1* Mutation**
MyoDOA+(1)	48	F	+	+	-	-	-	c.889C>T
MyoDOA+(2)	59	M	+	+	-	-	-	c.876-878 del (TGT)
MyoDOA+(3)	55	F	+	-	+	-	-	c.870+5g>a
MyoDOA+(4)	36	F	+	-	+	-	-	c.870+5g>a
OA Group								
MyoOA(1)	41	M	+	-	-	-	-	c.876-878 del (TGT)
MyoOA(2)	59	M	+	-	-	-	-	Exon 1-5 Deletion
MyoOA(3)	60	F	+	-	-	-	-	c.2713C>T
MyoOA(4)	65	M	+	-	-	-	-	c.2818+5g>a
***WFS1* Group**								***WFS1* Mutation**
WFS1(1)	36	F	+	-	-	+	+	c.409_424dup16

Table 5-1 Clinical characteristics of controls and optic atrophy patients with known pathogenic mutations.

5.2.2 Seeding of patient myoblasts and differentiation into myotubes

A 50 µg/ml collagen solution was prepared (Collagen: Life Technologies A10483-01) in filtered sterilised 20 mM acetic acid solution (Sigma-Aldrich). 1 ml of this collagen solution was added to a glass-bottomed confocal dish (Wilco) and left to incubate at room temperature overnight. The collagen solution was carefully aspirated and each dish was washed three times with autoclaved PBS solution (Oxoid) and used either immediately for myoblast cell seeding or left at 4^{o}C.

From a T25 flask, primary DOA and WFS1 myoblasts were seeded onto glass-bottomed confocal dishes (Wilco) as previously described (**Section 3.14.1.**) at a density of 75,000 cells/ dish. These cells were left to incubate overnight or until the cell density reached 50-70% confluence. Once this cell density threshold was achieved, the Skeletal Muscle Cell Growth Medium (Promocell) was aspirated from each dish and washed with PBS (Oxoid). Myoblasts were then incubated with Skeletal Muscle Differentiation Medium (Ready-to-use) (Promocell C-23061) for 24 hours before this media was aspirated and replaced with fresh differentiation medium. These cells were incubated in fresh differentiation medium every 2-3 days and primary myotubes were ready for imaging on day 6 of this protocol. Seeding and differentiation of myoblasts was performed by Dr. Florence Burté.

5.2.3 MitoTracker® Red CMXRos and Quant-iT™ PicoGreen® staining

On the day of imaging, cells were incubated with 1ml 3µl/ml stock Quant-iT™ PicoGreen® solution (Life Technologies) diluted in Skeletal Muscle Differentiation Medium (PromoCell: C-23061) for 1 hour at 37˚C. Thirty minutes mid-incubation of Quant-iT™ PicoGreen® stain, the staining medium was aspirated and 1ml of Skeletal Muscle Differentiation Medium containing 3µl/ml Quant-iT™ PicoGreen® (Life Technologiesnologies) and an optimised concentration of MitoTracker® Red CMXRos (50, 75 and 100nM) was added. Both Quant-iT™ PicoGreen® andMitoTracker® Red CMXRos were incubated for a further 30 minutes. This staining medium was aspirated and the cells were washed twice with PBS (oxoid) before they were added to DMEM (25mM glucose/phenol red free)(Gibco, Life Sciences) with 2% FBS ,1% Penicillin-Streptomycin and 25mM Hepes (All obtained from Sigma-Aldrich).

5.2.4 Optimisation of myotube image capture

Optimisation of MitoTracker® Red CMXRos loading, Quant-iT™ PicoGreen® staining and confocal image acquisition settings were required before standardised mitochondrial network morphology and mtDNA/nucleoid capture of primary myotubes was achieved. Initial attempts to load 75nM MitoTracker® Red CMXRos (as in **Section 4.2.3** for fibroblasts) and 3µl/ ml stock Quant-iT™ PicoGreen® (Life Technologies) with a specific cutoff threshold for HV settings resulted in both low level and saturated signal variation in both channels preventing accurate image capture (**Figure 5-2**). To minimise this variation, two control myotubes (MyoControl (1) and MyoControl (3)) were analysed under twelve different conditions for MitoTracker® Red CMXRos and four different conditions for Quant-iT™ PicoGreen® .

Briefly, to correct for signal variation using the Quant-iT™ PicoGreen® channel, myotubes were loaded with 3ul/ml stock Quant-iT™ PicoGreen® for 1 hour at 37ºC before confocal HV and laser power was adjusted and three myotubes were captured for analysis to determine the optimal acquisition settings as described in **Table 5-2**.

To correct for MitoTracker® Red CMXRos, myotubes were loaded with 50, 75 or 100 nM MitoTracker® Red CMXRos at 37ºC for 30 minutes before confocal HV and laser power was adjusted as described in **Table 5-2** for each concentration. Both Quant-iT™ PicoGreen® and MitoTracker® Red CMXRos signals were analysed using Huygens Essential Analyser (Scientific Volume Imaging, Hilversum, the Netherlands) to determine fluorescent signal intensity.

This analysis highlighted a greater variation in MitoTracker® Red CMXRos which led to either a saturated or an extremely weak signal which was problematic for image capture. In order to correct for this variation, myotubes were incubated with 75nM MitoTracker® Red CMXRos as previously described and HV was manually adjusted. A linear relationship exists between HV and signal fluorescent intensity and so MitoTracker® Red CMXRossignal was adjusted both to saturation and to the lower threshold of signal intensity to determine signal range. The mitochondrial network in each primary myotube line was captured 20% below the signal saturation threshold (**corrected condition**) to acquire the mitochondrial network in these cells. This signal was subsequently analysed with Huygens Essential Analyser (Scientific Volume Imaging, Hilversum, the Netherlands) and statistically assessed through a

Student's unpaired T-test of average mitochondrial length and volume to determine that there were no significant differences between control cells analysed (**Figure 5-2**)

	HV-Green	488-Green Channel (%)	HV-Red	561-Red Channel (%)
Original Settings	90	3	90	1
Condition 1	80	3	90	2
Condition 2	100	3	100	1
Condition 3	90	2	80	1
Condition 4	90	1	80	1

Table 5-2 Parameters used to analyse primary myotubes during image acquisition optimisation.

5.2.5 Mitochondrial network and nucleoid distribution and image acquisition

Excitation wavelength for MitoTracker® Red CMXRos and Quant-iT™ PicoGreen® were 561nm and 488nm, respectively. Primary myotubes were z-stacked with a section interval of 0.2um for 79 slices. Both the mitochondrial network (561nm excitation) and mtDNA/nucleoid (488nm excitation) were captured simultaneously. Laser power and PTM were carefully optimised to avoid both saturation and low level signal during image acquisition.

5.2.6 Image deconvolution

Following acquisition of live-cell images, the files were converted to TIFF format and each channel was stacked using ImageJ. ImageJ was also used to process these images by using the rolling-ball algorithm (Castle and Keller, 2007: Available at **rsb.info.nih.gov/ij/plugins/rolling-ball.html**) to average background intensity variation before the files were imported to Huygens Essential Software (Scientific Volume Imaging, Hilversum, the Netherlands) for deconvolution. Each channel was deconvolved independently with a standardised background threshold until confidence level approached 99% or the number of iterations approached 40.

5.2.7 Image analysis

Images were subsequently analysed with Huygens Essential Software (Scientific Volume Imaging, Hilversum, the Netherlands) using a standardised set of parameters for each channel (561nm channel (Mitotracker® Red CMXRos); Threshold 10%, Seed 11%, Garbage 40; 488nm channel (Quant-iT™ PicoGreen®); Threshold 8%, Seed 6%, Garbage 4. A region of interest (ROI) was selected in each cell analysed for each channel. The final analysis was corrected for the size of this ROI as a mean of standardisation for each cell measured.

A minimum of 12 myotubes were imaged for each primary myotube cell line ($N \leq 12$). Three parameters were quantified while measuring the morphology of the mitochondrial network: (1) Average length/volume, (2) total length/volume and (3) the number of fragments detected in the network. The total length/volume is the sum total of the length and volume of all mitochondrial fragments within the network of each cell. The number of fragments is the number of objects detected by Huygens Essential Software Object Analyser (Scientific Volume Imaging, Hilversum, the Netherlands) using optimised thresholds for detecting mitochondrial organelles in each cell analysed. The average length/volume is a metric calculated from the ratio between the total length/volume and the number of fragments of each cell. Similarly, the number and distribution of mtDNA/nucloids was quantifed using Quant-iT™ PicoGreen® staining using an optimised signal threshold.

The number, mean and standard error of the mean were generated from the analyses of these parameters calculated for each myotube disease group analysed. These parameters were corrected by there respective cell's ROI. The number of objects was also corrected by the ROI and distribution was calculated by determining Log_{10} of the number of objects defined between an upper and lower threshold of object size.

5.2.8 Statistical analysis

Statistical analysis was performed with excel (Microsoft, Reading, UK) and Graphpad™ V. 5 (Graphpad software). Comparison between groups was carried out using a Student's unpaired t-test.

5.3 Results

5.3.1 Optimisation of myotube image acquisition

Two control myotube lines were analysed and their signal fluorescence quantified in either corrected (refer to **Section 5.2.4**) or uncorrected conditions. This analysis showed that there were no significant differences between quantifying each individual line under corrected or non-corrected conditions. There appeared to be a mildly greater variation along the Z-axis (volume) in uncorrected values. Therefore, it was decided to analyse all myotube lines under a corrected threshold to ensure no information loss due to signal variation (**Figure 5-2**).

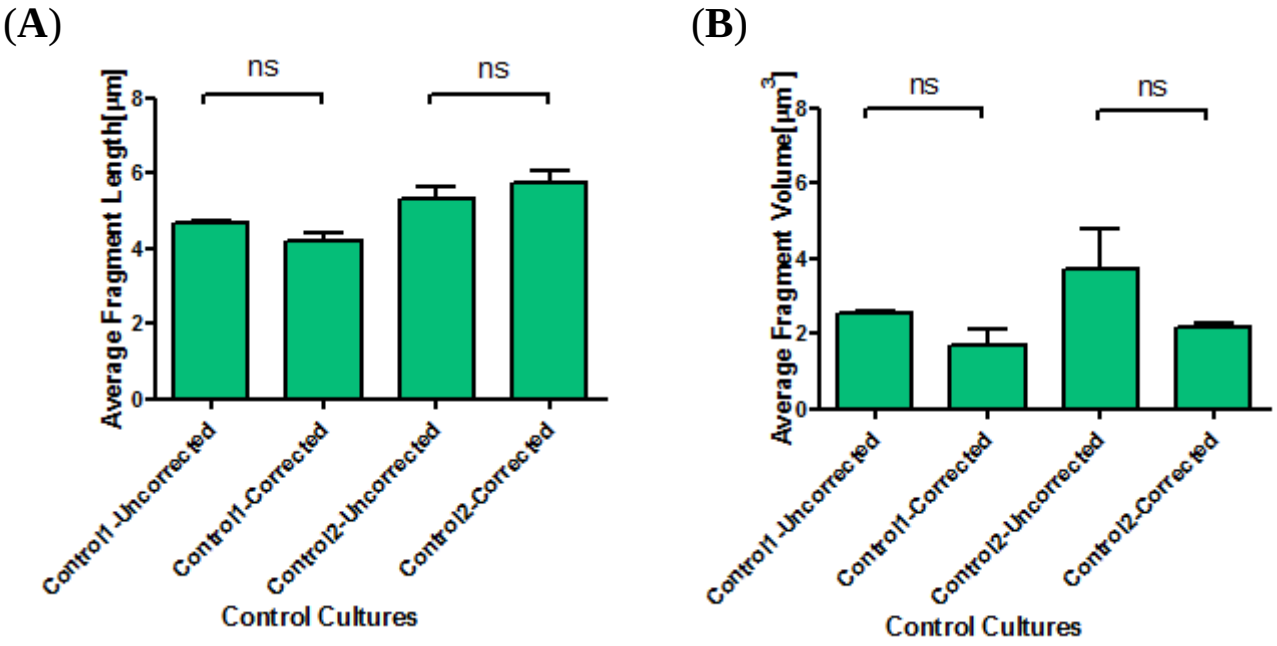

Figure 5-2 Optimisation of mitochondrial network capture in primary control myotubes.

The mitochondrial network was captured and quantified in the same myotube control line manually adjusted 20% below the point of saturation. Average fragment length (A) and average fragment volume were calculated (B) for each cell ($n \geq 3$) in two different control cell lines (Control1 and Control2). The signal of the mitochondrial network was captured and quantified in each myotube line using the same standardised settings throughout. Graphs were statistically compared using a Student's unpaired t-test

5.3.2 Mitochondrial network analysis in myotubes from DOA patients.

5.3.2.1 Mitochondrial network variation analysis between control cell lines

Total mitochondrial length was determined in each of the three primary myoblast lines, myoControl(1), myoControl(2) and myoControl(3) (n = 33, **Figure 5-3**). The greatest total length was observed in line myoControl(1) (Mean = 432.11, SEM = 25.14) and the least total length was detected in line myoControl(2) (Mean = 278.97, SEM = 37.16). A statistically significant difference was noted between total length of these two myoblast lines (P = 0.0023; $p < 0.01$) using a Student's unpaired t-test. No significant difference was detected between lines myoControl(1) and myoControl(3) (p = 0.1569) or lines myoControl(3) and myoControl(2) (p = 0.2372).

Measurement of total mitochondrial volume indicated that the greatest total volume was found in primary line myoControl(1) (Mean = 409.13, SEM = 45.09) and the least total volume was found in myoControl(2) (Mean = 163.97, SEM = 40.01). Statistical comparison between these two lines was significant (p = 0.0006; $p < 0.001$) which is consistent with the previous data generated for total mitochondrial length. Again, no significant difference in total volume was detected between myoControl(2) and myoControl(3) (p = 0.5486), however a significant difference was detected between lines myoControl(1) and myoControl(3) (p = 0.0059, $p < 0.01$).

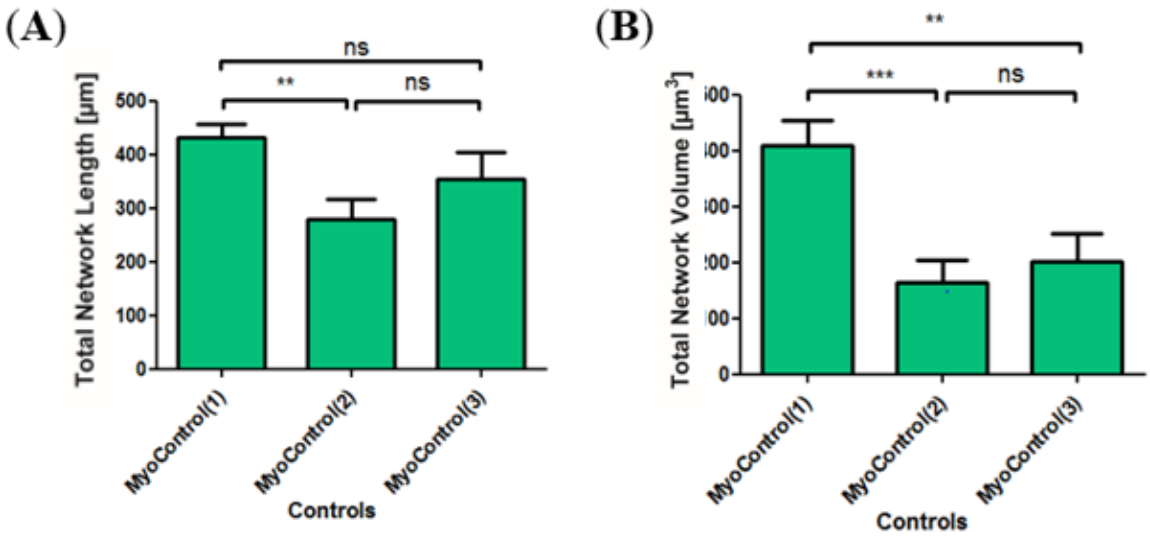

Figure 5-3 Variability in total network morphology between control myotube lines

Total mitochondrial length (A) and total volume (B) were measured using Huygens Object analyser module in control myotubes. Error bars represent the standard error of the mean (SEM). ns non-significant, ** $p \leq 0.01$ and *** $p \leq 0.001$ using a Student's unpaired t-test against controls ($n \geq 10$).

Comparing the average mitochondrial length between myoControl(1), myoControl(2) and myoControl(3) (**Figure 5-4B**), primary line myoControl(1) had the greatest average value (Mean = 3.88, SEM = 0.24) while myoControl(3) was of least average length (Mean = 3.20, SEM = 0.18) with a statistical significance ($p< 0.001$). The average length of myoControl(3) however was not significantly different from myoControl(2) (P = 0.0794). This is consistent with previous measured parameters.

Investigation of average mitochondrial volume reveals a similar trend (**Figure 5-4C**). The greatest average mitochondrial volume is found in line myoControl(1) (Mean = 3.96, SEM = 0.74) while myoControl(2) has the least mitochondrial volume (Mean = 1.86, SEM = 0.41). This difference in average volume between myoControl(1) and myoControl(2) is statistically significant (P = 0.0247, $p < 0.01$) while the difference in average volume between myoControl(3) and myoControl(2) is not significant (P = 0.8133).

The total number of mitochondrial fragments was also determined in myoControl(1), myoControl(2) and myoControl(3) (**Figure 5-4A**). Again the same trend in variability was seen with myoControl(1) having the greatest number of mitochondrial fragments (Mean = 115.79, SEM = 8.39) and myoControl(2) having the least number of fragments (Mean = 81.63, SEM = 10.77). Statistical significance was noted between lines myoControl(1) and myoControl(2) ($p = 0.0197$; $p < 0.05$) while no statistical significance was found between lines myoControl(1) and myoControl(3) ($p = 0.0695$) and lines myoControl(2) and myoControl(3) ($p = 0.5905$).

Overall, Variations between cell lines were more obvious when analysing volume parameters compared with length parameters. Also, total mitochondrial network was very similar between MyoControl(2) and MyoControl(3), whilst Myocontrol(1) appeared as an outlier compared to the other cell lines. This difference could be due to the older age or the gender of the healthy control and should be included to take in account the variations due to age and gender differences when comparing with the patient cell lines.

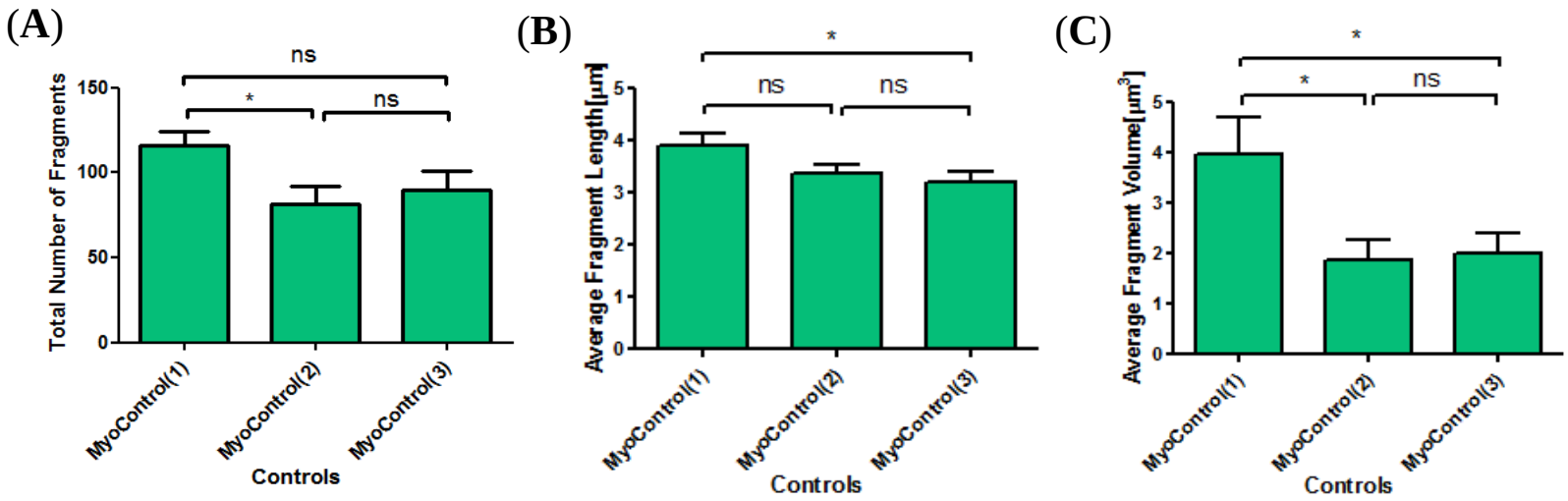

Figure 5-4 Variability in mitochondrial fragment morphology between control myotube lines

Average number of mitochondrial fragments (A) were measured using Huygens Object analyser software in imaged control myotubes. Average fragment length (B) and average fragment volume (C) were calculated as described in section **5.2.6**. Error bars represent the standard error of the mean (SEM). ns non-significant, * $p \leq 0.05$ using a Student's unpaired t-test against controls ($n \geq 10$).

5.3.2.2 Mitochondrial fragmentation analysis in patient primary myotubes

Mitochondrial network analysis was visualised using the mitochondria specific stain MitoTracker® Red CMXRos in all the cell lines in the myotube cohort and morphology was compared between each disease group. **Figure 5-5** shows representative images for each disease group.

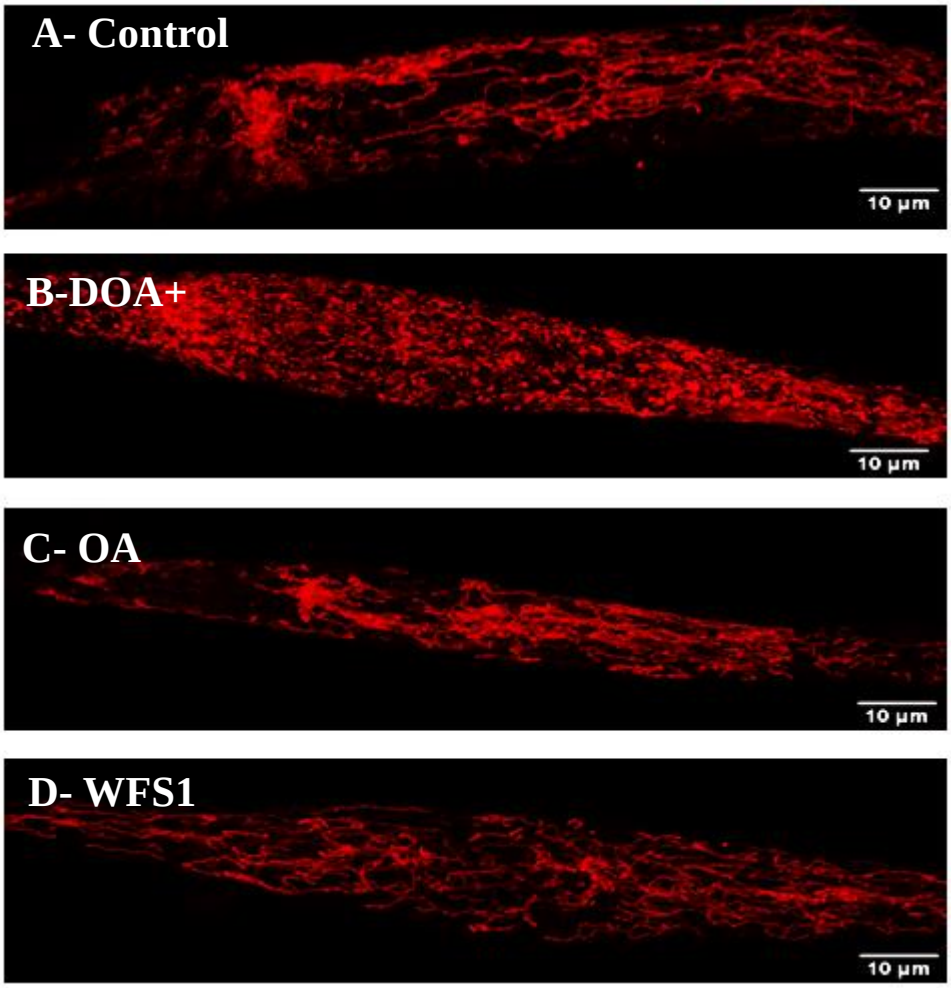

Figure 5-5 Representative image of primary myotubes from control, DOA+, OA and WFS1 patient-derived cell lines

Staining of the mitochondrial network was performed with MitoTracker® Red CMXRos (Molecular Probes, Life technologies). Images of primary myotubes were captured using (Nikon) Ti confocal microscope objective (x63) followed by Computerised Image deconvolution using Huygens Essential deconvolution wizard. Representative images of a myotube from control (A), myotubes from DOA+ (B), OA (C) and WFS1 patients (D). Scale bars represent 10µm.

Total network length was increased in all DOA+ patient myotubes from 1.5 to 2-fold (**Appendix Figure F-1A**). Consequently, the DOA+ patient group showed an overall total network extension compared to controls. In the OA group, three out of the four patients showed very mild total mitochondrial network length increase, with an average not significantly different to controls and significantly lower than in the DOA+ group. The WFS1 patient cell line did not show gross changes in total mitochondrial network length compared with control and OA groups (**Figure 5-6A**).

Among the cell lines derived from DOA+ patients, total network volume showed more variation leading to an overall mean similar to the control group (**Appendix Figure F-1B**). In the OA group, three out of four cell lines showed a very mild decrease or normal total mitochondrial network volume. Strikingly, MyoOA(4) showed an overly increased total mitochondrial network. WFS1 did not present any gross changes in total network volume (**Figure 5-6B**).

Despite a significant increased number of fragment in all cell lines, mitochondria were not fragmented in all DOA+ myotube cell lines (**Appendix Figure F-2A-B**) as indicated by the average fragment length parameter. Despite an overall indication of no fragmentation in the OA group (**Figure 5-7A-B**), MyoOA(1) was very fragmented (**Appendix Figure F-4B**).

Average mitochondrial volume did not show significant changes in each disease group when compared to controls (**Figure 5-7C**). This is mainly due to a high variation between myotubes derived from DOA+ patients for the DOA+ group (**Appendix Figure F-2C**) and for the OA group it is mainly due to the high increase in average volume in OA cell line, MyoOA(4), whilst the other cell lines did not show changes (**Appendix Figure F-4C**).

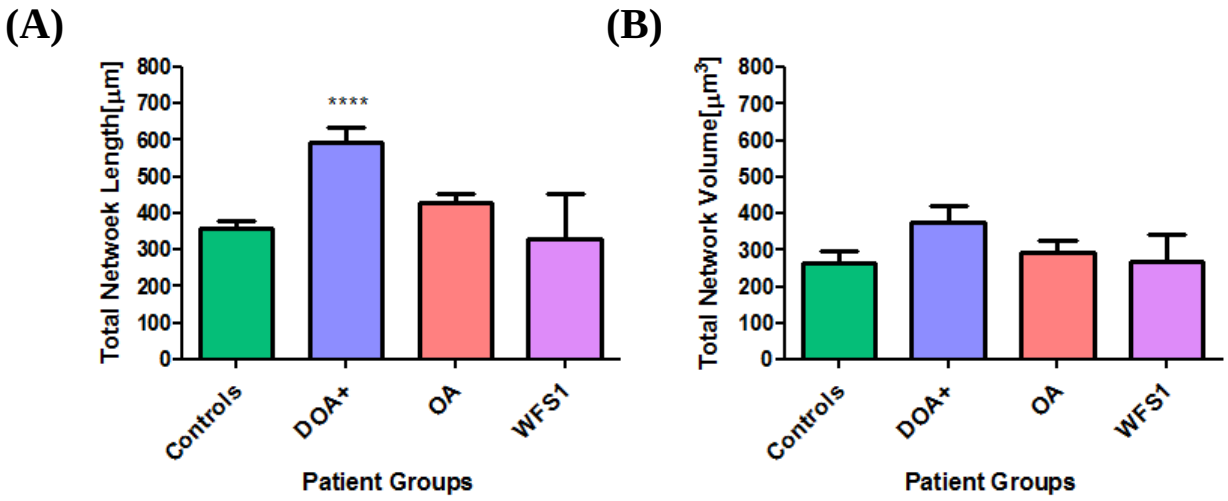

Figure 5-6 Total length and volume measurements of the mitochondrial network in patients and control primary myotubes

Total mitochondrial length (A) and total volume (B) were measured using Huygens Object analyser module in myotubes derived from different optic atrophy and control groups. Error bars represent Standard Error of the Mean (SEM). ns non-significant, **** $p \leq 0.0001$ using a Student's unpaired t-test against controls ($n \geq 12$).

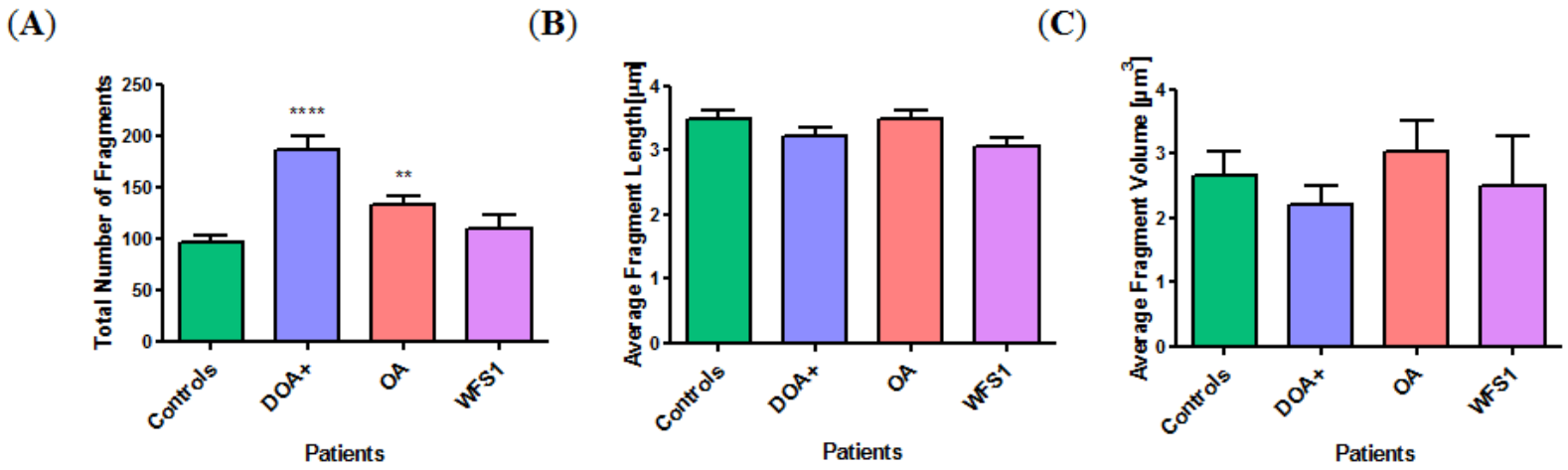

Figure 5-7 Mitochondrial fragmentation of the mitochondrial network in patient and control primary myotubes.

Average number of mitochondrial fragments **(A)** were measured using Huygens Object analyser software in fibroblasts imaged. Average fragment length **(B)** and average fragment volume **(C)** were calculated as described in section **5.2.6.** Error bars represent the standard error of the mean (SEM). ** $p \leq 0.01$, and **** $p \leq 0.0001$ using a Student's unpaired t-test against controls ($n \geq 12$).

5.3.3 Mitochondrial nucleoid distribution in myotubes from optic atrophy patients

Investigation of nucleoid distribution was conducted concurrently with mitochondrial fragmentation analysis in DOA+, OA and Wolfram syndrome primary myotubes using DNA staining followed by confocal microscopy and parametric image analysis (**Figure 5-8**). Staining with the DNA-specific dye Quant-iT™ PicoGreen® ® allowed the measurement of mitochondrial nucleoid size distribution and their object number within cells.

The Object Analyzer module from Huygens software allowed the measurement of volume of each DNA object within a specific region of interest (ROI) of a cell. Each object volume was standardised by the cell's ROI area and then expressed as a logarithmic function. Resulting size ranges were divided into bins and expressed as percentage per analysed cell. The number fragment within each bin from each cell was averaged ($n \geq 12$ cells) for each cell line. The resulting distribution of object size standardised to respective ROIs was then expressed as a percentage number fragment /cell line /size bin and represented as a distribution graph. The result from each cell line was then average per disease group (**Figures 5-9 to 5-11**).

The modified Kolmogorov-Smirnov test can be used as a distribution normality test. This statistical test indicated that the percentage nucleoid distribution in each group was not normally distributed (KS test for normality: Control, $p > 0.0001$; DOA+, $p > 0.0001$, OA, $p > 0.0001$; WFS1, $p > 0.0001$; **Table 5-3**). This was represented by the presence of a slight tail for highest size ranges for all disease groups.

The non parametric Mann-Whitney test comparing overall size distribution in heathy controls with those from patient cell lines revealed no significant difference (DOA+: $p = 0.8455$; OA: $p = 0.7290$ and WFS1: $p = 0.7869$; **Table 5-3**). .

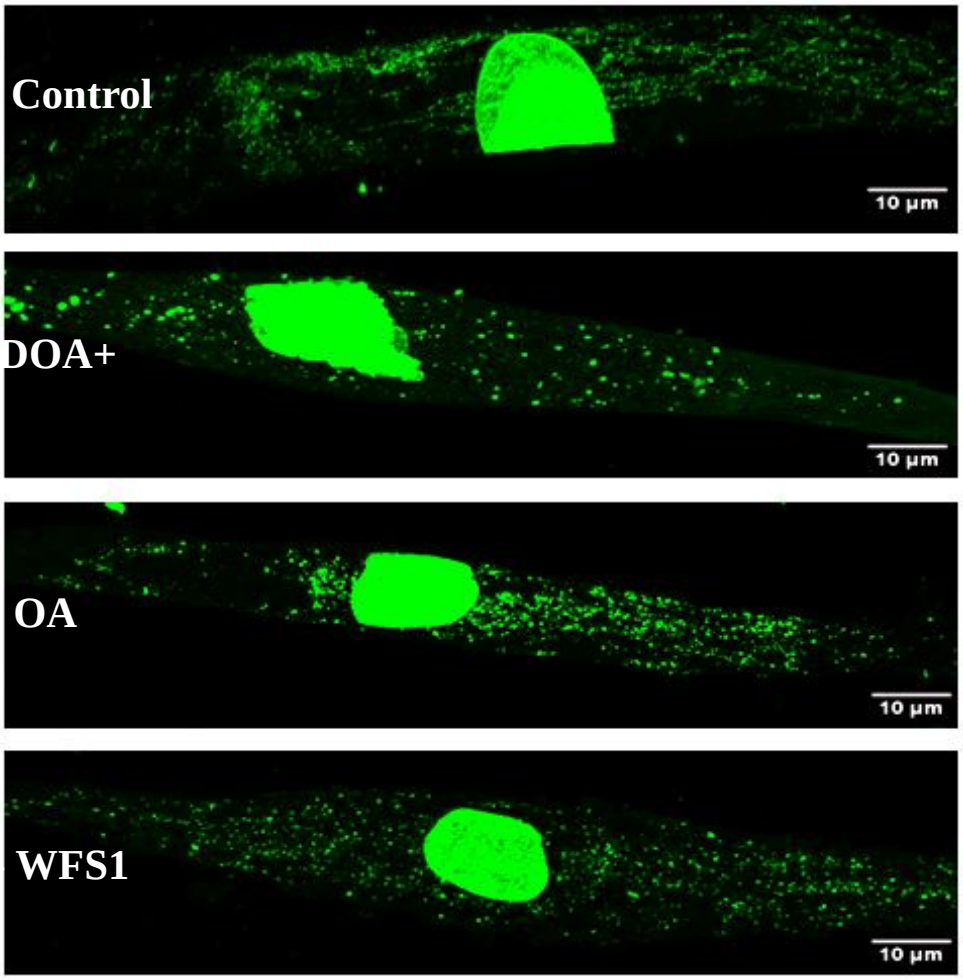

Figure 5-8 Maximum intensity projection of Quant-iT™ PicoGreen® staining within primary myotube lines

Staining of DNA/nucleoid molecules was performed with PicoGreen® (Molecular Probes, Life technologies). Images of primary myotubes were captured using Nikon Ti confocal microscope objective (x63) followed by Computerised Image deconvolution using Huygens Essential deconvolution wizard. Representative images of a myotube from control (A) and myotubes from DOA+ (B), OA (C) and WFS1 patients (D). Scale bars represent 10µm.

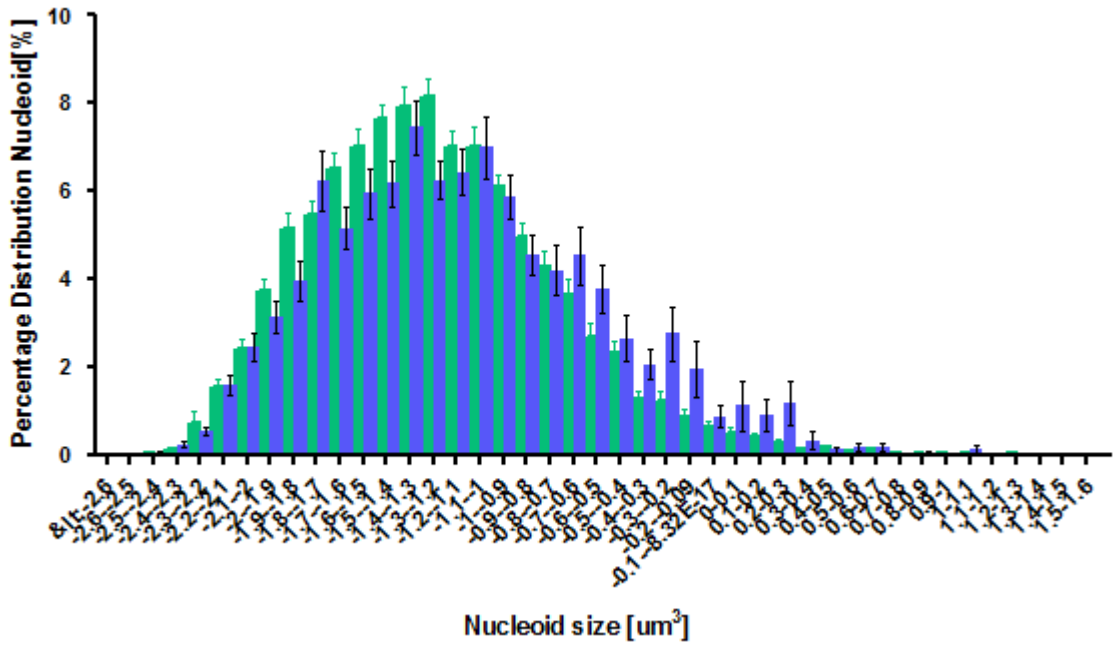

Figure 5-9 Distribution of mtDNA\nucleoid size in DOA+ (A) and control (B) primary myotubes

Percentage distribution of nucleoid size in DOA+ patient myotubes (blue bars) compared with the distribution of nucleoids found in the control group (green bars). All values were corrected for unit area and percentage distribution of nucleoids in each cell analysed. Error bars represent the standard error of the mean (SEM). Statistical analysis found in **Table 5-3.**

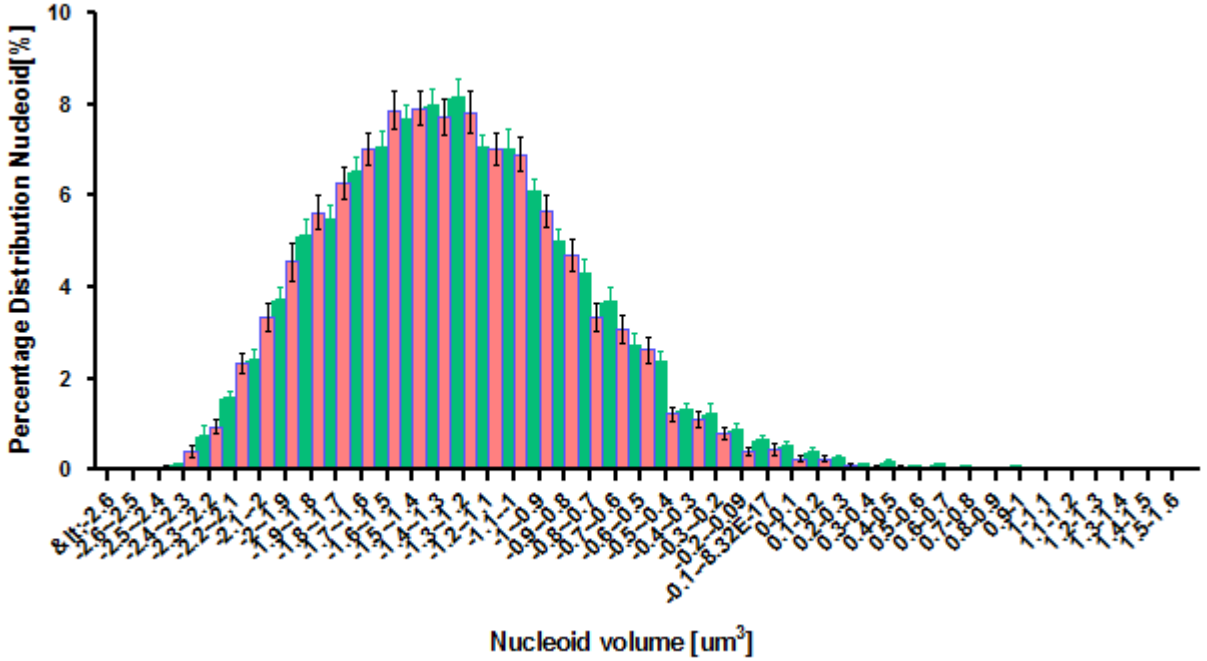

Figure 5-10 Distribution of mtDNA/nucleoid size in OA (A) and control (B) primary myotubes

Percentage distribution of nucleoid size in OA-derived myotubes (pink bars) compared with the distribution of nucleoids found in the control group (green bars). All values were corrected for unit area and percentage distribution of nucleoids in each cell analysed. Error bars represent the standard error of the mean (SEM). Statistical analysis found in **Table 5-3.**

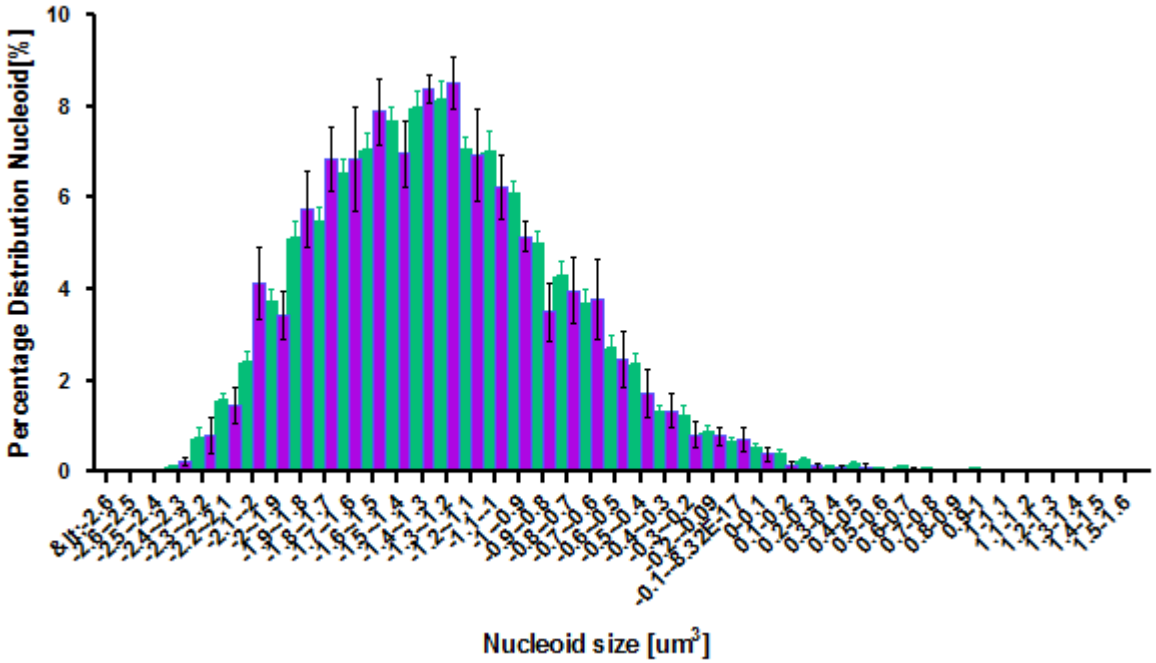

Figure 5-11 Distribution of mtDNA/nucleoid size in WFS1 (A) and control (B) primary myotubes

Percentage distribution of nucleoid size in WFS1-derived myotubes (purple bars) compared with the distribution of nucleoids found in the control group (green bars). All values were corrected for unit area and percentage distribution of nucleoids in each cell analysed. Error bars represent the standard error of the mean (SEM). Statistical analysis found in **Table 5-3.**

	Kolmogorov-Smirnoff test of normality			
	Control	**DOA+**	**OA**	**WFS1**
Passsed Normality:	<0.0001	<0.0001	<0.0001	<0.0001
	No	No	No	No
	Mann-Whitney test of significance			
		DOA+	**OA**	**WFS1**
Vs Controls:		0.8456	0.729	0.7869

Table 5-3 Statistical analysis of nucleoid/mtDNA distribution in control, DOA+, OA and WFS1 primary myotubes

A Kolmogorov –Smirnoff test was used to quantify deviance from normal distribution of mitochondrial nucleoids in control (N = 33), DOA+ (N = 47), OA (N = 45) and WFS1 (N =10) groups. A Mann –Whitney test was used to measure any significant bias in percentage nucleoid distribution between control and patient group. ($p \leq 0.05$ is * significance; $p \leq 0.01$ is ** significance, $p \leq 0.001$ is *** significance, $p \leq 0.0001$ is **** significance).

Despite no statistical difference between healthy controls and disease groups, **Figure 5-9** shows a slight shift in size distribution towards the right indicating a slight increase in nucleoid size. Analysis of size distribution within each individuals, which was carried out by Dr Ian Wilson, detected that the shift was mainly due to one patient (MyoDOA+ (2)) who presented with significantly bigger mitochondrial DNA clumps than other patients (**Appendix G-1 and G-2**).

In addition to the analysis of mitochondrial nucleoid size distribution, total number of nucleoid objects in ROI within each cell was also measured and averaged per cell line and then by disease group. This analysis revealed a marked decrease in object numbers in the individuals MyoDOA+(2) ($p<0.0001$), MyoDOA+(3) ($p = 0.0003$) and MyoDOA+(4) ($p = 0.0205$) (**Appendix Figure G-3**). Overall nucleoid number was then statisticaly reduced in the DOA+ group. There was greater variation in the OA group with a proliferation of objects detected in MyoOA(2)($p = 0.0246$) and a depletion in MyoOA(4) (Pp = 0.0012) (**Appendix Figure G-3**), leading to a similar trend overall in the OA group compared to the healthy control group (**Figure 5-12**). The cell line derived from the WFS1 patient had normal numbers of mtDNA objects/area analysed ($P = 0.2189$) (**Figure 5-12**).

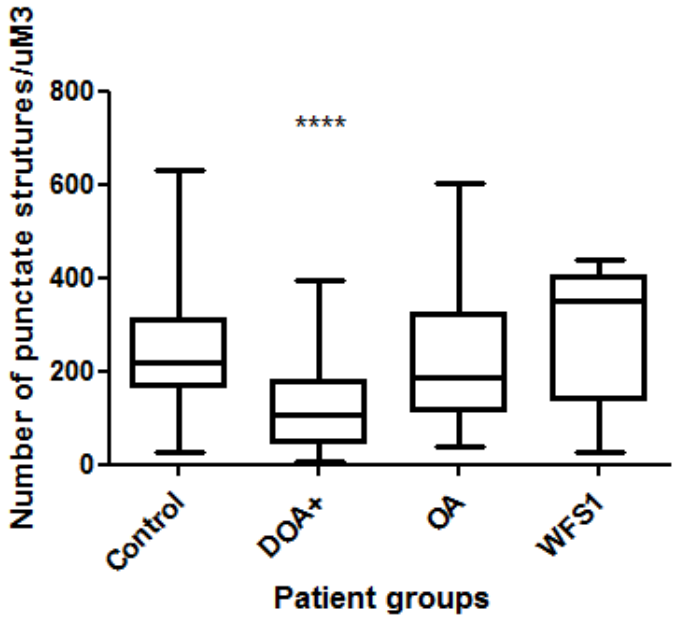

Figure 5-12 Total number of mtDNA objects detected per unit area of cell analysed.

The mean of the number of nucleoid/mtDNA objects detected per unit area of the cell in DOA+ (n = 47), OA (n = 45) and WFS1 (n = 10) was quantified and compared against control (n = 33). Error bars represent the standard error of the mean. *** $P \leq 0.001$ using a Student's unpaired t-test.

5.3.4 Mitochondrial nucleoid distribution within mitochondrial network in patients with optic atrophy

To investigate the distribution of nucleoids within the mitochondrial network (**Figure 5-13**) two parameters were analysed, 'Total number of nucleoids/ mitochondrial fragment' and 'Total number of nucleoids/ total mitochondrial length'.

The first parameter indicated a non-significant difference in the number of nucleoids per mitochondrial fragment between control, OA ($p = 0.0780$) and WFS1 ($p = 0.8306$) groups. A significant decrease in the number of nucleoids/mitochondrial fragment was detected in the DOA+ group ($p < 0.0001$), suggesting that each mitochondrial fragment contained significantly less nucleoids in the DOA+ group than in the control group (**Figure 5-14A**).

The second parameter 'Total number of nucleoids/ total mitochondrial length' also indicated a significant decrease in the number of nucleoids within the 'DOA+' group ($P < 0.0001$). A significant decrease in the number of nucleoids distributed along the total mitochondrial length was also detected in the OA group when compared against controls ($p < 0.0009$) while the number of nucleoids/ total length was non-significant for the WFS1 group ($p = 0.3702$) (**Figure 5-14B**).

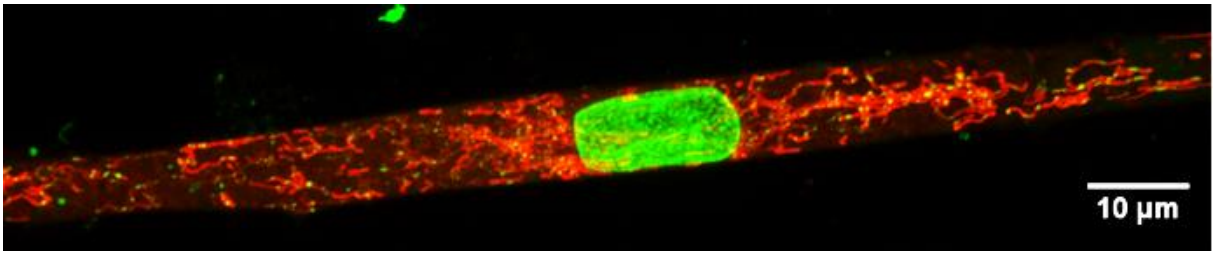

Figure 5-13 Mitochondrial DNA distribution within the mitochondrial network

Composite image of combined MitoTracker® Red CMXRos and Quant-iT™ PicoGreen® ® staining illustrating the mtDNA/nucleoid distribution (green) within the mitochondrial network (red) of a representative DOA+ primary myotube

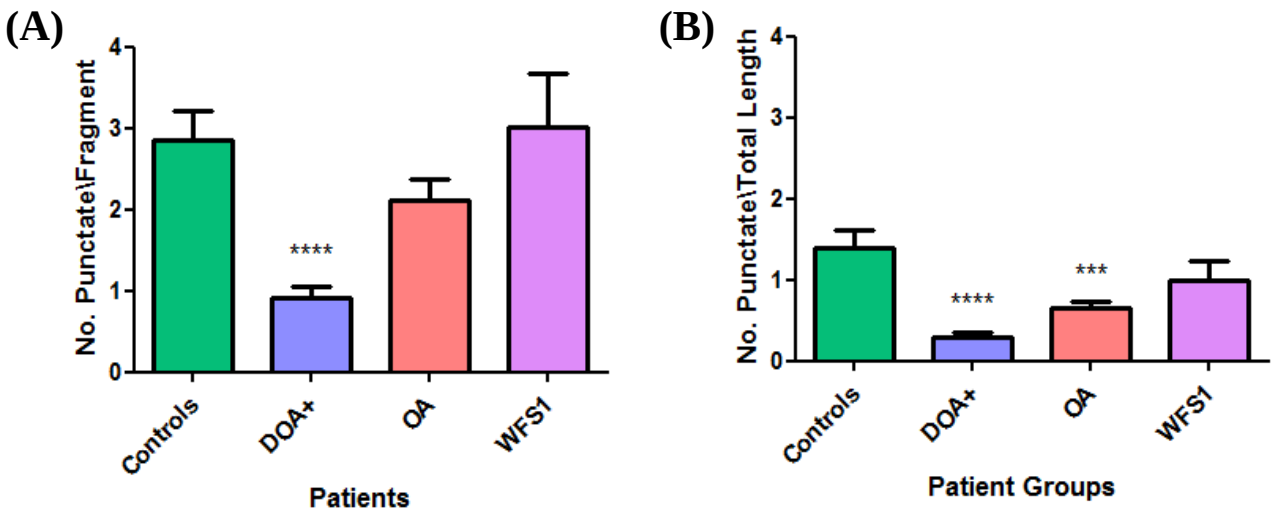

Figure 5-14 Quantification of the number of nucleoid\ mitochondrial fragment and the number of nucleoids\total mitochondrial length.

(A) The mean of the number of nucleoid objects corrected against the number of mitochondrial fragments in each cell was quantified per group, Control (N=33); DOA+ (N= 47); OA (N= 45); *WFS1* (N= 10). DOA+, OA and WFS1 groups were statistically compared against control. (**B**)The total number of nucleoid objects corrected against the total mitochondrial length in each cell was also quantified per group; Control (N = 33); DOA+ (N = 47); OA (N = 45); *WFS1* (N = 10) and statistically compared against control. A Student's unpaired t-test was used in all statistical analyses to measure significance. ($P < 0.05$ is non-significant; $P \leq 0.05$ is * of significance; $p \leq 0.01$ is ** significance; $p \leq 0.001$ is *** significance, $P \leq 0.0001$ is **** significance.

5.4 Discussion

5.4.1 Mitochondrial network fragmentation in DOA+ and OA patient myotubes

The present study indicated increased fragmentation of the mitochondrial network in DOA+ and OA myotubes, however no significant morphological difference was detected in Wolfram syndrome myotubes. This increase in mitochondrial fragmentation in DOA was consistent with previous reports (Chen *et al.*, 2005; Agier *et al.*, 2012). In addition, greater fragmentation was detected in the DOA+ network when compared with mitochondria from the OA network, an observation which was consistent with the analysis of primary fibroblasts from DOA+ and OA patients (**Section 4.3.3).** Consistently, a similar trend between fibroblast and myotube lines from both cohorts of patients was detected with total mitochondrial length. Although trends were similar, more obvious changes in morphology were observed in DOA fibroblasts compared with controls than in the myotube study. This might be more related to the sample size included in the respective cohorts than cell type related (Fibroblast study: n=200, Myotube study: n~46), although this hypothesis can not be neglected.

As discussed in the previous chapter in fibroblast cell lines (**Section 4.4.2**), mitochondrial expansion and fragmentation in DOA cell lines is in agreement with experimental validation studies performed by *Agier and colleagues* (2012) who also found an increased aspect ratio score indicating greater total mitochondrial length when compared against controls. This increase in total length was not attributed to OPA1 or DRP1 steady-state (Agier *et al.*, 2012) but instead may be a compensatory mechanism due to *Opa1* mutations. Mutated *OPA1* may result in disrupted cristae, impaired mitochondrial dynamics efficiency and a reduced efficiency to assemble respiratory chain complexes and supercomplexes (Cogliati *et al.*, 2013). Although the study in fibroblasts did not give evidence of it, this may culminate in a reduced rate of ATP production (Zanna *et al.*, 2008), however in view of recent reports linking OPA1 and mitochondrial maintenance, this remodelling of mitochondrial network might be associated with remodelling of mitochondrial nucleoid structure and numbers.

5.4.2 mtDNA size distribution is mildly affected in DOA+ myotubes associated with marked mtDNA nucleoid depletion

Previous experimental endeavours in the field have quantified the level and/or distribution of mtDNA/nucleoids both in primary human lines and animal models of mtDNA disturbance. In this study, a significant depletion of total mtDNA/nucleoids was found in the DOA+ group while no significant change in level was found in either OA or WFS1 primary myotubes. This observation is consistent with OPA1/MFN1 and two mouse models in which disruption of either outer or inner mitochondrial membrane fusion can result in both mtDNA depletion and multiple mtDNA deletions (Chen *et al.,* 2010; 2012). It is also consistent with data obtained from mouse embryonic fibroblasts (MEFS) showing that increased mitochondrial fragmentation and reduced fusion efficiency could result in a depletion of nucleoids and mtDNA content (Chen *et al.*, 2007).

MtDNA instability can also arise secondary to pathogenic mutations in *POLG,* a core mtDNA replication factor found within the nucleoid structure, *TFAM,* a peripheral factor involved in packaging and stability of mtDNA and *Twinkle,* a mitochondrial helicase essential for mtDNA replication. These constituents of the mitochondrial nucleoid all demonstrated a marked depletion of mtDNA either in animal models or primary patient-derived tissues. (Ashley *et al.*, 2008; Dai *et al.*, 2013; Milenkovic *et al.*, 2013; Larsson *et al.*, 1998; Ekstrand *et al.*, 2004 ; Sanchez-Martinez *et al.,* 2012; Matsushima and Kaguni, 2007). Based on these observations, it is therefore not surprising that a subset of *OPA1* mutations found in the GTPase domain may disrupt mtDNA maintenance and lead to a depletion of mtDNA molecules.

The experiments conducted in the present study have not only quantified the mtDNA/nucleoid population, but they have also demonstrated the number of mtDNA/nucleoids relative to both the size and number of fragments within the mitochondrial network. Our data indicate a severe depletion of mtDNA/nucleoids coupled with excessive mitochondrial fragmentation in DOA+ primary myotubes. Quantification of mtDNA/nucleoids relative to the total length and number of fragments within the mitochondrial network also showed this depletion in the DOA+ mitochondrial network. No significant difference in nucleoid number per total fragments or total mitochondrial length was detected in either OA or WFS1 primary myotubes. Quantifying mtDNA number by this

technique is more semiquantitative than RTqPCR, however, RTqPCR analysis conducted by a colleague subsequenct to this analysis in myoblasts confirmed a trend for mitochondrial depletion (unpublished).

Quantification of the percentage distribution and size of nucleoid foci and statistical analysis using a Mann-Whitney test for non-normal distribution indicated there was no disruption of nucleoid morphology (clumping) found in DOA+, OA and WFS1 myotube groups. A decrease in the number of detectable nucleoids without a shift in nucleoid distribution (clumping) was noted in primary fibroblasts with Alpers syndrome (Ashley *et al.*, 2008). This may indicate that DOA+ mtDNA/nucleoids may generally deplete by a similar mechanism. The existence of this mechanism warrants further investigation. A second hypothesis to explain this observation includes the topological status of these mtDNA molecules. *He and Colleagues* observed a decrease of the cytochemical Quant-iT™ PicoGreen® staining upon silencing of ATAD3 (He *et al.*, 2007). They concluded that although Quant-iT™ PicoGreen® is a useful cytochemical stain for marking mtDNA, the signal intensity is dependent on whether the mtDNA molecule is present in a relaxed or supercoiled state. A relaxed mitochondrial state results in a greater uptake of Quant-iT™ PicoGreen® and produces a signal of greater intensity, whereas supercoiled mtDNA molecules do not take up Quant-iT™ PicoGreen® as efficiently and therefore, they produce a lower intensity stain. Further investigation would require separation and identification of topoisomerases through a 1D or 2D agarose gel electrophoresis which would determine the supercoiled state of mtDNA in a qualitative manner. Overall, it may be that *OPA1* mutations lead to a disruption of mtDNA structure, which could have consequences for both mitochondrial transcription and replication rates. Both hypotheses suggest a defect in mtDNA homeostasis.

Analysis of mtDNA/nucleoid distribution in individual myotube lines found both mild clumping and a reduction in the total number of mtDNA/nucleoids in MyoDOA+(2). Mitochondria found in this line were significantly larger than controls, with longer average length and volume, consistent with possible swelling. This clumping and abnormal mitochondrial morphology may be due to an impairment of fusion caused by abnormal OPA1 processing and further investigations are needed. Impaired mitochondrial fusion in MEFs has

previously been linked with altered nucleoid distribution and morphology, and these abnormalities likely contribute to the observed mtDNA depletion (Chen *et al.*, 2007).

Our results are also consistent with the work by Elachouri and colleagues who showed a skew in mtDNA/nucleoid distribution towards a subpopulation of nucleoids with higher fluorescent intensity, indicative of either an increase in nucleoid size or nucleoid clumping in OPA1 exon 4b silenced Hela cells. These observations also agrees with the overexpression of TFAM or Twinkle which has been attributed to an increase of nucleoid size, however this increase in Quant-iT™ PicoGreen® fluorescence may also be a consequence of a shift in distribution towards increased clumping.

Analysis of *WFS1* myotubes, as a disease control, showed no significant difference in the number of nucleoids with respect to each mitochondrial fragment or with respect to the total mitochondrial length. Therefore, it would appear that, at least for this *WFS1* primary myotube line, the c.409_424dup16 mutation does not have a direct effect on mitochondrial fragmentation or nucleoid distribution within the network.

5.4.3 Conclusion

Consisent with our previous study using patient-derived *OPA1* fibroblasts, mitochondrial fragmentation was more pronounced in DOA+ patients. This was accompanied by a decrease in mitochondrial DNA objects suggesting a depletion in nucleoids/mitochondria along the mitochondrial network, and this could possibly be due to an impairment of fusion. This observation emphasises the biochemical disparity between the dominant-negative effect of *OPA1* misense mutations compared with mutations, such as deletions and slice site mutations, which result in haploinsufficiency. Interestingly, myotubes derived from a patient carrying a pathogenic *WFS1* mutation (c.409_424dup16) did not display aberrant mitochondrial morphology or nucleoid distribution when compared with controls. This would indicate that the pathogenic mechanisms linked to this specific *WFS1* mutation is not directly related with impaired mitochondrial dynamics or abnormal nuceloid distribution within the mitochondrial network.

Chapter 6

Novel Homozygous *OPA1* Mutation in a Consanguineous Israeli Family

6.1 Introduction

Infantile mitochondrial encephalopathy and congenital hypertrophic cardiomyopathy are defined as a group of primary mitochondrial heterogenous disorders which present with severe OXPHOS impairment primarily in patient neuronal tissue (cerebellum, spinal cord, brain stem, thalamus, basal ganglia) but also in heart and liver. These disorders usually manifest either in the prenatal stage or in the first year of life and can manifest with severe neurological, hepatic and respiratory disturbances (Uziel *et al.,* 2011). Individually rare, disorders of the OXPHOS system affect up to 1 in 5,000 individuals in the European population (Thorburn *et al.,* 2004).

The underlying genetic aetiology of these disorders is complex with many pathogenic variants recently discovered in both mitochondrial and nuclear encoded OXPHOS subunits, assembly factors of OXPHOS, factors which affect mtDNA replication and maintenance and factors involved in mitochondrial translation **(Table 6-1)**. Pathogenic variants which affect mtDNA replication and maintenance have been shown to either cause a severe depletion of mtDNA copy number or a proliferation of mtDNA deletions associated with an inherent error in replication (Naviaux *et al.,*1999; Naviaux and Nguyen, 2004; Spinazzola *et al.,* 2006; Elpeleg *et al.,* 2005; Ghezzi *et al.,* 2010; Goto *et al.,* 1990; Hammans *et al.,* 1991; Silvestri *et al.,* 1993). This disruption of mtDNA maintenance can have a deleterious effect on the efficiency of OXPHOS to produce chemical ATP energy. Given the fact that approximately 1,500 proteins are believed to be within the mitochondria and contribute to its function (Lopez *et al.,* 2000), eliciting the underlying pathological variants of these conditions can be a clinical challenge.

A novel homozygous *OPA1* variant, c.1601T>G (p.Leu534Arg), was identified in two affected sisters from a consanguineous family of Arab-Muslim origin using a combination of homozygosity mapping (performed with an Affymetrix Gene-Chip Human Mapping 50k Xba array and a Gene-Chip Human Mapping 250k MspI array) to identify regions of genomic homozygosity and whole exome analysis (Hiseq 2000, mean coverage depth x65.9) to identify any potential pathogenic variants in these regions. The c.1601T>G *OPA1* variant has not been previously reported in the 63,000 exome sequences found in the Exome Aggregation Consortium (ExAC) and it was not detected in 120 in-house controls. The two sisters

presented with similar neurological defects including optic atrophy, failure to thrive, neuromuscular weakness, cardiomyopathy and a fatal mitochondrial encephalopathy. Both of them died within 12 months after birth.

Previous biochemical exploration of these sisters obtained from a collaboration with Dr. Ann Saada and Dr. Ronen Spiegel revealed elevated serum alanine and lactate levels detected in both patients, indicative of a metabolic disorder. COX/SDH histopathological staining of muscle biopsy did not reveal any COX deficiency. Transmission electron microscopy (TEM) provided evidence of a defect in mitochondrial inner mitochondrial fusion (**Figure 6-1**) and complex activity of mitochondrial OXPHOS demonstrated a marked global decrease, which was more severely depressed for complexes I and IV (**Table 6-2**). This disruption of OXPHOS may have a pathological impact on tissues with high energy consumption (nervous, cardiac, hepatic and retinal), as represented by the symptoms.

In this study, I further investigated the pathogenic nature of this novel homozygous *OPA1* variant, c.1601T>G (p.Leu534Arg) as the likely cause of the fatal clinical phenotype in these two affected sisters.

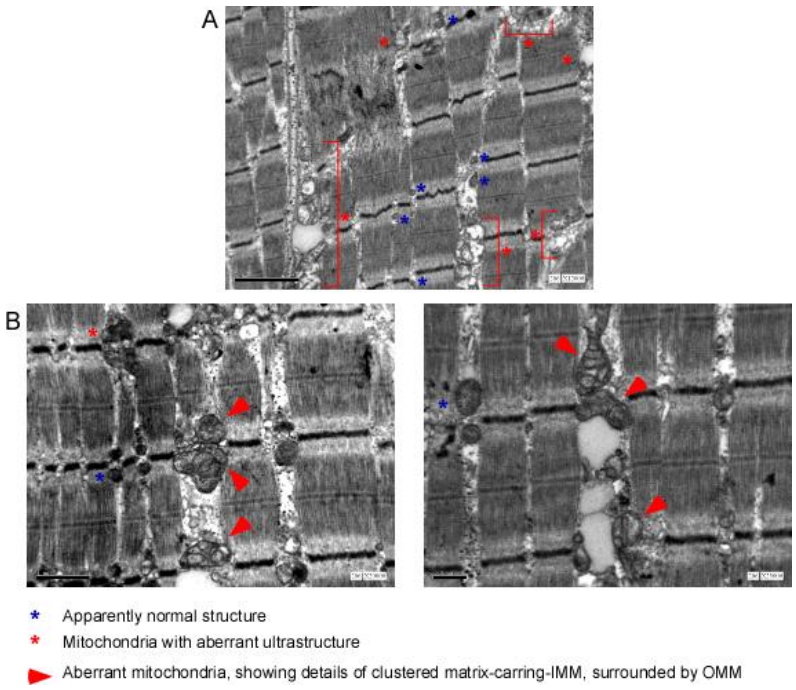

Figure 6-1 Mitochondrial ultrastructure imaged using transmission electron microscopy of patient III-4 muscle biopsy.

Enlarged mitochondria with a fusion defect were detected in patient III-2 (A) and (B). Irregular mitochondrial ultrastructure in the IMM of patient III-2 (B) Electron microscopy image obtained from collaboration with Drs Ronan Spiegal and Ann Saada

Figure reproduced from Spiegel, Saada, Flannery *et al.*, 2016, supplementary material.

Disease	OXPHOS Complex Affected	Genotype
Infantile-onset spinocerebellar ataxia		
Leigh Syndrome	I	MTND2,MTND3,MTND5, MTND6
		NDUFS1,NDUFS3,NDUFS4,NDUFS7,NDUFS8,NDUFA2,NDUFV1,NDUFAF2
		C8ORF38, C200RF7, FOXRED1
	II	SHDA
	III	UQCRQ
	IV	COX10,COX15, SURF1,TACO1
	V	MTATP6
	Multiple complexes	C12ORF65,EFG1
French-Canadian Leigh Syndrome	IV	LRPPRC
Leuko-encephalopathy	I	NDUFV1, NUBPL
	II	SDHAF1
	IV	COX6B1, SURF1
	I,III	TUFM
	I,III,IV	EARS2
Leuko-encephalopathy with Ataxia	I	MARS2

Disease	OXPHOS Complex affected	Genotype
Encephalo-cardiomyopathy		
Encephalo-cardiomyopathy	I	NDUFS2, NDUFV2, NDUFA11,NDUFAF4, ACAD9
	II	SDHA
	III	MTO1
	IV	SCO2,COX15
Cardiomyopathy	V	TMEM70, SLC25A3
	Unknown	DNAJC19, TAZ
Hepatoencephalopathy		
Hepatoencephalopathy	I	Twinkle
	IV	SCO1
	Multiple Complexes	EFG1
Alpers-Huttenlocher Syndrome	I,III,IV	POLG1, MPV17, DGOUK,FARS2

Table 6-1 Causative genes identified in patients with mitochondrial OXPHOS disorders.

Table adapted from Uziel *et al.*, 2011.

Assay	Patient III-2	Patient III-4	Controls±SD (n=50)
Complex I	0.047 (24%)	0.050 (25%)	0.199±0.043
Complex I+III	0.087 (40%)	n.d.	0.217±0.599
Complex II	0.099 (64%)	0.091 (59%)	0.154±0.024
Complex II+III	0.100 (65%)	0.053 (34%)	0.153±0.039
Complex III	0.934 (46%)	n.d.	2.01±0.40
Complex IV	0.270 (21%)	0.230 (22%)	1.03±0.24
Complex V	0.151 (44%)	n.d.	0.34±0.096

Table 6-2 Measurement of enzymatic activities of the OXPHOS system in Patient III-2, III-4 and control tissue

mU/U citrate synthase (% of control levels); n.d.-not determined. Data from OXPHOS complex activities obtained from the collaboration with Drs Ronan Spiegal and Ann Saada Table data reproduced from Spiegal, Saada, Flannery *et al.*, 2015.

6.2 Materials and Methods

6.2.1 Family history

Two consanguineous female patients of Arab-Muslim origin were investigated. Patient III-2 was born prematurely at 35 weeks. She presented with multiple episodes of hypotonic, opisthotonic posturing, weak cry and abnormal eye pursuits. Progression was characterised with a failure to thrive and severe neurodevelopmental delay. Following the onset of hypertrophic cardiomyopathy, the patient died at 10 months of age from an apnoeic episode.

Patient III-4 was born at term but quickly developed (within 2 days) generalised hypotonia and opisthotonic postering. Echocardioraphy detected a thickening of the left ventricular myocardium. Disease progression was again characterised by a failure to thrive, hypertrophic cardiomyopathy, neurodevelopmental delay, muscle wasting and sensorineural deafness. Opthalmological investigation conducted at 6 months revealed a mild disc pallor and electrophysiological investigation showed weakened visual-evoked potentials indicative of degeneration.The patient died at 11 months of age from an apnoeic episode.

The parents are first degree cousins with no apparent neurological or visual disruption. Exome sequencing analysis revealed that both sisters had a homozygous OPA1 variant (c.1601T>G; p.Leu534Arg). Further analysis confirmed that each parent and the two brothers carried this heterozygous *OPA1* variant but were apparently healthy. The mode of inheritance appears to be recessive with no other known affected family members (**Figure 6-2**).

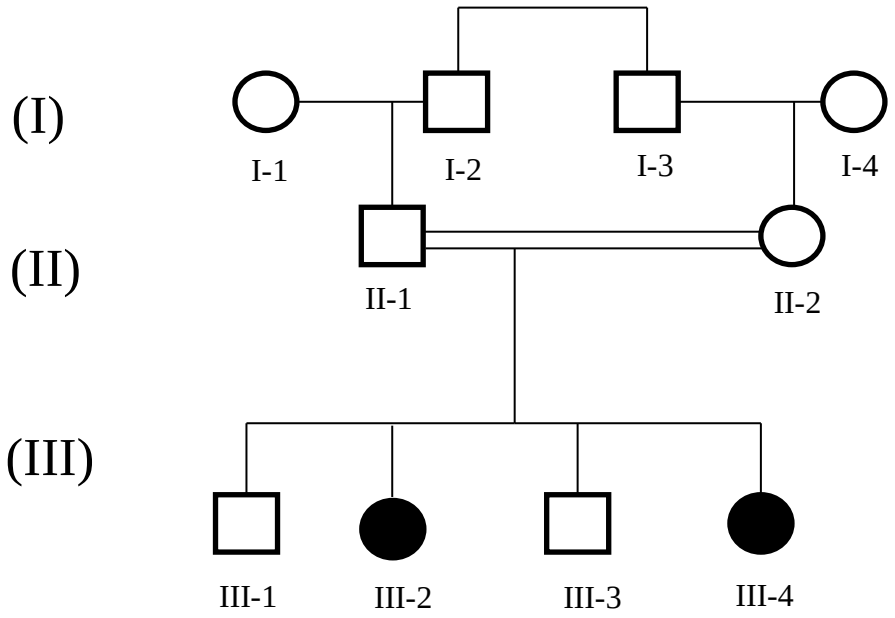

Figure 6-2: Pedigree from Israeli family with suspected pathogenic OPA1 mutation

Affected family members are coloured in black. Parents are first-degree cousins of Arab-Muslim origin. Individuals III-2 and III-4 are affected daughters with the homozygous c.1601T>G (p.Leu534Arg) *OPA1* variant.

6.2.2 Protein extraction from Muscle Tissue

Muscle biopsies were performed at 11 months and 1 month of age in patient III-2 and III-4, respectively. Protein was extracted from muscle homogenates from patient III-2 and four biological controls (four females aged between 19-23 years old).

6.2.3 Western blot analysis

Western blot analysis was conducted as described in **Section 3.3**. Briefly, 25µg of protein was loaded onto each lane from four control muscle homogenates and muscle homogenate from patient III-2. Following SDS-PAGE and blotting protein transfer, PVDF membrane was probed for OPA1 and GAPDH (1:1000 dilution) for 1 hour at room temperature. Membrane was incubated with secondary anti-mouse antibody (1:1000) for 1 hour / room temperature and visualised using biospectrum 500 imaging system. Densitometric analysis of western blot bands was conducted using ImageJ.

6.2.4 DNA extraction from Muscle Tissue

DNA was extracted from muscle tissue from patients' III-2, III-4 and two biological controls (two females aged between 19-20 years old) using the protocol described in **Section 3.5.2**.

6.2.5 mtDNA multiple deletion measurement

To investigate the presence of multiple mtDNA deletions in patient and control samples a 11kb long range PCR was conducted with the TaKaRa LA Taq$^{TM\ pcr}$ system on DNA muscle homogenate as described in **Section 3.12**.

6.2.6 Real-Time PCR analysis of mtDNA copy number

The mtDNA copy number quantification in control and patient tissue was investigated using a qPCR (*ND1/B2M*) assay as described in **Section 3.10.** The assay was used to quantify mtDNA content in two patients (Patient III-2 and Patient III-4) and two controls from extracted muscle biopsy. These two control muscle biopsies were gender-matched and the youngest muscle biopsies in storage were used for quantification with a mean age of 20 years. Real-time quantification of mtDNA was conducted in triplicate.

6.2.7 Conservation analysis and pathogenicity scoring

To determine if the leucine residue was evolutionarily conserved, the OPA1 amino acid sequence from a select group of outlying species was chosen for alignment. These sequences were acquired from the National Centre for Biotechnology Information (NCBI) protein database. In each case, OPA1 isoform 1 was chosen for alignment. These sequences were imported and aligned with BioEdit Sequence Alignment Editor (Obtained from http://www.mbio.ncsu.edu/bioedit/bioedit.html)

6.2.8 Modelling of OPA1 protein structure

Homology modelling was performed between residues 220-960 of human OPA1 (gi 18860834 ref NM.130833.1) based on the closest known structural homologue of OPA1 (June 2015), Interferon-Induced GTP-binding protein MX2: FFAS Score -82.7, sequence identity 16% (http://ffas.sanfordburnham.org/ffas-cgi/cgi/ffas.pl) This template was modelling with SCWRL server (http://www1.jcsg.org/scripts/prod/scwrl) with settings set to default.

Mutagenesis of p.Leu534Arg in protein model and illustration of GTP-binding domain of OPA1 was performed manually using PyMOL (Delano Scientific).

6.2.9 Statistical Analysis

Unpaired Student's t-test was performed using Graphpad prism version 5.0 for windows, Graphpad software , San Diego California USA, www.graphpad.com

6.3 Results

6.3.1 Conservation of OPA1 p.Leu534Arg residue

A multiple sequence alignment was generated to determine the evolutionary conservation of OPA1 p.Leu534Arg relative in six other outlying species (**Figure 6.3**). The leucine amino acid appears to be highly conserved in both mammalian and lower invertebrate species. Evolutionary divergence occurs in yeast (S. *Cerevisiae* and S. *Pombe*) indicating that this mutated region of *OPA1* has been conserved since early evolutionary history and may impart an important structural or functional role.

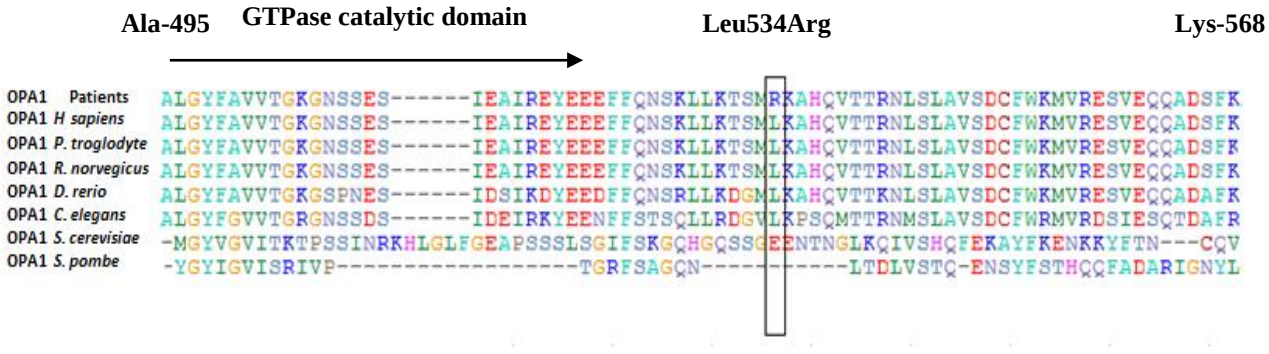

Figure 6-3 Multiple Sequence Alignment of OPA1 protein

Multiple sequence alignment of OPA1 gene region (residue Ala495- Lys568) with suspected pathogenic OPA1 missense variant in different species. The black rectangle indicates the position of the missense variant p.Leu534Arg in Homo sapiens and six other outlying species. Sequences were aligned using BioEdit Sequence Alignment Editor.

6.3.2 Pathogenicity scoring of OPA1 p.Leu534Arg variant

Pathogenicity scoring is an *in silico* method used to predict the likelihood of a genetic variant to result in a pathological change which may be responsible for a disease phenotype. This *in silico* analysis was applied to the Leu534Arg OPA1 mutation with online pathogenicity software 'Mutation Taster' and 'SIFT' (Sorting Intolerant from Tolerant). Both pathogenicity programs predicted a disease causing pathogenic variant for p.Leu534Arg with a Mutation Taster prediction of 'disease causing' with a probability of 0.999 and SIFT prediction of 'Damaging' with a score of 100% (**Table 6-2**).

Program	Score
Mutation Taster	Disease causing; probability 0.999
SIFT	Damaging; Score 100%

Table 6-3 Pathogenicity Scoring of *OPA1* variant

OPA1 variant p.Leu534Arg pathogenicity report generated by online software Mutation Taster and SIFT.

6.3.3 Modelling of OPA1 p.Leu534Arg mutant protein

A theoretical model of OPA1 protein was generated to illustrate any structural changes which may occur as a consequence of the pathogenic p.Leu534Arg mutation. This OPA1 model was created by first using the FFAS server to identify the most structurally homologous protein to OPA1 and then modelled using the SCWRL online modeller with default settings, and manipulated using PyMol (Delano Scientific). The L534 residue (white) is in close proximity to the GTP binding domain of OPA1 (red). The missense change to Arginine introduces a much larger and more polar amino acid to this site which may result in structural instability near this GTP binding domain (**Figure 6-4**).

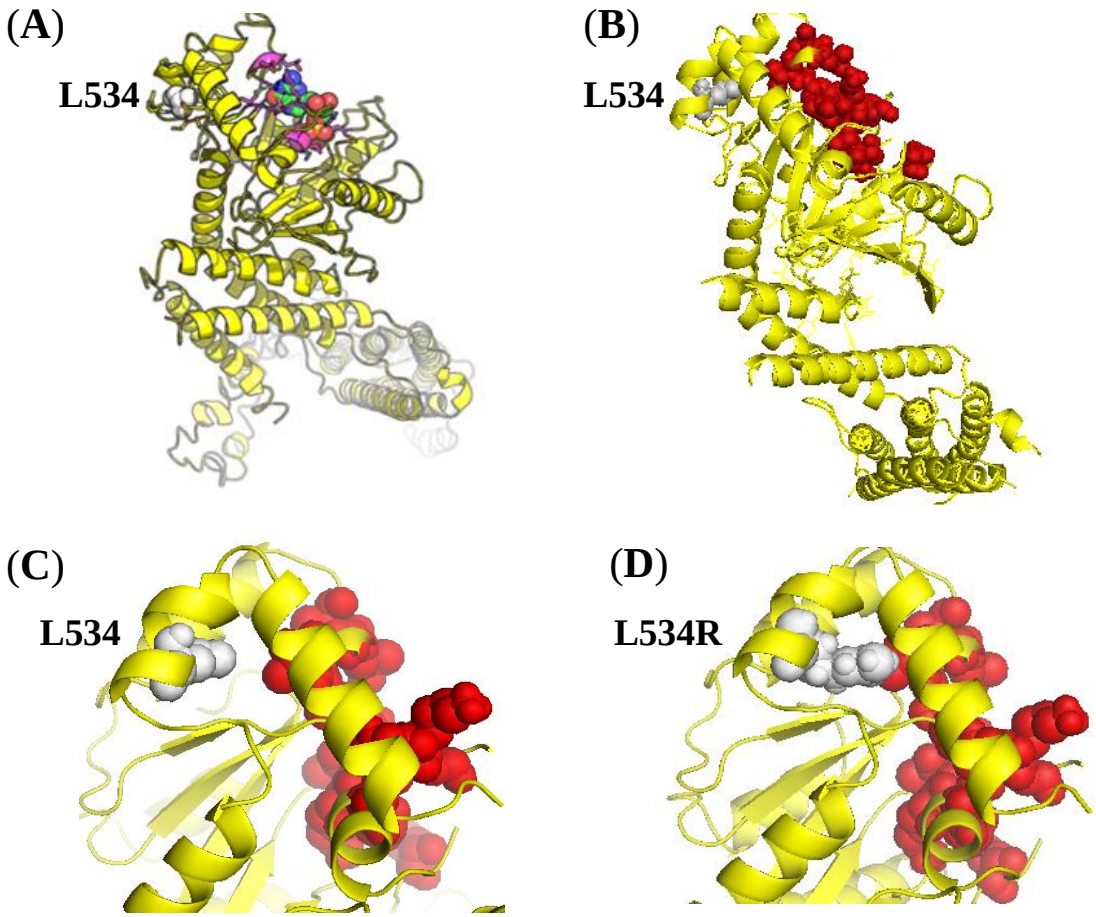

Figure 6-4 *In Silico* Modelling of OPA1

(A) Modelling performed by Devorah Soiferman (Professor Ora Sheuler-Furman's collaboration, Isreal) which illustrates the proximity of the L534 residue (white) to the GTP-binding domain (multi-coloured) The GTP domain binding site is illustrated in magenta. Modelling was performed using I-tasser server (Yang *et al.*, 2015). The template for modelling was derived from Yan *et al.*, 2011b; **(B)** Homologous modelling performed by Padraig Flannery (Dr Yu-Wai-Mans lab) of OPA1 protein using the 'Fold and Functions Assignment System (FFAS)' server to determine the most structurally homologous protein to OPA1 (Interferon –Induced GTP-binding protein MX2 (FFAS Score -84; Seq Id: 15%) to use as model. SCWRL modeller and PyMol for generation of protein model and manual manipulation of image. White spheres illustrate the position o f the L534R variant , red spheres illustrate the relative position of the catalytic GTPase domain **(C)** maginified position

of the L534 residue in wild-type OPA1 **(D)** Magnified position of the L534R residue in mutated OPA1 protein.

6.3.4 Proband OPA1 protein expression

Western blot analysis was conducted on muscle homogenate from patient III-2 and four biological controls (age approximately 20 years old). Blotting of patient III-4 could not be conducted due to limited sample size. Analysis revealed a significant reduction of OPA1 protein levels ($p \leq 0.05$) compared with controls indicating that the c.1601T>G; p.Leu534Arg change resulted in a marked decrease of OPA1 expression in muscle tissue (**Figure 6-5**).

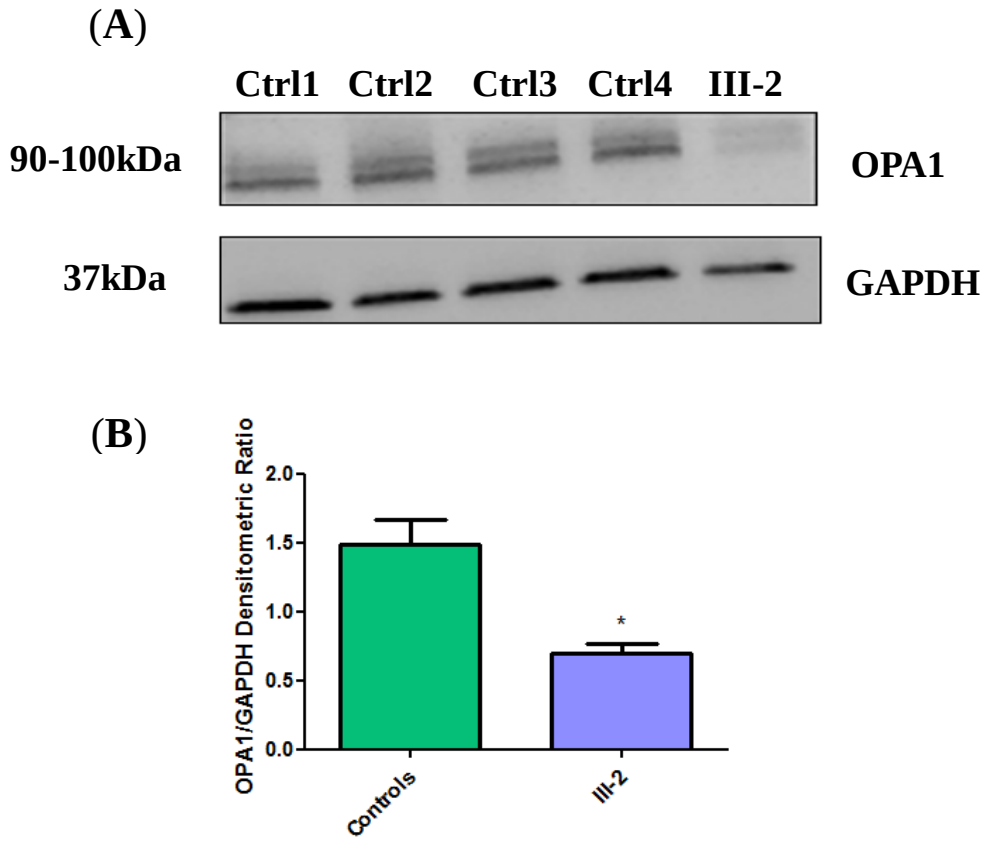

Figure 6-5 Western blot analysis conducted between patient III-2 and controls.

Representative western blot analysis of OPA1 normalised against GAPDH and mean of four biological controls (**A**). Quantification analysis performed in three independent experiments on patient muscle with three females and one male muscle controls aged between19-23. Control in green bar and patient value in purple bar are shown. Error bars represent standard error of the mean. An unpaired Student's t-test was used in statistical comparison between patient and controls (* $p < 0.05$)(**B**).

6.3.5 MtDNA copy number analysis

Investigation of mtDNA copy number in patient muscle tissue was conducted using a real-time PCR assay to measure the ratio of mtDNA (*ND1* gene) relative to Nuclear DNA (*B2M* gene). Analysis was conducted from the muscle homogenate of two negative controls (age approximately 20 years old) and two patients (patient III-2, Patient III-4). A significant mtDNA depletion (78% in both affected sisters) was detected in both affected patients relative to controls ($p<0.0001$) (**Figure 6-6**)

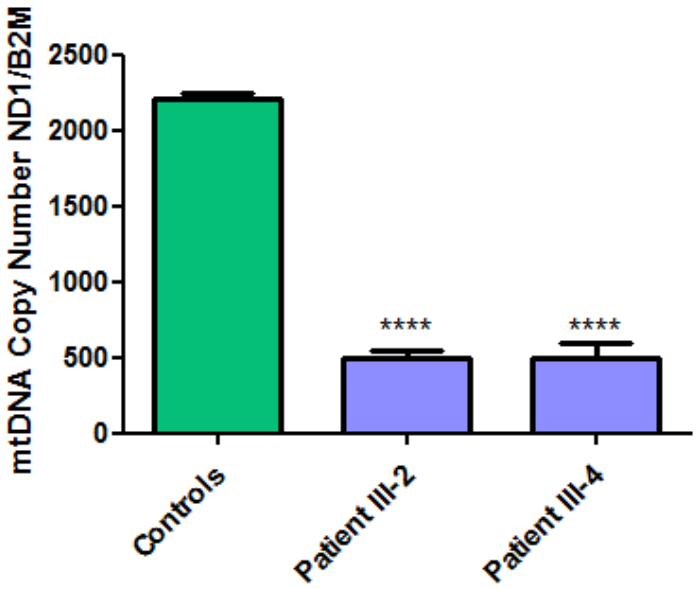

Figure 6-6 Comparison of mtDNA copy number between OPA1 patients and controls

mtDNA copy number was assessed using real-time PCR measuring ND1 mtDNA gene copy number and normalised to nuclear B2M gene. Controls: n=2); *OPA1* Patients: Patient III-2 and Patient III-4. Error bars represent standard error of the mean. Statistical analysis performed with Student's unpaired t-test (**** $p < 0.0001$).

6.3.6 mtDNA deletion analysis

To determine if the reduction of OPA1 protein levels may result in the accumulation of mtDNA deletions which may lead to an inhibition of OXPHOS, a long-range PCR was conducted in muscle tissue to detect alternative mtDNA species at a lower molecular weight than the wild-type molecule (16,569 bps). Analysis was performed on three controls (two negative controls (lane 1 and 2) and one positive control (lane 3)) and both patients (patient III-2, patient III-4). Fig 6.4. Amplification of patient mtDNA revealed no additional mtDNA species other than wild-type amplicon (11kbs). This indicates that there are no mtDNA deletions detected in patient mtDNA (**Figure 6-7**).

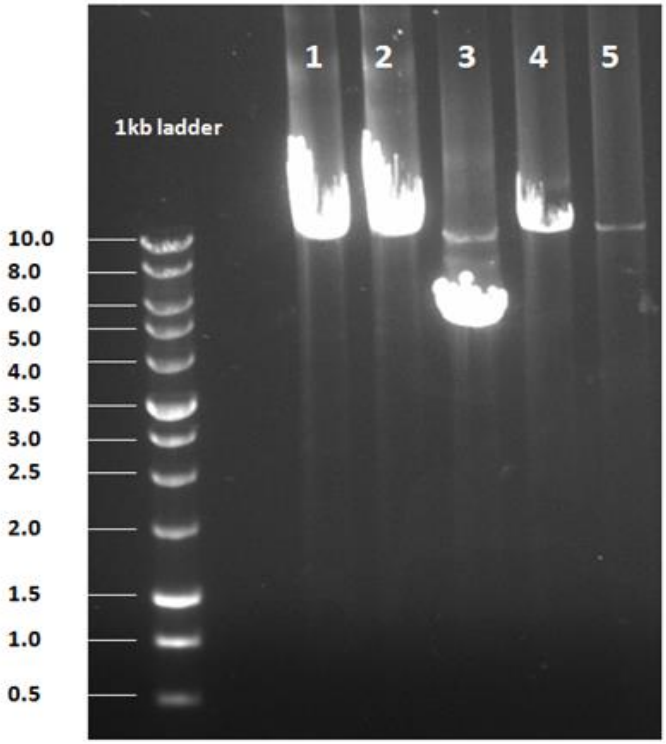

Figure 6-7 Long-range PCR of mtDNA derived from control and patient muscle homogenates

Long range PCR amplification products of human muscle mtDNA. Forward primers nt6222-6240 and reverse primers nt16122-16153 of mtDNA yielded an amplicon of 11kbs. Lane 1 and 2 are amplicons of negative control mtDNA from muscle homogenate. Lane 3 is an amplicon of mtDNA from a multiple deletion positive control. Lane 4 and 5 are amplicons from patients III-2 and III-4.

6.4 Discussion

Two sisters of Arab Muslim origin were diagnosed with fatal mitochondrial encephalopathy and congenital hypertrophic cardiomyopathy. Due to a family history of consanguinuity, these patients were investigated using a combination of homozygosity mapping and whole-exome sequencing analysis which highlighted a novel homozygous variant (p.Leu534Arg) in the *OPA1* gene.

To further confirm *OPA1* involvement in the syndrome, both *in silico* and biochemical analyses were carried out. Bioinformatic analysis of *OPA1* sequence conservation indicated that the p.Leu534Arg change occurred in a highly conserved region of *OPA1* within the GTPase domain. Variants which display a high degree of evolutionary conservation are likely to impart an important structural or functional role and are more likely to be deleterious than variants within regions without evolutionary constraint. This was confirmed using online pathogenicity software Mutation taster2 and SIFT, which predicted the OPA1 change to be highly likely pathogenic.

Significantly reduced levels of OPA1 protein in patient III-2 muscle biopsy suggested that the homozygous p.Leu534Arg may have deleterious effects on the protein function and/or structure. Dysfunction of OPA1 is demonstrated through abnormal IMM fusion and ultrastructure detected through TEM analysis (**Figure 6-1**). Although not located strictly within the GTPase domain, modelling of the OPA1 protein illustrated the proximity of the mutated residue to the GTPase domain. Pathogenic missense variants found in the GTPase domain of OPA1 are typically associated with a more severe form of DOA with extra-ocular features which include sensorineural deafness, ataxia, myopathy and peripheral neuropathy (DOA+). Novel *OPA1* GTPase variants have also been found which extend the clinical spectrum of DOA+ by presentation with oththalmoplegia, ptosis, polyneuropathy and PEO (Liskova *et al.,* 2013; Zeviani *et al.,* 2008; Hudson *et al.,* 2008). This illustrates how the pathological disruption of OPA1 may lead to complex multisystemic neurological disorders. (Liskova *et al.,* 2013). The severe clinical phenotype of these two patients would appear to be consistent with these previous observations.

Dysfunction of mtDNA replication in encephalopathy can manifest as either depletion in mtDNA copy number or the accumulation of mtDNA deletions which may lead to a

proliferation of mutated mtDNA copies. Both of these mechanisms may explain the generalised dysfunction of the OXPHOS system. Previous investigation of patients with *OPA1* defect and broad multisystemic features found in DOA+ have shown the accumulation of mtDNA mutations to be an important pathogenic mechanism responsible for this broad symptomatic spectrum (Amati-Bonneau *et al.,* 2008; Husdon *et al.,* 2008). Our patients, however, did not harbour multiple mitochondrial deletions. This could be linked to the premature age of fatality of these two patients (under 1 year-old). Indeed, the accumulation of mtDNA deletions at detectable levels is often not observed before adolescence (Elpeleg *et al.,* 2002).

Despite no mtDNA deletions detected, investigation of both affected sisters revealed a striking depletion of the mtDNA copy number (78% reduction). A marked depletion of mtDNA is typical in cases of infantile mitochondrial encephalopathy because multiple mtDNA deletions which are also known to underpin these disorders, are first required to clonally expand before they reach a threshold in the mtDNA population sufficient for a clinical presentation within an affected tissue (Elpeleg *et al.,* 2002; Stewart and Chinnery, 2015). This may be linked to the recently observed role of *OPA1* in mtDNA replication (Elachouri *et al.,* 2011). *Elachouri and colleagues* demonstrated that isoforms of OPA1 which contain exon 4b have a role in anchoring the mitochondrial nucleoid to the IMM, a necessary step for mtDNA replication (Elachouri *et al.,* 2011). This was supported by siRNA knockdown of *OPA1* in Hela cells and isolated rat RGCs which resulted in a depletion of mtDNA and a partial inhibition of OXPHOS (Kushnareva *et al.,* 2013).

The suggested mechanism for OPA1 pathogenicity in this mitochondrial encephalopathy may consist of a multi-prolonged attack to reduce OXPHOS efficiency. The decrease in structural stability and potential decrease in GTPase activity induced by the p.Leu534Arg change may hamper mtDNA maintenance, disrupt cristae structure as revealed by TEM and supported by siRNA knockdown of *OPA1* (Kushnareva *et al.,* 2013) and disrupt OXPHOS complex assembly (Zanna et al,. 2008; Cogliati *et al.,* 2013). Dysregulation of cristae may also promote the release of pro-apoptotic factors such as cytochrome c which may contribute to fatal encephalopathy and cardiomyopathy. Recent investigation of an *OPA1* mouse model support the involvement of pathogenic *OPA1* variants which contribute to mtDNA instability and late-onset cardiomyopathy (Chen *et al.,* 2012).

Investigation of *OPA1* during embyogenesis in zebrafish has revealed its requirement for normal development (Rahn *et al.,* 2013). In parallel, a previous homozygous *OPA1* mouse model, introducing an OPA1 protein truncation in all four OPA1 transcripts was developed by *Chen and colleagues* (2012). It was hypothesised to lead to a complete reduction of OPA1 expression and, consequently, embryonic lethality further reinforcing OPA1 involvement in development. The presence of a homozygous missense variant rather than a nonsense mutation may explain why this variant persisted to the post-natal stage. The rarity of pathological homozygous *OPA1* variants is highlighted by the fact that this is the first recorded case found in the general population.

In addition to being the first report of *OPA1* homozygosity, these two cases have broadened the clinical spectrum of *OPA1*-inherited disorders to include infantile mitochondrial encephalomyopathy and cardiomyopathy. It also further highlights the diagnostic power of whole-exome analysis for patients with molecularly undefined genetic disorders.

The collaborative work presented in this chapter has been published in the Journal of Medical Genetics.

Spiegel, R. Saada, A., **Flannery, P.J.**, Burté, F., Soiferman, S., Khayat, M., Eisner Sagüés, V., Vladovski, E., Taylor, R.W., Bindoff, L.A., Shaag, A., Mandel, H., Furman, O., Shalev, S.A., Elpeleg, O., Yu-Wai-Man, P. Fatal infantile mitochondrial encephalomyopathy and hypertrophic cardiomyopathy associated with homozygous *OPA1* mutations. J Med Genet. 2016;53(2):127-31.

Chapter 7

Whole-Exome Analysis of a Patient Cohort with Inherited Optic Atrophy

7.1 Introduction

In recent years, the advancement of next-generation sequencing (NGS) technologies has allowed the development of a useful tool in the diagnostic assessment of patient genetic disorders (Shashi *et al.,* 2014; Liew *et al.,* 2013; Lee *et al.,* 2014; Yang *et al.,* 2013, 2014). This has been especially possible given decreased costs, increased speed of sequencing and increased shared annotation of genetic variants (Jamuar and Tan, 2015). NGS can be defined as either a whole-genome sequencing (WGS) or whole-exome sequencing (WES) technology.

For WGS, patient DNA is extracted and isolated to determine the complete sequence of the genome. This sequence is aligned and compared against a reference sequence and the variants are annotated to identify distinct mutations in a patients' genetic code. This WGS analysis may typically identify three to four million variants in an individual patient (Biesecker *et al.,* 2012). A search algorithm can also be implemented to determine if any distinct variants are known to be disease causing (Rizzo *et al.,* 2012). However, even after this bioinformatic analysis, there may be hundreds of false positive disease causing variants identified.

WES is similar to WGS except that sequencing and analysis is confined to exons which collectively compose the exome. The exome represents only 1% of the whole genome. The rationale behind WES to analyse the genetic code lies in the observation that 85% of known disease causing genes are located in the exome, which may represent an enriched subset of the genome containing pathogenic variants (Botstein *et al.,* 2003; Majewski *et al.,* 2011). Similar to WGS, sequences from these exons are aligned against a reference and variants annotated to identify disease causing mutations. Approximately 10,000 or more variants may be identified in an individual exome (Rabbani *et al.,* 2014). This may increase the efficiency of identifying the underlying aetiology of a genetic disorder.

To conduct NGS analysis, genomic DNA is typically extracted from patient blood to undergo library preparation and whole genome or targeted exon capture using an appropriate kit. Samples are subsequenctly sequenced using a next generation sequencing platform to generate raw sequence reads of the exome in the form of FASTQ files of each patient sample.

FASTQ files are then transferred to an in-house bioinformatics team who process this data using an established in-house pipeline for (1) sequence quality control, (2) alignment to a genetic reference and (3) annotation. These processes are briefly described in **Section 7.2.** This pipeline generates an excel-tabulated format of the analysed sequencing data for further clinical and genetic analysis.

In silico analysis of novel variant pathogenicity is conducted with publically available online pathogenicity softwares. SIFT is an algorithm designed by *Kumar and colleagues* (2009) which predicts potential pathogenicity of detected variant by identifying evolutionary constrained regions through sequence homology with the PSI-BLAST algorithm. SIFT then compiles an alignment of these homologous sequences and calculates the effect of every type of amino acid substitution at a particular position on protein function. It then uses this information to predict if a specific mutation is pathogenic.

Polyphen-2 is another online algorithm developed by *Adzhubei and colleagues* (2010) which was designed to predict the pathogenicity of missense mutations. The algorithm uses eight sequence-based and three structure-based modes of prediction. The mutant and wild-type alleles are compared to each other and a set of parameters are applied to multiple homologous sequence alignments (MHSA). These parameters include the probability of this variant allele arising from a polymorphism which is determined from amino-acid changes in these MHSA and how different the human protein is from the closest evolutionary divergant protein. The hypermutability of the site is also accounted for when predicting pathogenic probability. Finally, functional impact of this mutant allele is calculated using a naïve Bayes classifier (Bayes classifier is a machine learning classifier based upon Bayes mathematical model of probability assessment).

Mutation taster is a third pathogenecity algorithm developed by *Schwarz and colleagues* (2014) designed to not only identify pathogenic variants which create alternative amino acid sequences but also predict pathogenicity of synonymous variants and variants in intronic regions. MutationTaster 2 also contains publically available SNP and indel data generated from the 1,000 genomes project (Abecasis *et al.,* 2010), ClinVar (Landrum *et al.,* 2014) and HGMD (Human Gene Mutation Database) (Stenson *et al.,* 2014). An annotated variant can be categorized as neutral if it has been detected in a homozygous state more than four times within either the 1,000 genomes or HapMap databases. If the variant is already

known to be pathogenic, this information can be retrieved from the ClinVar database. Similar to SIFT and Polyphen-2, MutationTaster2 scores the pathogenicity of a variant based on evolutionary conservation of the surrounding region and uses a number of integrated analyses based on genetic regulatory elements. In addition, the algorithm approximately predicts the pathogenicity of splice site defects only at known intron-exon boundaries. MutationTaster2 improves upon older versions of MutationTaster by investigating variants at intron-exon junctions. Similar to these previous versions, MutationTaster2 uses a Bayes classifier to create genetic variant predictions.

In the present study, WES analysis was performed on a cohort of fourteen patients (Ten females and four males), all clinically diagnosed with optic atrophy with ages ranging from 20-79 years. The underlying genetic aetiology of this cohort was unknown and previous mutation screenings performed in-house have excluded these patients for *OPA9* and *OPA1* pathogenic variants. The overall aim of the study was to use WES analysis as a tool to explore the genetic aetiology underpinning this cohort of patients diagnosed with either pure optic atropy or optic atrophy associated with other systemic features which afflict the central or peripheral nervous systems.

7.2 Materials and Methods

7.2.1 Assessment of appropriate control datasets for whole exome analysis

To identify the most appropriate control exome database for WES analysis of this patient cohort, individual samples were filtered using a defined minor allele frequency (MAF) threshold of 5% to quantify the number of potential variants that were not found in control exomes: 1000 Genome Project, the National Heart, Lung and Blood Institute Exome Sequencing Project 6500 (http://evs.gs.washington.edu/EVS/), and the CG69 dataset (Abecasis *et al.*, 2010, Drmanac *et al.*, 2010) (**Table 7-1**). This analysis demonstrated which databases contained the most variants found within the British population. The 1000 genomes project had the greatest number of variants in our patient cohort whereas the ESP6500 dataset had the least number of variants.

	PFC-340	PFC-341	PFC-342	PFC-344	PFC-345	PFC-346	PFC-347	PFC-348	PFC-349	PFC-350	PFC-351	PFC-352	PFC-353
Exonic/Splicing/non-synon	10912	10728	10862	10950	10812	10716	10844	9819	10866	11028	12091	11220	11141
Not in ESP6500	2292	2188	2219	2182	2226	2169	2224	1516	2194	2304	2667	2260	2386
Not in 1000G	996	986	948	962	1003	983	994	833	1003	1014	1385	1047	1295
Not in CG69	1492	1467	1420	1470	1504	1469	1494	1323	1508	1506	1933	1547	1697
Not in ESP6500, 1000G, CG69													
Dominant	1368	1361	1396	1351	1434	1350	1347	1311	1398	1415	2272	1846	1561
Recessive	201	168	146	181	164	181	199	182	176	186	191	155	188

Table 7-7-1 Calling of variants in published databases for each individual patient.

The number of single nucleotide polymorphisms (SNPs) and their relative frequency in each database were then analysed by Dr. Gavin Hudson to determine the most appropriate databases to use for data filtration of the excel tabulated pipeline output.

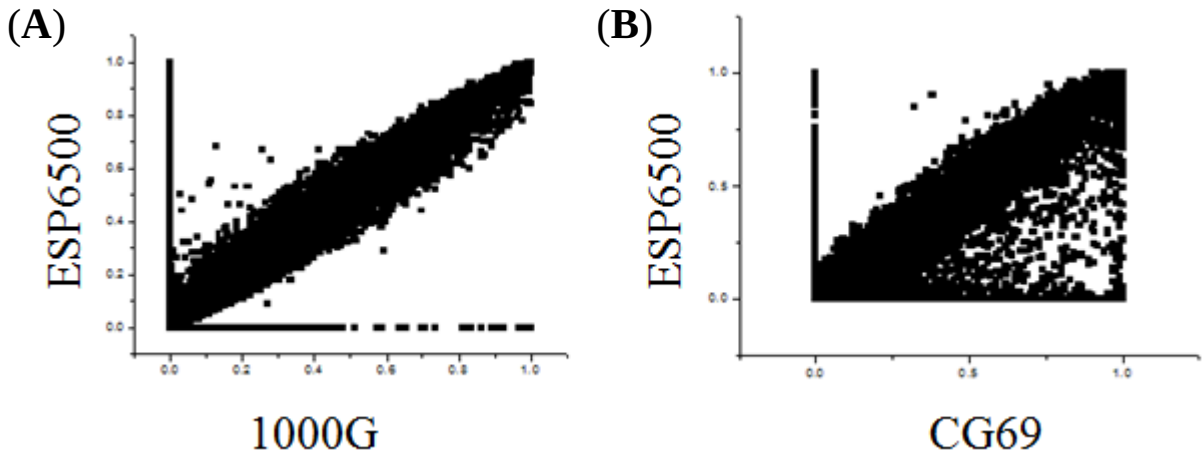

Figure 7-1 Distribution of variant frequency in the 1000 genomes project, ESP6500 and CG69.

Comparison of these datasets highlighted a tight linear concordance of variant frequency (A) between the ESP6500 and the 1000 Genomes dataset. However when comparing variants between the 1000 genomes dataset and CG69 (B), there was a skew in the frequency of detected polymorphisms which highlight underlying differences either in the analysis and annotation pipelines used to generate these variants and/ or genetic frequency stratification between the populations used in these projects.

A skew in the frequency of detected polymorphisms was observed when comparing the CG69 and the ESP6500 datasets, whilst the ESP6500 and 1000 Genomes projects showed a linear relationship **(Figure 7-1)**. Consequently, for analysis of my patient cohort, it was determined that the 1000 genomes project and the ESP6500 were to be used as a reference population for intersection filtering of genetic variation generated as an excel tabulated output from the WES in-house pipline.

7.2.2 Whole exome capture, alignment and annotation

Patient genomic DNA was previously isolated from whole blood (DNeasy®,Qiagen,Valencia,CA) for whole exome analysis and outsourced to AROS (AROS Applied Biotechnology A/S, Aarhus, Denmark) where DNA underwent library preparation and enrichment with a Nextera Rapid Capture Expanded Exomes Kit (Illumina Inc., San Diego, USA). This kit includes greater than 340,000 95mer probes designed using the hg19 reference genome (Manolio *et al.*, 2009). It allows greater coverage of exons and includes sequencing data in surrounding non-coding regions (UTRS and miRNA binding sites). Raw sequencing data was generated with an Illumina HiSeq2500 platform in the form of a FASTQ file (Illumina Inc., San Diego, USA). The quality of these sequences was analysed using 'FASTQC' and sequences deemed low quality are removed (reads with poly-N tail). High quality reads were then input into a WES pipeline for data processing before the final results were generated in excel format.

7.2.3 GATK and Freebayes in-house pipelines

These in-house pipelines were designed by the in-house bioinformatics team for WES analysis. Briefly, sequence reads were aligned to UCSC hg19 with the (Barrows-Wheeler) aligner (BWA) (Li and Durbin, 2009) and variants were detected with either the GATK or Freebayes callers using filtering parameters as defined by GATK Best Practise Recommendations. Detected variants were annotated using Ingenuity Variant Analysis (IVA) or Annovar (Wang *et al.*, 2010). Annotated variants were tabulated into Excel (Microsoft Office) along with other parameters such as variant location, type, frequency, associated gene, etc for further clinical and biological analyses. These analyses are described below.

7.2.4 Comparison of Freebayes and GATK variant callers

In order to determine the best exome variant caller to use in whole exome analysis specific to my patient cohort, the cohort was first subdivided into categories based on disease phenotype (**Table 7-3**). These groups of patients were then analysed using the BWA aligner with either a GATK or Freebayes caller to detect variants by the in-house Mitochondria Bioinformatics

Team, IGM. The output generated by both of these callers was then filtered using the 1000 genomes project and ESP6500 datasets to detect >1% of variants and annotated using IVA which uses a biological context filter with curatted data from the Ingenuity knowledge base to determine how many of these annotated variants are detected in either known optic atrophy genes or genetic diseases associated with optic atrophy.

IVA is an online tool designed to work as a functional annotator for whole genome and whole exome data. It integrates both analytical tools and curated integrated content from online publication to analyse called genetic variants. IVA is a more versatile tool than ANNOVAR as it permits filtering of variants based on a number of adjustable predefined parameters such as mode of inheritance, quality of reads or variant frequency in population exome databases. Data readout includes all known relevant information on the variants of interest including pathogenicity and links to any relevant publications. The predefined filters used for the analysis of GATK and Freebayes variants included 'Confidence', 'Common variants', 'Predicted Deleterious' and 'Biological Context' (as detailed in **Table 7-2**).

Confidence	Call quality is at least 20 reads in any case or control Outside top 5% most exonically variable 100bp windows in healthy public genomes
Common Variants	Exclude common variants found greater than 1% of the exome (1) 1000 genomes project and (2) ESP6500 project.
Predicted Deleterious	Disease associated according to computed ACMG guidelines classification (1)Pathogenic (2)Likely Pathogenic Or are associated with Loss of Gene Function (1)Frameshift, in-frame indel or start\stop codon change (2)Missense
Biological Context	Optic Atrophy

Table 7-2 Predefined parameters in Ingenuity Variant Analysis (IVA) used to filter variants obtained from both the GATK and Freebayes Caller

Variants which were predicted deleterious according to IVA were defined according to the American College of Medical Genetics and Genomics (ACMG) guidelines.

7.2.5 Quality control usingT_i/T_v ratio in WES

The T_i/T_v ratio is a metric of genetic polymorphisms generation. Development of a next-generation sequencing framework for analysing genetic variation in combination with previous inter-species sequencing projects have demonstrated that the ratio between genetic transitions and transvertions is approximately 2.1 in human whole genomic samples and 2.8 in human whole exonic samples (Depristo *et al.,* 2011; Ebersberger *et al.,* 2002; Freudenberg-Hua *et al.,* 2003). The reason for a higher T_i/T_v ratio in whole exome samples is because there are a greater degree of methylated cytosine found within C_pG nucleotides within these samples which can easily undergo a deamination and transition to thymine. This number may vary depending on the individual sequenced or between different human populations. If this number is appreciably lower it could indicate false positive enrichment. The T_i/T_V ratio was quantified by IVA in each whole exome sample and used as a parameter of WES caller quality.

7.2.6 Filtering of WES excel data generated through GATK pipeline

Once WES data in excel format was output from the in-house GATK pipeline, annotated variants were filtered according to variant type, frequency in control exome databases and other parameters such as predicted pathogenicity, evolutionary conservation and quality of WES reads. In addition, patients with a common phenotype were compared in a process known as ‘intersection filtering’ (**Table 7-3**) (Robinson *et al.,* 2011).

Patient	Gender	Age	OA	Ataxia	Peripheral Neuropathy	Deafness	Nystagmus	Spasticity	Epilepsy	Dementia	Diabetes
Isolated OA											
PFC-346	F	37	+	-	-	-	-	-	-	-	
PFC-347	M	33	+	-	-	-	-	-	-	-	
PFC-348	F	27	+	-	-	-	-	-	-	-	
PFC-349	F	61	+	-	-	-	-	-	-	-	
PFC-351	F	20	+	-	-	-	-	-	-	-	
OA and deafness											
PFC-344	F	78	+	-	-	+	-	-	-	-	
PFC-352	M	25	+	-	-	+	-	-	-	-	
OA and diabetes											
PFC-341	F	38	+								+
OA and peripheral neuropathy											
PFC-340	F	64	+	+	-	-	-	-	-	-	
PFC-342	F	54	+	+	+	-	-	-	-	-	
PFC-345		53	+	+	-	-	-	-	-	-	
Recessive OA											
PFC-350	F	20	+	-	-	-	+	-	-	-	
PFC-351	F	20	+	-	-	-	-	-	-	-	
PFC-353	F	45	+	-	-	-	-	+	+	+	

Table 7-3 Cohort of patients investigated through whole exome analysis with clinical phenotype. OA group 1; Isolated OA, OA group 2; OA and Deafness, OA group 3; OA and diabetes, OA group 4; OA and Peripheral Neuropathy, OA group 5; Recessive OA.

Briefly, annotated variants were first filtered according to whether they were present in the exome or at intronic splice sites as opposed to surrounding intronic regions which may not impact protein quality, are less probable to impart on pathogenicity and have poorer coverage due to the design of WES.

Due to the relative rareness of these conditions, annoted variants were selected at a minor allele frequency of either 1% or 5% within both the 1000 genomes project and the ESP 6500 project to provide a subset of potential pathogenic variants.

At this stage a number of different strategies may be employed, potential pathogenic variants in individuals may be further refined to identify those only in evolutionarily conserved regions using the GERP2 filter (Cooper *et al.,* 2005). The '*a priori*' hypothesis behind this filtering process suggests that pathogenic variants are likely to be located in functional regions of the genome which are not subject to selective evolutionary pressure. Pathogenicity of variants in these regions as determined through four alternative pathogenicity programs is typically high, given that mutations in evolutionary conserved regions is one of the main parameters often used to judge whether a variant may be pathogenic.

For the remaining variants, patients with a common clinical phenotype may be selected for comparison, filtering out non-common genes and only selecting those which 'intersect' or are common to both individuals (Li *et al.*, 2012). This process may further limit the number of potential pathogenic candidates and is a typical strategy used to analyse sporadic cases or cases of non-related individuals. This intersection filtering may also be employed prior to the use of the GERP2 filter, particularly if no relavent variants are identified.

Identified common variants between individuals with a similar or identical clinical phenotype are a strong candidate for potential pathogenicity. These variants can then be further analysed with pathogenicity programs SIFT, PolyPhen2 and Mutationtaster2 to estimate the pathogenic probability of these variants. A summary of the methods used to sequence and identify potential pathogenic variants in this cohort and illustrated in **Figure 7-2**.

7.2.7 Coverage of common genes associated with optic atrophy-related disorders

Data analysis of relative gene coverage was calculated from sample alignment files using Bedtools v. 2.15.0 and Perl script. This analysis was conducted by Doctor Yaobo Xu PhD. Data was further analysed and graphed using excel (Microsoft, Reading, UK).

7.2.8 Pathogenicity scoring

Pathogenicity scoring was performed using three online tools designed to predict the probability of a variant identified through next-generation sequencing as being pathogenic. These tools included 'Sorting Tolerant From inTolerant (SIFT), Polyphen-2 and Mutation taster (Kumar *et al.*, 2009; Ng *et al.*,2001; 2003;2006)

- SIFT threshold parameters to denote the degree of probability associated with variant pathogenicity which include 'deleterious' (<=0.05) and 'tolerated' (.0.05).
- Parameters used to classify variants analysed by polyphen-2 pathogenicity software include 'probably damaging (0.85), 'possibly damaging' (0.85-0.15) and 'benign' (≤ 0.15) and MutationTaster2 uses the following labels ' disease automatic', 'disease causing',' polymorphism', 'polymorphism automatic' with a higher score indicating an increased probability of pathogenicity.
- When analysing potential pathogenic variants from the optic atrophy cohort, these variants were analysed in parallel by MutationTaster2, SIFT and Polyphen-2 and variants was determined to be 'likely' pathogenic if two of these three algorithms determined the variant to be pathogenic.

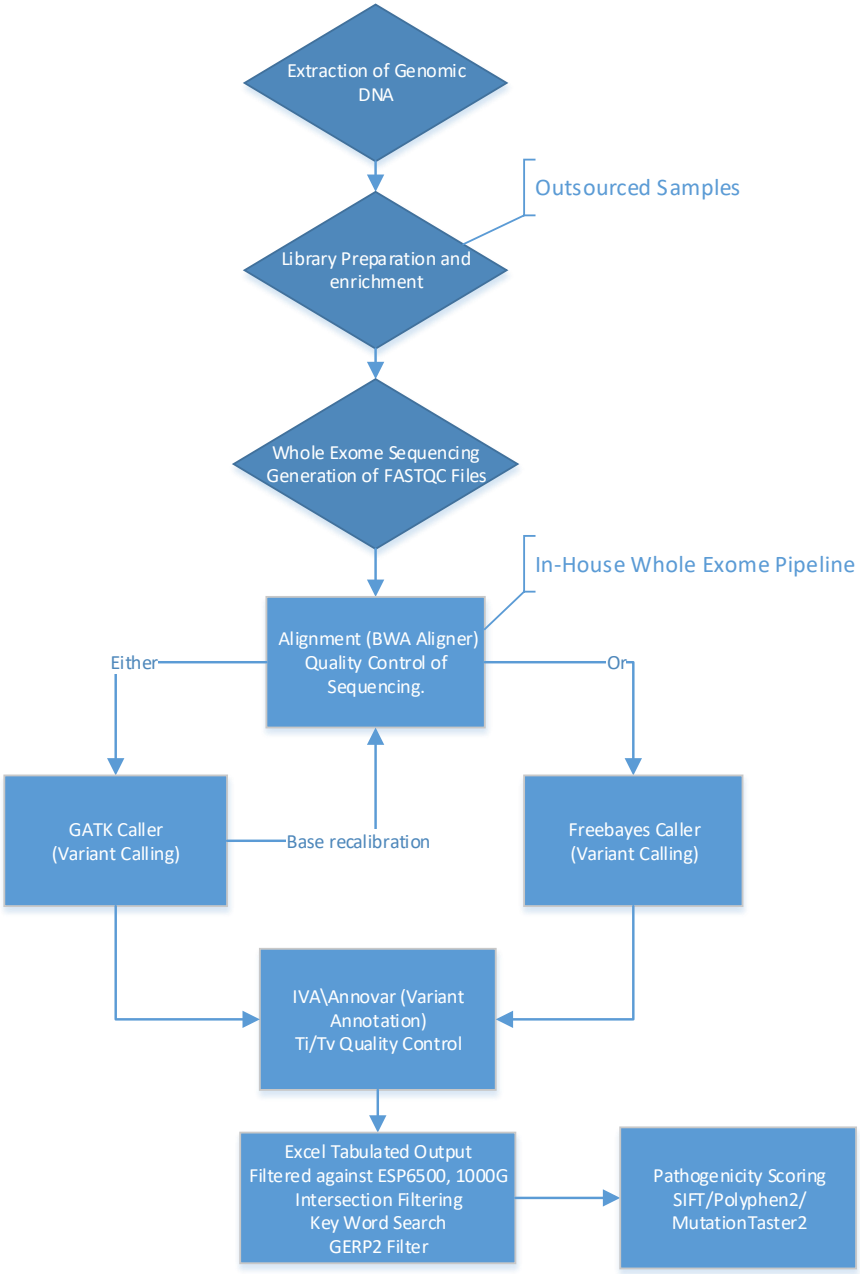

Figure 7-2 Flowthrough schematic summarising the different stages necessary to sequence, align, call and annotate genetic variants in whole exome analysis.

Excel tabulated output is further filtered and analysed to determine potential pathogenic variants. The probability of variant pathogenicity is determined using online tools.

7.3 Results

7.3.1 Comparison of the data resulting from different exonic pipeline callers

Genomic variant location and translational variant impact were two parameters generated and compared following IVA of the annotated data (**Figures 7-3 and 7-4; Table 7-4**). This analysis produced the distribution of variants called by both GATK and Freebayes variant callers from each of the defined phenotypic groups. This showed a 3.4%-7.8% degree of crossover for heterozygous variants in OA groups 1 to 4 (described in **Table 7-2**). There was also a 19.7% 'mutual' detection for homozygous variants in OA group 5 (**Table 7-4**).

Variants associated only with an optic atrophy phenotype also showed an 8.1%-22.2% of shared heterozygous variants for the OA group 1 to 4 and 17.4% homozygous variants between GATK and Freebayes. However more variants in known optic atrophy genes were detected in the GATK pipeline. This discrepancy may be due to a greater generation of novel variants by Freebayes, possibly due to a greater degree of false positive detection.

The T_i/T_v ratio which was detected in samples called by Freebayes was between 1.3-1.8 for 93% of our patient cohort, while exomes called using GATK generated a T_i/T_v ratio between 2.1 and 2.5 also in 93% of my patient cohort (**Table 7-4**). This ratio was probably lower than the 2.8 standard metric for whole-exome analysis as described in **Section 7.2.5** due to Nextera whole-exome capture which also allows for genetic regions surrounding exons to be sequenced at a cost cheaper than whole genomic sequencing.

	GATK and Freebayes shared variants
Heterozygous	3.4-7.8%
Homozygous	19.70%
GATK and Freebayes shared variants (Biological context OA)	
Heterozygous	8.1-22.2%
Homozygous	17.40%
	T_i/T_v
Optimum	2.8
Freebayes	1.3-1.8
GATK	2.1-2.5

Table 7-4 Crossover and quality scores of variants found between GATK and FreeBayes callers

Identification of both shared heterozygous and homozygous variants between GATK and Freebayes callers and shared variants identified using the biological context filter (variants identified only in known optic atrophy related genes).

The location and type of detected variants were also disparate between the two whole exome callers.These variants were mostly detected in intergenic regions by the Freebayes caller while the variants detected by GATK were detected in exonic regions (**Figure 7-3**). In addition, the Freebayes variant caller detected a greater proportion of SNPs, insertions and deletions as well as substitutions and complex variants not detected by the GATK caller (**Figure 7-4**).

Given the T_i/T_v ratio indicating a lesser degree of false positive discovery in the GATK pipeline, a greater degree of variants detected in known optic atrophy genes and in exonic regions and the fact that the genetic variance called in the 1000 genomes project and the ESP6500 datasets was generated using GATK, the GATK caller was chosen for the analysis of the present patient cohort.

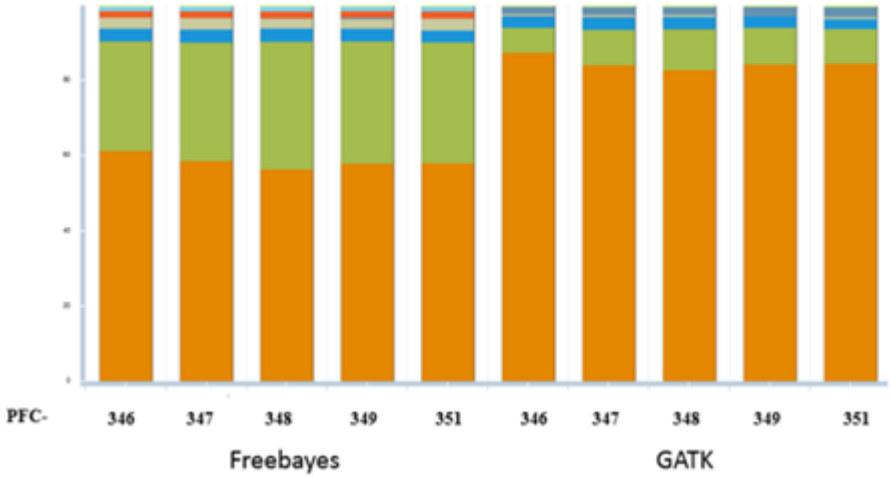

Figure 7-3 Representative distribution of genomic locations

Orange = exonic; Green = Intronic; Blue = ncRNA; Gray = 3'UTR; Red = Promotor; Light Blue = 5' UTR. (B) Orange = SNP; Green = Deletion; Blue = Insertion; Gray = Insertion.

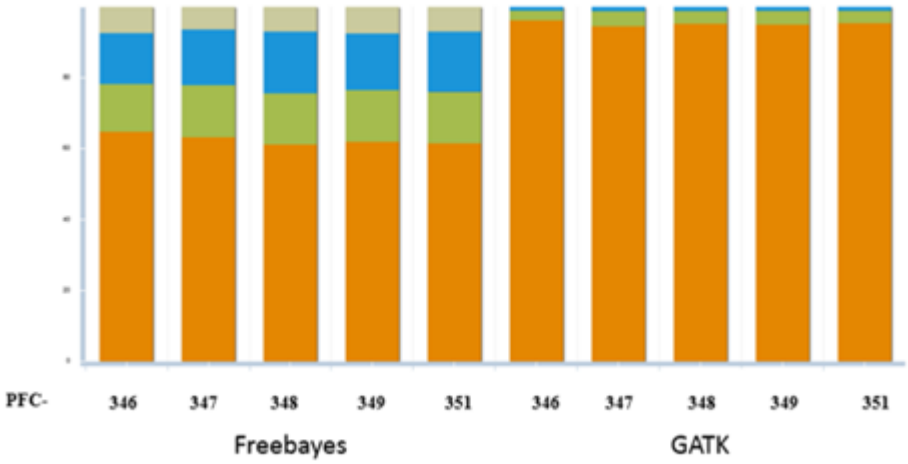

Figure 7-4 Representative distribution of the type of genetics variants with Freebayes and GATK caller.

Orange = SNP; Green = Deletion ; Blue = Insertion ; Gray = Substitution

7.3.2 Whole-exome coverage of known optic atrophy genes

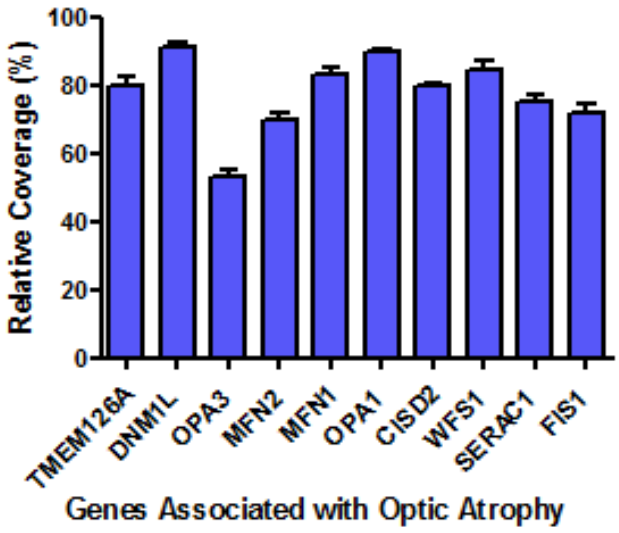

Figure 7-5 Whole- exome coverage data of ten representative genes associated with optic atrophy

To determine the relative whole-exome sequencing coverage of the optic cohort, ten common genes associated with optic atrophy were selected and coverage data of the sequencing reads from these genes was determined by the in-house bioinformatics team (**Figure 7-5**). An average coverage of 78% was achived at a 20x sequencing depth across this panel of genes which conforms to the accepted coverage standard for whole exome analysis (Sims *et al.*, 2014).

7.3.3 Intersection filtering by clinical phenotype

Two alternative strategies were employed to analyse the present patient cohort, one based on intersection filtering of phenotypic groupings and the second based on filtering between patients irrespective of clinical presentation. The four phenotypic groups mentioned in **Section 7.2.6** were first screened against the 1000 genomes and ESP6500 datasets to

determine the number of novel variants within each group. The MAF was set at 5% in order to capture as many rare variants as possible (**Tables 7-5** and **7-6**).

Each grouping was filtered for both heterozygous and homozygous variants. Each of these genes was then investigated using the gene ontology database developed by the gene ontology consortium. This database provides classifications relating to several domains of cellular and molecular biology and provides an overview of known gene function. Once candidate gene lists were generated for each of the phenotypic groups, the number of gene hits in each group was quantified in an attempt to find a common novel optic atrophy candidate gene. The variants found in these genes were then manually assessed to determine if detected variants were due to obvious PCR read duplication error in low complexity regions. Most of the genes found using this method were detected due to common variants generated through sequencing bias and error in these low complexity regions. However it did highlight a SNP in *WFS1* identified in OA group 2 ((c.2051C>T; Ala684Val) 1000 genomes project percentage frequency: 0; ESP6500 percentage frequency: 0; ExAc database: 0). Mutations in *WFS1* are responsible for Wolfram syndrome, a disease characterised by optic atrophy, hearing loss and diabetes and so this was considered a likely pathogenic candidate. To further define the propensity of *WFS1* variant c.2051C>T; p.Ala684Val to be disease causing in patients PFC-344 and PFC-352, the probability of pathogenicity of the variant was further investigated using online pathogenicity tools as described in **Section 7.2.8.** This analysis highlighted the pathogenicity of the c.1505C>T; Ala684Val variant (scores in **Section 7.3.5**) and furthermore it was previously documented in the literature as a variant known to cause optic atrophy and sensorineural deafness. This description matched the clinical presentation of patients PFC-344 and PFC-352 (Rendtorrf *et al.*, 2011).

	OA and Peripheral Neuropathy	OA and Deafness	Isolated OA	Recessive OA
	PFC-340	PFC-344	PFC-346	PFC-350
	PFC-342	PFC-352	PFC-347	PFC-351
	PFC-345		PFC-348	PFC-353
			PFC-349	
			PFC-351	
Dominant	111	193	41	
Recessive	93	104	52	79

Table 7-5 Number of dominant and recessive variants after phenotypic intersection filtering of each phenotypic group.

	Isolated OA	OA and Deafness		OA and Peripheral Neuropathy		Isolated OA	OA and Deafness	OA and Peripheral Neuropathy	Recessive OA group
Dominant candidate genes	FOXD4L5	ABCA12	OR1D5	FOXD4L5	**Recessive candidate genes**	COL18A1	AHSA1	ACSL6	COL18A1
	KCNN2	ATN1	OR6C76	KCNN2		CYFIP2	COL18A1	ATG3	DIXDC1
	NEK3	C2orf71	PIGQ	NEK3		DIXDC1	DIXDC1	COL18A1	FOXD2
	OR11H12	CHL1	POU2F1	OR11H12		FOXD2	FOXD2	CTSA	GRIA3
	POU2F1	CLYBL	PRKCSH	POU2F1		GRIA3	GRIA3	DIXDC1	GRM7
	TIMM23	CNTNAP2	PXDN	TIMM23		HADHB	GRM7	FOXD2	HADHB
		EOMES	SEPN1			MAPK8IP2	OLFM1	GRIA3	KCNN3
		FOXC1	TIMM23			NCOR2	OR7C2	MAP3K1	MAP3K1
		FOXD4L5	TOP1MT			OLFM1	OR8K3		MAPK8IP2
		FSIP2	TPRN			OR7C2	POU4F2		NCOR2
		OBP2A	TSC2			PCLO	SMPD1		OLFM1
		OR11G2	UNQ514				TMIE		OR7C2
		WFS1							PCLO
									STAU2

Table 7-6 Dominant and recessive candidate genes after phenotypic intersection filtering.

7.3.4 Intersection filtering of individual patients

A second approach was adopted to analyse remaining patients for any potential gene candidates. This involved using a similar method previously described by *Fogel and colleagues* (2014). Two whole exome samples from non-optic atrophy patients sequenced in parallel were used as controls to screen for false positive variants generated through technical error that were detected in the analysis described previously in **Section 7.2.5**. These patients were diagnosed with vasovagal syncope with no known optic disturbances. Patients were screened using the 1000 genomes and ESP6500 datasets at a MAF frequency less than or equal to 1% to identify extremely rare pathogenic variants. A threshold of 1% was chosen as a reasonable threshold to limit the number of potential candidate genes. Only exonic and splicing regions were investigated in this analysis. Given the likelihood of pathogenic variants which lie in highly conserved genomic regions, only regions with a genomic evolutionary rate profiling (GERP) score greater than or equal to 2 were investigated. Once variants were filtered according to these parameters, a key word search was used to identify any relevant genes which included terms such as 'eye', 'nervous system', 'endoplasmic reticulum (ER)' and 'mitochondria'. This generated a list of potential candidate genes which were further filtered by comparing between any two patients in the entire optic atrophy cohort. This analysis resulted in 90 potential genes which were then screened using gene card, web of science, google scholar and the Ingenuity Knowledge Base to identify any genes related to optic atrophy or any secondary symptom.

These genes were further investigated to select those which contained any two or more pathogenic variants present in at least two individuals of the cohort. Pathogenic variants were defined as any variant which was identified as potentially pathogenic in at least two different online pathogenicity tools. This analysis was to identify any potential common pathogenic gene between any two individuals underpinning an optic atrophy phenotype. These genes are listed in **Table 7-7.** Two potential pathogenic variant in *WFS1* (c.977C>T; p.Ala326Val (1000 genomes project percentage frequency: 0; ESP6500 percentage frequency: 0.00008; ExAc percentage frequency 0.000025) and c.2452C>T; p.Arg818Cys (1000 genomes project precentage frequency 0.002; ESP6500 precentage frequency 0.005; ExAc: 0.0049) and numerous patients containing *ATF5* variants were discovered following this analysis. Since the majority of cases of Wolfram Syndrome are recessivly inherited as previously described,

PFC-341 and PFC-351 were further scrutinised to determine if any other variants were detected by WES but filtered out due to the stringent parameters used to detect any potential pathogenic variants. This revealed a second variant in patient PFC-341 (c.1309G>C; p. Gly437Arg; ExAc percentage frequency:0.0000082) . Further analysis to determine inheritance pattern of these variants in described in **Chapter 8**.

Genes	cDNA	Protein	PFC-
ATP7B	c.1682C>T	p.Thr561Met	348
	c.1763C>T	p.Ala588Val	353
CACNA1S	c.773G>A	p.G258D	346,349
KCND3	c.497G>A	p.Arg166His	340;349
	c.5C>A	p.Ala2Glu	147
GRIN2A	c.2909G>A	p.Arg970Gln	342
	c.2626A>T	p.Ile876Phe	350
NBAS	c.1093G>C	p.Asp365His	345,350
WFS1	c.977C>T	p.Ala326Val	341
	c.2452C>T	p.Arg818Cys	351
SYNE1	c.4162C>T	p.Arg1388Trp	341
	c.13696G>A	p.Asp4566Asn	147
ATF5	c.365T>C	p.Leu122Pro	341,342,348,353,147
	c.376T>C	p.Ser126Pro	341,342,348,353
CTSB	c.203G>A	p.Arg68His	147
	c.391G>A	p.Val131Met	348
CUL7	c.3253C>T	p.Arg1085Cys	353
	c.2570C>T	p.Thr857Met	340
CEP290	c.2417G>A	p.Arg806Gln	353
	c.245G>A	p.Arg82Gln	348
COL24A1	c.4235A>T	p.Asp1412Val	350
	c.20G>A	p.Arg7Lys	353
TRPV4	c.219G>A	p.Glu733Lys	147
	c.1363G>A	p.Val455Ile	348
HDGF	c.709C>T	p.His237Tyr	341
	c.622C>T	p.Arg208Trp	340
DRAXIN	c.178C>T	p.Arg60Trp	350,347

Table 7-7 Candidate gene list generated for each optic atrophy patient

This table illustrates genes containing at least one pathogenic variant in two or more patients which are associated with either an OA phenotype or any other additional phenotype which presents in this patient cohort. Only genes which have been predicted to be pathogenic in at least two pathogenicity tools are included. Genes are ranked in order of decreasing probability of pathogenicity.

7.3.5 Investigation of the probability of *WFS1* variant pathogenicity

The pathogenicity of the four *WFS1* variants (p.Ala684Val, p.Ala326Val, p.Gly437Arg and p.Arg818Cys) identified were analysed using Mutationtaster2, Polyphen-2 and SIFT. The c.2505C>T (p.Ala684Val) variant found in PFC-344 and PFC-352 patients was identified as pathogenic by all three prediction programs with a Polyphen2 score of '0.992' and a SIFT score of '0'. MutationTaster2 predicted the variant to be disease causing with a probability of 0.999 because it was a known disease mutation identified through HGMD.

Investigation of patient PFC-341 identified the p.Ala326Val variant in Polyphen2 as probably damaging with a score of 0.997, SIFT predicted a tolerated variant with a score of 0.356 and MutationTaster2 predicting a disease causing gene with a probability of 0.999. MutationTaster2 also determined the variant to be a known disease mutation. An investigation of the p.Gly437Arg variant revealed that both Polyphen2 and MutationTaster2 predicted the variant to be benign with a Polyphen2 score of 0.029, MutationTaster2 score of predicted of 1.42e-5. Further investigation of these three *WFS1* variants was conducted in patient PFC-341 in **Chapter 8.** Patient PFC-351, who harboured the p.Arg818Cys *WFS1* variant, had a Polyphen2 score of '1', a SIFT score of 0.03 and a MutationTaster2 score of '0.999'. MutationTaster2 also annotated the variant as a known disease mutation. Further investigation of these three *WFS1* variants was conducted in patient PFC-341 in **Chapter 8.**

7.3.6 Identification of two potential pathogenic variants in *ATF5*

Intersection filtering of the WES cohort also identied two potential pathogenic missense variants in *ATF5* p.Leu122Pro and p.Ser126Pro (**Table 7-7**). The presence of these two variants in a relatively large subset of optic atrophy patients (PFC-341, PFC-342, PFC-348, PFC-353 and PFC-147) may warrant further investigation.

7.4 Discussion

Typically, WES study design includes either a cohort of family trios consisting for two unaffected parents and an affected child or as singleton cases in which a large cohort of unrelated affected individuals is analysed.

Evaluation of family trios can improve the accuracy and detection of causative pathogenic mutations by allowing variant filtration based on the genetic background of the affected individual (Hunt *et al*., 2014). As a consequence, many polymorphisms, both common and rare in the general population, may be removed from the analysis. This is best for recessive conditions in which homozygous or compound heterozygous variants can be segregated in both parents and child. Furthermore, variants found in affected individuals but not in unaffected parents due to artefactual sequencing error may also be determined.

On the other hand, the use of sequencing data from family trios may also introduce additional cost and complexity in the analysis. It would require detailed clinical assessment of both parents and child with a reduced cohort of affected individuals in the final assessment. Technical complexity could also be introduced due to sample 'missingness' referring to alternative loci of low coverage within a family trio (Browning *et al*., 2009). 'This may increase the number of polymorphisms and false positives after the filtration process. Other difficulties can also arise due to reduced penetrance of a pathogenic variant. A large and detailed pedigree would therefore be beneficial for segregation analysis in these cases.

In this study, we opted to analyse a cohort of rigorously phenotyped OPA1-negative singleton cases who presented with optic atrophy. This design was chosen to provide a large cohort of affected individuals of unknown genetic aetiology but with similar clinical presentation. In addition, although it would be useful to include other unaffected family members for segregation analysis, limited access to parental DNA for many of these cases limited the scope of the analysis which could be performed.

Based on this study design, variant frequencies within the patient cohort were associative and based upon population frequencies found within the 1000 genome and ESP6500 datasets.

Two different in-house bioinformatics pipelines with either a GATK haplotype or Freebayes caller were developed by the mitochondria bioinformatics team, IGM. In order to assess the best caller for sequencing analysis of this patient cohort, FASTQ files were processed through either the GATK or Freebayes pipelines and annotated using IVA. This investigation revealed that the GATK caller generated more SNPs in the exonic region than Freebayes with a lower Ti/Tv false positive variant score. Freebayes also called a number of insertions and deletions in the intergenic region which were not detected by GATK. Given the likelihood that Freebayes may be detecting greater degree of variants that are false-positive both in exonic regions and regions not likely to result in protein functional pathogenicity, the GATK caller was then chosen to perform variant calling for the optic atrophy cohort.

Numerous different study designs with different capture kits have been implemented to achieve the greatest depth and coverage of the human exome. Despite a significant reduction in recent years, sequencing costs still remain substantial and a fine balance must be achieved between cost and robust sequencing with adequate depth and coverage in each sample analysed (Sims *et al.,* 2014). The minimum threshold to achieve this is 10x deep sequencing coupled with 80% targeted capture of the exome, regardless of the exome capture kit or WES pipeline used to detect variants (Zhou *et al.,* 2012; Thauvin-Robinet *et al.,* 2013; Yu *et al.,* 2013). This means a significant portion of the exome may not be covered due to LCRs and poor hybridisation of sequence capture probes in GC rich regions.

To assess the degree of coverage in the optic atrophy cohort through this selected pipeline, a selection of ten optic atrophy genes were chosen and their coverage analysed by the mitochondria bioinformatics team, IGM. The percentage of bases captured in each gene across the entire cohort was quantified and ranged between 50-90% coverage. Average coverage was approximately 80% at 20x sequencing depth which is the quality standard required for WES analysis (Sims *et al.,* 2014).

Initial filtering of the entire optic atrophy cohort did not detect variants common to all patients, suggesting underlying genetic heterogeneity in patient presentation. In order to prevent pathogenic variants from being screened through whole cohort filtering, each of the patients was stratified according to their phenotype. This divided the cohort into five phenotypic groups described as OA group 1 ‘Isolated optic atrophy’, OA group 2 ‘Optic atrophy and deafness’, OA group 3 ‘Optic atrophy and diabetes, OA group 4 ‘Optic atrophy

and peripheral neruopathy' and OA group 5 'Suspected recessive inheritance'. Patients from OA groups 1-5 which had more than one individual with a similar clinical phenotype other than OA were used in this analysis (Exception for OA and diabetes which contained a single patient member).

In the initial intersection filtration method, the patient cohort were stratified according to their common phenotypic presentations. This led to the identification of a dominant *WFS1* variant identified in patients characterised with optic atrophy secondary to hearing impairment (OA group 2). Further investigation of this variant indicated that it was disease causing. A literature search revealed two publications by Rendtorff *et al.* (2011) and Tessa *et al.* (2001) describing dominant inheritance of the pathogenic *WFS1* phenotype of two patients harboring the p.Ala684Val *WFS1* variant. Additional heterozygous/homozygous variants detected in each of these groupings were found to be caused by misalignment error or PCR bias which occurred at LCRs of the genome.

In the second method of intersection filtering which involved filtering of any two patients irrespective of clinical presentation, false-positives due to technical errors were minimised by using two 'no optic atrophy' disease controls. Also, to help reduce the number of likely polymorphic variants in the cohort, variants were screened using a GERP2 filter. This was used to screen for variants located in evolutionarily conserved regions of the genome. Investigation of these evolutionary conserved regions highlighted a number of interesting variants. A *WFS1* missense variants (p.Ala326Val) was detected in PFC-341, **Table 7-7**. This patient presented with optic atrophy and diabetes, a common clinical phenotype associated with Wolfram syndrome. (Wolfram and Wagner, 1938; Cooper *et al.*, 1950; Paley and Tunbridge, 1956). Wolfram syndrome is typically a recessive condition which is acquired through compound heterozygous or homozygous inheritance. A literature search indicated that this variant was one of a number of variants that were identified through genetic screening of a cohort of patients diagnosed with Wolfram syndrome and psychiatric illness. However it has not yet been proven to be causally linked to the manifestation of Wolfram syndrome (Torres *et al.*, 2001). Further analysis of this patient is described in **Chapter 8**.

Furthermore, a second WFS1 variant (p.Arg818Cys) was also detected using this second method of intersection filtering. This variant has been annotated as 'disease causing'

according to HGMD however a literature search indicated that there is much controversy surrounding the pathogenicity of this variant. It was initially described in a consanguineous Spanish family with homozygous inheritance diagnosed with Wolfram syndrome (Gomez-Zaera *et al.,* 2001). However it has also been detected in control cohorts of independent studies investigating Wolfram syndrome (Cryns *et al.,* 2002; Martorell *et al.,* 2003). Functional analysis is required to determine if it is truly pathogenic. Unfortunately, we were unable to obtain the relevent biological material to perform this analysis.

Interestingly two potential pathogenic ATF5 heterozygous variants (p.Leu122Pro and p.Ser126Pro) were both discovered in four patients in the optic atrophy cohort and a single p.L122P variant was detected in a fifth (**Table 7-7**). ATF5 is a transcription factor that belongs to the response element binding protein family (CREB) and is involved in the ER stress reponse (Vinson, 2002). It is expressed as two alternative transcripts (ATFα and ATFβ) that differ only in their 5' untranslated region (UTR) (Hansen *et al.,* 2002). This UTR is similar to the one found in *ATF4* and allows *ATF4* and *ATF5* transcripts to be preferentially translated upon induction of ER stress due to an overload of misfolded proteins. It typically operates to promote cellular/protein homeostasis in conjunction with ATF4, ATF6 and XBP1 downsteam of phosphorylated EIF2α. However, once ER stress conditions reach a critical threshold, it can instead promote apoptotic cell death (Teske *et al.,* 2013). Previously, ATF5 was not thought to be expressed in differentiated neuronal tissue however recent experimental work conducted by *Torres-Pereza and colleagues* (2013) showed that ATF5 is widely expressed in differentiated mouse neurons. The ATF5 gene is not particularly large with only 5,235 bases which encode a 282 amino acid protein. Further functional work would be required to confirm these potential pathological variants in optic atrophy. Other ER components involved of the UPR such as WFS1 have been associated with optic atrophy illustrating that, ER components involved in maintaining ER homeostasis may also have an impact on optic nerve degeneration.

In conclusion, intersection filtering was employed both between individual patients and groups of patient with a similar clinical phenotype. These strategies aided in the identification of a number of pathogenic or potential pathogenic *WFS1* variants which may suggest a greater incidence of Wolfram syndrome than has previously been reported in the British population.

The number of confirmed and potential *WFS1* cases (3/14 patients – 21%) is consistent with the current documented success rate for WES in monogenic disorders (25%) (Yang *et al.*, 2013). Further functional work to validate some of these variants is described in **Chapter 8**. Furthermore, stringent analysis between individual patients to identify highly rare potentially pathogenic variants in evolutionary conserved genomic regions have highlighted two novel ATF5 variants in 36% of my cohort (5/14 patients). Further investigation is required to determine if these variants influence an underlying clinical phenotype through *in vitro* manipulation of ER stress induced pathways.

Inability to detect potential pathogenic variants in other member of the OA cohort reflect three limitations of study design. The first is that variant frequencies used in this analysis are merely associative. Variants of low frequency may reflect regions of poor coverage within each of the independent control studies used in this analysis or individuals within these control cohorts may only possess wild-type alleles for regions enriched with variants sequenced by our in-house pipeline. This can increase the number of polymorphisms left after intersection filtering. The second is that WES is limited to only the exonic regions which are not of low complexity. Therefore, mutations in promotor regions, intronic regions and copy number variants will go undetected. Lastly, the lack of any definitive pathogenic gene other than *WFS1* also likely reflects the genetic heterogeneity of optic neuropathies which could be ameliorated by a larger OA cohort.

Chapter 8

WFS1 Mutations in Patients with Inherited Optic Atrophy

8.1 Introduction

Wolfram syndrome was first described by Dr Donald Wolfram from the Mayo Clinic in 1938 in a case series of four siblings diagnosed diabetes insipidus, diabetes mellitus, optic atrophy and deafness (DIDMOAD) (Wolfram and Wagner, 1938). The condition has been characterised with classical symptoms: diabetes insipidus, diabetes mellitus, optic atrophy and/or deafness (DIDMOAD). The EURO-WABB is an EU rare diseases registry for Wolfram syndrome, Alström syndrome, Bardet-Biedl syndrome and other rare diabetes syndromes (Farmer *et al*., 2013). Based on the latest EURO-WABB consensus guidelines, both optic atrophy and diabetes mellitus are considered as major criteria for the diagnosis of Wolfram syndrome(http://www.orpha.net/national/data/IEEN/www/uploads/Wolfram2014.pdf, accessed July 10, 2016).

Autosomal recessive *WFS1* mutations were identified in patients with classical Wolfram syndrome (Strom *et al*., 1998). *WFS1* encodes for Wolframin, a transmembrane endoplasmic reticulum protein that plays a critical role in calcium homeostasis and stress in the unfolded protein response (Takei *et al.*, 2006; Yamada *et al.*, 2006; Yamaguchi *et al.*, 2004).With the advent of genetic screening and through clinical assessment, the manifestations and mutational spectrum of pathogenic *WFS1* mutations has expanded rapidly over the past few years. Over 200 case reports have been published so far and in addition to the classical DIDMOAD, other associated features include neurological deficits, psychiatric disturbances, urological dysfunction and gastrointestinal abnormalities. Fatal complications such as central apnea leading to aspiration pneumonia can also arise and the average lifespan of a patient diagnosed with Wolfram syndrome is 30-40 years old (De Heredia *et al.*, 2013). Patients can also present with a more limited form of the disease, referred to as Wolfram-like syndromes, including isolated sensorineural hearing loss, cataracts and diabetes (Bai et al., 2014; Goncalves et al., 2014; Berry et al., 2013; Chacon-Camacho et al., 2013; Bonnycastle et al., 2013; Valero et al., 2008).

The majority of patients with Wolfram syndrome or Wolfram-like syndromes, harbour homozygous or compound heterozygous *WFS1* mutations. More recently, there have been a number of reports of patients carrying dominant *WFS1* mutations, especially in association with low frequency sensorineural hearing loss, diabetes mellitus and autosomal dominant

optic atrophy (Rendtorrf *et al.,* 2011; Khanim *et al.,*2001; Middle *et al.,* 2000; Hogewind *et al.,* 2010; Eiberg *et al.,* 2006; Wasson *et al.,* 2008). The studies that have been published so far have revealed variable genotype-phenotype correlations for recessive and dominant *WFS1* mutations. A recent study performed by *Chaussenot and colleagues* suggested that *WFS1* mutations located at or near the C-terminus are more likely to be associated with psychiatric illness whereas those located at or near the N-terminus have a lower likelihood of causing neurological complications (Chaussenot *et al*., 2011). In addition, they also found that homozygous loss-of-function mutations, such as nonsense or frameshift mutations, which result in a marked reduction in WFS1 protein level are more likely to be associated with early-onset diabetes mellitus and optic atrophy. This early onset of optic atrophy and diabetes is consistent with the findings of other independent studies (Cano *et al.,* 2007; Rohayem *et al.,* 2011; Matsunaga *et al.,* 2014).

A systematic review of 49 published studies was performed by *De Heredia and colleagues* in which patients were stratified into groups based upon: (1) complete loss of WFS1 protein level, (2) dominant-negative *WFS1* mutations, or (3) haploinsufficient *WFS1* mutations (De Heredia *et al*., 2013). Compared with the other studies mentioned earlier, this analysis of 412 patients came up with different genotype-phenotype correlations. Interestingly, in this patient cohort, diabetes mellitus and optic atrophy were not always the first two manifesting clinical features. Disease progression was characterised by the development of diabetes mellitus (10 years old), optic atrophy (10-20 years old), diabetes insipidus (10-30 years old), sensorineural hearing loss (10-38 years old), and/or neurological defects (5-55 years old) (De Heredia *et al.,* 2013). The age at onset of diabetes mellitus, hearing defects, and diabetes insipidus were found to depend on the patient's genotypic class. In terms of disease severity, dominant negative *WFS1* mutations were associated with more rapid progression, in particular for optic atrophy, sensorineural deafness and diabetes mellitus (De Heredia *et al.,* 2013)

In this part of my PhD project, I further investigated the functional consequences of the *WFS1* variants that have been identified with WES in our cohort of patients with undiagnosed inherited optic atrophy (**Table 8-1**). Moreover, given the unexpected high prevalence of pathogenic *WFS1* mutations, Sanger sequencing was carried out for the

remaining patients in our optic atrophy cohort to look for possible WFS1 *variants* that might have been missed in regions not well covered by WES.

Patient	Gender	Age	Clinical Presentation	cDNA	Protein
341	F	38	OA and diabetes mellitus	c.977C>T	p.Ala326Val
341	F	38	OA and diabetes mellitus	c.1309G>C	p.Gly437Arg
344	F	78	OA and hearing loss	c.2051C>T	p.Ala684Val
352	M	25	OA and hearing loss	c.2051C>T	p.Ala684Val
351	F	19	OA	c.2452C>T	p.Arg818Cys

Table 8-1 Cohort of patients with *WFS1* variants identified through WES.

8.2 Materials and Methods

8.2.1 DNA extraction from blood

Whole Blood Genomic Extraction kit (Nucleon) was used to extract DNA from the blood of the parents of patient PFC-341 as described in **Section 3.5.1.** In addition, DNA previously extracted from patients PFC-341, PFC-344 and PFC-352's blood and stored at -80°C were used.

8.2.2 *WFS1* Sanger sequencing

Pathogenicity of *WFS1* variants was determined '*in silico'*as described in **Section 7.2.4** using online programs MutationTaster2, SIFT and Polyphen-2. The *WFS1* variants identified with whole-exome sequencing was confirmed with both forward and reverse Sanger sequencing as described in **Section 3.13**. These sequenced amplicons were compared against *WFS1* mRNA transcript variant 1 (NM_006005.3) and protein (NP_005996.2)) using Seqscape v 2.6 (Applied Biosystems). DNA was extracted from blood samples obtained from the parents of patient PFC-341 to confirm the mode of inheritance.

8.2.3 Western blot analysis of patient with compound heterozygous *WFS1* variants

Western blot analysis of patient 'PFC-341' was carried out as described in **Section 3.3.** Briefly, protein from three primary fibroblast biological replicates was extracted and probed using a primary WFS1 anti-rabbit antibody (cat: 11558-1-AP; Proteintech) overnight using a 1:1000 antibody dilution. This was washed three times in TTBS (Sigma-Aldrich) for 10 minutes before an anti-rabbit secondary antibody was applied for 1 hour at room temperature. The western blot membrane was re-washed with TTBS 4 times with each wash lasting 5 minutes before antibody detection. Protein bands were imaged using an ECL kit (Biorad) and an Amersham Imager 600 (GE Healthcare Lifesciences).

8.2.4 Modelling of WFS1 protein

A theoretical model of the WFS1 protein was generated to illustrate any structural changes induced by mutations in *WFS1*. Similar to the model generated for OPA1 as described previously in **Section 6.3.3**, the WFS1 structural model was generated by using the FFAS server to locate the most structurally homologous protein to WFS1, namely, maltose-binding periplasmic protein (score: -8.69; sequence identity: 9%, http://ffas.sanfordburnham.org/ffas-cgi/cgi/ffas.p). This protein was then modelled using the SCWRL server with default settings. Pymol (Delano Scientific, https://www.pymol.org/) was used to manipulate the WFS1 model and introduce any changes due to specific mutations using the mutagenesis tool.

8.2.5 *WFS1* screening

Exons 2-8 and surrounding intronic regions were PCR amplified and sequenced using 11 M13-tagged primer pairs (**Table 8-2**). Sanger sequencing of *WFS1* in my whole exome cohort was carried out as previously described in **Section 3.13**. These sequenced amplicons were also compared against *WFS1* mRNA transcript variant 1 (NM_006005.3) and protein (NP_005996.2)) using Seqscape v 2.6 (Applied Biosystems). The genetic variants identified were analysed for pathogenicity using MutationTaster2, SIFT and Polyphen-2 as previously described (**Section 7.3.3**). Any identified *WFS1* variants were reversed sequenced to exclude any errors due to PCR amplification.

Exon	Size (bp)	Forward (Sequence 5'-3')	Reverse Sequence (3'-5')
2	491	TCAGCGAGATCCTGTATGGA	AGCTGCACAATGCTGAACTG
4	579	TCCATGCATTGATGGTGAGC	AATTTCCCAACAGCATCACC
5	495	CCCTGGTAACCAAGTCCTGA	GCACGGTCTCTACAGGAAGG
7	684	GTCACCCGTGCTGTGAGAA	GGCACGGCTGTAAGACACTC
8(a)	482	TTTCAAGGGCACCTACTGCT	CCATGTTGGTCTCCTTCCAG
8(b)	599	ACATGCTCCCGTTCTTCATC	CACTGGTGCATGCCTGTC
8(c)	384	GGTCAAGCTCATCCTGGTGT	AGCAGCTTAAGGCGACAGAG
8(d)	540	AAGAGGAAGTAGCCGATGGA	CAACCTGGATGTGGAGCAG
8(e)	497	GTCAGAGGGAGGCGTGAGAT	GGGATGCAGTCCTTGCTG

Table 8-2 Primers details in PCR amplification of select WFS1 exons.

Exons of WFS1 which were not covered through 20x whole exome sequencing were selectively targeted,PCR amplified and Sanger sequenced to determine if any pathogenic variants of WFS1 may lie hidden in these genomic regions. All primers were designed using Genbank accession number NM_006005. Each primer contains an M13 tag to facilitate single primer sequencing. Sequencing conditions used to quantify mtDNA copy number are described in **Section 3.10.2.**

8.3 Results

8.3.1 Confirmation of variant c.3452C>T(p.Arg818Cys) in patient PFC -351

The c.C3452T (p.R818C) *WFS1* variant in patient PFC-351 that was detected with WES was confirmed by both forward and reverse Sanger sequencing (**Figure 8-1**).

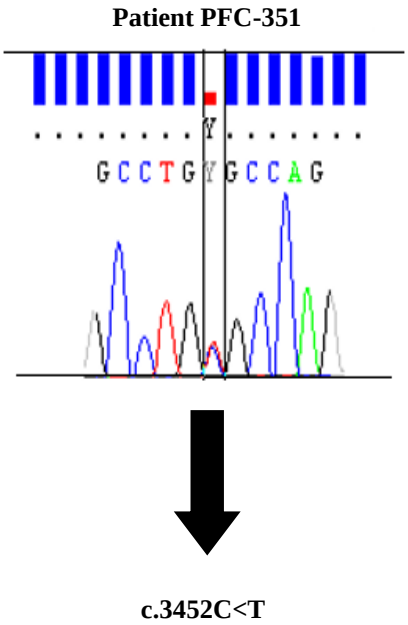

Figure 8-1 Sequencing chromatogram illustrating the c.C3452T *WFS1* variant detected in patient PFC-351

8.3.2 Confirmation of variants c.1309G<C (p.Gly437Arg) and c.977C>T (p.Ala326Val) in patient PFC -341

Clinical examination of patient PFC-341 was performed by Dr Yu-Wai-Man. Fundus examination showed bilateral optic atrophy and significant thinning of the peripapillary retinal nerve fibre layer was confirmed with optical coherence tomography (OCT) imaging (**Figure 8-2**). Sanger sequencing confirmed the c.1309G<C (p.Gly437Arg) and c.977C<T (p.Arg326Val) *WFS1* variants in patient PFC-341. Sanger sequencing was also carried out in both parents to confirm the mode of inheritance (**Figure 8-3A**). The father harboured the c.1309G>C (p.Gly437Arg) variant whereas the mother harboured the c.977C<T (p.Ala326Val) variant, indicating a compound heterozygous mode of inheritance for patient PFC-341 (**Figure 8-3B**).

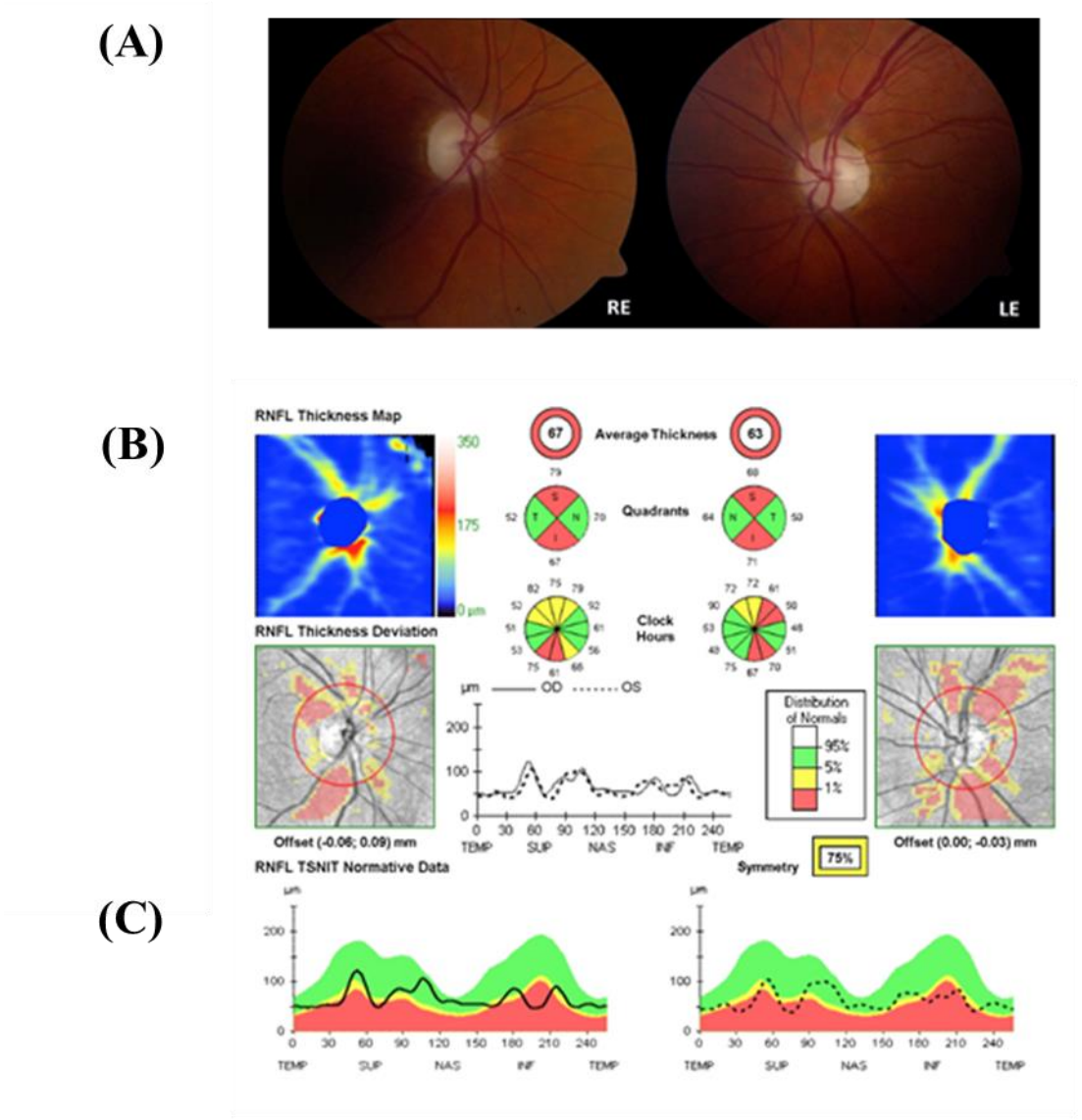

Figure 8-2 Ophthalmological findings for patient PFC-341

(A) Bilateral optic atrophy is demonstrated on fundoscopic examination (RE = right eye, LE = left eye). **(B)** Optical coherence tomography (OCT) measurements were obtained with the high-resolution spectral-domain Cirrus^{TM} platform (Carl Zeiss Meditec, Dublin, CA). The average retinal nerve fibre layer thickness was 67µm in the right eye (OD) and 63µm in the left eye (OS). **(C)** The analysis software automatically selects the appropriate normative range for the patient and the peripapillary RNFL measurements (dark traces) are represented within colour-coded distribution centiles (bottom panel): (i) red < 1%, (ii) yellow 1-5%, and (iii) green 5-95%.

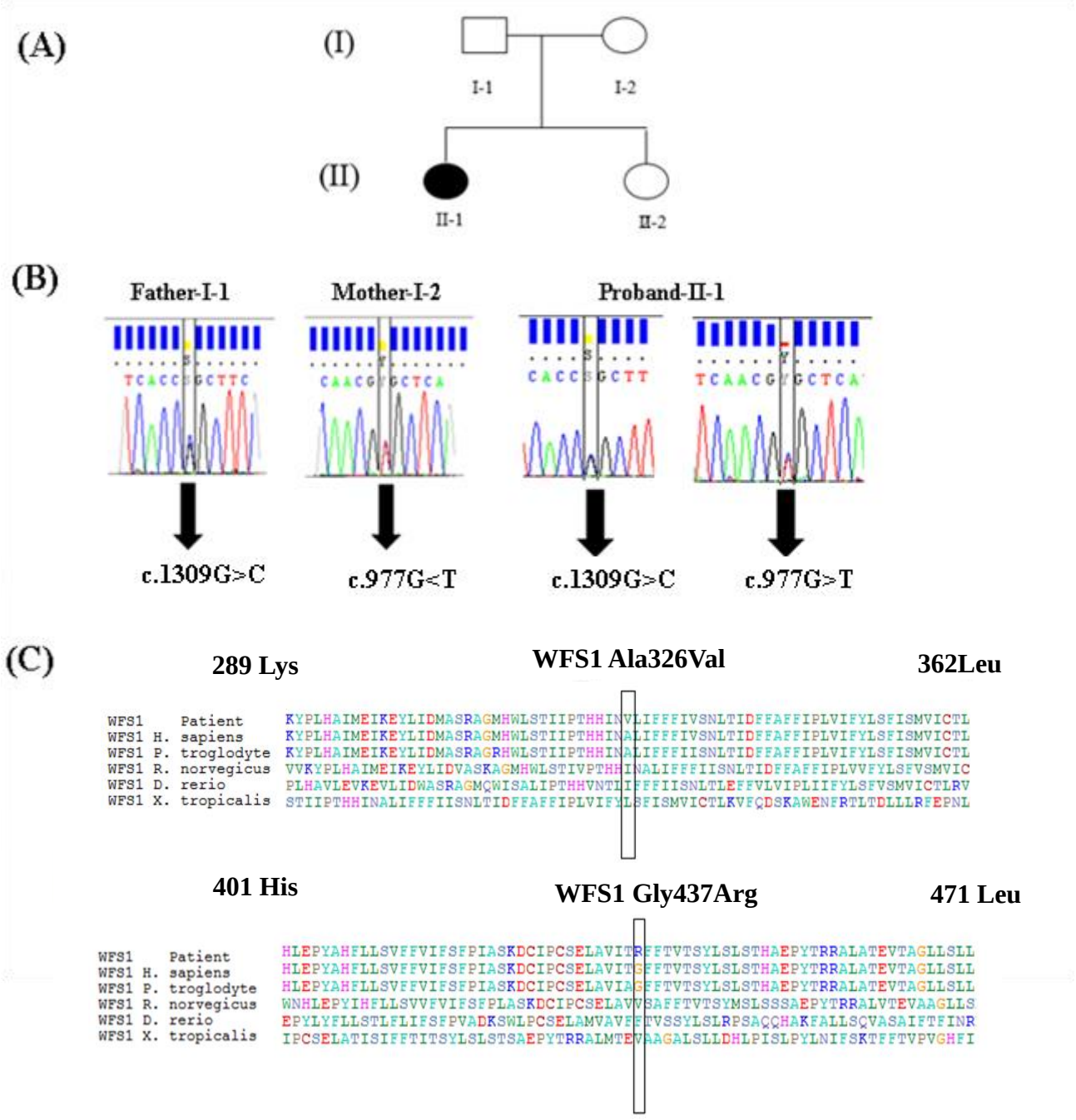

Figure 8-3 (A) Family pedigree; (B) Sequencing chromatogram of the proband and his unaffected parents; and (C) WFS1 protein alignment and degree of evolutionary conservation.

The pathogenicity of the *WFS1* variants found in patient PFC-341, c.1309G<C (p.Gly437Arg) and c.977C<T (p.Ala326Val), was further investigated with western blot analysis. WFS1 protein levels in the patient's fibroblasts showed a significant decrease compared with controls to about half normal levels.

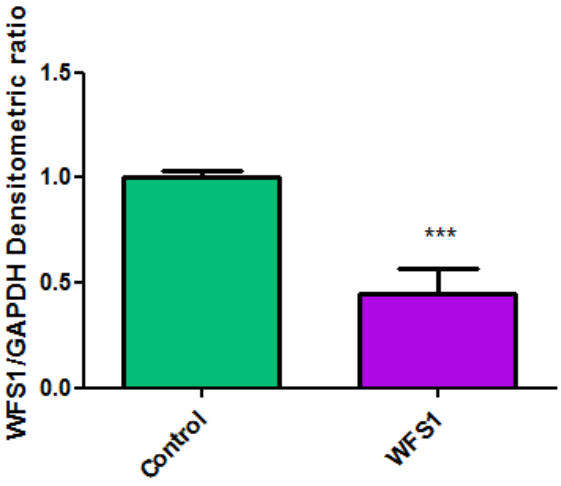

Figure 8-4 Western blot analysis of WFS1 in patient PFC-341.

Western blot normalised against GAPDH and mean of two biological controls. An unpaired Student's T-test was used for statistical comparison ($p \leq 0.001$, *** significance).

8.3.3 Confirmation of variant c.2051C<T (p.Ala684Val) in patients PFC-344 and PFC-352

Clinical examination of patient PFC-344 was performed by Dr Yu-Wai-Man (**Figure 8-5**). Sanger sequencing confirmed the presence of the c.2051C<T (p.Ala684Val) *WFS1* variant that was detected with WES (**Figure 8-5**).

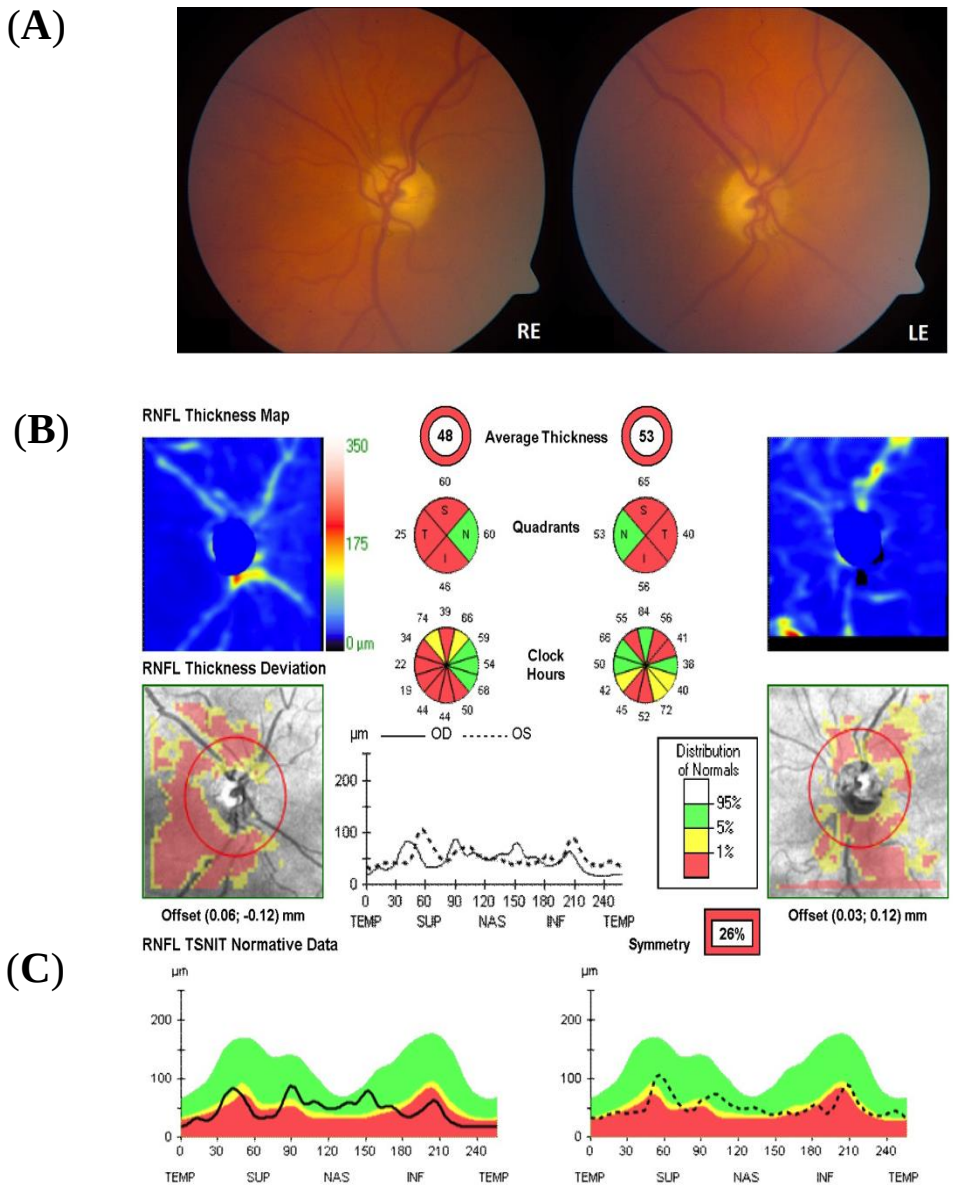

Figure 8-5 Ophthalmological findings for patient PFC-344

(A) Bilateral optic atrophy was observed on fundoscopic examination (RE = right eye, LE = left eye). **(B)** Optical coherence tomography (OCT) measurements were obtained with the high-resolution spectral-domain Cirrus^{TM} platform (Carl Zeiss Meditec, Dublin, CA). The average retinal nerve fibre layer thickness was 48µm in the right eye (OD) and 53µm in the left eye (OS). **(C)** The analysis software automatically selects the appropriate normative range for the patient and the peripapillary RNFL measurements (dark traces) are represented within colour-coded distribution centiles (bottom panel): (i) red < 1%, (ii) yellow 1-5%, and (iii) green 5-95%.

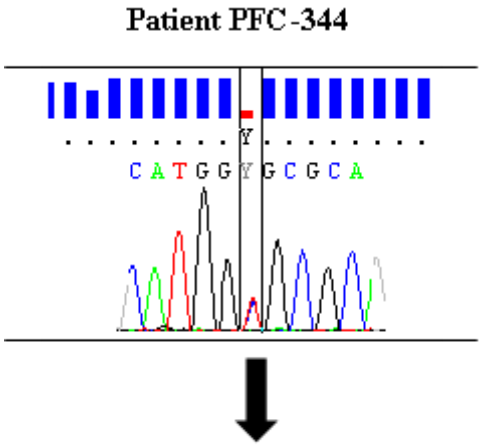

Figure 8-6 Sequencing chromatogram illustrating the c.2051C<T *WFS1* variant detected in patient PFC-344

8.3.4 Confirmation of variant c.2051C<T (p.Ala684Val) in patient PFC-352

Sanger sequencing confirmed the c.2051C<T (p.Ala684Val) *WFS1* variant in patient PFC-352 (**Figure 8-7**).

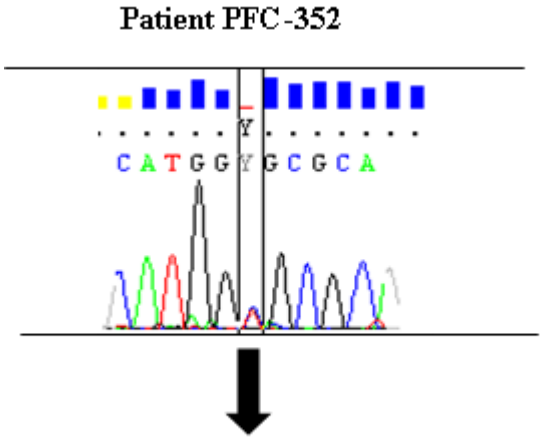

Figure 8-7 Sequencing chromatogram illustrating the c.2051C<T *WFS1* variant detected in patient PFC-352

8.3.5 Protein modelling of the impact of *WFS1* mutations

WFS1 is an 890 amino acid protein with the closest known structural homologue being Maltose-binding periplasmic protein (sequence identity: 9%) (**Figure 8-8**). The precise protein folding of WFS1 and how pathogenic mutations may impact on its structure and function are still poorly defined in the literature. Modelling of the c.2051C<T (p.Ala684Val) variant indicates that it lies structurally within the degron, a target for Smurf-1 mediated degradation of WFS1 by the ubiquitin-proteasome system, which is an important mechanism for regulating the unfolded protein response in the ER (Guo *et al.*, 2011). Interestingly, an investigation of single heterozygous variants identified in patients with wolfram syndrome in the Euro-Wabb WFS1 database (https://lovd.euro-wabb.org/home.php?select_db=WFS1) indicate that almost all of these variants are located in exon 8 and they affect protein regions located within the ER (membrane and lumen) rathen than the cytoplasmic compartment. Heterozygous *WFS1* mutations that have been linked specifically with optic atrophy and sensorineural hearing loss also appear to cluster exclusively in the protein region located within the ER lumen, with the exception of a single sporadic case reported by *Cryns and colleagues* (2002). The *WFS1* missense variants, c.977C<T (p.Ala326Val) and c.1309G<C (p.Gly437Arg) are both located within the ER membrane, but due to the compound heterozygous nature of these variants with both contributing to disease pathogenicity, it is more difficult to structurally ascertain their impact on WFS1 protein function.

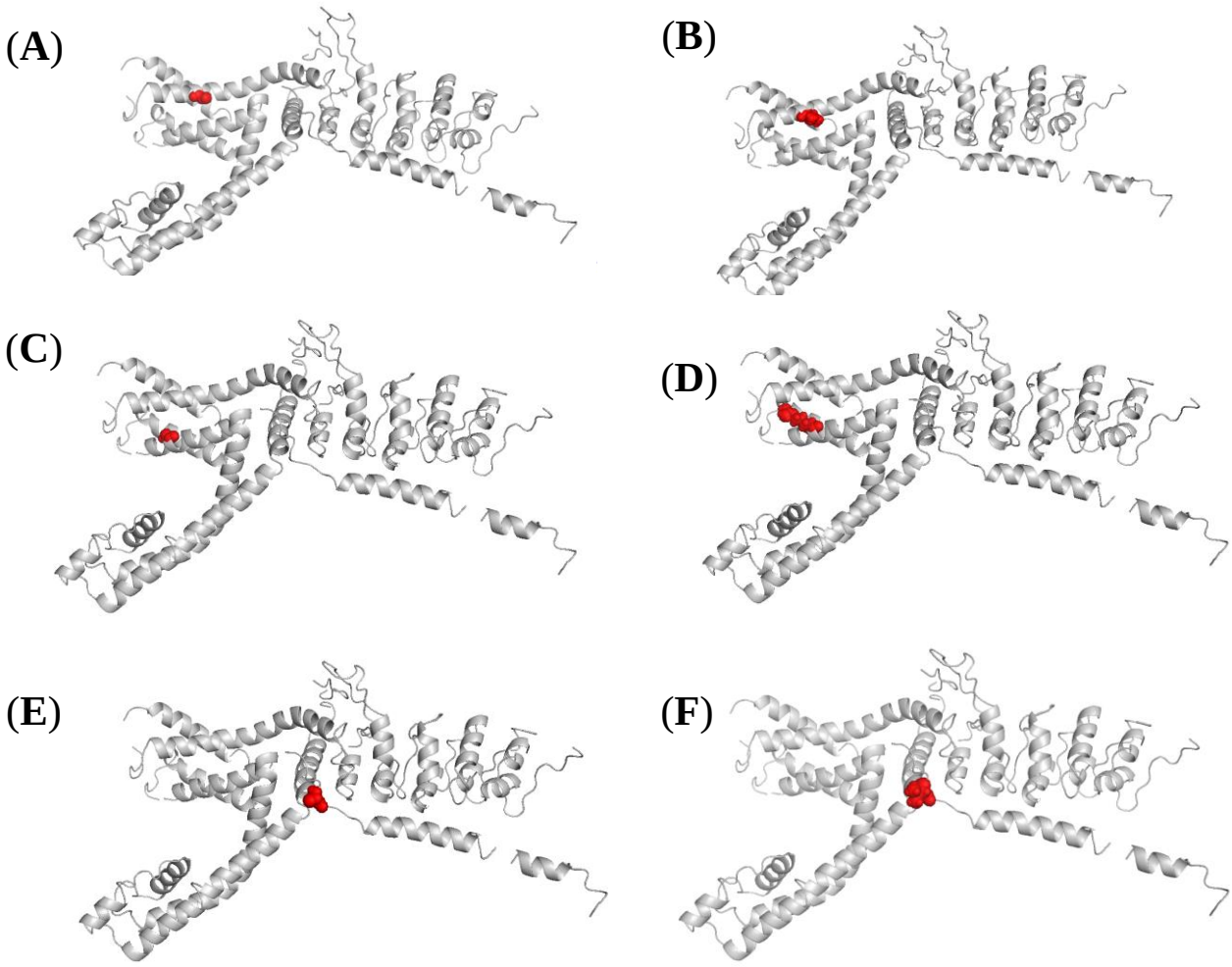

Figure 8-8 *In silico* modelling of the WFS1 protein and induced conformational changes.

Structural protein modelling of WFS1 was determined with the 'Fold and Functions Assignment (FFAS)' server, SCWRL modeller and PyMol for manual manipulation of image. The red spheres indicate the position of the either the wild type or mutant amino acid. WFS1 model with: **(A)** Ala326 amino acid; **(B)** Ala326Val amino acid change; **(C)** Gly437 amino acid; **(D)** Gly437Arg amino acid change; **(E)** Ala684 amino acid; **(F)** Ala684Val amino acid change. **(A)**, **(B)**, **(C)** and **(D)** illustrate recessive *WFS1* mutations, whereas **(E)** and **(F)** illustrate dominant *WFS1* mutations.

8.3.6 Screening of the remaining patients in our whole-exome cohort for potentially pathogenic *WFS1* variants

Analysis of our WES raw data indicate that only approximately 80% of the *WFS1* gene is covered and called by the Illumina HiSeq2500 and GATK in-house pipeline. To ensure that no other pathogenic *WFS1* variants were missed in these unsequenced regions, *WFS1* Sanger sequencing was carried out for the other patients in our whole-exome cohort. **Table 8-3** indicates the *WFS1* variants that were detected and confirmed with reverse sequencing within the 20% uncovered WES region. These *WFS1* variants were then analysed using three online pathogenicity programs to determine whether these could account for the patient's optic atrophy phenotype. Most of the identified missense variants were predicted to be benign in nature (**Appendix Table H1**). However, the c.631G<C (p.Asp211Gly), c.2165T<C (p.Met722Thr), c.2653C<G (p.Pro885Thr), and c.1810T<A (p.Cys604Ser) variants were identified as potentially pathogenic and require further investigation**.**

Nucleotide Change	Protein Change	ExAC database	Euro-WAB database	SIFT	POLYPHEN2	Provean	SIFT	Polyphen2	Provean	PFC-
c.631G<C	p.Asp211Gly	NA	NA	Damaging	benign	Deleterious	0.03	0.001	-2.78	147
c.2165T<C	p.Met722Thr	NA	NA	Tolerated	possibly damaging	Deleterious	0.09	0.95	-2.56	342
c.2653C<G	p.Pro885Thr	NA	NA	Tolerated	probably damaging	Deleterious	2.86	1	-6.75	346
c.1810T<A	p.Cys604Ser	NA	NA	Tolerated	possibly damaging	Deleterious	0.27	0.82	-2.95	347

Table 8-3 Potentially pathogenic *WFS1* missense variants detected and confirmed with Sanger sequencing and their relative pathogenicity scores.

SIFT, POLYPHEN2 and Provean were used to analyse each variant and their respective scores are indicated. The presence of these variants in the Euro-WABB WFS1 database, which contains the largest collection of up-to-date variants, was also investigated (September 2015).

8.4 Discussion

WES was performed on a cohort of 14 patients with optic atrophy and/or additional extra-ocular features and four of these patients (28%) harboured potentially pathogenic *WFS1* variants. Sanger sequencing confirmed the presence of each of these variants: c.2051C<T (p.Ala684Val), c.977C<T (p.Ala326Val), c.1309G<C (p.Gly437Arg) and c.2452C<T (p.Arg818Cys). Two patients (PFC-344 and PFC-352) with optic atrophy and deafness carried a previously reported pathogenic variant c.2051C<T (p.Ala684Val), which was identified in a family with multiple affected family members segregating both optic atrophy and sensorineural deafness (Rendtorff *et al.*, 2011). The pathogenic nature of this variant was confirmed functionally in Hek293 cells with a significant decrease in WFS1 level indicative of either structural instability or haploinsufficiency. The mechanisms by which the mutant WFS1 protein (p.Ala684Val) result in optic atrophy and deafness remain unclear, but it might be associated with mtDNA instability, which is a mechanism that has also been observed with the *OPA1* p.Arg455His mutation (Rendtorff *et al.*, 2011).

Based on the Euro-Wabb WFS1 database, almost all heterozygous missense variants that result in optic atrophy and deafness, or isolated sensorineural hearing loss, are located near the C-terminal domain within the ER lumen. These missense mutations appear to cluster around the degron locus (Guo *et al.*, 2011), which is located in the final 100 amino acids before the C terminus. *Chassenot and colleagues* have also reported that the majority of patients with Wolfram syndrome who developed neurological symptoms had compound heterozygous missense mutations located either within the transmembrane domains or towards the C-terminus of the protein (Chaussenot *et al*., 2011). Therefore, heterozygous missense mutations, such as c.2051C<T (p.Ala684Val), may lead to cellular dysfunction by interfering with ER stress mechanisms or the interaction between WFS1 and another transmembrane protein ATF6α, a mechanism which acts as a negative regulator of the unfolded protein response (UPR) (Fonseca *et al*., 2010) In addition, the fact that many of these missense mutations are located at or near the degron may suggest that ER stress mechanisms are impaired because of a dysfunctional interaction between WFS1 and SMURF1, which is a ligase required for maintaining steady-state WFS1 levels under different physiological conditions (Guo *et al.*, 2011). Further research is currently ongoing to

determine how *WFS1* mutations lead to neurological complications in patients with Wolfram syndrome.

Patient PFC-341 harboured two previously unreported *WFS1* variants, c.C977T (p.Ala326Val) and c.1309G<C (p.Gly437Arg). Patient PFC-341 presented with optic atrophy and diabetes mellitus. Both of his parents were clinically unaffected with no evidence of subclinical optic nerve dysfunction or diabetes. Segregation analysis revealed that each parent harboured one of these two variants and the proband was therefore compound heterozygous. Further functional analysis to assess the pathogenicity of these variants was conducted using western blot analysis and a significant decrease in level of the WFS1 protein was found, indicative of a possible haploinsufficient mechanism or instability of the mutant protein. Pathogenic *WFS1* mutations are typically either homozygous or compound heterozygous with the majority of mutations classified as inactivating (Cryns *et al.,* 2003). Compound heterozygosity with pathogenic missense variants is rare and it has been speculated that these mutation carriers would present with a clinically milder form of Wolfram syndrome, limited to optic atrophy and diabetes mellitus (Rigoli *et al.,* 2011). This hypothesis would be consistent with the milder phenotype of patient PFC-341. Sanger sequencing confirmed the c.2452C<T (p.Arg818Cys) *WFS1* variant in patient PFC-351 and additional functional analysis will be required to fully determine its pathogenicity.

As detailed in the WES analysis of our optic atrophy patient cohort (**Chapter 7**), the genetic aetiology of ten patients remains unknown. It is interesting that two SNPs in *ATF5* (**Table 7-6**), which is a gene associated with the ER stress response, were found in 5/14 (36%) patients. These SNPS are extremely rare in control population databases (1000 genomes project and ESP6500). They were not present in two controls sequenced on the same plate to exclude technical PCR bias and they were also not found in our in-house control database. The relevance of these *ATF5* variants will need to be investigated to determine if they are a possible risk factors for the development of optic neuropathy.

Only 80% of the *WFS1* exonic regions were appropriately covered with WES analysis and it is possible that other pathogenic variants might have been missed in the unsequenced regions. These regions were therefore screened with Sanger sequencing and the detected variants were analysed using the online SIFT, POLYPHEN2 and Provean pathogenicity programmes. A number of missense *WFS1* variants were detected, which were confirmed by

reverse sequencing, and determined as possibly pathogenic (**Table 8-2**). Although these variants were not found in the Euro-WABB *WFS1* database, further functional work is needed to determine if they are truly pathogenic.

The prevalence of Wolfram syndrome has previously been estimated at 1 in 770,000 in the UK population, but this was based on a clinical diagnostic criteria before the identification of *WFS1* as the major causative gene (Barrett *et al.*, 1995). Other reported prevalence figures are 1 in 500,000 in Germany (Rohayem *et al.*, 2011) and 1 in 710,000 in Japan (Matsunaga *et al.*, 2014). A much higher figure of 1 in 68,000 has been found in Lebanon and this has been ascribed to higher level of consanguinity and/or a potential founder even this region of the world (Zalloua *et al.*, 2008). Lombardo and colleagues suggest that Wolfram syndrome and the prevalence of pathogenic *WFS1* mutations may be underreported in non-consanguineous European populations (Lombardo *et al.*, 2014). Our data is consistent with this as evidenced by the identification of confirmed pathogenic *WFS1* mutations in 3/14 patients with suspected inherited optic atrophy that had previously been found to be *OPA1*-negative. Furthemore, it is clear that dominant *WFS1* mutations represent an important genetic subgroup and the spectrum of clinical features has expanded from classical DIDMOAD to more limited forms of the disease characterised by varying combinations of optic atrophy, deafness and diabetes mellitus. Long-term prospective studies are needed to better assess the natural history of dominant and recessive *WFS1* mutations, which will be crucial for designing future treatment trials.

Chapter 9

General Discussion

Inherited optic neuropathies are an important cause of chronic visual morbidity and they affect at least 1 in 10,000 individuals in the UK population (Yu-Wai-Man *et al.,* 2014). The pathophysiology of this group of disorders is intrinsically linked with mitochondrial dysfunction and the two classical paradigms are LHON, which is caused by primary mtDNA mutations, and DOA secondary to pathogenic *OPA1* mutations. Recessive forms of optic neuropathy are rarer and they are characterised by both genetic and phenotypic heterogeneity, with clinical features ranging from isolated optic atrophy to severe early-onset syndromic optic atrophy associated with debilitating neurological features and neurodevelopmental defects. Wolfram syndrome is the most common recessive optic atrophy and interestingly, the major causative gene, *WFS1*, encodes for an ER transmembrane protein, highlighting the complex interplay and crosstalk between the mitochondrial and ER compartments. A growing list of nuclear genes causing optic atrophy is being identified with the technological revolution of next-generation exome and whole genome sequencing. These exciting discoveries are providing major insights into the pathological mechanisms that eventually contribute to RGC loss and neurodegeneration. In addition to impaired mitochondrial bioenergetics and elevated ROS levels, it is now clear that disturbed mitochondrial dynamics, mtDNA instability and impaired mitochondrial quality control also play a role in triggering or potentiating RGC loss (**Figure 9-1**) (Burté *et al*., 2015; Yu-Wai-Man and Chinnery, 2012). We are still at the start of a long road to fully understand the complex interplay between these pathological pathways and how these ultimately result in tissue specificity and progressive neurodegeneration.

As part of my PhD work, I have further investigated the expanding clinical manifestations and the disease mechanisms that contribute to *OPA1*-related dominant optic atophy. To do so, I made use of primary fibroblast cell lines established from two contrasting phenotypic patient groups, one with pure optic atrophy (OA) and the other with patients that had developed more severe extraocular features (DOA+). The data obtained with this *OPA1* cell model revealed a striking mitochondrial fragmentation pattern when compared to controls. Interestingly, there was significantly greater fragmentation in the DOA+ group compared with the OA group, which had not been reported previously. The differences in mitochondrial fragmentation might be associated with the underlying subtype of *OPA1* mutations that are more likely to be associated with DOA+ phenotypes (Zeviani, 2008; Yu-

Wai-Man *et al*., 2010b). Missense *OPA1* mutations involving the GTPase domain carry an increased risk of DOA+ phenotypes, presumably because the mutant mRNA is translated and the resulting aberrant protein is not immediately degraded by cellular quality control mechanisms. This hypothesis is consistent with the normal levels of OPA1 found in fibroblast cell lines from patients with DOA+ phenotypes. In contrast, the majority of *OPA1* mutations result in haploinsufficiency due to nonsense mediated decay and with the wild-type allele accounting for the approximately 50% expression of OPA1 (Schimpf *et al.* 2008).

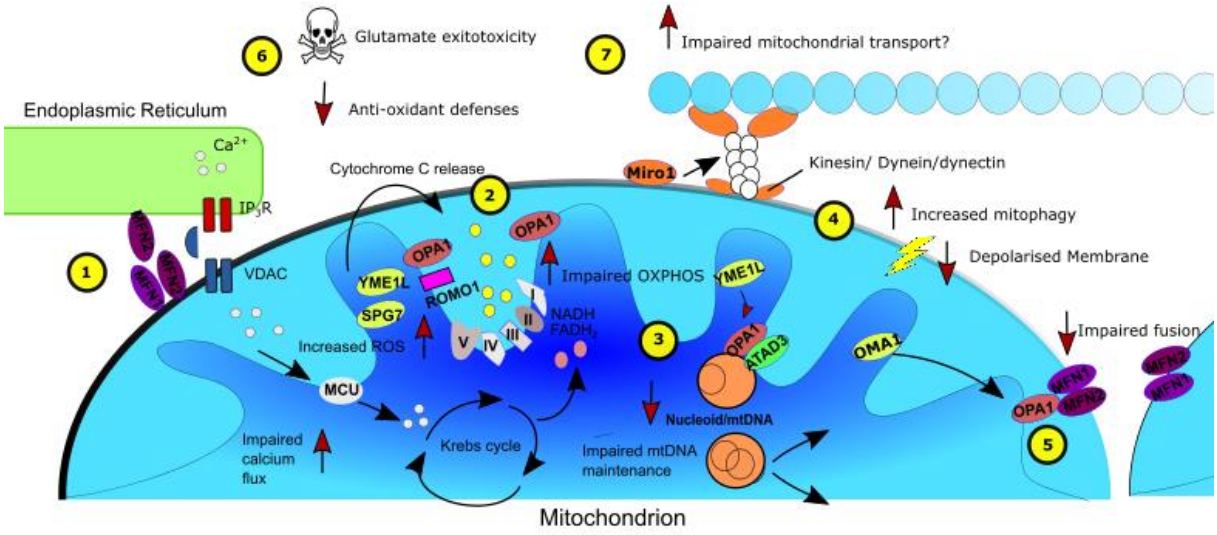

Figure 9-1 Disease mechanisms implicated in common inherited optic neuropathies - LHON, DOA and Wolfram syndrome

(1) Disturbed calcium homoeostasis from both the ER and cytosol have been implicated as potential dysfunctions in DOA and Wolfram syndrome(Jahani-Asl *et al*., 2011; Kamei *et al*., 2005; Dayanithi *et al*., 2010; Cagalinec *et al*., 2016) Increased calcium retention within the mitochondrial compartment could induce mitochondrial swelling and impaired SIMH in DOA as detected in chapter 4. Hypothetically, this calcium could alter the Krebs cycle as a compensatory effect to OXPHOS dysfunction (Traaseth *et al*., 2004). (2) Impaired rate of ATP production from OXPHOS implicating either a complex I (LHON)(Wallace *et al*., 1988; Huoponen *et al*., 1991; Johns *et al*., 1992) and/or complex IV (DOA) defect (Zanna et al., 2008; Chevrollier *et al*., 2008) which could also exasperate levels of ROS (Carelli et al., 2004; Tang et

al., 2009; Millet *et al*., 2016). Disturbed cristae morphology may also impinge on the efficiency of OXPHOS while the release of cytochrome C, typically sequestered within these cristae compartments, can induce apoptosis (Gonzalves *et al*., 2005; Kuwana *et al*., 2002; Lutter *et al*., 2000). (3) Dysfunctional mtDNA maintenance in models of optic neuropathy can induce mtDNA depletion (Kim *et al*., 2005; Chen *et al*., 2012; Speigal *et al*., 2016; Chapter 5 results), mtDNA proliferation as a potential OXPHOS compensatory effect, (Sitarz *et al*., 2012; Yu-Wai-Man *et al*., 2010b; Yen *et al*., 2002) or disturb the distribution of mtDNA within the mitochondrial network (Elachouri *et al*., 2011; Chapter 5 results) (4) Increased mitophagy has been detected in models of DOA (White *et al*., 2009; Sarzi *et al*., 2012) and Wolfram syndrome (Caglinec *et al*., 2016). (5) Mitochondrial fragmentation is a hallmark of DOA (Olichon *et al.*, 2003; Zanna *et al*., 2008; Chevrollier *et al*., 2012) with DOA+ displaying a more severe fragmentation pattern than OA (Chapter 4). In addition, OA mitochondrial morphology demonstrates abnormal SIMH under stressed metabolic conditions (Chapter 4). Mitochondrial fusion rates were also impaired in DOA (Zanna *et al*., 2008) and Wolfram syndrome (Cagalinec *et al*., 2016). This may disturb complementation between mitochondrial organelles.(6) Glutatemate excitotoxicity and reduced anti-oxidant defences are especially pertinent for retinal ganglion cells (Nguyen *et al*., 2011; Millet *et al*., 2016). (7) The anterograde/retrograde transport of mitochondria are dependent on ATP and mitochondrial dynamics and so may be particularly pertinent to retinal gangion cell dysfunction (Safiulina and Kaasik, 2013).

Once translated, the OPA1 protein is targeted for integration into the IMM where short and long isoforms oligomerise into multimeric complexes (Yamaguchi *et al.*, 2008; Frezza *et al.*, 2006). A possible explanation for the increased fragmentation of the mitochondrial network in DOA+ may be that both wild-type and pathogenic OPA1 oligomers self assemble to create malformed and unstable OPA1 complexes, which further impair normal IMM fusion. In OA, the wild-type OPA1 oligomers form fewer multimeric complexes, but they are functional and therefore, these could minimise the impact on mitochondrial morphology. Based on our results, the increase in mitochondrial fragmentation in DOA+ and OA fibroblasts does not seem to be secondary to a severe mitochondrial OXPHOS defect or to

disruption of mtDNA maintenance, suggesting that the observed fragmentation is more likely the direct consequence of the impaired OPA1 fusional abilities (**Chapter 4**). Quantification of the mitochondrial network showed an exaggerated increase in both mitochondrial length and volume, consistent with pathological mitochondrial swelling. A more pronounced effect was observed in the OA group under stressful oxidative conditions and this could reflect activation of SIMH as a compensatory protective mechanism **(**Tondera *et al*., 2009).

To further investigate the link between *OPA1* mutations and mtDNA instability, I quantified mtDNA/nucleoid level and distribution, and how these relate with the mitochondrial fragmentation patterns observed in DOA+ and OA fibroblasts and myotubes. In both cell models, DOA+ was associated with a significantly higher number of mitochondrial fragments compared with OA or controls. This further supports our hypothesis that the severity of mitochondrial fragmentation is an important parameter that correlates with disease severity. It will be very interesting to investigate other tissue types, in particular RGCs, which are the neuronal populations that are prefentially affected in DOA. The greater extent of mitochondrial fragmentation could also impact on mitochondrial quality control by impairing the complementation of mutant mtDNA molecules by wild-type molecules through content mixing (Chen *et al.,* 2010; Nakada *et al.,* 2009). An elegant study performed by *Elachouri and colleagues* demonstrated mechanistically how a specific OPA1 peptide sequence encoded by exon 4b was likely responsible for anchoring mtDNA nucleoids to the IMM, thereby facilitating proper mtDNA replication (Elachouri *et al*., 2011). It is therefore plausible that a reduction in the level of OPA1 could impact on mtDNA number and nucleoid distribution. Of note, a recently published study has highlighted how ER-mitochondria contacts regulate mtDNA replication in relation to mitochondrial division in human cells **(**Lewis *et al*., 2016). MtDNA replication is undoubtedly a complex process and it is clear that disturbance at any point can result in human disease. In our study, I did not find any major difference in mtDNA/nucleoid distribution between DOA+ and OA compared with controls, but there was a significant decrease in the number of mtDNA/nucleoids when correlated with the mitochondrial fragmentation patterns. A significant decrease in mtDNA/nucleoid content was detected in both DOA+ and OA groups relative to total mitochondrial length. This difference is likely due to the greater total mitochondrial length that has been reported in *OPA1*-mutant fibroblasts (Agier *et al.,* 2012), but it could also indicate a relative depletion of

mtDNA/nucleoid copies due to impaired fusion or mtDNA maintenance. Further work is required to explore the mechanisms that underlie these observations and the possible pathological link with mitochondrial quality control.

Although optic atrophy remains the defining feature of DOA, the clinical manifestations observed in *OPA1*-related disease have now expanded to include chronic progressive external ophthalmoplegia (CPEO) and other extraocular features such as ataxia, myopathy and peripheral neuropathy. The association of optic atrophy with spastic paraplegia, resembling cases that fit the historical description of Behr syndrome, has been well described in several unrelated *OPA1* mutation carriers (Bonneau *et al*., 2014; Carelli *et al*., 2015b; Yu-Wai-Man and Chinnery, 2015). The development of this syndromic form of DOA has been ascribed to the deleterious synergistic consequences of compound heterozygous OPA1 mutations, in particular the recurrent c.1146A>G (p.Ile382Met) missense mutation, which can occur in combination with a deep intronic mutation (Bonifert et al., 2014). Remarkably, two Italian families carrying different *OPA1* missense mutations have been reported with an atypical combination of parkinsonism, dementia and CPEO, but with only subclinical optic neuropathy (Carelli et al., 2015). In my PhD project, I have further extended the genetic complexity of *OPA1* disease by confirming a novel homozygous *OPA1* mutation as the underlying molecular defect in two affected sisters of Arab Muslim origin, born to consanguineous parents, and who developed a fatal infantile encephalomyopathy with hypertrophic cardiomyopathy and optic atrophy. Intriguingly, the muscle biopsy from one sister instead showed marked mtDNA depletion rather than multiple mtDNA deletions, which could explain the severity of the clinical phenotype (Spiegel *et al*., 2016). The expanding clinical and genetic heterogeneity linked to DOA plus phenotypes only serves to emphasize the more global neurodegenerative impact of pathogenic *OPA1* mutations, which can extend far beyond the inner retina and the anterior visual pathways.

Whole-exome sequencing (WES) has proven a powerful tool in determining the underlying genetic basis of rare monogenic disorders. As part of my PhD project, I analysed WES data for a cohort of 14 patients with suspected inherited optic atrophy, but who had been found to be negative for a number of known optic atrophy genes, namely *OPA1*, *OPA3*, *C12orf65* and *RTN4IP1*. Pathogenic *WFS1* mutations were identified in 3 patients and highly suspected in one additional patient, accounting for a nearly 30% positive hit rate. The genetic

aetiology for the remaining patients in our cohort remain unknown and further work, including whole genome sequencing, and ongoing collaborations will be crucial if we are to uncover new, but relatively rare, optic atrophy genes. Recessive *WFS1* mutations were originally found in patients with early-onset severe Wolfram syndrome that developed diabetes insipidus, diabetes mellitus, optic atrophy and deafness (DIDMOAD) (Barrett *et al*., 1995). *WFS1* encodes for wolframin, a transmembrane endoplasmic reticulum protein that plays a critical role in calcium homeostasis and interorganellar cross-talk at mitochondria associated membranes (MAMs) (Lu *et al*., 2014; Hoppins and Nunnari, 2012). The molecular elucidation of Wolfram syndrome has uncovered the intimate dynamic interactions between mitochondria and the endoplasmic reticulum, and how dysfunction in one compartment can detrimentally affect the other, and vice versa (Burté *et al*., 2015; Murley and Nunnari, 2016). Importantly, these disturbances are highly relevant to normal RGC physiology and it is highly likely that new optic atrophy genes will be uncovered that directly or indirectly affect MAM function. *WFS1* mutations have now been confirmed to be an important cause of DOA and they can cause a more limited phenotype, which, remarkably, can sometimes be restricted to the optic nerve. The variable tissue specificity observed with both *OPA1* and *WFS1* mutations raise fundamental questions about the secondary genetic and environmental modifiers, including possible epigenetic influence, that are influencing their downstream consequences on cellular function.

In conclusion, my PhD work has provided new insights into *OPA1*-related disease mechanisms and how these might impact on the severity of the patient's phenotype. *OPA1* mutations can sometimes behave recessively and we have described the first report of a novel homozygous *OPA1* mutation, which was associated with a fatal infantile mitochondrial encephalomyopathy, hypertrophic cardiomyopathy and optic atrophy. The phenotypic manifestations of DOA+ will likely expand further with wider clinical access to WES. A similar development has occurred for *WFS1* mutations and screening for this specific gene should no longer be limited to patients with the DIDMOAD "full house". Indeed, *WFS1* mutations should now be actively sought in patients with suspected inherited optic atrophy who have been found to be *OPA1* negative. There are currently no effective treatments for patients with inherited optic neuropathies and there are significant challenges in drug development and clinical trials for this group of disorders. Despite these difficulties, there

have been major advances in our understanding of the genetic and pathophysiological basis of inherited optic neuropathies, and the hope is that these breakthroughs will eventually translate into tangible benefits for patients experiencing progressive visual loss.

Appendix A OPA1 protein levels

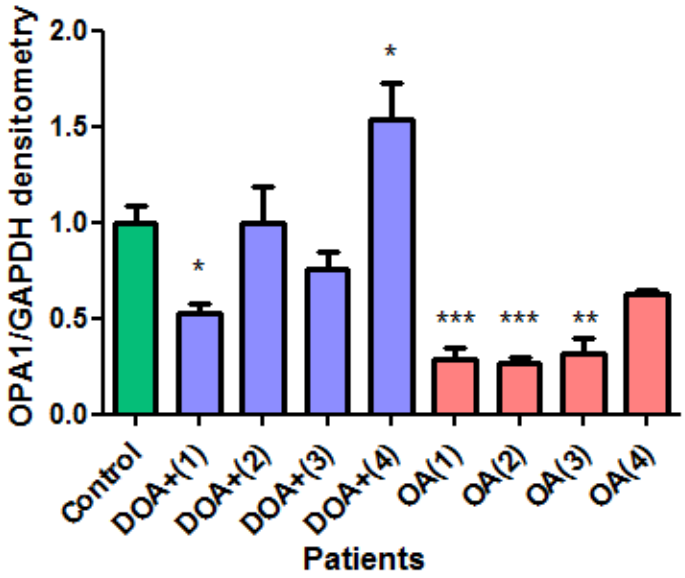

Figure A-1 Quantification of OPA1 in primary patient fibroblasts witt pure dominant optic atrophy and dominant optic atrophy plus

Levels of OPA1 were standardised to GAPDH and control lines (N = 4) for each DOA+ and OA fibroblast cell line. Error bars represent the standard error of the mean (SEM). The individual DOA+ and OA fiboblast cell lines were analysed using the Student's unpaired t-test to determine the level of significance compared with controls (ns > 0.05; * ≤ 0.05; ** ≤ 0.01; *** ≤ 0.001; **** ≤ 0.0001).

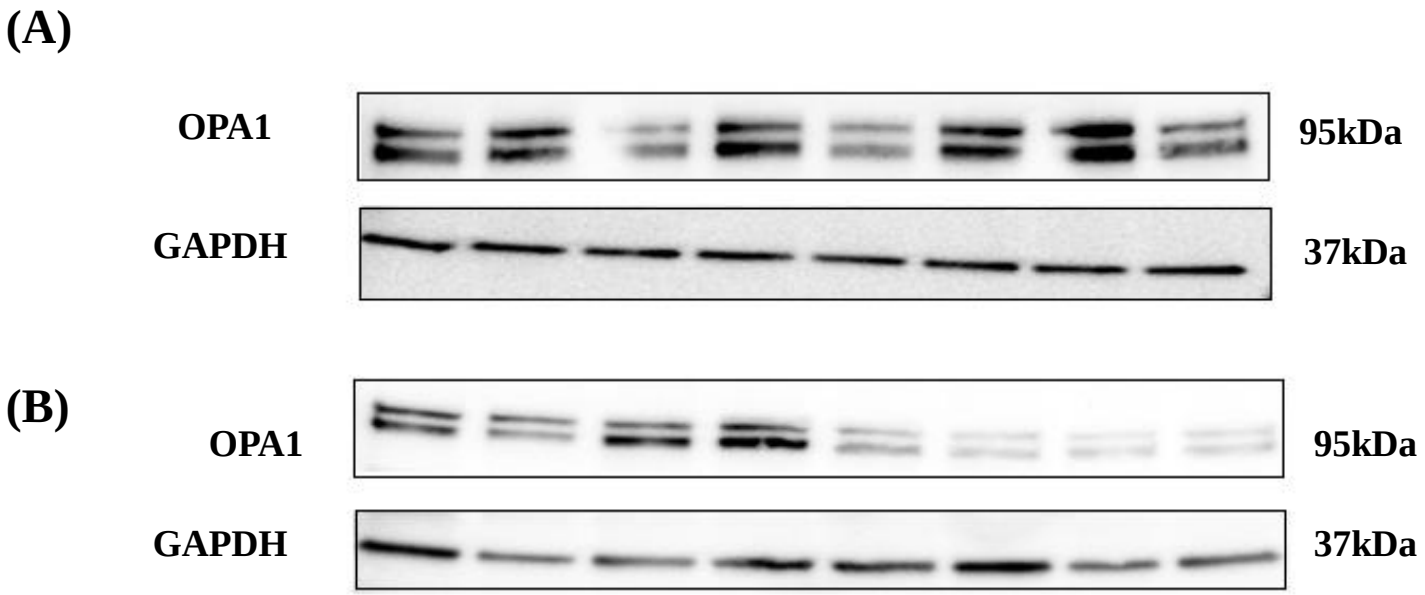

Figure A-2 Representative western blot of OPA1 and GAPDH in (A) DOA+ and (B) OA primary fibroblasts

Appendix B OPA1 gene expression

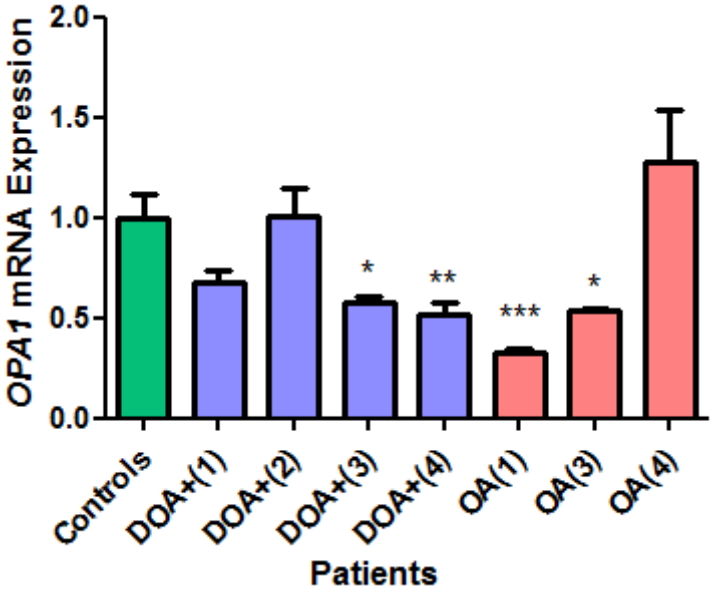

Figure B-1Quantification of OPA1 mRNA expression in individual DOA+ and OA primary fibroblasts.

Error bars represent the standard error of the mean (SEM). A Student's unpaired t-test was used to statistically measure DOA+ and OA groups relative to controls (ns > 0.05; * ≤ 0.05; ** ≤ 0.01; *** ≤ 0.001; **** ≤ 0.0001).

Appendix C Mitochondrial network analysis

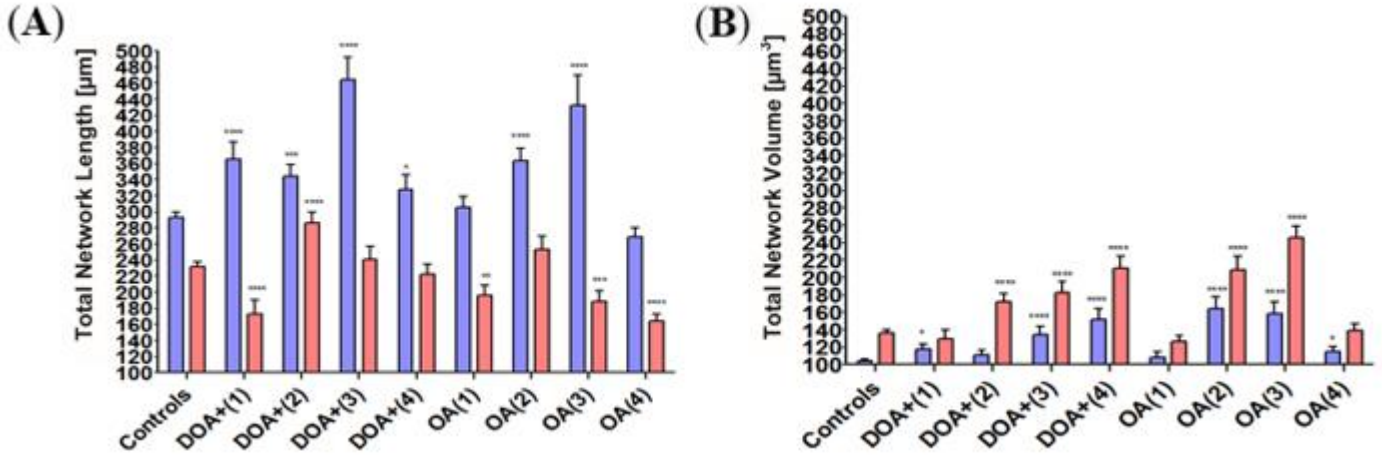

Figure C-1Quantification of the Total length and Volume of individual lines from both DOA+ and OA groups under glucose (5mM) and galactose (5mM) conditions.

Total network length **(A)** and total network volume **(B)** were quantified under glucose (blue) and galactose (red) conditions. Error bars represent the standard error of the mean. A Student's unpaired t-test was used for statistical comparison between DOA+, OA and controls. control (ns > 0.05; * ≤ 0.05; ** ≤ 0.01; *** ≤ 0.001; **** ≤ 0.0001).

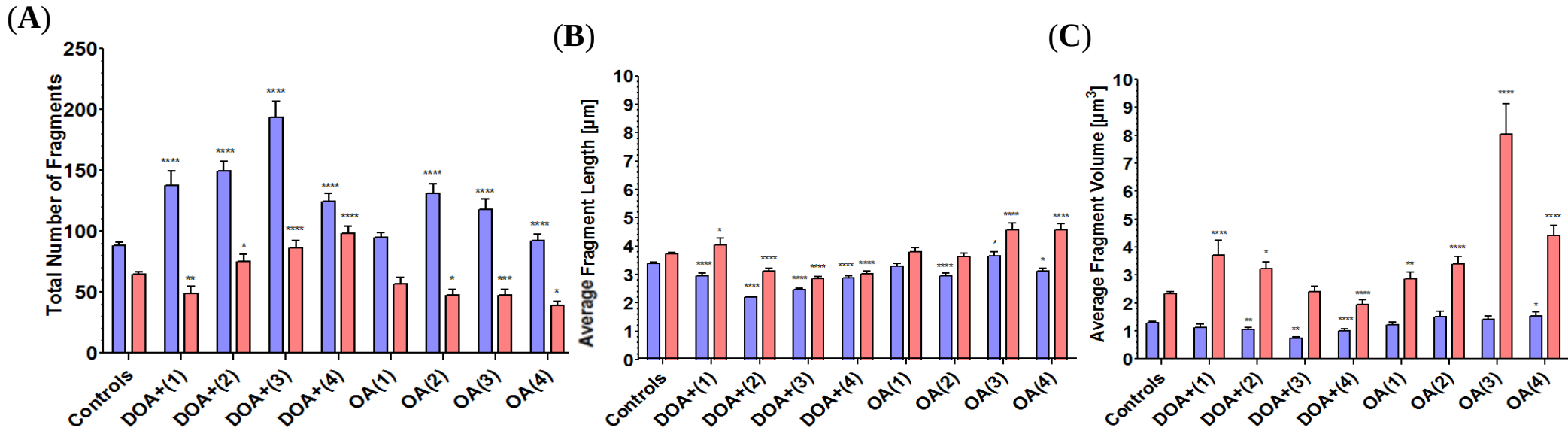

Figure C-2Mitochondrial fragmentation of the network in individual patient and control primary fibroblasts.

Average number of mitochondrial fragments **(A)** were measured using Huygens Object analyser software in fibroblasts imaged following either 24 hour incubation with 5mM glucose (blue) or 48 hour incubation with 5mM galactose (red). Average fragment length **(B)** and average fragment volume **(C)** were calculated as described in section **4.2.4.** Error bars represent the standard error of the mean (SEM).* $p \leq 0.05$, ** $p \leq 0.01$, *** $p \leq 0.001$ and **** $p \leq 0.0001$ using a Student's unpaired t-test against controls (n=200).

Appendix D Mitochondrial maintenance analysis

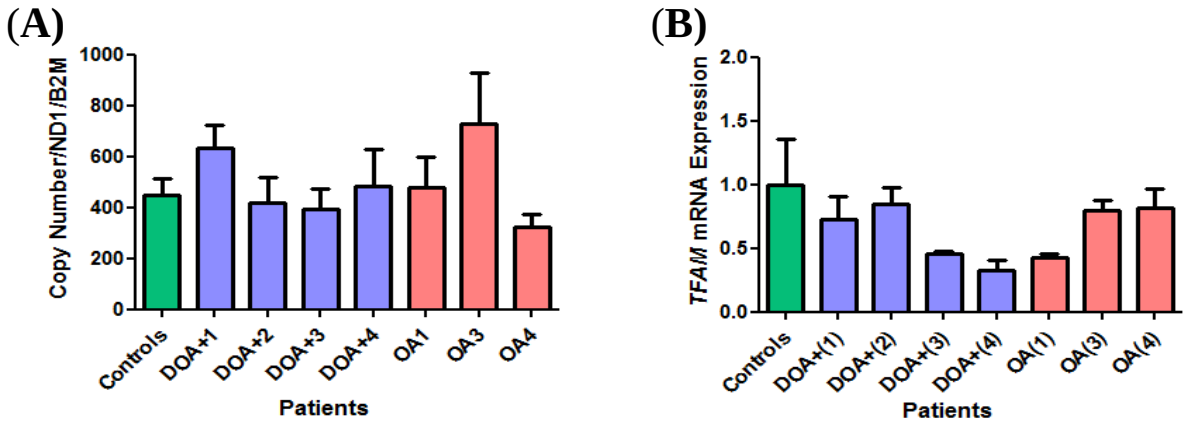

Figure D-1 mtDNA maintenance markers in individual primary fibroblast lines from DOA+ and OA patients.

MtDNA copy number was measured using real-time PCR and normalised to nuclear encoded *B2M* copy number **(A)**. TFAM was measured using real-time PCR and standardised against mean *β-actin* and *B2M* gene expression **(B)**. Both mitochondrial maintenance markers were expressed compared to mean of three different control cell lines (n=3). Error bars represent the standard error of the mean (SEM). * $p \leq 0.05$ using a Student's unpaired t-test against controls.

Appendix E OXPHOS disturbances

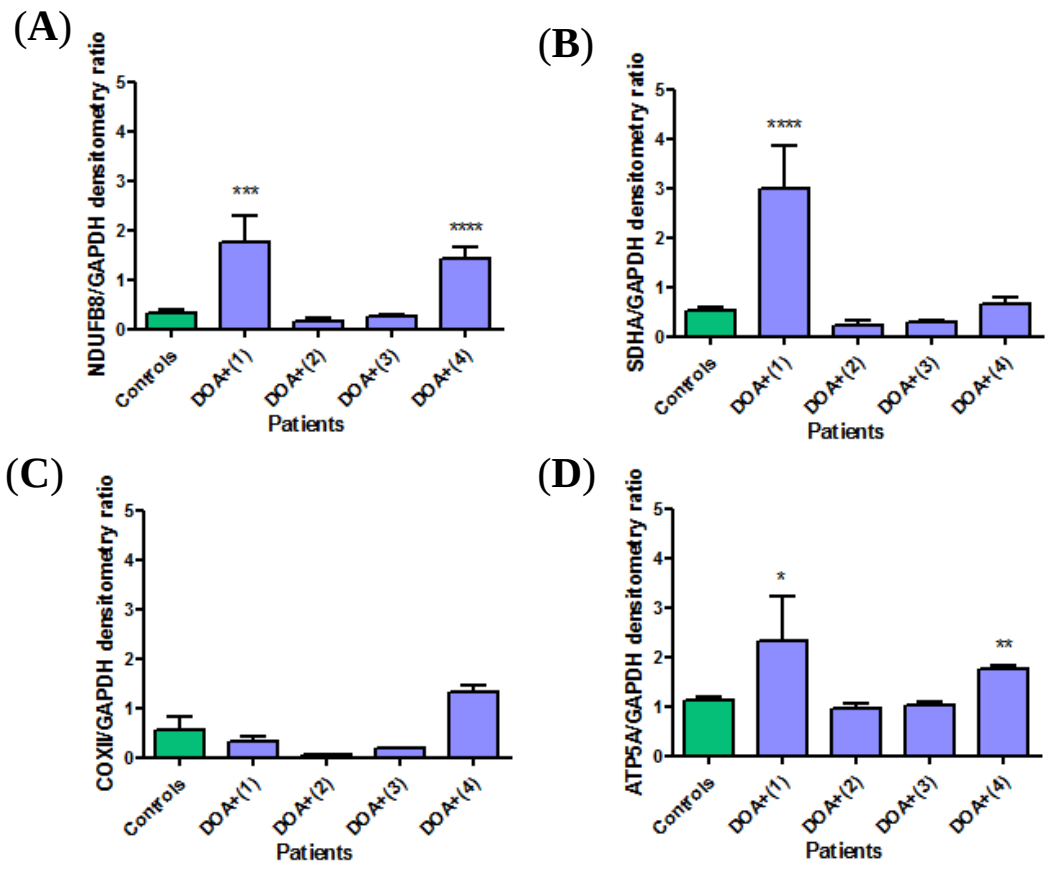

Figure E-1 Relative expression of OXPHOS complex subunits corrected against GAPDH in individual DOA+ primary fibroblasts compared to control.

Densitometric analysis of NDUFB8 **(A)**, SDHA **(B)**, COXII **(C)** and ATP5A **(D).** OXPHOS subunit immunoblots was performed using ImageJ and each subunit densitometry normalised to GAPDH. Ratios were expressed compared to mean of three different control cell lines (n=3). Error bars represent standard error of the mean. A Student's unpaired t-test was used to statistically compare DOA+and OA with control (ns > 0.05; * ≤ 0.05; ** ≤ 0.01; *** ≤ 0.001; **** ≤ 0.0001).

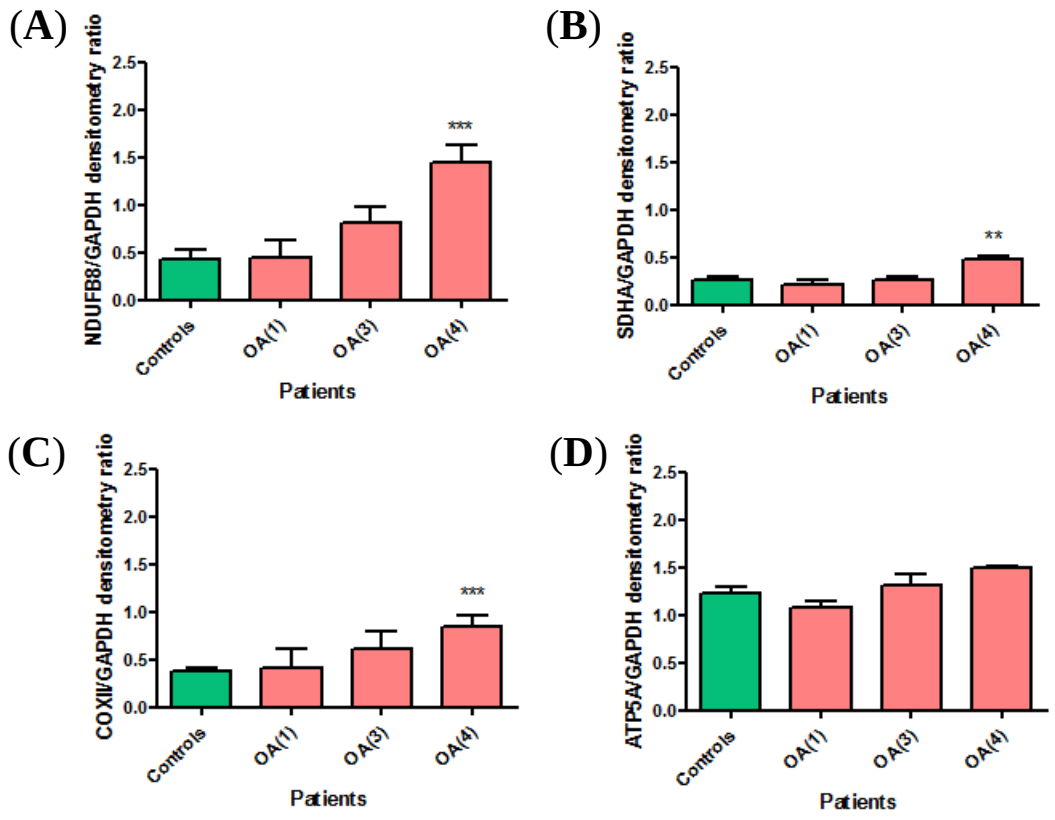

Figure E-2 Relative expression of OXPHOS complex subunits corrected against GAPDH in individual OA primary fibroblasts compared to control.

Densitometric analysis of NDUFB8 **(A)**, SDHA **(B)**, COXII **(C)** and ATP5A **(D).** OXPHOS subunit immunoblots was performed using ImageJ and each subunit densitometry normalised to GAPDH. Ratios were expressed compared to mean of three different control cell lines (n=3). Error bars represent standard error of the mean. A Student's unpaired t-test was used to statistically compare DOA+and OA with control (ns >0.05; * ≤ 0.05; ** ≤ 0.01; *** ≤ 0.001; ****≤ 0.0001).

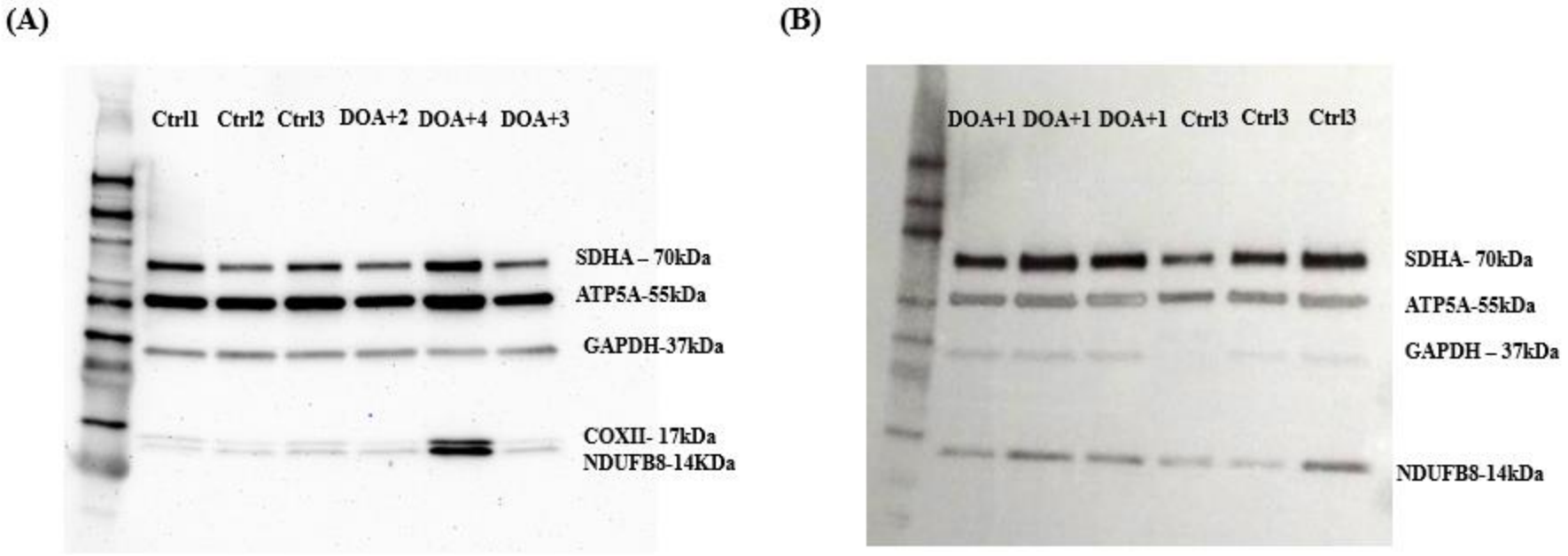

Figure E-3 Representative western blots of mitochondrial OXPHOS complex subunits in (A) DOA+(2), DOA+(3) and DOA+(4) and (B) DOA+(1) primary fibroblasts

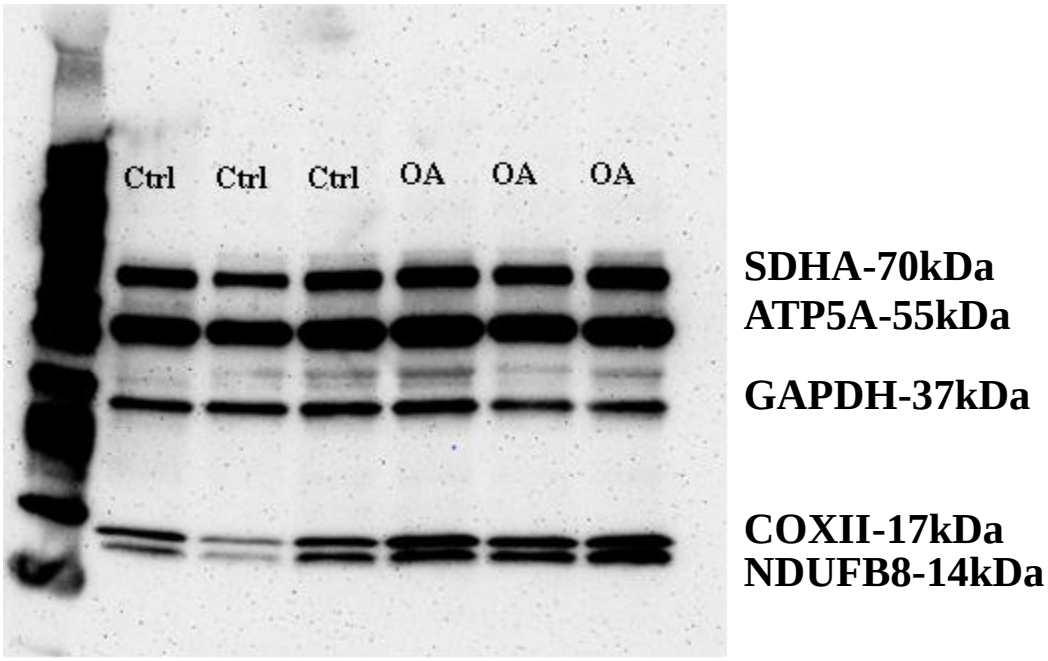

Figure E-4 Representative western blot of mitochondrial OXPHOS complex subunits in OA primary fibroblasts

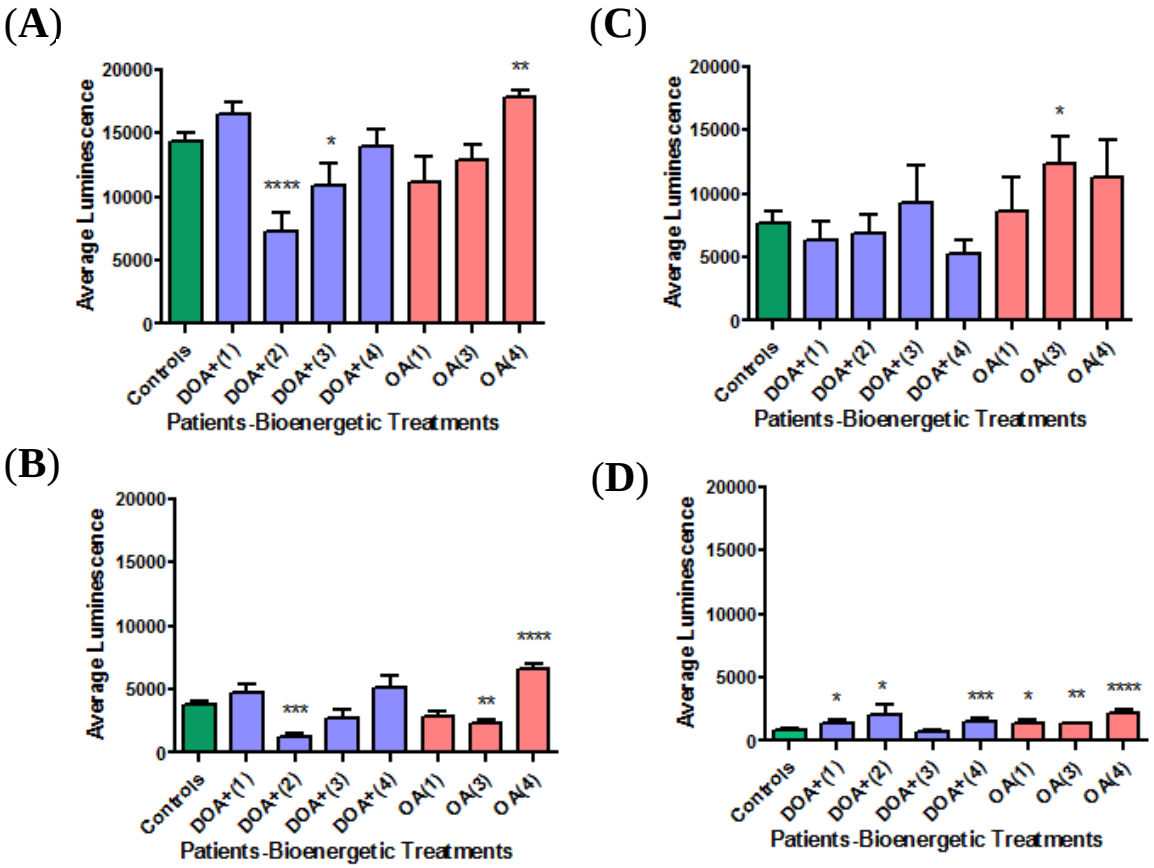

Figure E-5 Quantification of the levels of ATP produced through OXPHOS and the glycolytic pathway incubated in (A) 5mM glucose, (B) 5mM glucose and oligomycin, (C) 5mM glucose and d-deoxyglucose and (D) 5mM glucose with d-deoxyglucose and oligomycin within control DOA+ and OA groups.

A Student's unpaired t-test was used to statistically compare DOA+ and OA with controls (ns > 0.05; * ≤ 0.05; ** ≤ 0.01; *** ≤ 0.001; ****≤ 0.0001).

Appendix F Mitochondrial network analysis in myotubes

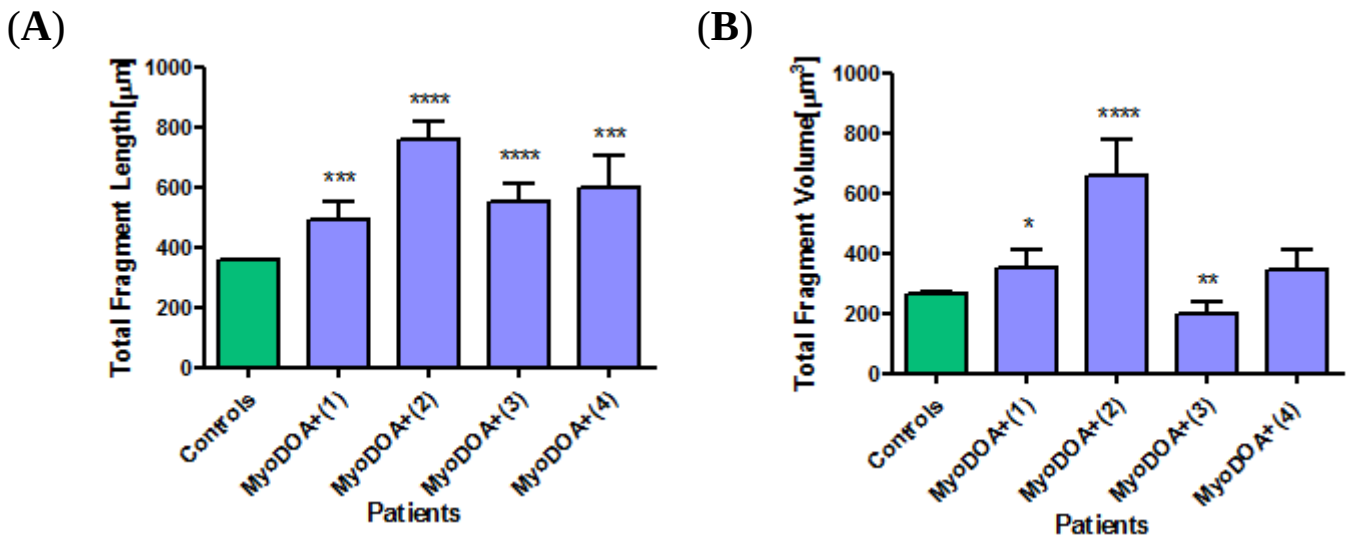

Figure F-1 Total mitochondrial length and volume measured in individual DOA+ primary myotube lines.

Total fragment length **(A)** and **(B)** Total fragment volume of primary myotube DOA+ lines were compared statistically against group primary control myotubes using a Student's umpaired t-test (* $p \leq 0.05$; ** $p \leq 0.01$; *** $p \leq 0.001$; **** $p \leq 0.0001$).

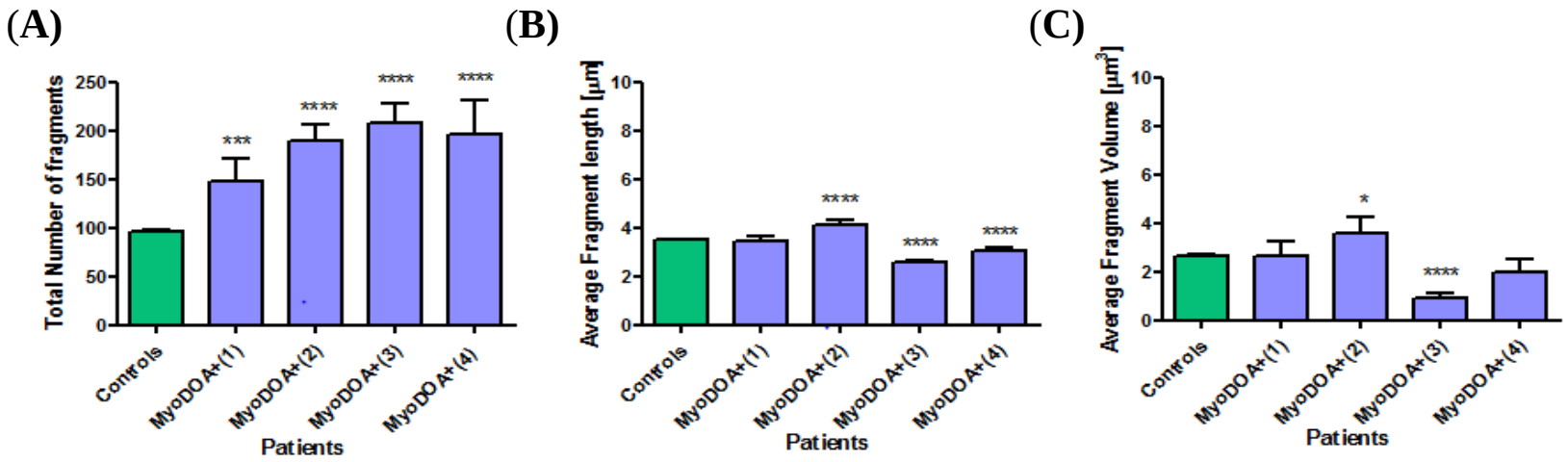

Figure F-2Average mitochondrial length, volume measured and total number of mitochondrial fragments in DOA+ primary myotubes

Average mitochondrial length **(B)** and volume **(C)** were calculated as a ratio between total length/ volume and total number of mitochondrial fragments **(A)**. Variation between DOA+ primary myotube lines and grouped control was statistically analysed using a Student's unpaired t-test (* $p \leq 0.05$; ** $p \leq 0.01$; *** $p \leq 0.001$; **** $p \leq 0.0001$)

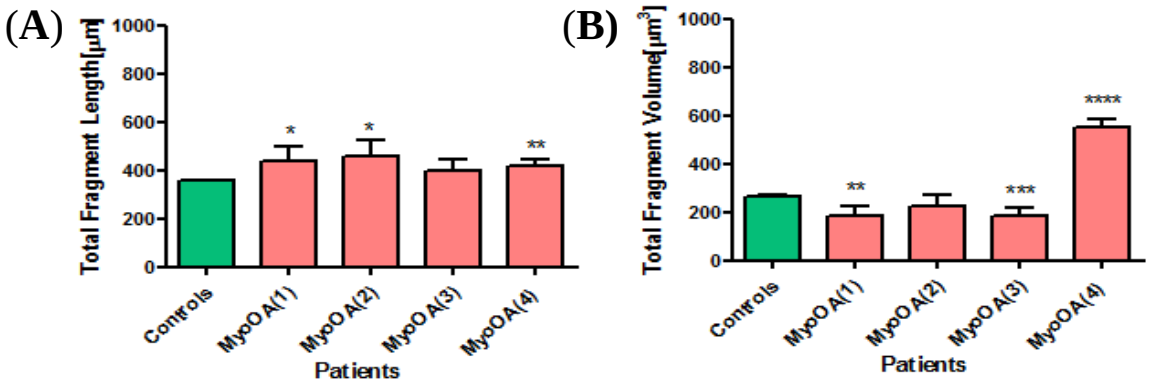

Figure F-3Total mitochondrial length and volume measured in primary OA myotubes.

Variation of total mitochondrial length **(A)** and volume **(B)** between individual myotubes lines and grouped control was statistically analysed using a Student's unpaired t-test (* $p \leq 0.05$; ** $p \leq 0.01$; *** $p \leq 0.001$; **** $p \leq 0.0001$)

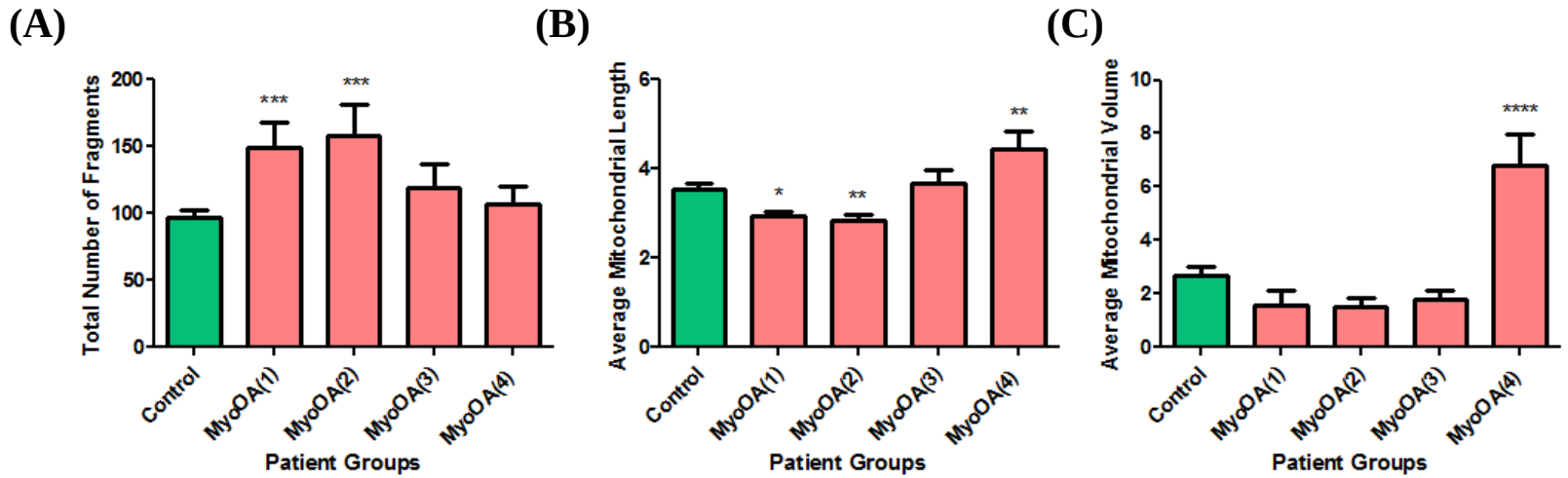

Figure F-4Average mitochondrial length, volume and total number of mitochondrial fragments in individual OA primary myotube lines.

Average mitochondrial length **(B)** and volume **(C)** was calculated as a ratio between total length/volume and the total number of mitochondrial fragments **(A)**. Variation between average mitochondrial OA myotube lines was compared statistically to control using a Student's unpaired t-test (* $p \leq 0.05$; ** $p \leq 0.01$; *** $p \leq 0.001$; **** $p \leq 0.0001$)

Appendix G Mitochondrial nucleoid distribution

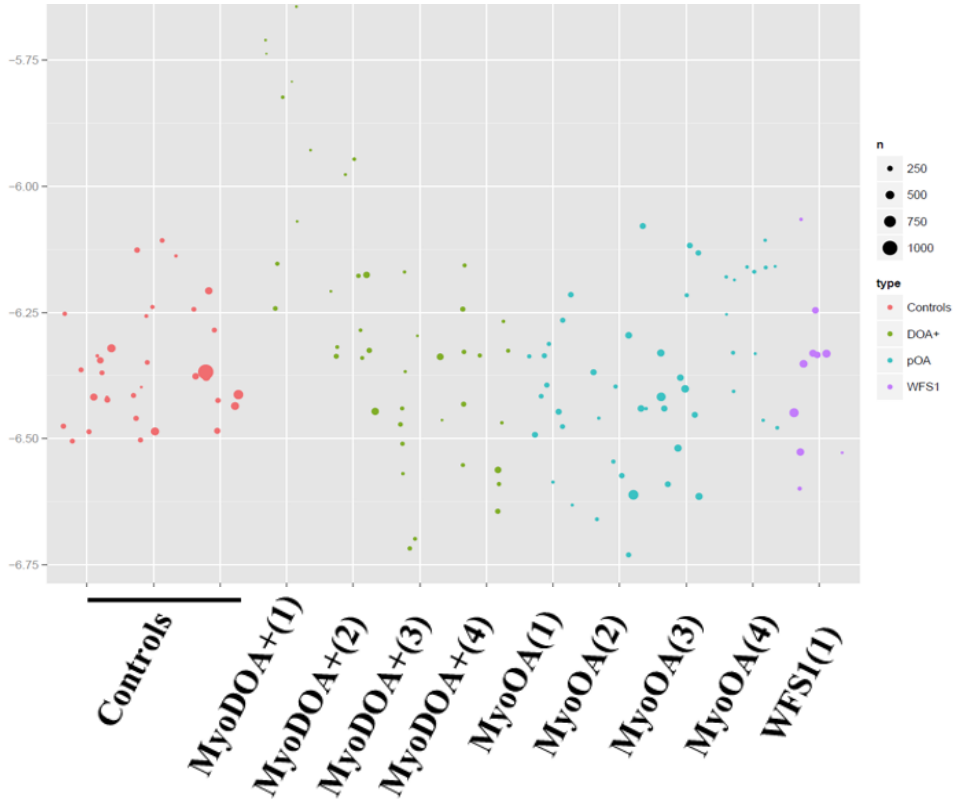

Figure G-1 Nucleoid distribution dot plot of individual DOA+ and OA primary myoblasts

The size of each blot represents the weighted number of mtDNA/ nucleoid objects present in each individual myoblast cell. Graph was generated by Dr. Ian Wilson.

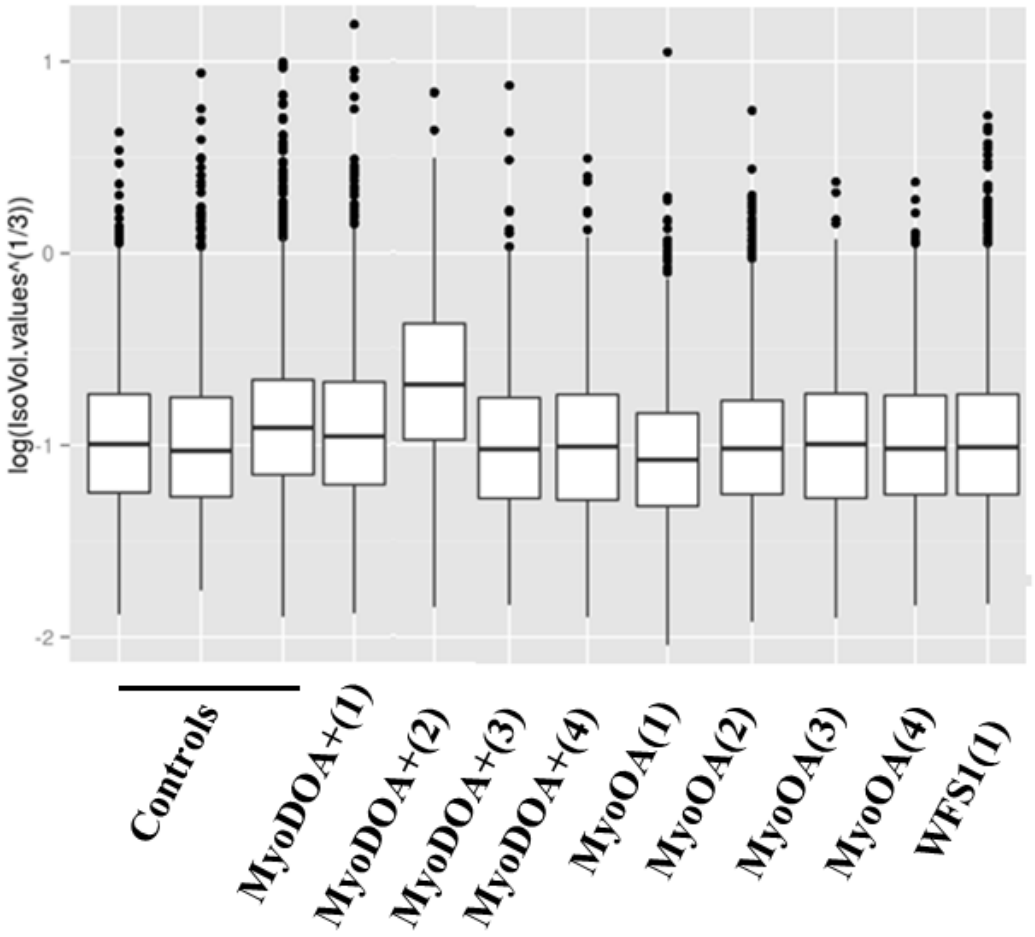

Figure G-2 Box-plot of average mtDNA/nucleoid distribution in each individual myoblast line

Box-plot generated by Dr. Ian Wilson.

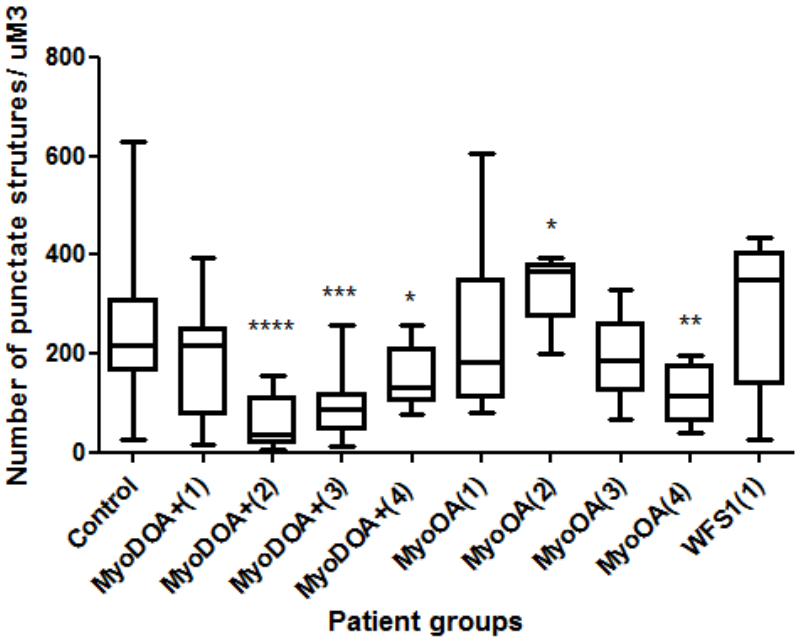

Figure G-3 Total number of nucleoids/mtDNA in each individual primary line per unit area of cell analysed

The mean of the number of nucleoid/mtDNA objects detected per unit area of the cell in DOA+, OA and WFS1 lines (N ~ 11) was quantified and compared against control (N = 33). Error bars represent standard error of the mean. ($p > 0.05$ is non-significant; $p \leq 0.05$ * of significance; $p \leq 0.01$ is ** of significance; $p \leq 0.001$ is *** of significance; $p \leq 0.0001$ is **** significance).

Appendix H Benign variants found in *WFS1* screen

DNA	Missense Change	Euro-WAB database	ExAc Frequency	SIFT	POLYPHEN2	Provean	SIFT	Polyphen2	Provean	PFC-
c.634G<C	p.Gly212Ala	NA	0	Tolerated	possibly damaging	Neutral	0.26	0.571	-1.41	147
c.637G<A	p.Gly213Arg	NA	0	Tolerated	Benign	Neutral	0.14	0.216	-2.06	147
c.640G<A/641C<T/642G<T	p.Ala214Ile	NA	0	Tolerated	Benign	Neutral	0.22	0.221	-0.95	147
c.645G<C	p.Gln215His	NA	0	Tolerated	possibly damaging	Neutral	0.13	0.884	-1.74	147
c.977G<A	p.Val333Ile	Ganie *et al.*, 2011	0.7818	Tolerated	Benign	Neutral	0.92	0.0001	0.36	147;349;350;342;345;346;351
c.2470G<A	p.Glu824Lys	NA	0.000084	Tolerated	probably damaging	Neutral	2.86	1	-1.63	345
c.56C<T	p.Pro19Lys	NA	0.000042	Damaging(low confidence)	Benign	Neutral	0.03	0	-0.99	349
c.1832G<A	p.Arg611His	NA	0.5367	Tolerated	Benign	Neutral	0.1	0.146	-1.82	350;147;353;346;341
c.2565A<G	p.Ser855Pro	NA	0.00058	Tolerated	Benign	Neutral	0.28	0.34	-2.023	353
c.1367G<A	p.Arg456His	NA	0.057	Tolerated	Probably damaging	Neutral	0.12	1	-1.31	349

Table H-1*WFS1* Missense variants detected and confirmed with Sanger sequencing and their relative pathogenicity scores.

SIFT, POLYPHEN2 and Provean were used to analyse each variant and their respective scores are indicated. The presence of these variants in the Euro-Wab WFS1 database which contains the largest collection of up-to-date variants was also investigated (September 2015)

Bibliography

Abbott, J.A., Francklyn, C.S., Robey-Bond, S.M., (2014) 'Transfer RNA and human disease', Frontiers in Genetics (5)158

Abecasis, G.R., Altshuler, D., Auton, A., Brooks, L.D., Durbin, R.M., Gibbs, R.A., Hurles, M.E., McVean, G.A. and Genomes Project, C. (2010) 'A map of human genome variation from population-scale sequencing', *Nature*, 467(7319), pp. 1061-73.

Abrahams, J.P., Leslie, A.G.W., Lutter, R. and Walker, J.E. (1994) 'Structure at 2.8-angstrom resolution of f1-atpase from bovine heart-mitochondria', *Nature*, 370(6491), pp. 621-628.

Acin-Perez, R., Bayona-Bafaluy, M.P., Fernandez-Silva, P., Moreno-Loshuertos, R., Perez-Martos, A., Bruno, C., Moraes, C.T. and Enriquez, J.A. (2004) 'Respiratory complex III is required to maintain complex I in mammalian mitochondria', *Molecular Cell*, 13(6), pp. 805-815.

Adzhubei, I.A., Schmidt, S., Peshkin, L., Ramensky, V.E., Gerasimova, A., Bork, P., Kondrashov, A.S. and Sunyaev, S.R. (2010) 'A method and server for predicting damaging missense mutations', *Nature Methods*, 7(4), pp. 248-249.

Agier, V., Oliviero, P., Laine, J., L'Hermitte-Stead, C., Girard, S., Fillaut, S., Jardel, C., Bouillaud, F., Bulteau, A.L. and Lombes, A. (2012) 'Defective mitochondrial fusion, altered respiratory function, and distorted cristae structure in skin fibroblasts with heterozygous OPA1 mutations', *Biochimica Et Biophysica Acta-Molecular Basis of Disease*, 1822, pp. 1570-1580.

Alam, T.I., Kanki, T., Muta, T., Ukaji, K., Abe, Y., Nakayama, H., Takio, K., Hamasaki, N. and Kang, D.C. (2003) 'Human mitochondrial DNA is packaged with TFAM', *Nucleic Acids Research*, 31(6), pp. 1640-1645.

Alavi, M.V., Bette, S., Schimpf, S., Schuettauf, F., Schraermeyer, U., Wehrl, H.F., Ruttiger, L., Beck, S.C., Tonagel, F., Pichler, B.J., Knipper, M., Peters, T., Laufs, J. and Wissinger, B. (2007) 'A splice site mutation in the murine OpaI gene features pathology of autosomal dominant optic atrophy', *Brain*, 130, pp. 1029-1042
.
Alberts, B., Johnson A., Lewis, J., Raff, M., Roberts, K. and Walter, P. (2002) 'The Genetic System of Mitochondria and Plasmids', *Molecular Biology of the Cell. 4th Edition.*

Alexander, C., Votruba, M., Pesch, U.E.A., Thiselton, D.L., Mayer, S., Moore, A., Rodriguez, M., Kellner, U., Leo-Kottler, B., Auburger, G., Bhattacharya, S.S. and Wissinger, B. (2000) 'OPA1, encoding a dynamin-related GTPase, is mutated in autosomal dominant optic atrophy linked to chromosome 3q28', *Nature Genetics*, 26, pp. 211-215.

Alexeyev, M., Shokolenko, I., Wilson, G. and LeDoux, S. (2013) 'The Maintenance of Mitochondrial DNA Integrity-Critical Analysis and Update', *Cold Spring Harbor Perspectives in Biology*, 5(5).

Allen, K.F., Gaier, E.D. and Wiggs, J.L. (2015) 'Genetics of Primary Inherited Disorders of the Optic Nerve: Clinical Applications', *Cold Spring Harbor Perspectives in Medicine*, 5(7).

Amati-Bonneau, P., Guichet, A., Olichon, A., Chevrollier, A., Viala, F., Miot, S., Ayuso, C., Odent, S., Arrouet, C., Verny, C., Calmels, M.N., Simard, G., Belenguer, P., Wang, J., Puel, J.L., Hamel, C., Malthiery, Y., Bonneau, D., Lenaers, G. and Reynier, P. (2005) 'OPA1 R445H mutation in optic atrophy associated with sensorineural deafness', *Annals of Neurology*, 58(6), pp. 958-963.

Amati-Bonneau, P., Valentino, M.L., Reynier, P., Gallardo, M.E., Bornstein, B., Boissiere, A., Campos, Y., Rivera, H., de la Aleja, J.G., Carroccia, R., Iommarini, L., Labauge, P., Figarella-Branger, D., Marcorelles, P., Furby, A., Beauvais, K., Letournel, F., Liguori, R., La Morgia, C., Montagna, P., Liguori, M., Zanna, C., Rugolo, M., Cossarizza, A., Wissinger, B., Verny, C., Schwarzenbacher, R., Martin, M.A., Arenas, J., Ayuso, C., Garesse, R., Lenaers, G., Bonneau, D. and Carelli, V. (2008) 'OPA1 mutations induce mitochondrial DNA instability and optic atrophy plus phenotypes', *Brain*, 131, pp. 338-351.

Amr, S., Heisey, C., Zhang, M., Xia, X.-J., Shows, K.H., Ajlouni, K., Pandya, A., Satin, L.S., El-Shanti, H. and Shiang, R. (2007) 'A homozygous mutation in a novel zinc-finger protein, ERIS, is responsible for Wolfram syndrome 2', *American Journal of Human Genetics*, 81(4), pp. 673-683.

Amunts, A., Brown, A., Toots, J., Scheres, S.H.W. and Ramakrishnan, V. (2015) 'The structure of the human mitochondrial ribosome', *Science*, 348(6230), pp. 95-98.
Anand, R., Wai, T., Baker, M.J., Kladt, N., Schauss, A.C., Rugarli, E. and Langer, T. (2014) 'The i-AAA protease YME1L and OMA1 cleave OPA1 to balance mitochondrial fusion and fission', *Journal of Cell Biology*, 204(6), pp. 919-929.

Anderson, C.T.M. and Friedberg, E.C. (1980) 'presence of nuclear and mitochondrial uracil-dna glycosylase in extracts of human kb-cells', *Nucleic Acids Research*, 8(4), pp. 875-888.
Anderson, S., Bankier, A.T., Barrell, B.G., Debruijn, M.H.L., Coulson, A.R., Drouin, J., Eperon, I.C., Nierlich, D.P., Roe, B.A., Sanger, F., Schreier, P.H., Smith, A.J.H., Staden, R. and Young, I.G. (1981) 'Sequence and organization of the human mitochondrial genome', *Nature*, 290(5806), pp. 457-465.

Andrews, R.M., Griffiths, P.G., Johnson, M.A. and Turnbull, D.M. (1999) 'Histochemical localisation of mitochondrial enzyme activity in human optic nerve and retina', *British Journal of Ophthalmology*, 83(2), pp. 231-235.

Angebault, C., Guichet, P.O., Talmat-Amar, Y., Charif, M., Gerber, S., Fares-Taie, L., Gueguen, N., Halloyn, F., Moore, D., Amati-Bonneau, P., Manes, G., Hebrard, M., Bocquet, B., Quiles, M., Piro-Megy, C., Teigell, M., Delettre, C., Rossel, M., Meunier, I., Preising, M., Lorenz, B., Carelli, V., Chinnery, P.F., Yu-Wai-Man, P., Kaplan, J., Roubertie, A., Barakat, A., Bonneau, D., Reynier, P., Rozet, J.M., Bomont, P., Hamel, C.P. and Lenaers, G. (2015) 'Recessive

Mutations in RTN4IP1 Cause Isolated and Syndromic Optic Neuropathies', *American Journal of Human Genetics*, 97(5), pp. 754-760.

Anikster, Y., Kleta, R., Shaag, A., Gahl, W.A. and Elpeleg, O. (2001) 'Type III 3-methylglutaconic aciduria (optic atrophy plus syndrome, or Costeff optic atrophy syndrome): Identification of the OPA3 gene and its founder mutation in Iraqi Jews', *American Journal of Human Genetics*, 69(6), pp. 1218-1224.

Ashley, N., O'Rourke, A., Smith, C., Adams, S., Gowda, V., Zeviani, M., Brown, G.K., Fratter, C. and Poulton, J. (2008) 'Depletion of mitochondrial DNA in fibroblast cultures from patients with POLG1 mutations is a consequence of catalytic mutations', *Human Molecular Genetics*, 17(16), pp. 2496-2506.

Assink, J.J.M., Tijmes, N.T., tenBrink, J.B., Oostra, R.J., Riemslag, F.C., deJong, P. and Bergen, A.A.B. (1997) 'A gene for X-linked optic atrophy is closely linked to the Xp11.4-Xp11.2 region of the X chromosome', *American Journal of Human Genetics*, 61(4), pp. 934-939.

Bacman, S.R., Williams, S.L., Garcia, S. and Moraes, C.T. (2010) 'Organ-specific shifts in mtDNA heteroplasmy following systemic delivery of a mitochondria-targeted restriction endonuclease', *Gene Therapy*, 17(6), pp. 713-720.

Bacman, S.R., Williams, S.L., Pinto, M., Peralta, S. and Moraes, C.T. (2013) 'Specific elimination of mutant mitochondrial genomes in patient-derived cells by mitoTALENs', *Nature Medicine*, 19(9), pp. 1111-1113.

Bai, X., Lv, H., Zhang, F., Liu, J., Fan, Z., Xu, L., Han, Y., Chai, R., Li, J. and Wang, H. (2014) 'Identification of a Novel Missense Mutation in the WFS1 Gene as a Cause of Autosomal Dominant Nonsyndromic Sensorineural Hearing Loss in All-Frequencies', *American Journal of Medical Genetics Part A*, 164(12), pp. 3052-3060.

Bailie, M., Votruba, M., Griffiths, P.G., Chinnery, P.F. and Yu-Wai-Man, P. (2013) 'Visual and psychological morbidity among patients with autosomal dominant optic atrophy', *Acta Ophthalmologica*, 91(5), pp. E413-E414.

Ban-Ishihara, R., Ishihara, T., Sasaki, N., Mihara, K. and Ishihara, N. (2013) 'Dynamics of nucleoid structure regulated by mitochondrial fission contributes to cristae reformation and release of cytochrome c', *Proceedings of the National Academy of Sciences of the United States of America*, 110(29), pp. 11863-11868.

Baracca, A., Solaini, G., Sgarbi, G., Lenaz, G., Baruzzi, A., Schapira, A.H.V., Martinuzzi, A. and Carelli, V. (2005) 'Severe impairment of complex I-Driven adenosine triphosphate synthesis in Leber hereditary optic neuropathy cybrids', *Archives of Neurology*, 62(5), pp. 730-736.

Barbet, F., Gerber, S., Hakiki, S., Perrault, I., Hanein, S., Ducroq, D., Tanguy, G., Dufier, J.L.,

Munnich, A., Rozet, J.M. and Kaplan, J. (2003) 'A first locus for isolated autosomal recessive optic atrophy (ROA1) maps to chromosome 8q', *European Journal of Human Genetics*, 11(12), pp. 966-971.
Barbet, F., Hakiki, S., Orssaud, C., Gerber, S., Perrault, I., Hanein, S., Ducroq, D., Dufier, J.L., Munnich, A., Kaplan, J. and Rozet, J.M. (2005) 'A third locus for dominant optic atrophy on chromosome 22q', *Journal of Medical Genetics*, 42(1).

Barbiroli, B., Montagna, P., Cortelli, P., Iotti, S., Lodi, R., Barboni, P., Monari, L., Lugaresi, E., Frassineti, C. and Zaniol, P. (1995) 'Defective brain and muscle energy-metabolism shown by in-vivo p-31 magnetic-resonance spectroscopy in nonaffected carriers of 11778-mtdna mutation', *Neurology*, 45(7), pp. 1364-1369.

Barrell, B.G., Bankier, A.T. and Drouin, J. (1979) 'Different genetic-code in human mitochondria', *Nature*, 282(5735), pp. 189-194.

Barrett, T.G. and Bundey, S.E. (1997) 'Wolfram (DIDMOAD) syndrome', *Journal of Medical Genetics*, 34(10), pp. 838-841.

Barrett, T.G., Bundey, S.E. and Macleod, A.F. (1995) 'Neurodegeneration and diabetes - uk nationwide study of wolfram (didmoad) syndrome', *Lancet*, 346(8988), pp. 1458-1463.

Bell, J.A., Reed, M.A., Consitt, L.A., Martin, O.J., Haynie, K.R., Hulver, M.W., Muoio, D.M. and Dohm, G.L. (2010) 'Lipid Partitioning, Incomplete Fatty Acid Oxidation, and Insulin Signal Transduction in Primary Human Muscle Cells: Effects of Severe Obesity, Fatty Acid Incubation, and Fatty Acid Translocase/CD36 Overexpression', *Journal of Clinical Endocrinology & Metabolism*, 95(7), pp. 3400-3410.

Bellance, N., Lestienne, P. and Rossignol, R. (2009) 'Mitochondria: from bioenergetics to the metabolic regulation of carcinogenesis', *Frontiers in bioscience (Landmark edition)*, 14, pp. 4015-34.

Berry, V., Gregory-Evans, C., Emmett, W., Waseem, N., Raby, J., Prescott, D., Moore, A.T. and Bhattacharya, S.S. (2013) 'Wolfram gene (WFS1) mutation causes autosomal dominant congenital nuclear cataract in humans', *European Journal of Human Genetics*, 21(12), pp. 1356-1360.

Bessahraoui, M., Paquis, V., Rouzier, C., Bouziane-Nedjadi, K., Naceur, M., Niar, S., Zennaki, A., Boudraa, G. and Touhami, M. (2014) 'Familial Wolfram syndrome', *Archives De Pediatrie*, 21(11), pp. 1229-1232.

Biesecker, L.G., Burke, W., Kohane, I., Plon, S.E. and Zimmern, R. (2012) 'Next-generation sequencing in the clinic: are we ready?', *Nature Reviews Genetics*, 13(11), pp. 818-824.
Bogenhagen, D. and Clayton, D.A. (1977) 'Mouse l-cell mitochondrial-dna molecules are selected randomly for replication throughout cell-cycle', *Cell*, 11(4), pp. 719-727.

Bonifert, T., Karle, K.N., Tonagel, F., Batra, M., Wilhelm, C., Theurer, Y., Schoenfeld, C., Kluba, T., Kamenisch, Y., Carelli, V., Wolf, J., Gonzalez, M.A., Speziani, F., Schuele, R., Zuechner, S., Schoels, L., Wissinger, B. and Synofzik, M. (2014) 'Pure and syndromic optic atrophy explained by deep intronic OPA1 mutations and an intralocus modifier', *Brain*, 137, pp. 2164-2177.

Bonneau, D., Colin, E., Oca, F., Ferre, M., Chevrollier, A., Gueguen, N., Desquiret-Dumas, V., N'Guyen, S., Barth, M., Zanlonghi, X., Rio, M., Desguerre, I., Barnerias, C., Momtchilova, M., Rodriguez, D., Slama, A., Lenaers, G., Procaccio, V., Amati-Bonneau, P. and Reynier, P. (2014) 'Early-onset Behr syndrome due to compound heterozygous mutations in OPA1', *Brain*, 137.

Bonnycastle, L.L., Chines, P.S., Hara, T., Huyghe, J.R., Swift, A.J., Heikinheimo, P., Mahadevan, J., Peltonen, S., Huopio, H., Nuutila, P., Narisu, N., Goldfeder, R.L., Stitzel, M.L., Lu, S., Boehnke, M., Urano, F., Collins, F.S. and Laakso, M. (2013) 'Autosomal Dominant Diabetes Arising From a Wolfram Syndrome 1 Mutation', *Diabetes*, 62(11), pp. 3943-3950.
Botstein, D. and Risch, N. (2003) 'Discovering genotypes underlying human phenotypes: past successes for mendelian disease, future approaches for complex disease', *Nature Genetics*, 33, pp. 228-237.

Bowmaker, M., Yang, M.Y., Yasukawa, T., Reyes, A., Jacobs, H.T., Huberman, J.A. and Holt, I.J. (2003) 'Mammalian mitochondrial DNA replicates bidirectionally from an initiation zone', *Journal of Biological Chemistry*, 278(51), pp. 50961-50969.

Boyer, P.D. (1997) 'The ATP synthase - A splendid molecular machine', *Annual Review of Biochemistry*, 66, pp. 717-749.

Bristow, E.A., Griffiths, P.G., Andrews, R.M., Johnson, M.A. and Turnbull, D.M. (2002) 'The distribution of mitochondrial activity in relation to optic nerve structure', *Archives of Ophthalmology*, 120(6), pp. 791-796.

Brown, T.A., Tkachuk, A.N., Shtengel, G., Kopek, B.G., Bogenhagen, D.F., Hess, H.F. and Clayton, D.A. (2011) 'Superresolution Fluorescence Imaging of Mitochondrial Nucleoids Reveals Their Spatial Range, Limits, and Membrane Interaction', *Molecular and Cellular Biology*, 31(24), pp. 4994-5010.

Browning, B.L. and Browning, S.R. (2009) 'A Unified Approach to Genotype Imputation and Haplotype-Phase Inference for Large Data Sets of Trios and Unrelated Individuals', *American Journal of Human Genetics*, 84(2), pp. 210-223.

Buono, L.M., Foroozan, R., Sergott, R.C. and Savino, P.J. (2002) 'Is normal tension glaucoma actually an unrecognized hereditary optic neuropathy? New evidence from genetic analysis', *Current opinion in ophthalmology*, 13(6), pp. 362-70.

Burte, F., Carelli, V., Chinnery, P.F. and Yu-Wai-Man, P. (2015) 'Disturbed mitochondrial dynamics and neurodegenerative disorders', *Nature Reviews Neurology*, 11(1), pp. 11-24.

Bustamante, E. and Pedersen, P.L. (1977) 'High aerobic glycolysis of rat hepatoma-cells in culture - role of mitochondrial hexokinase - (l-lactic acid-d-glucose-d-galactose-liver-neoplasia)', *Proceedings of the National Academy of Sciences of the United States of America*, 74(9), pp. 3735-3739.

Cagalinec, M., Liiv, M., Hodurova, Z., Hickey, M.A., Vaarmann, A., Mandel, M., Zeb, A., Choubey, V., Kuum, M., Safiulina, D., Vasar, E., Veksler, V. and Kaasik, A. (2016) 'Role of Mitochondrial Dynamics in Neuronal Development: Mechanism for Wolfram Syndrome', *Plos Biology*, 14(7).

Campbell, C.T., Kolesar, J.E. and Kaufman, B.A. (2012) 'Mitochondrial transcription factor A regulates mitochondrial transcription initiation, DNA packaging, and genome copy number', *Biochimica Et Biophysica Acta-Gene Regulatory Mechanisms*, 1819(9-10), pp. 921-929.

Cann, R.L. (2001) 'Genetic clues to dispersal in human populations: Retracing the past from the present', *Science*, 291(5509), pp. 1742-1748.

Cano, A., Rouzier, C., Monnot, S., Chabrol, B., Conrath, J., Lecomte, P., Delobel, B., Boileau, P., Valero, R., Procaccio, V., Paquis-Flucklinger, V., Vialettes, B. and French Grp Wolfram, S. (2007) 'Identification of novel mutations in WFS1 and genotype-phenotype correlation in Wolfram syndrome', *American Journal of Medical Genetics Part A*, 143A(14), pp. 1605-1612.

Cantatore, P. and Attardi, G. (1980) 'Mapping of nascent light and heavy strand transcripts on the physical map of hela-cell mitochondrial-dna', *Nucleic Acids Research*, 8(12), pp. 2605-2625.

Carelli, V., Ghelli, A., Ratta, M., Bacchilega, E., Sangiorgi, S., Mancini, R., Leuzzi, V., Cortelli, P., Montagna, P., Lugaresi, E. and Esposti, M.D. (1997) 'Leber's hereditary optic neuropathy: Biochemical effect of 11778/ND4 and 3460/ND1 mutations and correlation with the mitochondrial genotype', *Neurology*, 48(6), pp. 1623-1632.

Carelli, V., La Morgia, C., Valentino, M.L., Barboni, P., Ross-Cisneros, F.N. and Sadun, A.A. (2009) 'Retinal ganglion cell neurodegeneration in mitochondrial inherited disorders', *Biochimica Et Biophysica Acta-Bioenergetics*, 1787(5), pp. 518-528.

Carelli, V., La Morgia, C., Valentino, M.L., Rizzo, G., Carbonelli, M., De Negri, A.M., Sadun, F., Carta, A., Guerriero, S., Simonelli, F., Sadun, A.A., Aggarwal, D., Liguori, R., Avoni, P., Baruzzi, A., Zeviani, M., Montagna, P. and Barboni, P. (2011a) 'Idebenone Treatment In Leber's Hereditary Optic Neuropathy', *Brain*, 134.

Carelli, V., Musumeci, O., Caporali, L., Zanna, C., La Morgia, C., Del Dotto, V., Porcelli, A.M., Rugolo, M., Valentino, M.L., Iommarini, L., Maresca, A., Barboni, P., Carbonelli, M.,

Trombetta, C., Valente, E.M., Patergnani, S., Giorgi, C., Pinton, P., Rizzo, G., Tonon, C., Lodi, R., Avoni, P., Liguori, R., Baruzzi, A., Toscano, A. and Zeviani, M. (2015a) 'Syndromic parkinsonism and dementia associated with OPA1 missense mutations', *Annals of Neurology*, 78(1), pp. 21-38.

Carelli, V., Ross-Cisneros, F.N. and Sadun, A.A. (2004) 'Mitochondrial dysfunction as a cause of optic neuropathies', *Progress in Retinal and Eye Research*, 23(1), pp. 53-89.
Carelli, V., Saadati, H.G., Cortelli, P., Barboni, P., Madigan, M. and Sadun, A.A. (1999) 'A histopathologic analysis of the optic nerve in a case of Leber's hereditary optic neuropathy (LHON) with 3460/ND1 mt DNA mutation', *Investigative Ophthalmology & Visual Science*, 40(4), pp. S445-S445.

Carelli, V., Sabatelli, M., Carrozzo, R., Rizza, T., Schimpf, S., Wissinger, B., Zanna, C., Rugolo, M., La Morgia, C., Caporali, L., Carbonelli, M., Barboni, P., Tonon, C., Lodi, R. and Bertini, E. (2015b) "Behr syndrome' with OPA1 compound heterozygote mutations', *Brain*, 138.

Carelli, V., Schimpf, S., Fuhrmann, N., Valentino, M.L., Zanna, C., Iommarini, L., Papke, M., Schaich, S., Tippmann, S., Baumann, B., Barboni, P., Longanesi, L., Rugolo, M., Ghelli, A., Alavi, M.V., Youle, R.J., Bucchi, L., Carroccia, R., Giannoccaro, M.P., Tonon, C., Lodi, R., Cenacchi, G., Montagna, P., Liguori, R. and Wissinger, B. (2011b) 'A clinically complex form of dominant optic atrophy (OPA8) maps on chromosome 16', *Human Molecular Genetics*, 20(10), pp. 1893-1905.

Carelli, V., Schimpf, S., Valentino, M.L., Fuhrmann, N., Papke, M., Schaich, S., Tippmann, S., Baumann, B., Barboni, P., Ghelli, A., Bucchi, L., Lodi, R., Barbiroli, B., Liguori, R., Carroccia, R., Villanova, M., Montagna, P., Baruzzi, A. and Wissinger, B. (2007) 'Dominant optic atrophy (DOA) and sensorineural hearing loss: Clinical, biochemical, spectroscopic and molecular genetic study of a large Italian pedigree linked to a new locus an chromosome 16', *Neurology*, 68(12), pp. A42-A42.

Caspi, R.R. (2010) 'A look at autoimmunity and inflammation in the eye', *Journal of Clinical Investigation*, 120(9), pp. 3073-3083.

Castle, M. and Keller, J. (2007)'Rolling Ball Background Subtraction' **rsb.info.nih.gov/ij/plugins/rolling-ball.html**

Chacon-Camacho, O., Arce-Gonzalez, R., Granillo-Alvarez, M., Flores-Limas, S., Ramirez, M. and Zenteno, J.C. (2013) 'Expansion of the Clinical Ocular Spectrum of Wolfram Syndrome in a Family Carrying a Novel WFS1 Gene Deletion', *Ophthalmic Genetics*, 34(4), pp. 243-248.

Chaussenot, A., Bannwarth, S., Rouzier, C., Vialettes, B., El Mkadem, S.A., Chabrol, B., Cano, A., Labauge, P. and Paquis-Flucklinger, V. (2011) 'Neurologic Features and Genotype-Phenotype Correlation in Wolfram Syndrome', *Annals of Neurology*, 69(3), pp. 501-508.

Chaussenot, A., Rouzier, C., Quere, M., Plutino, M., Ait-El-Mkadem, S., Bannwarth, S., Barth, M., Dollfus, H., Charles, P., Nicolino, M., Chabrol, B., Vialettes, B. and Paquis-Flucklinger, V. (2015) 'Mutation update and uncommon phenotypes in a French cohort of 96 patients with WFS1-related disorders', *Clinical Genetics*, 87(5), pp. 430-439.

Chen, H., McCaffery, J.M. and Chan, D.C. (2007) 'Mitochondrial fusion protects against neurodegeneration in the cerebellum', *Cell*, 130(3), pp. 548-562.

Chen, H., Vermulst, M., Wang, Y.E., Chomyn, A., Prolla, T.A., McCaffery, J.M. and Chan, D.C. (2010) 'Mitochondrial Fusion Is Required for mtDNA Stability in Skeletal Muscle and Tolerance of mtDNA Mutations', *Cell*, 141(2), pp. 280-289.

Chen, H.C. and Chan, D.C. (2005) 'Emerging functions of mammalian mitochondrial fusion and fission', *Human Molecular Genetics*, 14, pp. R283-R289.

Chen, H.C., Detmer, S.A., Ewald, A.J., Griffin, E.E., Fraser, S.E. and Chan, D.C. (2003) 'Mitofusins Mfn1 and Mfn2 coordinately regulate mitochondrial fusion and are essential for embryonic development', *Journal of Cell Biology*, 160(2), pp. 189-200.

Chen, L., Liu, T., Alice, T., Lu, X., Tomilov, A.A., Davies, V., Cortopassi, G., Chiamvimonvat, N., Bers, D.M., Votruba, M. and Knowlton, A.A. (2012) 'OPA1 Mutation and Late-Onset Cardiomyopathy: Mitochondrial Dysfunction and mtDNA Instability', *Journal of the American Heart Association*, 1(5).

Chevrollier, A., Cassereau, J., Ferre, M., Alban, J., Desquiret-Dumas, V., Gueguen, N., Amati-Bonneau, P., Procaccio, V., Bonneau, D. and Reynier, P. (2012) 'Standardized mitochondrial analysis gives new insights into mitochondrial dynamics and OPA1 function', *International Journal of Biochemistry & Cell Biology*, 44, pp. 980-988.

Chevrollier, A., Guillet, V., Loiseau, D., Gueguen, N., de Crescenzo, M.A.P., Verny, C., Ferre, M., Dollfus, H., Odent, S., Milea, D., Goizet, C., Amati-Bonneau, P., Procaccio, V., Bonneau, D. and Reynier, P. (2008) 'Hereditary optic neuropathies share a common mitochondrial coupling defect', *Annals of Neurology*, 63, pp. 794-798.

Chinnery, P.F. (2015) 'Mitochondrial disease in adults: what's old and what's new?', *Embo Molecular Medicine*, 7(12), pp. 1503-1512.

Chinnery, P.F., Craven, L., Mitalipov, S., Stewart, J.B., Herbert, M. and Turnbull, D.M. (2014) 'The Challenges of Mitochondrial Replacement', *Plos Genetics*, 10(4).

Cipolat, S., de Brito, O.M., Dal Zilio, B. and Scorrano, L. (2004) 'OPA(1) requires mitofusin-1 to promote mitochondrial fusion', *Biochimica Et Biophysica Acta-Bioenergetics*, 1658, pp. 38-38.

Cipolat, S., Rudka, T., Hartmann, D., Costa, V., Serneels, L., Craessaerts, K., Metzger, K., Frezza, C., Annaert, W., D'Adamio, L., Derks, C., Dejaegere, T., Pellegrini, L., D'Hooge, R., Scorrano, L. and De Strooper, B. (2006) 'Mitochondrial rhomboid PARL regulates cytochrome c release during apoptosis via OPA1-dependent cristae remodeling', *Cell*, 126(1), pp. 163-175.

Clayton, D.A. (1982) 'Replication of animal mitochondrial-dna', *Cell*, 28(4), pp. 693-705.

Cogliati, S., Frezza, C., Soriano, M.E., Varanita, T., Quintana-Cabrera, R., Corrado, M., Cipolat, S., Costa, V., Casarin, A., Gomes, L.C., Perales-Clemente, E., Salviati, L., Fernandez-Silva, P., Enriquez, J.A. and Scorrano, L. (2013) 'Mitochondrial Cristae Shape Determines Respiratory Chain Supercomplexes Assembly and Respiratory Efficiency', *Cell*, 155(1), pp. 160-171.

Cohn, A.C., Toomes, C., Hewitt, A.W., Kearns, L.S., Inglehearn, C.F., Craig, J.E. and Mackey, D.A. (2008) 'The natural history of OPA1-related autosomal dominant optic atrophy', *British Journal of Ophthalmology*, 92(10), pp. 1333-1336.

Cohn, A.C., Toomes, C., Potter, C., Towns, K.V., Hewitt, A.W., Inglehearn, C.F., Craig, J.E. and Mackey, D.A. (2007) 'Autosomal dominant optic atrophy: Penetrance and expressivity in patients with OPA1 mutations', *American Journal of Ophthalmology*, 143(4), pp. 656-662.

Cooper, G.M., Stone, E.A., Asimenos, G., Green, E.D., Batzoglou, S., Sidow, A. and Progra, N.C.S. (2005) 'Distribution and intensity of constraint in mammalian genomic sequence', *Genome Research*, 15(7), pp. 901-913.

Cooper, I.S., Rynearson, E.H., Bailey, A.A. and MacCarty, C.S. (1950) 'The relation of spinal cord diseases to gynecomastia and testicular atrophy', *Proceedings of the staff meetings. Mayo Clinic*, 25(12), pp. 320-6.

Craven, L., Tuppen, H.A., Greggains, G.D., Harbottle, S.J., Murphy, J.L., Cree, L.M., Murdoch, A.P., Chinnery, P.F., Taylor, R.W., Lightowlers, R.N., Herbert, M. and Turnbull, D.M. (2010) 'Pronuclear transfer in human embryos to prevent transmission of mitochondrial DNA disease', *Nature*, 465(7294), pp. 82-U89.

Crimi, M., Galbiati, S., Perini, M.P., Bordoni, A., Malferrari, G., Sciacco, M., Biunno, I., Strazzer, S., Moggio, M., Bresolin, N. and Comi, G.P. (2003) 'A mitochondrial tRNA(His) gene mutation causing pigmentary retinopathy and neurosensorial deafness', *Neurology*, 60(7), pp. 1200-1203.

Cryns, K., Pfister, M., Pennings, R.J.E., Bom, S.J.H., Flothmann, K., Caethoven, G., Kremer, H., Schatteman, I., Koln, K.A., Toth, T., Kupka, S., Blin, N., Nurnberg, P., Thiele, H., van de Heyning, P.H., Reardon, W., Stephens, D., Cremers, C., Smith, R.J.H. and Van Camp, G. (2002) 'Mutations in the WFS1 gene that cause low-frequency sensorineural hearing loss are small non-inactivating mutations', *Human Genetics*, 110(5), pp. 389-394.

Cryns, K., Sivakumaran, T.A., Van den Ouweland, J.M.W., Pennings, R.J.E., Cremers, C., Flothmann, K., Young, T.L., Smith, R.J.H., Lesperance, M.M. and Van Camp, G. (2003) 'Mutational spectrum of the WFS1 gene in Wolfram syndrome, nonsyndromic hearing impairment, diabetes mellitus, and psychiatric disease', *Human Mutation*, 22(4), pp. 275-287.

Czabotar, P.E., Lessene, G., Strasser, A. and Adams, J.M. (2014) 'Control of apoptosis by the BCL-2 protein family: implications for physiology and therapy', *Nature Reviews Molecular Cell Biology*, 15(1), pp. 49-63.

Dahlmann-Noor, A., Vijay, S., Jayaram, H., Limb, A. and Khaw, P.T. (2010) 'Current approaches and future prospects for stem cell rescue and regeneration of the retina and optic nerve', *Canadian Journal of Ophthalmology-Journal Canadien D Ophtalmologie*, 45(4), pp. 333-341.

Dai, Y., Kiselak, T., Clark, J., Clore, E., Zheng, K., Cheng, A., Kujoth, G.C., Prolla, T.A., Maratos-Flier, E. and Simon, D.K. (2013) 'Behavioral and metabolic characterization of heterozygous and homozygous POLG mutator mice', *Mitochondrion*, 13(4), pp. 282-291.

Davies, V.J., Hollins, A.J., Piechota, M.J., Yip, W., Davies, J.R., White, K.E., Nicols, P.P., Boulton, M.E. and Votruba, M. (2007) 'Opa1 deficiency in a mouse model of autosomal dominant optic atrophy impairs mitochondrial morphology, optic nerve structure and visual function', *Human Molecular Genetics*, 16(11), pp. 1307-1318.

Davies, V.J., Powell, K.A., White, K.E., Yip, W., Hogan, V., Hollins, A.J., Davies, J.R., Piechota, M., Brownstein, D.G., Moat, S.J., Nichols, P.P., Wride, M.A., Boulton, M.E. and Votruba, M. (2008) 'A missense mutation in the murine Opa3 gene models human Costeff syndrome', *Brain*, 131, pp. 368-380.

Dayanithi, G., Chen-Kuo-Chang, M., Viero, C., Hamel, C., Muller, A. and Lenaers, G. (2010) 'Characterization of Ca2+ Signalling in Postnatal Mouse Retinal Ganglion Cells: Involvement of OPA1 in Ca2+ Clearance', *Ophthalmic Genetics*, 31(2), pp. 53-65.

de Heredia, M.L., Cleries, R. and Nunes, V. (2013) 'Genotypic classification of patients with Wolfram syndrome: insights into the natural history of the disease and correlation with phenotype', *Genetics in Medicine*, 15(7), pp. 497-506.

Delettre, C., Lenaers, G., Griffoin, J.M., Gigarel, N., Lorenzo, C., Belenguer, P., Pelloquin, L., Grosgeorge, J., Turc-Carel, C., Perret, E., Astarie-Dequeker, C., Lasquellec, L., Arnaud, B., Ducommun, B., Kaplan, J. and Hamel, C.P. (2000) 'Nuclear gene OPA1, encoding a mitochondrial dynamin-related protein, is mutated in dominant optic atrophy', *Nature Genetics*, 26(2), pp. 207-210.

DePristo, M.A., Banks, E., Poplin, R., Garimella, K.V., Maguire, J.R., Hartl, C., Philippakis, A.A., del Angel, G., Rivas, M.A., Hanna, M., McKenna, A., Fennell, T.J., Kernytsky, A.M.,

Sivachenko, A.Y., Cibulskis, K., Gabriel, S.B., Altshuler, D. and Daly, M.J. (2011) 'A framework for variation discovery and genotyping using next-generation DNA sequencing data', *Nature Genetics*, 43(5), pp. 491-+.

Detmer, S.A. and Chan, D.C. (2007) 'Functions and dysfunctions of mitochondrial dynamics', *Nature Reviews Molecular Cell Biology*, 8(11), pp. 870-879.

DiMauro, S., Schon, E.A., Carelli, V. and Hirano, M. (2013) 'The clinical maze of mitochondrial neurology', *Nature Reviews Neurology*, 9(8), pp. 429-444.

Ding, W.-X. and Yin, X.-M. (2012) 'Mitophagy: mechanisms, pathophysiological roles, and analysis', *Biological Chemistry*, 393(7), pp. 547-564.

Dodson, M.L. and Lloyd, R.S. (2002) 'Mechanistic comparisons among base excision repair glycosylases', *Free Radical Biology and Medicine*, 32(8), pp. 678-682.

Drmanac, R., Sparks, A.B., Callow, M.J., Halpern, A.L., Burns, N.L., Kermani, B.G., Carnevali, P., Nazarenko, I., Nilsen, G.B., Yeung, G., Dahl, F., Fernandez, A., Staker, B., Pant, K.P., Baccash, J., Borcherding, A.P., Brownley, A., Cedeno, R., Chen, L., Chernikoff, D., Cheung, A., Chirita, R., Curson, B., Ebert, J.C., Hacker, C.R., Hartlage, R., Hauser, B., Huang, S., Jiang, Y., Karpinchyk, V., Koenig, M., Kong, C., Landers, T., Le, C., Liu, J., McBride, C.E., Morenzoni, M., Morey, R.E., Mutch, K., Perazich, H., Perry, K., Peters, B.A., Peterson, J., Pethiyagoda, C.L., Pothuraju, K., Richter, C., Rosenbaum, A.M., Roy, S., Shafto, J., Sharanhovich, U., Shannon, K.W., Sheppy, C.G., Sun, M., Thakuria, J.V., Tran, A., Vu, D., Zaranek, A.W., Wu, X., Drmanac, S., Oliphant, A.R., Banyai, W.C., Martin, B., Ballinger, D.G., Church, G.M. and Reid, C.A. (2010) 'Human Genome Sequencing Using Unchained Base Reads on Self-Assembling DNA Nanoarrays', *Science*, 327(5961), pp. 78-81.

Droge, W. (2002) 'Free radicals in the physiological control of cell function', *Physiological Reviews*, 82(1), pp. 47-95.

Ebersberger, I., Metzler, D., Schwarz, C. and Paabo, S. (2002) 'Genomewide comparison of DNA sequences between humans and chimpanzees', *American Journal of Human Genetics*, 70(6), pp. 1490-1497.

Eiberg, H., Hansen, L., Kjer, B., Hansen, T., Pedersen, O., Bille, M., Rosenberg, T. and Tranebjaerg, L. (2006) 'Autosomal dominant optic atrophy associated with hearing impairment and impaired glucose regulation caused by a missense mutation in the WFS1 gene', *Journal of Medical Genetics*, 43(5), pp. 435-440.

Eiberg, H., Kjer, B., Kjer, P. and Rosenberg, T. (1994) 'Dominant optic atrophy (opa1) mapped to chromosome 3q region .1. linkage analysis', *Human Molecular Genetics*, 3(6), pp. 977-980.

Ekstrand, M.I., Falkenberg, M., Rantanen, A., Park, C.B., Gaspari, M., Hultenby, K., Rustin, P.,

Gustafsson, C.M. and Larsson, N.G. (2004) 'Mitochondrial transcription factor A regulates mtDNA copy number in mammals', *Human Molecular Genetics*, 13(9), pp. 935-944.

El-Shanti, H., Lidral, A.C., Jarrah, N., Druhan, L. and Ajlouni, K. (2000) 'Homozygosity mapping identifies an additional locus for Wolfram syndrome on chromosome 4q', *American Journal of Human Genetics*, 66(4), pp. 1229-1236.

Elachouri, G., Vidoni, S., Zanna, C., Pattyn, A., Boukhaddaoui, H., Gaget, K., Yu-Wai-Man, P., Gasparre, G., Sarzi, E., Delettre, C., Olichon, A., Loiseau, D., Reynier, P., Chinnery, P.F., Rotig, A., Carelli, V., Hamel, C.P., Rugolo, M. and Lenaers, G. (2011) 'OPA1 links human mitochondrial genome maintenance to mtDNA replication and distribution', *Genome Research*, 21, pp. 12-20.

Ellouze, S., Augustin, S., Bouaita, A., Bonnet, C., Simonutti, M., Forster, V., Picaud, S., Sahel, J.-A. and Corral-Debrinski, M. (2008) 'Optimized allotopic expression of the human mitochondrial ND4 prevents blindness in a rat model of mitochondrial dysfunction', *American Journal of Human Genetics*, 83(3), pp. 373-387.

Elpeleg, O., Mandel, H. and Saada, A. (2002) 'Depletion of the other genome-mitochondrial DNA depletion syndromes in humans', *Journal of Molecular Medicine-Jmm*, 80(7), pp. 389-396.

Elpeleg, O., Miller, C., Hershkovitz, E., Bitner-Glindzicz, M., Bondi-Rubenstein, G., Rahman, S., Pagnamenta, A., Eshhar, S. and Saada, A. (2005) 'Deficiency of the ADP-forming succinyl-CoA synthase activity is associated with encephalomyopathy and mitochondrial DNA depletion', *American Journal of Human Genetics*, 76(6), pp. 1081-1086.

Endo, T., Yamano, K. and Kawano, S. (2011) 'Structural insight into the mitochondrial protein import system', *Biochimica Et Biophysica Acta-Biomembranes*, 1808(3), pp. 955-970.

Farmer, A., Ayme, S., de Heredia, M.L., Maffei, P., McCafferty, S., Mlynarski, W., Nunes, V., Parkinson, K., Paquis-Flucklinger, V., Rohayem, J., Sinnott, R., Tillmann, V., Tranebaerg, L. and Barrett, T.G. (2013) 'EURO-WABB: an EU rare diseases registry for Wolfram syndrome, Alstrom syndrome and Bardet-Biedl syndrome', *Bmc Pediatrics*, 13.

Ferree, A. and Shirihai, O. (2012) 'Mitochondrial Dynamics: The Intersection of Form and Function', *Mitochondrial Oxidative Phosphorylation: Nuclear-Encoded Genes, Enzyme Regulation, and Pathophysiology*, 748, pp. 13-40.

Fogel, B.L., Lee, H., Deignan, J.L., Strom, S.P., Kantarci, S., Wang, X., Quintero-Rivera, F., Vilain, E., Grody, W.W., Perlman, S., Geschwind, D.H. and Nelson, S.F. (2014) 'Exome Sequencing in the Clinical Diagnosis of Sporadic or Familial Cerebellar Ataxia', *Jama Neurology*, 71(10), pp. 1237-1246.

Fonseca, S.G., Fukuma, M., Lipson, K.L., Nguyen, L.X., Allen, J.R., Oka, Y. and Urano, F.

(2005) 'WFS1 is a novel component of the unfolded protein response and maintains homeostasis of the endoplasmic reticulum in pancreatic beta-cells', *Journal of Biological Chemistry*, 280(47), pp. 39609-39615.

Fonseca, S.G., Ishigaki, S., Oslowski, C.M., Lu, S.M., Lipson, K.L., Ghosh, R., Hayashi, E., Ishihara, H., Oka, Y., Permutt, M.A. and Urano, F. (2010) 'Wolfram syndrome 1 gene negatively regulates ER stress signaling in rodent and human cells', *Journal of Clinical Investigation*, 120(3), pp. 744-755.

Fournier, A.V., Damji, K.F., Epstein, D.L. and Pollock, S.C. (2001) 'Disc excavation in dominant optic atrophy', *Ophthalmology*, 108(9), pp. 1595-1602.

Freudenberg-Hua, Y., Freudenberg, J., Kluck, N., Cichon, S., Propping, P. and Nothen, M.M. (2003) 'Single nucleotide variation analysis in 65 candidate genes for CNS disorders in a representative sample of the European population', *Genome Research*, 13(10), pp. 2271-2276.
Frey, T.G. and Mannella, C.A. (2000) 'The internal structure of mitochondria', *Trends in Biochemical Sciences*, 25(7), pp. 319-324.

Frezza, C., Cipolat, S., de Brito, O.M., Micaroni, M., Beznoussenko, G.V., Rudka, T., Bartoli, D., Polishuck, R.S., Danial, N.N., De Strooper, B. and Scorrano, L. (2006) 'OPA1 controls apoptotic cristae remodeling independently from mitochondrial fusion', *Cell*, 126(1), pp. 177-189.

Fueloep, L., Szanda, G., Enyedi, B., Varnai, P. and Spaet, A. (2011) 'The Effect of OPA1 on Mitochondrial Ca2+ Signaling', *Plos One*, 6(9).

Gangelhoff, T.A., Mungalachetty, P.S., Nix, J.C. and Churchill, M.E.A. (2009) 'Structural analysis and DNA binding of the HMG domains of the human mitochondrial transcription factor A', *Nucleic Acids Research*, 37(10), pp. 3153-3164.

Garcin, R., Raverdy, P., Delthil, S., Man, H.X. and Chimenes, H. (1961) 'On a heredo-familial disease combining cataract, optic atrophy, extrapyramidal symptoms and certain defects of Friedreich's disease. (Its nosological position in relation to the Behr's syndrome, the Marinesco-Sjogren syndrome and Friedreich's disease with ocular symptoms', *Revue neurologique*, 104, pp. 373-9.

Ghezzi, D., Sevrioukova, I., Invernizzi, F., Lamperti, C., Mora, M., D'Adamo, P., Novara, F., Zuffardi, O., Uziel, G. and Zeviani, M. (2010) 'Severe X-Linked Mitochondrial Encephalomyopathy Associated with a Mutation in Apoptosis-Inducing Factor', *American Journal of Human Genetics*, 86(4), pp. 639-649.

Gibbons, C., Montgomery, M.G., Leslie, A.G.W. and Walker, J.E. (2000) 'The structure of the central stalk in bovine F-1-ATPase at 2.4 angstrom resolution', *Nature Structural Biology*, 7(11), pp. 1055-1061.

Gilkerson, R.W., De Vries, R.L.A., Lebot, P., Wikstrom, J.D., Torgyekes, E., Shirihai, O.S., Przedborski, S. and Schon, E.A. (2012) 'Mitochondrial autophagy in cells with mtDNA mutations results from synergistic loss of transmembrane potential and mTORC1 inhibition', *Human Molecular Genetics*, 21(5), pp. 978-990.

Gilkerson, R.W., Schon, E.A., Hernandez, E. and Davidson, M.M. (2008) 'Mitochondrial nucleoids maintain genetic autonomy but allow for functional complementation', *Journal of Cell Biology*, 181(7), pp. 1117-1128.

Giordano, C., Montopoli, M., Perli, E., Orlandi, M., Fantin, M., Ross-Cisneros, F.N., Caparrotta, L., Martinuzzi, A., Ragazzi, E., Ghelli, A., Sadun, A.A., d'Amati, G. and Carelli, V. (2011) 'Oestrogens ameliorate mitochondrial dysfunction in Leber's hereditary optic neuropathy', *Brain*, 134, pp. 220-234.

Giorgi, C., Missiroli, S., Patergnani, S., Duszynski, J., Wieckowski, M.R. and Pinton, P. (2015) 'Mitochondria-Associated Membranes: Composition, Molecular Mechanisms, and Physiopathological Implications', *Antioxidants & Redox Signaling*, 22(12), pp. 995-1019.
Gomez-Zaera, M., Strom, T.M., Rodriguez, B., Estivill, X., Meitinger, T. and Nunes, V. (2001) 'Presence of a major WFS1 mutation in Spanish wolfram syndrome pedigrees', *Molecular Genetics and Metabolism*, 72(1), pp. 72-81.

Goncalves, A.C., Matos, T.D., Simoes-Teixeira, H.R., Machado, M.P., Simao, M., Dias, O.P., Andrea, M., Fialho, G. and Caria, H. (2014) 'WFS1 and non-syndromic low-frequency sensorineural hearing loss: A novel mutation in a Portuguese case', *Gene*, 538(2), pp. 288-291.

Gonzalvez, F., Pariselli, F., Dupaigne, P., Budihardjo, I., Lutter, M., Antonsson, B., Diolez, P., Manon, S., Martinou, J.C., Goubern, M., Wang, X., Bernard, S. and Petit, P.X. (2005a) 'tBid interaction with cardiolipin primarily orchestrates mitochondrial dysfunctions and subsequently activates Bax and Bak', *Cell Death and Differentiation*, 12(6), pp. 614-626.

Gonzalvez, F., Pariselli, F., Dupaigne, P., Budihardjo, I., Lutter, M., Antonsson, B., Diolez, P., Manon, S., Martinou, J.C., Goubern, M., Wang, X., Bernard, S. and Petit, P.X. (2005b) 'tBid interaction with cardiolipin primarily orchestrates mitochondrial dysfunctions and subsequently activates Bax and Bak', *Cell Death and Differentiation*, 12(6), pp. 614-626.

Gorman, G.S., Schaefer, A.M., Ng, Y., Gomez, N., Blakely, E.L., Alston, C.L., Feeney, C., Horvath, R., Yu-Wai-Man, P., Chinnery, P.F., Taylor, R.W., Turnbull, D.M. and McFarland, R. (2015) 'Prevalence of Nuclear and Mitochondrial DNA Mutations Related to Adult Mitochondrial Disease', *Annals of Neurology*, 77(5), pp. 753-759.

Goto, Y., Nonaka, I. and Horai, S. (1990) 'A mutation in the transfer rnaleu(uur) gene associated with the melas subgroup of mitochondrial encephalomyopathies', *Nature*, 348(6302), pp. 651-653.

Grau, T., Burbulla, L.F., Engl, G., Delettre, C., Delprat, B., Oexle, K., Leo-Kottler, B., Roscioli, T., Krueger, R., Rapaport, D., Wissinger, B. and Schimpf-Linzenbold, S. (2013) 'A novel heterozygous OPA3 mutation located in the mitochondrial target sequence results in altered steady-state levels and fragmented mitochondrial network', *Journal of Medical Genetics*, 50(12), pp. 848-858.

Gray, M.W., Burger, G. and Lang, B.F. (1999) 'Mitochondrial evolution', *Science*, 283(5407), pp. 1476-1481.

Green, D.R. and Reed, J.C. (1998) 'Mitochondria and apoptosis', *Science*, 281, pp. 1309-1312.
Grigorieff, N. (1999) 'Structure of the respiratory NADH : ubiquinone oxidoreductase (complex I)', *Current Opinion in Structural Biology*, 9(4), pp. 476-483.

Griparic, L., van der Wel, N.N., Orozco, I.J., Peters, P.J. and van der Bliek, A.M. (2004) 'Loss of the intermembrane space protein Mgm1/OPA1 induces swelling and localized constrictions along the lengths of mitochondria', *Journal of Biological Chemistry*, 279(18), pp. 18792-18798.

Gropman, A., Chen, T.J., Perng, C.L., Krasnewich, D., Chernoff, E., Tifft, C. and Wong, L.J.C. (2004) 'Variable clinical manifestation of homoplasmic G14459A mitochondrial DNA mutation', *American Journal of Medical Genetics Part A*, 124A(4), pp. 377-382.

Guo, X., Shen, S., Song, S., He, S., Cui, Y., Xing, G., Wang, J., Yin, Y., Fan, L., He, F. and Zhang, L. (2011) 'The E3 Ligase Smurf1 Regulates Wolfram Syndrome Protein Stability at the Endoplasmic Reticulum', *Journal of Biological Chemistry*, 286(20), pp. 18037-18047.

Guy, J., Carelli, V., Lewin, A., Qi, X.P., Martinuzzi, A., Schon, E., Manfredi, G., Pallotti, F. and Hauswirth, W. (2002) 'Gene therapy with the ND4 subunit gene recoded in the universal genetic code reverses a mitochondrial deficiency causing Leber hereditary optic neuropathy (LHON)', *Neurology*, 58(7), pp. A508-A508.

Guy, J., Qi, X., Koilkonda, R.D., Arguello, T., Chou, T.-H., Ruggeri, M., Porciatti, V., Lewin, A.S. and Hauswirth, W.W. (2009) 'Efficiency and Safety of AAV-Mediated Gene Delivery of the Human ND4 Complex I Subunit in the Mouse Visual System', *Investigative Ophthalmology & Visual Science*, 50(9), pp. 4205-4214.

Hammans, S.R., Sweeney, M.G., Brockington, M., Morganhughes, J.A. and Harding, A.E. (1991) 'Mitochondrial encephalopathies - molecular genetic diagnosis from blood-samples', *Lancet*, 337(8753), pp. 1311-1313.

Hammarsund, M., Wilson, W., Corcoran, M., Merup, M., Einhorn, S., Grander, D. and Sangfelt, O. (2001) 'Identification and characterization of two novel human mitochondrial elongation factor genes, hEFG2 and hEFG1, phylogenetically conserved through evolution', *Human Genetics*, 109(5), pp. 542-550.

Hanein, S., Perrault, I., Roche, O., Gerber, S., Khadom, N., Rio, M., Boddaert, N., Jean-Pierre, M., Brahimi, N., Serre, V., Chretien, D., Delphin, N., Fares-Taie, L., Lachheb, S., Rotig, A., Meire, F., Munnich, A., Dufier, J.-L., Kaplan, J. and Rozet, J.-M. (2009) 'TMEM126A, Encoding a Mitochondrial Protein, Is Mutated in Autosomal-Recessive Nonsyndromic Optic Atrophy', *American Journal of Human Genetics*, 84(4), pp. 493-498.

Hansen, M.B., Mitchelmore, C., Kjaerulff, K.M., Rasmussen, T.E., Pedersen, K.M. and Jensen, N.A. (2002) 'Mouse Atf5: Molecular cloning of two novel mRNAs, genomic organization, and odorant sensory neuron localization', *Genomics*, 80(3), pp. 344-350.

Hatefi, Y. and Galante, Y.M. (1980) 'Isolation of cytochrome-b560 from complex ii (succinate-ubiquinone oxidoreductase) and its reconstitution with succinate-dehydrogenase', *Journal of Biological Chemistry*, 255(12), pp. 5530-5537.

He, J., Mao, C.-C., Reyes, A., Sembongi, H., Di Re, M., Granycome, C., Clippingdale, A.B., Fearnley, I.M., Harbour, M., Robinson, A.J., Reichelt, S., Spelbrink, J.N., Walker, J.E. and Holt, I.J. (2007) 'The AAA(+) protein ATAD3 has displacement loop binding properties and is involved in mitochondrial nucleoid organization', *Journal of Cell Biology*, 176(2), pp. 141-146.

Herrington, J., Park, Y.B., Babcock, D.F. and Hille, B. (1996) 'Dominant role of mitochondria in clearance of large Ca2+ loads from rat adrenal chromaffin cells', *Neuron*, 16, pp. 219-228.

Herrnstadt, C., Elson, J.L., Fahy, E., Preston, G., Turnbull, D.M., Anderson, C., Ghosh, S.S., Olefsky, J.M., Beal, M.F., Davis, R.E. and Howell, N. (2002) 'Reduced-median-network analysis of complete mitochondrial DNA coding-region sequences for the major African, Asian, and European haplogroups', *American Journal of Human Genetics*, 70(5), pp. 1152-1171.

Herrnstadt, C. and Howell, N. (2004) 'An evolutionary perspective on pathogenic mtDNA mutations: haplogroup associations of clinical disorders', *Mitochondrion*, 4(5-6), pp. 791-798.
Hinchliffe, P. and Sazanov, L.A. (2005) 'Organization of iron-sulfur clusters in respiratory complex I', *Science*, 309(5735), pp. 771-774.

Hofmann, S. and Bauer, M.F. (2006) 'Wolfram syndrome-associated mutations lead to instability and proteasomal degradation of wolframin', *Febs Letters*, 580(16), pp. 4000-4004.

Hofmann, S., Philbrook, C., Gerbitz, K.D. and Bauer, M.F. (2003) 'Wolfram syndrome: structural and functional analyses of mutant and wild-type wolframin, the WFS1 gene product', *Human Molecular Genetics*, 12(16), pp. 2003-2012.

Hogewind, B.F.T., Pennings, R.J.E., Hol, F.A., Kunst, H.P.M., Hoefsloot, E.H., Cruysberg, J.R.M. and Cremers, C.W.R.J. (2010) 'Autosomal dominant optic neuropathy and sensorineual hearing loss associated with a novel mutation of WFS1', *Molecular Vision*, 16(4), pp. 26-35.

Holt, I.J., He, J., Mao, C.-C., Boyd-Kirkup, J.D., Martinsson, P., Sembongi, H., Reyes, A. and Spelbrink, J.N. (2007) 'Mammalian mitochondrial nucleoids: Organizing an independently minded genome', *Mitochondrion*, 7(5), pp. 311-321.

Holt, I.J., Lorimer, H.E. and Jacobs, H.T. (2000) 'Coupled leading- and lagging-strand synthesis of mammalian mitochondrial DNA', *Cell*, 100(5), pp. 515-524.

Hoppins, S. and Nunnari, J. (2012) 'Mitochondrial Dynamics and Apoptosis-the ER Connection', *Science*, 337(6098), pp. 1052-1054.

Howell, N., Kubacka, I. and Mackey, D.A. (1996) 'How rapidly does the human mitochondrial genome evolve?', *American Journal of Human Genetics*, 59(3), pp. 501-509.

Howell, N., Kubacka, I., Xu, M. and McCullough, D.A. (1991) 'Leber hereditary optic neuropathy - involvement of the mitochondrial ndi gene and evidence for an intragenic suppressor mutation', *American Journal of Human Genetics*, 48(5), pp. 935-942.

Hudson, G., Amati-Bonneau, P., Blakely, E.L., Stewart, J.D., He, L., Schaefer, A.M., Griffiths, P.G., Ahlqvist, K., Suomalainen, A., Reynier, P., McFarland, R., Turnbull, D.M., Chinnery, P.F. and Taylor, R.W. (2008) 'Mutation of OPA1 causes dominant optic atrophy with external ophthalmoplegia, ataxia, deafness and multiple mitochondrial DNA deletions: a novel disorder of mtDNA maintenance', *Brain*, 131, pp. 329-337.

Huizing, M., Dorward, H., Ly, L., Klootwijk, E., Kleta, R., Skovby, F., Pei, W., Feldman, B., Gahl, W.A. and Anikster, Y. (2010) 'OPA3, mutated in 3-methylglutaconic aciduria type III, encodes two transcripts targeted primarily to mitochondria', *Molecular Genetics and Metabolism*, 100(2), pp. 149-154.

Hunt, D., Leventer, R.J., Simons, C., Taft, R., Swoboda, K.J., Gawne-Cain, M., Magee, A.C., Turnpenny, P.D., Baralle, D. and Study, D.D.D. (2014) 'Whole exome sequencing in family trios reveals de novo mutations in PURA as a cause of severe neurodevelopmental delay and learning disability', *Journal of Medical Genetics*, 51(12), pp. 806-813.

Huoponen, K., Vilkki, J., Aula, P., Nikoskelainen, E.K. and Savontaus, M.L. (1991) 'A new mtdna mutation associated with leber hereditary optic neuroretinopathy', *American Journal of Human Genetics*, 48(6), pp. 1147-1153.

Iborra, F.J., Kimura, H. and Cook, P.R. (2004) 'The functional organization of mitochondrial genomes in human cells', *Bmc Biology*, 2.

Inoue, H., Tanizawa, Y., Wasson, J., Behn, P., Kalidas, K., Bernal-Mizrachi, E., Mueckler, M., Marshall, H., Donis-Keller, H., Crock, P., Rogers, D., Mikuni, M., Kumashiro, H., Higashi, K., Sobue, G., Oka, Y. and Permutt, M.A. (1998) 'A gene encoding a transmembrane protein is mutated in patients with diabetes mellitus and optic atrophy (Wolfram syndrome)', *Nature*

Genetics, 20(2), pp. 143-148.

Ishihara, N., Fujita, Y., Oka, T. and Mihara, K. (2006) 'Regulation of mitochondrial morphology through proteolytic cleavage of OPA1', *Embo Journal*, 25(13), pp. 2966-2977.
Jamuar, S.S. and Tan, E.-C. (2015) 'Clinical application of next-generation sequencing for Mendelian diseases', *Human Genomics*, 9.

Jahani-Asl, A., Pilon-Larose, K., Xu, W., MacLaurin, J.G., Park, D.S., McBride, H.M. and Slack, R.S. (2011) 'The Mitochondrial Inner Membrane GTPase, Optic Atrophy 1 (Opa1), Restores Mitochondrial Morphology and Promotes Neuronal Survival following Excitotoxicity', *Journal of Biological Chemistry*, 286(6), pp. 4772-4782.

Jazin, E., Soodyall, H., Jalonen, P., Lindholm, E., Stoneking, M. and Gyllensten, U. (1998) 'Mitochondrial mutation rate revisited: hot spots and polymorphism', *Nature Genetics*, 18(2), pp. 109-110.

Jin, S.M., Lazarou, M., Wang, C.X., Kane, L.A., Narendra, D.P. and Youle, R.J. (2010) 'Mitochondrial membrane potential regulates PINK1 import and proteolytic destabilization by PARL', *Journal of Cell Biology*, 191(5), pp. 933-942.

Jinek, M., Chylinski, K., Fonfara, I., Hauer, M., Doudna, J.A. and Charpentier, E. (2012) 'A Programmable Dual-RNA-Guided DNA Endonuclease in Adaptive Bacterial Immunity', *Science*, 337(6096), pp. 816-821.

Johns, D.R., Smith, K.H. and Miller, N.R. (1992) 'Lebers hereditary optic neuropathy - clinical manifestations of the 3460 mutation', *Archives of Ophthalmology*, 110(11), pp. 1577-1581.

Johns, D.R., Heher, K.L., Miller, N.R. and Smith, K.H. (1993) 'Lebers hereditary optic neuropathy - clinical manifestations of the 14484 mutation', *Archives of Ophthalmology*, 111(4), pp. 495-498.

Kadenbach, B., Jarausch, J., Hartmann, R. and Merle, P. (1983) 'Separation of mammalian cytochrome-c-oxidase into 13 polypeptides by a sodium dodecyl-sulfate gel-electrophoretic procedure', *Analytical Biochemistry*, 129(2), pp. 517-521.

Kamei, S., Chen-Kuo-Chang, M., Cazevieille, C., Lenaers, G., Olichon, A., Belenguer, P., Roussignol, G., Renard, N., Eybalin, M., Michelin, A., Delettre, C., Brabet, P. and Hamel, C.P. (2005) 'Expression of the Opa1 mitochondrial protein in retinal ganglion cells: Its downregulation causes aggregation of the mitochondrial network', *Investigative Ophthalmology & Visual Science*, 46(11), pp. 4288-4294.

Kao, S.-H., Yen, M.-Y., Wang, A.-G., Yeh, Y.-L. and Lin, A.-L. (2015) 'Changes in Mitochondrial Morphology and Bioenergetics in Human Lymphoblastoid Cells With Four Novel OPA1 Mutations', *Investigative Ophthalmology & Visual Science*, 56(4), pp. 2269-2278.

Karbowski, M., Lee, Y.J., Gaume, B., Jeong, S.Y., Frank, S., Nechushtan, A., Santel, A., Fuller, M., Smith, C.L. and Youle, R.J. (2002) 'Spatial and temporal association of Bax with mitochondrial fission sites, Drp1, and Mfn2 during apoptosis', *Journal of Cell Biology*, 159(6), pp. 931-938.

Karbowski, M., Norris, K.L., Cleland, M.M., Jeong, S.Y. and Youle, R.J. (2006) 'Role of Bax and Bak in mitochondrial morphogenesis', *Nature*, 443(7112), pp. 658-662.

Kasiviswanathan, R., Collins, T.R.L. and Copeland, W.C. (2012) 'The interface of transcription and DNA replication in the mitochondria', *Biochimica Et Biophysica Acta-Gene Regulatory Mechanisms*, 1819(9-10), pp. 970-978.

Kayalar, C., Rosing, J. and Boyer, P.D. (1977) 'Alternating site sequence for oxidative-phosphorylation suggested by measurement of substrate binding patterns and exchange-reaction inhibitions', *Journal of Biological Chemistry*, 252(8), pp. 2486-2491.

Kerrison, J.B., Arnould, V.J., Sallum, J.M.F., Vagefi, M.R., Barmada, M.M., Li, Y.Y., Zhu, D.P. and Maumenee, I.H. (1999) 'Genetic heterogeneity of dominant optic atrophy, Kjer type - Identification of a second locus on chromosome 18q12.2-12.3', *Archives of Ophthalmology*, 117(6), pp. 805-810.

Khanim, F., Kirk, J., Latif, F. and Barrett, T.G. (2001) 'WFS1/Wolframin mutations, Wolfram syndrome, and associated diseases', *Human Mutation*, 17(5), pp. 357-367.

Kijima, K., Numakura, C., Izumino, H., Umetsu, K., Nezu, A., Shiiki, T., Ogawa, M., Ishizaki, Y., Kitamura, T., Shozawa, Y. and Hayasaka, K. (2005) 'Mitochondrial GTPase mitofusin 2 mutation in Charcot-Marie-Tooth neuropathy type 2A', *Human Genetics*, 116(1-2), pp. 23-27.

Kim, J.Y., Hwang, J.M., Ko, H.S., Seong, M.W., Park, B.J. and Park, S.S. (2005) 'Mitochondrial DNA content is decreased in autosomal dominant optic atrophy', *Neurology*, 64(6), pp. 966-972.

Kirkman, M.A., Yu-Wai-Man, P., Korsten, A., Leonhardt, M., Dimitriadis, K., De Coo, I.F., Klopstock, T. and Chinnery, P.F. (2009) 'Geneenvironment interactions in Leber hereditary optic neuropathy', *Brain*, 132, pp. 2317-2326.

Kjer, B., Eiberg, H., Kjer, P. and Rosenberg, T. (1996) 'Dominant optic atrophy mapped to chromosome 3q region .2. Clinical and epidemiological aspects', *Acta Ophthalmologica Scandinavica*, 74(1), pp. 3-7.

Kjer, P. (1959) 'Infantile optic atrophy with dominant mode of inheritance: a clinical and genetic study of 19 Danish families', *Acta ophthalmologica. Supplementum*, 164(Supp 54), pp. 1-147.

Klebe, S., Depienne, C., Gerber, S., Challe, G., Anheim, M., Charles, P., Fedirko, E., Lejeune,

E., Cottineau, J., Brusco, A., Dollfus, H., Chinnery, P.F., Mancini, C., Ferrer, X., Sole, G., Destee, A., Mayer, J.M., Fontaine, B., de Seze, J., Clanet, M., Ollagnon, E., Busson, P., Cazeneuve, C., Stevanin, G., Kaplan, J., Rozet, J.M., Brice, A. and Durr, A. (2012) 'Spastic paraplegia gene 7 in patients with spasticity and/or optic neuropathy', *Brain*, 135, pp. 2980-2993.

Ko, Y.H., Hullihen, J., Hong, S. and Pedersen, P.L. (2000) 'Mitochondrial F(0)F1 ATP synthase - Subunit regions on the F-1 motor shielded by F-0, functional significance, and evidence for an involvement of the unique F-0 subunit F-6', *Journal of Biological Chemistry*, 275(42), pp. 32931-32939.

Kobayashi, Y., Momoi, M.Y., Tominaga, K., Momoi, T., Nihei, K., Yanagisawa, M., Kagawa, Y. and Ohta, S. (1990) 'A POINT MUTATION IN THE MITOCHONDRIAL TRANSFER RNALEU(UUR) GENE IN MELAS (MITOCHONDRIAL MYOPATHY, ENCEPHALOPATHY, LACTIC-ACIDOSIS AND STROKE-LIKE EPISODES)', *Biochemical and Biophysical Research Communications*, 173(3), pp. 816-822.

Koopman, W.J.H., Verkaart, S., Visch, H.J., van Emst-de Vries, S., Nijtmans, L.G.J., Smeitink, J.A.M. and Willems, P.H.G.M. (2007) 'Human NADH: ubiquinone oxidoreductase deficiency: radical changes in mitochondrial morphology?', *American Journal of Physiology-Cell Physiology*, 293(1), pp. C22-C29.

Kornmann, B., Osman, C. and Walter, P. (2011) 'The conserved GTPase Gem1 regulates endoplasmic reticulum-mitochondria connections', *Proceedings of the National Academy of Sciences of the United States of America*, 108(34), pp. 14151-14156.

Kriegenburg, F., Ellgaard, L. and Hartmann-Petersen, R. (2012) 'Molecular chaperones in targeting misfolded proteins for ubiquitin-dependent degradation', *Febs Journal*, 279(4), pp. 532-542.

Kubli, D.A. and Gustafsson, A.B. (2012) 'Mitochondria and Mitophagy The Yin and Yang of Cell Death Control', *Circulation Research*, 111(9), pp. 1208-1221.

Kucej, M., Kucejova, B., Subramanian, R., Chen, X.J. and Butow, R.A. (2008) 'Mitochondrial nucleoids undergo remodeling in response to metabolic cues', *Journal of Cell Science*, 121(11), pp. 1861-1868.

Kukat, C., Wurm, C.A., Spahr, H., Falkenberg, M., Larsson, N.-G. and Jakobs, S. (2011) 'Super-resolution microscopy reveals that mammalian mitochondrial nucleoids have a uniform size and frequently contain a single copy of mtDNA', *Proceedings of the National Academy of Sciences of the United States of America*, 108(33), pp. 13534-13539.

Kumar, P., Henikoff, S. and Ng, P.C. (2009) 'Predicting the effects of coding non-synonymous variants on protein function using the SIFT algorithm', *Nature Protocols*, 4(7), pp. 1073-1082.

Kushnareva, Y.E., Gerencser, A.A., Bossy, B., Ju, W.K., White, A.D., Waggoner, J., Ellisman, M.H., Perkins, G. and Bossy-Wetzel, E. (2013) 'Loss of OPA1 disturbs cellular calcium homeostasis and sensitizes for excitotoxicity', *Cell Death and Differentiation*, 20(2), pp. 353-365.

Kushnareva, Y., Seong, Y., Andreyev, A.Y., Kuwana, T., Kiosses, W.B., Votruba, M. and Newmeyer, D.D. (2016) 'Mitochondrial dysfunction in an Opa1(Q285STOP) mouse model of dominant optic atrophy results from Opa1 haploinsufficiency', *Cell Death & Disease*, 7.

Kuwana, T., Mackey, M.R., Perkins, G., Ellisman, M.H., Latterich, M., Schneiter, R., Green, D.R. and Newmeyer, D.D. (2002) 'Bid, Bax, and lipids cooperate to form supramolecular openings in the outer mitochondrial membrane', *Cell*, 111(3), pp. 331-342.

Kytovuori, L., Seppanen, A., Martikainen, M.H., Moilanen, J.S., Kamppari, S., Sarkioja, T., Remes, A.M., Rasanen, P., Ronnemaa, T. and Majamaa, K. (2013) 'WFS1 variants in Finnish patients with diabetes mellitus, sensorineural hearing impairment or optic atrophy, and in suicide victims', *Journal of Human Genetics*, 58(8), pp. 495-500.

La Morgia, C., Carbonelli, M., Barboni, P., Sadun, A.A. and Carelli, V. (2014) 'Medical management of hereditary optic neuropathies', *Frontiers in Neurology*, 5.

Lancaster, C.R.D. and Kroger, A. (2000) 'Succinate: quinone oxidoreductases: new insights from X-ray crystal structures', *Biochimica Et Biophysica Acta-Bioenergetics*, 1459(2-3), pp. 422-431.

Landes, T., Leroy, I., Bertholet, A., Diot, A., Khosrobakhsh, F., Daloyau, M., Davezac, N., Miquel, M.C., Courilleau, D., Guillou, E., Olichon, A., Lenaers, G., Arnaune-Pelloquin, L., Emorine, L.J. and Belenguer, P. (2010) 'OPA1 (dys)functions', *Seminars in Cell & Developmental Biology*, 21(6), pp. 593-598.

Landrum, M.J., Lee, J.M., Riley, G.R., Jang, W., Rubinstein, W.S., Church, D.M. and Maglott, D.R. (2014) 'ClinVar: public archive of relationships among sequence variation and human phenotype', *Nucleic Acids Research*, 42(D1), pp. D980-D985.

Lang, B.F., Burger, G., Okelly, C.J., Cedergren, R., Golding, G.B., Lemieux, C., Sankoff, D., Turmel, M. and Gray, M.W. (1997) 'An ancestral mitochondrial DNA resembling a eubacterial genome in miniature', *Nature*, 387(6632), pp. 493-497.

Larsson, N.G., Wang, J.M., Wilhelmsson, H., Oldfors, A., Rustin, P., Lewandoski, M., Barsh, G.S. and Clayton, D.A. (1998) 'Mitochondrial transcription factor A is necessary for mtDNA maintenance and embryogenesis in mice', *Nature Genetics*, 18(3), pp. 231-236.

Lee, H., Deignan, J.L., Dorrani, N., Strom, S.P., Kantarci, S., Quintero-Rivera, F., Das, K., Toy, T., Harry, B., Yourshaw, M., Fox, M., Fogel, B.L., Martinez-Agosto, J.A., Wong, D.A., Chang, V.Y., Shieh, P.B., Palmer, C.G.S., Dipple, K.M., Grody, W.W., Vilain, E. and Nelson, S.F.

(2014) 'Clinical Exome Sequencing for Genetic Identification of Rare Mendelian Disorders', *Jama-Journal of the American Medical Association*, 312(18), pp. 1880-1887.

Legros, F., Malka, F., Frachon, P., Lombes, A. and Rojo, M. (2004) 'Organization and dynamics of human mitochondrial DNA', *Journal of Cell Science*, 117(13), pp. 2653-2662.

Lenaers, G., Hamel, C., Delettre, C., Amati-Bonneau, P., Procaccio, V., Bonneau, D., Reynier, P. and Milea, D.C. (2012) 'Dominant optic atrophy', *Orphanet Journal of Rare Diseases*, 7.

Lewis, S.C., Uchiyama, L.F. and Nunnari, J. (2016) 'ER-mitochondria contacts couple mtDNA synthesis with mitochondrial division in human cells', *Science*, 353(6296), pp. 261-+.

Li, H. and Durbin, R. (2010) 'Fast and accurate long-read alignment with Burrows-Wheeler transform', *Bioinformatics*, 26(5), pp. 589-595.

Li, M.-X., Gui, H.-S., Kwan, J.S.H., Bao, S.-Y. and Sham, P.C. (2012) 'A comprehensive framework for prioritizing variants in exome sequencing studies of Mendelian diseases', *Nucleic Acids Research*, 40(7).

Liew, W.K.M., Ben-Omran, T., Darras, B.T., Prabhu, S.P., De Vivo, D.C., Vatta, M., Yang, Y., Eng, C.M. and Chung, W.K. (2013) 'Clinical Application of Whole-Exome Sequencing A Novel Autosomal Recessive Spastic Ataxia of Charlevoix-Saguenay Sequence Variation in a Child With Ataxia', *Jama Neurology*, 70(6), pp. 788-791.

Lin, C.S., Sharpley, M.S., Fan, W., Waymire, K.G., Sadun, A.A., Carelli, V., Ross-Cisneros, F.N., Baciu, P., Sung, E., McManus, M.J., Pan, B.X., Gil, D.W., MacGregor, G.R. and Wallace, D.C. (2012) 'Mouse mtDNA mutant model of Leber hereditary optic neuropathy', *Proceedings of the National Academy of Sciences of the United States of America*, 109(49), pp. 20065-20070.

Ling, M.F., Merante, F., Chen, H.S., Duff, C., Duncan, A.M.V. and Robinson, B.H. (1997) 'The human mitochondrial elongation factor tu (EF-Tu) gene: cDNA sequence, genomic localization, genomic structure, and identification of a pseudogene', *Gene*, 197(1-2), pp. 325-336.

Liskova, P., Ulmanova, O., Tesina, P., Melsova, H., Diblik, P., Hansikova, H., Tesarova, M. and Votruba, M. (2013) 'Novel OPA1 missense mutation in a family with optic atrophy and severe widespread neurological disorder', *Acta Ophthalmologica*, 91(3), pp. E225-E231.

Litonin, D., Sologub, M., Shi, Y., Savkina, M., Anikin, M., Falkenberg, M., Gustafsson, C.M. and Temiakov, D. (2010) 'Human Mitochondrial Transcription Revisited Only tfam and tfb2m are required for transcription of the mitochondrial genes in vitro', *Journal of Biological Chemistry*, 285(24), pp. 18129-18133.

Lodeiro, M.F., Uchida, A., Bestwick, M., Moustafa, I.M., Arnold, J.J., Shadel, G.S. and Cameron, C.E. (2012) 'Transcription from the second heavy-strand promoter of human mtDNA

is repressed by transcription factor A in vitro', *Proceedings of the National Academy of Sciences of the United States of America*, 109(17), pp. 6513-6518.

Lodi, R., Tonon, C., Valentino, M.L., Lotti, S., Clementi, V., Malucelli, E., Barboni, P., Longanesi, L., Schimpf, S., Wissinger, B., Baruzzi, A., Barbiroli, B. and Carelli, V. (2004) 'Deficit of in vivo mitochondrial ATP production in OPA1-related dominant optic atrophy', *Annals of Neurology*, 56(5), pp. 719-723.

Loiseau, D., Chevrollier, A., Verny, C., Guillet, V., Gueguen, N., de Crescenzo, M.-A.P., Ferre, M., Malinge, M.-C., Guichet, A., Nicolas, G., Amati-Bonneau, P., Malthiery, Y., Bonneau, D. and Reynier, P. (2007) 'Mitochondrial coupling defect in Charcot-Marie-Tooth type 2A disease', *Annals of Neurology*, 61(4), pp. 315-323.

Lombardo, F., Salzano, G., Di Bella, C., Aversa, T., Pugliatti, F., Cara, S., Valenzise, M., De Luca, F. and Rigoli, L. (2014) 'Phenotypical and genotypical expression of Wolfram syndrome in 12 patients from a Sicilian district where this syndrome might not be so infrequent as generally expected', *Journal of Endocrinological Investigation*, 37(2), pp. 195-202.

Lopez, M.F., Kristal, B.S., Chernokalskaya, E., Lazarev, A., Shestopalov, A.I., Bogdanova, A. and Robinson, M. (2000) 'High-throughput profiling of the mitochondrial proteome using affinity fractionation and automation', *Electrophoresis*, 21(16), pp. 3427-3440.

Loson, O.C., Song, Z., Chen, H. and Chan, D.C. (2013) 'Fis1, Mff, MiD49, and MiD51 mediate Drp1 recruitment in mitochondrial fission', *Molecular Biology of the Cell*, 24(5), pp. 659-667.

Lu, S.M., Kanekura, K., Hara, T., Mahadevan, J., Spears, L.D., Oslowski, C.M., Martinez, R., Yamazaki-Inoue, M., Toyoda, M., Neilson, A., Blanner, P., Brown, C.M., Semenkovich, C.F., Marshall, B.A., Hershey, T., Umezawa, A., Greer, P.A. and Urano, F. (2014) 'A calcium-dependent protease as a potential therapeutic target for Wolfram syndrome', *Proceedings of the National Academy of Sciences of the United States of America*, 111(49), pp. E5292-E5301.

Lutter, M., Fang, M., Luo, X., Nishijima, M., Xie, X.S. and Wang, X.D. (2000) 'Cardiolipin provides specificity for targeting of tBid to mitochondria', *Nature Cell Biology*, 2(10), pp. 754-756.

Ma, Q. (2013) 'Role of Nrf2 in Oxidative Stress and Toxicity', *Annual Review of Pharmacology and Toxicology, Vol 53, 2013*, 53, pp. 401-+.

Majander, A., Finel, M., Savontaus, M.L., Nikoskelainen, E. and Wikstrom, M. (1996) 'Catalytic activity of Complex I in cell lines that possess replacement mutations in the ND genes in Leber's hereditary optic neuropathy', *European Journal of Biochemistry*, 239(1), pp. 201-207.

Majewski, J., Schwartzentruber, J., Lalonde, E., Montpetit, A. and Jabado, N. (2011) 'What can exome sequencing do for you?', *Journal of Medical Genetics*, 48(9), pp. 580-589.

Man, P.Y.W., Griffiths, P.G., Brown, D.T., Howell, N., Turnbull, D.M. and Chinnery, P.F. (2003) 'The epidemiology of Leber hereditary optic neuropathy in the North East of England', *American Journal of Human Genetics*, 72(2), pp. 333-339.

Man, P.Y.W., Turnbull, D.M. and Chinnery, P.F. (2002) 'Leber hereditary optic neuropathy', *Journal of Medical Genetics*, 39(3), pp. 162-169.

Manolio, T.A., Collins, F.S., Cox, N.J., Goldstein, D.B., Hindorff, L.A., Hunter, D.J., McCarthy, M.I., Ramos, E.M., Cardon, L.R., Chakravarti, A., Cho, J.H., Guttmacher, A.E., Kong, A., Kruglyak, L., Mardis, E., Rotimi, C.N., Slatkin, M., Valle, D., Whittemore, A.S., Boehnke, M., Clark, A.G., Eichler, E.E., Gibson, G., Haines, J.L., Mackay, T.F.C., McCarroll, S.A. and Visscher, P.M. (2009) 'Finding the missing heritability of complex diseases', *Nature*, 461(7265), pp. 747-753.

Marchbank, N.J., Craig, J.E., Leek, J.P., Toohey, M., Churchill, A.J., Markham, A.F., Mackey, D.A., Toomes, C. and Inglehearn, C.F. (2002) 'Deletion of the OPA1 gene in a dominant optic atrophy family: evidence that haploinsufficiency is the cause of disease', *Journal of Medical Genetics*, 39(8).

Marchetti, V., Krohne, T.U., Friedlander, D.F. and Friedlander, M. (2010) 'Stemming vision loss with stem cells', *Journal of Clinical Investigation*, 120(9), pp. 3012-3021.

Marella, M., Seo, B.B., Thomas, B.B., Matsuno-Yagi, A. and Yagi, T. (2010) 'Successful Amelioration of Mitochondrial Optic Neuropathy Using the Yeast NDI1 Gene in a Rat Animal Model', *Plos One*, 5(7).

Marelli, C., Amati-Bonneau, P., Reynier, P., Layet, V., Layet, A., Stevanin, G., Brissaud, E., Bonneau, D., Durr, A. and Brice, A. (2011) 'Heterozygous OPA1 mutations in Behr syndrome', *Brain*, 134.

Maresca, A., la Morgia, C., Caporali, L., Valentino, M.L. and Carelli, V. (2013) 'The optic nerve: A "mito-window" on mitochondrial neurodegeneration', *Molecular and Cellular Neuroscience*, 55, pp. 62-76.

Margineantu, D.H., Cox, W.G., Sundell, L., Sherwood, S.W., Beechem, J.A. and Capaldi, R.A. (2002) 'Cell cycle dependent morphology changes and associated mitochondrial DNA redistribution in mitochondria of human cell lines', *Mitochondrion*, 1(5), pp. 425-435.

Margulis, L. (1971) 'Symbiosis and evolution', *Scientific American*, 225(2), pp. 48-57.
Marshall, B.A., Permutt, M.A., Paciorkowski, A.R., Hoekel, J., Karzon, R., Wasson, J., Viehover, A., White, N.H., Shimony, J.S., Manwaring, L., Austin, P., Hullar, T.E., Hershey, T. and Washington Univ Wolfram Study, G. (2013) 'Phenotypic characteristics of early Wolfram syndrome', *Orphanet Journal of Rare Diseases*, 8.

Martin, M., Cho, J.Y., Cesare, A.J., Griffith, J.D. and Attardi, G. (2005) 'Termination factor-mediated DNA loop between termination and initiation sites drives mitochondrial rRNA synthesis', *Cell*, 123(7), pp. 1227-1240.

Martorell, L., Zaera, M.G., Valero, J., Serrano, D., Figuera, L., Joven, J., Labad, A., Vilella, E. and Nunes, V. (2003) 'The WFS1 (Wolfram syndrome 1) is not a major susceptibility gene for the development of psychiatric disorders', *Psychiatric Genetics*, 13(1), pp. 29-32.

Mascialino, B., Leinonen, M. and Meier, T. (2012) 'Meta-analysis of the prevalence of Leber hereditary optic neuropathy mtDNA mutations in Europe', *European Journal of Ophthalmology*, 22(3), pp. 461-465.

Matsunaga, K., Tanabe, K., Inoue, H., Okuya, S., Ohta, Y., Akiyama, M., Taguchi, A., Kora, Y., Okayama, N., Yamada, Y., Wada, Y., Amemiya, S., Sugihara, S., Nakao, Y., Oka, Y. and Tanizawa, Y. (2014) 'Wolfram Syndrome in the Japanese Population; Molecular Analysis of WFS1 Gene and Characterization of Clinical Features', *Plos One*, 9(9).

Matsushima, Y. and Kaguni, L.S. (2007) 'Differential phenotypes of active site and human autosomal dominant progressive external ophthalmoplegia mutations in Drosophila mitochondrial DNA helicase expressed in Schneider cells', *Journal of Biological Chemistry*, 282(13), pp. 9436-9444.

McBride, H.M., Neuspiel, M. and Wasiak, S. (2006) 'Mitochondria: More than just a powerhouse', *Current Biology*, 16(14), pp. R551-R560.

Meeusen, S., DeVay, R., Block, J., Cassidy-Stone, A., Wayson, S., McCaffery, J.M. and Nunnari, J. (2006) 'Mitochondrial inner-membrane fusion and crista maintenance requires the dynamin-related GTPase Mgm1', *Cell*, 127(2), pp. 383-395.

Middle, F., Jones, I., McCandless, F., Barrett, T., Khanim, F., Owen, M.J., Lendon, C. and Craddock, N. (2000) 'Bipolar disorder and variation at a common polymorphism (A1832G) within exon 8 of the Wolfram gene', *American Journal of Medical Genetics*, 96(2), pp. 154-157.

Milenkovic, D., Matic, S., Kuhl, I., Ruzzenente, B., Freyer, C., Jemt, E., Park, C.B., Falkenberg, M. and Larsson, N.G. (2013) 'TWINKLE is an essential mitochondrial helicase required for synthesis of nascent D-loop strands and complete mtDNA replication', *Human Molecular Genetics*, 22(10), pp. 1983-1993.

Millet, A.M.C., Bertholet, A.M., Daloyau, M., Reynier, P., Galinier, A., Devin, A., Wissinguer, B., Belenguer, P., Davezac, N. (2016) 'Loss of functional OPA1 unbalances redox state: implications in dominant optic atrophy pathogenesis', *Annals of Clinical and Translational Neurology*, 3(6), pp. 408-421.

Minczuk, M., Papworth, M.A., Miller, J.C., Murphy, M.P. and Klug, A. (2008) 'Development of a single-chain, quasi-dimeric zinc-finger nuclease for the selective degradation of mutated human mitochondrial DNA', *Nucleic Acids Research*, 36(12), pp. 3926-3938.

Mishra, P., Carelli, V., Manfredi, G. and Chan, D.C. (2014) 'Proteolytic Cleavage of Opa1 Stimulates Mitochondrial Inner Membrane Fusion and Couples Fusion to Oxidative Phosphorylation', *Cell Metabolism*, 19(4), pp. 630-641.

Mitchell, P. (1976) 'Vectorial chemistry and molecular mechanics of chemiosmotic coupling - power transmission by proticity', *Biochemical Society Transactions*, 4(3), pp. 399-430.
Montoya, J., Christianson, T., Levens, D., Rabinowitz, M. and Attardi, G. (1982) 'Identification of initiation sites for heavy-strand and light-strand transcription in human mitochondrial-dna', *Proceedings of the National Academy of Sciences of the United States of America-Biological Sciences*, 79(23), pp. 7195-7199.

Moraes, C.T. (2001) 'What regulates mitochondrial DNA copy number in animal cells?', *Trends in Genetics*, 17(4), pp. 199-205.

Morozov, Y.I., Agaronyan, K., Cheung, A.C.M., Anikin, M., Cramer, P. and Temiakov, D. (2014) 'A novel intermediate in transcription initiation by human mitochondrial RNA polymerase', *Nucleic Acids Research*, 42(6), pp. 3884-3893.

Murley, A., Lackner, L.L., Osman, C., West, M., Voeltz, G.K., Walter, P. and Nunnari, J. (2013) 'ER-associated mitochondrial division links the distribution of mitochondria and mitochondrial DNA in yeast', *Elife*, 2.

Murley, A. and Nunnari, J. (2016) 'The Emerging Network of Mitochondria-Organelle Contacts', *Molecular Cell*, 61(5), pp. 648-653.

Myasnikov, A.G., Simonetti, A., Marzi, S. and Klaholz, B.P. (2009) 'Structure-function insights into prokaryotic and eukaryotic translation initiation', *Current Opinion in Structural Biology*, 19(3), pp. 300-309.

Nakada, K., Sato, A. and Hayashi, J.-I. (2009) 'Mitochondrial functional complementation in mitochondrial DNA-based diseases', *International Journal of Biochemistry & Cell Biology*, 41(10), pp. 1907-1913.

Nass, M.M. (1969) 'Mitochondrial DNA. I. Intramitochondrial distribution and structural relations of single- and double-length circular DNA', *Journal of molecular biology*, 42(3), pp. 521-8.

Naviaux, R.K. and Nguyen, K.V. (2004) 'POLG mutations associated with Alpers' syndrome and mitochondrial DNA depletion', *Annals of Neurology*, 55(5), pp. 706-712.

Naviaux, R.K., Nyhan, W.L., Barshop, B.A., Poulton, J., Markusic, D., Karpinski, N.C. and Haas, R.H. (1999) 'Mitochondrial DNA polymerase gamma deficiency and mtDNA depletion in a child with Alpers' syndrome', *Annals of Neurology*, 45(1), pp. 54-58.

Newman, N.J. (2012) 'Treatment of hereditary optic neuropathies', *Nature Reviews Neurology*, 8(10), pp. 545-556.

Newman, N.J. and Biousse, V. (2004) 'Hereditary optic neuropathies', *Eye*, 18(11), pp. 1144-1160.

Nijtmans, LGJ., Ugalde, C., van den Heuvel, LP., Smeitink, JA. (2004) 'Function and Dysfunction of the Oxidative Phosphorylation System', In: Bauer M and Koehler C, editors. *Topics in Current Genetics: Biogenesis of mitochondria and associated diseases. Heidelberg: Springer*, 149-176.

Ng, P.C. and Henikoff, S. (2001) 'Predicting deleterious amino acid substitutions', *Genome Research*, 11(5), pp. 863-874.

Ng, P.C. and Henikoff, S. (2003) 'SIFT: predicting amino acid changes that affect protein function', *Nucleic Acids Research*, 31(13), pp. 3812-3814.

Ng, P.C. and Henikoff, S. (2006) 'Predicting the effects of amino acid substitutions on protein function', *Annual Review of Genomics and Human Genetics*, 7, pp. 61-80.

Nguyen, D., Alavi, M., Kim, K.Y., Kang, T., Scott, R.T., Noh, Y.H., Lindsey, J.D., Wissinger, B., Ellisman, M.H., Weinreb, R.N., Perkins, G.A. and Ju, W.K. (2011) 'A new vicious cycle involving glutamate excitotoxicity, oxidative stress and mitochondrial dynamics', *Cell Death & Disease*, 2.

Nikoskelainen, E.K. (1994) 'Clinical picture of lhon', *Clinical Neuroscience*, 2(2), pp. 115-120.
Oca-Cossio, J., Kenyon, L., Hao, H.K. and Moraes, C.T. (2003) 'Limitations of allotopic expression of mitochondrial genes in mammalian cells', *Genetics*, 165(2), pp. 707-720.

Ohtsubo, T., Nishioka, K., Imaiso, Y., Iwai, S., Shimokawa, H., Oda, H., Fujiwara, T. and Nakabeppu, Y. (2000) 'Identification of human MutY homolog (hMYH) as a repair enzyme for 2-hydroxyadenine in DNA and detection of multiple forms of hMYH located in nuclei and mitochondria', *Nucleic Acids Research*, 28(6), pp. 1355-1364.

Ojala, D., Merkel, C., Gelfand, R. and Attardi, G. (1980) 'The transfer-rna genes punctuate the reading of genetic information in human mitochondrial-dna', *Cell*, 22(2), pp. 393-403.

Olichon, A., Baricault, L., Gas, N., Guillou, E., Valette, A., Belenguer, P. and Lenaers, G. (2003) 'Loss of OPA1 perturbates the mitochondrial inner membrane structure and integrity, leading to cytochrome c release and apoptosis', *Journal of Biological Chemistry*, 278(10), pp. 7743-7746.

Olichon, A., ElAchouri, G., Baricault, L., Delettre, C., Belenguer, P. and Lenaers, G. (2007) 'OPA1 alternate splicing uncouples an evolutionary conserved function in mitochondrial fusion from a vertebrate restricted function in apoptosis', *Cell Death and Differentiation*, 14(4), pp. 682-692.

Olichon, A., Emorine, L.J., Descoins, E., Pelloquin, L., Brichese, L., Gas, N., Guillou, E., Delettre, C., Valette, A., Hamel, C.P., Ducommun, B., Lenaers, G. and Belenguer, P. (2002) 'The human dynamin-related protein OPA1 is anchored to the mitochondrial inner membrane facing the inter-membrane space', *Febs Letters*, 523(1-3), pp. 171-176.

Osman, A.A., Saito, M., Makepeace, C., Permutt, M.A., Schlesinger, P. and Mueckler, M. (2003) 'Wolframin expression induces novel ion channel activity in endoplasmic reticulum membranes and increases intracellular calcium', *Journal of Biological Chemistry*, 278(52), pp. 52755-52762.

Paley, R.G. and Tunbridge, R.E. (1956) 'Primary optic atrophy in diabetes mellitus', *Diabetes*, 5(4), pp. 295-6.

Pan, B.X., Ross-Cisneros, F.N., Carelli, V., Rue, K.S., Salomao, S.R., Moraes-Filho, M.N., Moraes, M.N., Berezovsky, A., Belfort, R., Jr. and Sadun, A.A. (2012) 'Mathematically Modeling the Involvement of Axons in Leber's Hereditary Optic Neuropathy', *Investigative Ophthalmology & Visual Science*, 53(12), pp. 7608-7617.

Parker, W.D., Oley, C.A. and Parks, J.K. (1989) 'A defect in mitochondrial electron-transport activity (nadh-coenzyme-q oxidoreductase) in lebers hereditary optic neuropathy', *New England Journal of Medicine*, 320(20), pp. 1331-1333.

Pei, W.H., Kratz, L.E., Bernardini, I., Sood, R., Yokogawa, T., Dorward, H., Ciccone, C., Kelley, R.I., Anikster, Y., Burgess, H.A., Huizing, M. and Feldman, B. (2010) 'A model of Costeff Syndrome reveals metabolic and protective functions of mitochondrial OPA3', *Development*, 137(15), pp. 2587-2596.

Perkins, G., Bossy-Wetzel, E. and Ellisman, M.H. (2009) 'New insights into mitochondrial structure during cell death', *Experimental Neurology*, 218(2), pp. 183-192.

Perkins, G., Renken, C., Martone, M.E., Young, S.J. and Ellisman, M. (1997) 'Electron tomography of neuronal mitochondria: Three-dimensional structure and organization of cristae and membrane contacts', *Journal of Structural Biology*, 119(3), pp. 260-272.

Pesch, U.E.A., Leo-Kottler, B., Mayor, S., Jurklies, B., Kellner, U., Apfelstedt-Sylla, E., Zrenner, E., Alexander, C. and Wissinger, B. (2001) 'OPA1 mutations in patients with autosomal dominant optic atrophy and evidence for semi-dominant inheritance', *Human Molecular Genetics*, 10(13), pp. 1359-1368.

Pfeffer, G., Burke, A., Yu-Wai-Man, P., Compston, D.A.S. and Chinnery, P.F. (2013a) 'Clinical features of MS associated with Leber hereditary optic neuropathy mtDNA mutations', *Neurology*, 81(24), pp. 2073-2081.

Pfeffer, G., Horvath, R., Klopstock, T., Mootha, V.K., Suomalainen, A., Koene, S., Hirano, M., Zeviani, M., Bindoff, L.A., Yu-Wai-Man, P., Hanna, M., Carelli, V., McFarland, R., Majamaa, K., Turnbull, D.M., Smeitink, J. and Chinnery, P.F. (2013b) 'New treatments for mitochondrial disease-no time to drop our standards', *Nature Reviews Neurology*, 9(8), pp. 474-481.

Pfeffer, G., Majamaa, K., Turnbull, D.M., Thorburn, D. and Chinnery, P.F. (2012) 'Treatment for mitochondrial disorders', *Cochrane Database of Systematic Reviews*, (4).

Pineau, B., Mathieu, C., Gerard-Hirne, C., De Paepe, R. and Chetrit, P. (2005) 'Targeting the NAD7 subunit to mitochondria restores a functional complex I and a wild type phenotype in the Nicotiana sylvestris CMS II mutant lacking nad7', *Journal of Biological Chemistry*, 280(28), pp. 25994-26001.

Pisano, A., Preziuso, C., Iommarini, L., Perli, E., Grazioli, P., Campese, A.F., Maresca, A., Montopoli, M., Masuelli, L., Sadun, A.A., d'Amati, G., Carelli, V., Ghelli, A. and Giordano, C. (2015) 'Targeting estrogen receptor beta as preventive therapeutic strategy for Leber's hereditary optic neuropathy', *Human Molecular Genetics*, 24(24), pp. 6921-6931.

Pomeranz, H.D. and Lessell, S. (1999) 'A hereditary chiasmal optic neuropathy', *Archives of Ophthalmology*, 117(1), pp. 128-131.

Porcelli, A.M., Angelin, A., Ghelli, A., Mariani, E., Martinuzzi, A., Carelli, V., Petronilli, V., Bernardi, P. and Rugolo, M. (2009) 'Respiratory Complex I Dysfunction Due to Mitochondrial DNA Mutations Shifts the Voltage Threshold for Opening of the Permeability Transition Pore toward Resting Levels', *Journal of Biological Chemistry*, 284(4), pp. 2045-2052.

Puomila, A., Huoponen, K., Mantyjarvi, M., Hamalainen, P., Paananen, R., Sankila, E.M., Savontaus, M.L., Somer, M. and Nikoskelainen, E. (2005) 'Dominant optic atrophy: correlation between clinical and molecular genetic studies', *Acta Ophthalmologica Scandinavica*, 83(3), pp. 337-346.

Qi, X., Lewin, A.S., Sun, L., Hauswirth, W.W. and Guy, J. (2007a) 'Suppression of mitochondrial oxidative stress provides long-term neuroprotection in experimental optic neuritis', *Investigative Ophthalmology & Visual Science*, 48(2), pp. 681-691.

Qi, X., Sun, L., Hauswirth, W.W., Lewin, A.S. and Guy, J. (2007b) 'Use of mitochondrial antioxidant defenses for rescue of cells with a Leber hereditary optic neuropathy-causing mutation', *Archives of Ophthalmology*, 125(2), pp. 268-272.

Rabbani, B., Tekin, M. and Mahdieh, N. (2014) 'The promise of whole-exome sequencing in

medical genetics', *Journal of Human Genetics*, 59(1), pp. 5-15.

Raha, S. and Robinson, B.H. (2000) 'Mitochondria, oxygen free radicals, disease and ageing', *Trends in Biochemical Sciences*, 25(10), pp. 502-508.

Rahn, J.J., Stackley, K.D. and Chan, S.S.L. (2013) 'Opa1 Is Required for Proper Mitochondrial Metabolism in Early Development', *Plos One*, 8(3).

Ramonet, D., Perier, C., Recasens, A., Dehay, B., Bove, J., Costa, V., Scorrano, L. and Vila, M. (2013) 'Optic atrophy 1 mediates mitochondria remodeling and dopaminergic neurodegeneration linked to complex I deficiency', *Cell Death and Differentiation*, 20(1), pp. 77-85.

Rendtorff, N.D., Lodahl, M., Boulahbel, H., Johansen, I.R., Pandya, A., Welch, K.O., Norris, V.W., Arnos, K.S., Bitner-Glindzicz, M., Emery, S.B., Mets, M.B., Fagerheim, T., Eriksson, K., Hansen, L., Bruhn, H., Moller, C., Lindholm, S., Ensgaard, S., Lesperance, M.M. and Tranebjaerg, L. (2011) 'Identification of p.A684V Missense Mutation in the WFS1 Gene as a Frequent Cause of Autosomal Dominant Optic Atrophy and Hearing Impairment', *American Journal of Medical Genetics Part A*, 155A(6), pp. 1298-1313.

Reynier, P., Amati-Bonneau, P., Verny, C., Olichon, A., Simard, G., Guichet, A., Bonnemains, C., Malecaze, F., Malinge, M.C., Pelletier, J.B., Calvas, P., Dollfus, H., Belenguer, P., Malthiery, Y., Lenaers, G. and Bonneau, D. (2004) 'OPA3 gene mutations responsible for autosomal dominant optic atrophy and cataract', *Journal of Medical Genetics*, 41(9).

Rigoli, L., Lombardo, F. and Di Bella, C. (2011) 'Wolfram syndrome and WFS1 gene', *Clinical Genetics*, 79(2), pp. 103-117.

Rizzo, J.M. and Buck, M.J. (2012) 'Key Principles and Clinical Applications of "Next-Generation" DNA Sequencing', *Cancer Prevention Research*, 5(7), pp. 887-900.

Roberti, M., Musicco, C., Polosa, P.L., Milella, F., Gadaleta, M.N. and Cantatore, P. (1998) 'Multiple protein-binding sites in the TAS-region of human and rat mitochondrial DNA', *Biochemical and Biophysical Research Communications*, 243(1), pp. 36-40.

Robinson, P.N., Krawitz, P. and Mundlos, S. (2011) 'Strategies for exome and genome sequence data analysis in disease-gene discovery projects', *Clinical Genetics*, 80(2), pp. 127-132.

Rodriguez-Enriquez, S., Kim, I., Currin, R.T. and Lemasters, J.J. (2006) 'Tracker dyes to probe mitochondrial autophagy (mitophagy) in rat hepatocytes', *Autophagy*, 2(1), pp. 39-46.

Rohayem, J., Ehlers, C., Wiedemann, B., Holl, R., Oexle, K., Kordonouri, O., Salzano, G., Meissner, T., Burger, W., Schober, E., Huebner, A., Lee-Kirsch, M.A. and Wolfram Syndrome Diabet Writing, G. (2011) 'Diabetes and Neurodegeneration in Wolfram Syndrome A multicenter study of phenotype and genotype', *Diabetes Care*, 34(7), pp. 1503-1510.

Romagnoli, A., Aguiari, P., De Stefani, D., Leo, S., Marchi, S., Rimessi, A., Zecchini, E., Pinton, P. and Rizzuto, R. (2007) 'Endoplasmic reticulum/mitochondria calcium cross-talk', *Novartis Foundation symposium*, 287, pp. 122-31; discussion 131-9.

Ross-Cisneros, F.N., Pan, B.X., Silva, R.A., Miller, N.R., Albini, T.A., Tranebjaerg, L., Rendtorff, N.D., Lodahl, M., Moraes-Filho, M.N., Moraes, M.N., Salomao, S.R., Berezovsky, A., Belfort, R., Jr., Carelli, V. and Sadun, A.A. (2013) 'Optic nerve histopathology in a case of Wolfram Syndrome: A mitochondrial pattern of axonal loss', *Mitochondrion*, 13(6), pp. 841-845.

Rossignol, R., Gilkerson, R., Aggeler, R., Yamagata, K., Remington, S.J. and Capaldi, R.A. (2004) 'Energy substrate modulates mitochondrial structure and oxidative capacity in cancer cells', *Cancer Research*, 64(3), pp. 985-993.

Roucou, X., Artika, I.M., Devenish, R.J. and Nagley, P. (1999) 'Bioenergetic and structural consequences of allotopic expression of subunit 8 of yeast mitochondrial ATP synthase - The hydrophobic character of residues 23 and 24 is essential for maximal activity and structural stability of the enzyme complex', *European Journal of Biochemistry*, 261(2), pp. 444-451.

Rouzier, C., Bannwarth, S., Chaussenot, A., Chevrollier, A., Verschueren, A., Bonello-Palot, N., Fragaki, K., Cano, A., Pouget, J., Pellissier, J.F., Procaccio, V., Chabrol, B. and Paquis-Flucklinger, V. (2012) 'The MFN2 gene is responsible for mitochondrial DNA instability and optic atrophy 'plus' phenotype', *Brain*, 135, pp. 23-34.

Rugarli, E.I. and Langer, T. (2012) 'Mitochondrial quality control: a matter of life and death for neurons', *Embo Journal*, 31(6), pp. 1336-1349.

Rytomaa, M. and Kinnunen, P.K.J. (1995) 'Reversibility of the binding of cytochrome-c to liposomes - implications for lipid-protein interactions', *Journal of Biological Chemistry*, 270(7), pp. 3197-3202.

Rytomaa, M., Mustonen, P. and Kinnunen, P.K.J. (1992) 'Reversible, nonionic, and ph-dependent association of cytochrome-c with cardiolipin-phosphatidylcholine liposomes', *Journal of Biological Chemistry*, 267(31), pp. 22243-22248.

Sadun, A.A., Chicani, C.F., Ross-Cisneros, F.N., Barboni, P., Thoolen, M., Shrader, W.D., Kubis, K., Carelli, V. and Miller, G. (2012) 'Effect of EPI-743 on the Clinical Course of the Mitochondrial Disease Leber Hereditary Optic Neuropathy', *Archives of Neurology*, 69(3), pp. 331-338.

Sadun, A.A., Kashima, Y., Wurdeman, A.E., Dao, J., Heller, K. and Sherman, J. (1994) 'Morphological findings in the visual-system in a case of lebers hereditary optic neuropathy', *Clinical Neuroscience*, 2(2), pp. 165-172.

Safiulina, D. and Kaasik, A. (2013) 'Energetic and Dynamic: How Mitochondria Meet Neuronal Energy Demands', *Plos Biology*, 11(12).

Sanchez-Martinez, A., Calleja, M., Peralta, S., Matsushima, Y., Hernandez-Sierra, R., Whitworth, A.J., Kaguni, L.S. and Garesse, R. (2012) 'Modeling Pathogenic Mutations of Human Twinkle in Drosophila Suggests an Apoptosis Role in Response to Mitochondrial Defects', *Plos One*, 7(8).

Santel, A. (2006) 'Get the balance right: Mitofusins roles in health and disease', *Biochimica Et Biophysica Acta-Molecular Cell Research*, 1763(5-6), pp. 490-499.
Saraste, M. (1999) 'Oxidative phosphorylation at the fin de siecle', *Science*, 283(5407), pp. 1488-1493.

Sarzi, E., Angebault, C., Seveno, M., Gueguen, N., Chaix, B., Bielicki, G., Boddaert, N., Mausset-Bonnefont, A.L., Cazevieille, C., Rigau, V., Renou, J.P., Wang, J., Delettre, C., Brabet, P., Puel, J.L., Hamel, C.P., Reynier, P. and Lenaers, G. (2012) 'The human OPA1(delTTAG) mutation induces premature age-related systemic neurodegeneration in mouse', *Brain*, 135, pp. 3599-3613.

Satoh, M., Hamamoto, T., Seo, N., Kagawa, Y. and Endo, H. (2003) 'Differential sublocalization of the dynamin-related protein OPA1 isoforms in mitochondria', *Biochemical and Biophysical Research Communications*, 300(2), pp. 482-493.

Saxton, W.M. and Hollenbeck, P.J. (2012) 'The axonal transport of mitochondria', *Journal of Cell Science*, 125(9), pp. 2095-2104.

Sbisa, E., Tanzariello, F., Reyes, A., Pesole, G. and Saccone, C. (1997) 'Mammalian mitochondrial D-loop region structural analysis: identification of new conserved sequences and their functional and evolutionary implications', *Gene*, 205(1-2), pp. 125-140.

Schaaf, C.P., Blazo, M., Lewis, R.A., Tonini, R.E., Takei, H., Wang, J., Wong, L.-J. and Scaglia, F. (2011) 'Early-onset severe neuromuscular phenotype associated with compound heterozygosity for OPA1 mutations', *Molecular Genetics and Metabolism*, 103(4), pp. 383-387.

Schimpf, S., Fuhrmann, N., Schaich, S. and Wissinger, B. (2008) 'Comprehensive cDNA study and quantitative transcript analysis of mutant OPA1 transcripts containing premature termination codons', *Human Mutation*, 29(1), pp. 106-112.

Schwarz, J.M., Cooper, D.N., Schuelke, M. and Seelow, D. (2014) 'MutationTaster2: mutation prediction for the deep-sequencing age', *Nature Methods*, 11(4), pp. 361-362.

Schweingruber, C., Rufener, S.C., Zuend, D., Yamashita, A. and Muehlemann, O. (2013) 'Nonsense-mediated mRNA decay - Mechanisms of substrate mRNA recognition and degradation in mammalian cells', *Biochimica Et Biophysica Acta-Gene Regulatory Mechanisms*,

1829(6-7), pp. 612-623.

Sergouniotis, P.I., Perveen, R., Thiselton, D.L., Giannopoulos, K., Sarros, M., Davies, J.R., Biswas, S., Ansons, A.M., Ashworth, J.L., Lloyd, I.C., Black, G.C. and Votruba, M. (2015) 'Clinical and molecular genetic findings in autosomal dominant OPA3-related optic neuropathy', *Neurogenetics*, 16(1), pp. 69-75.

Shashi, V., McConkie-Rosell, A., Rosell, B., Schoch, K., Vellore, K., McDonald, M., Jiang, Y.-H., Xie, P., Need, A. and Goldstein, D.B. (2014) 'The utility of the traditional medical genetics diagnostic evaluation in the context of next-generation sequencing for undiagnosed genetic disorders', *Genetics in Medicine*, 16(2), pp. 176-182.

Shoffner, J.M., Lott, M.T., Lezza, A.M.S., Seibel, P., Ballinger, S.W. and Wallace, D.C. (1990) 'Myoclonic epilepsy and ragged-red fiber disease (merrf) is associated with a mitochondrial-dna transfer rnalys mutation', *Cell*, 61(6), pp. 931-937.

Silvestri, G., Ciafaloni, E., Santorelli, F.M., Shanske, S., Servidei, S., Graf, W.D., Sumi, M. and Dimauro, S. (1993) 'Clinical-features associated with the a- g transition at nucleotide-8344 of mtdna (merrf mutation)', *Neurology*, 43(6), pp. 1200-1206.

Sims, D., Sudbery, I., Ilott, N.E., Heger, A. and Ponting, C.P. (2014) 'Sequencing depth and coverage: key considerations in genomic analyses', *Nature Reviews Genetics*, 15(2), pp. 121-132.

Singaravelu, K., Nelson, C., Bakowski, D., de Brito, O.M., Ng, S.-W., Di Capite, J., Powell, T., Scorrano, L. and Parekh, A.B. (2011) 'Mitofusin 2 Regulates STIM1 Migration from the Ca2+ Store to the Plasma Membrane in Cells with Depolarized Mitochondria', *Journal of Biological Chemistry*, 286(14).
Sitarz, K.S., Chinnery, P.F. and Yu-Wai-Man, P. (2012) 'Disorders of the Optic Nerve in Mitochondrial Cytopathies: New Ideas on Pathogenesis and Therapeutic Targets', *Current Neurology and Neuroscience Reports*, 12(3), pp. 308-317.

Smith, D.P. (1972) 'Diagnostic criteria in dominantly inherited juvenile optic atrophy - report of 3 new families', *American Journal of Optometry and Archives of American Academy of Optometry*, 49(3), pp. 183-&.

Smits, P., Smeitink, J. and van den Heuvel, L. (2010) 'Mitochondrial Translation and Beyond: Processes Implicated in Combined Oxidative Phosphorylation Deficiencies', *Journal of Biomedicine and Biotechnology*.

Song, Z., Chen, H., Fiket, M., Alexander, C. and Chan, D.C. (2007) 'OPA1 processing controls mitochondrial fusion and is regulated by mRNA splicing, membrane potential, and Yme1L', *Journal of Cell Biology*, 178(5), pp. 749-755.

Spelbrink, J.N. (2010) 'Functional Organization of Mammalian Mitochondrial DNA in

Nucleoids: History, Recent Developments, and Future Challenges', *Iubmb Life*, 62(1), pp. 19-32.

Spiegel, R., Saada, A., Flannery, P.J., Burte, F., Soiferman, D., Khayat, M., Eisner, V., Vladovski, E., Taylor, R.W., Bindoff, L.A., Shaag, A., Mandel, H., Schuler-Furman, O., Shalev, S.A., Elpeleg, O. and Yu-Wai-Man, P. (2016) 'Fatal infantile mitochondrial encephalomyopathy, hypertrophic cardiomyopathy and optic atrophy associated with a homozygous OPA1 mutation', *Journal of Medical Genetics*, 53(2), pp. 127-131.

Spinazzi, M., Cazzola, S., Bortolozzi, M., Baracca, A., Loro, E., Casarin, A., Solaini, G., Sgarbi, G., Casalena, G., Cenacchi, G., Malena, A., Frezza, C., Carrara, F., Angelini, C., Scorrano, L., Salviati, L. and Vergani, L. (2008) 'A novel deletion in the GTPase domain of OPA1 causes defects in mitochondrial morphology and distribution, but not in function', *Human Molecular Genetics*, 17(21), pp. 3291-3302.

Spinazzola, A., Viscomi, C., Fernandez-Vizarra, E., Carrara, F., D'Adamo, P., Calvo, S., Marsano, R.M., Donnini, C., Weiher, H., Strisciuglio, P., Parini, R., Sarzi, E., Chan, A., DiMauro, S., Rotig, A., Gasparini, P., Ferrero, I., Mootha, V.K., Tiranti, V. and Zeviani, M. (2006) 'MPV17 encodes an inner mitochondrial membrane protein and is mutated in infantile hepatic mitochondrial DNA depletion', *Nature Genetics*, 38(5), pp. 570-575.

Stenson, P.D., Mort, M., Ball, E.V., Shaw, K., Phillips, A.D. and Cooper, D.N. (2014) 'The Human Gene Mutation Database: building a comprehensive mutation repository for clinical and molecular genetics, diagnostic testing and personalized genomic medicine', *Human Genetics*, 133(1), pp. 1-9.

Stewart, J.B. and Chinnery, P.F. (2015) 'The dynamics of mitochondrial DNA heteroplasmy: implications for human health and disease', *Nature Reviews Genetics*, 16(9), pp. 530-542.
Stiburek, L., Cesnekova, J., Kostkova, O., Fornuskova, D., Vinsova, K., Wenchich, L., Houstek, J. and Zeman, J. (2012) 'YME1L controls the accumulation of respiratory chain subunits and is required for apoptotic resistance, cristae morphogenesis, and cell proliferation', *Molecular Biology of the Cell*, 23(6), pp. 1010-1023.

Strom, T.M., Hortnagel, K., Hofmann, S., Gekeler, F., Scharfe, C., Rabl, W., Gerbitz, K.D. and Meitinger, T. (1998) 'Diabetes insipidus, diabetes mellitus, optic atrophy and deafness (DIDMOAD) caused by mutations in a novel gene (wolframin) coding for a predicted transmembrane protein', *Human Molecular Genetics*, 7(13), pp. 2021-2028.

Suissa, S., Wang, Z., Poole, J., Wittkopp, S., Feder, J., Shutt, T.E., Wallace, D.C., Shadel, G.S. and Mishmar, D. (2009) 'Ancient mtDNA Genetic Variants Modulate mtDNA Transcription and Replication', *Plos Genetics*, 5(5).

Svilar, D., Goellner, E.M., Almeida, K.H. and Sobol, R.W. (2011) 'Base Excision Repair and Lesion-Dependent Subpathways for Repair of Oxidative DNA Damage', *Antioxidants & Redox Signaling*, 14(12), pp. 2491-2507.

Tachibana, M., Sparman, M., Sritanaudomchai, H., Ma, H., Clepper, L., Woodward, J., Li, Y., Ramsey, C., Kolotushkina, O. and Mitalipov, S. (2009) 'Mitochondrial gene replacement in primate offspring and embryonic stem cells', *Nature*, 461(7262), pp. 367-372.

Takeda, K., Inoue, H., Tanizawa, Y., Matsuzaki, Y., Oba, J., Watanabe, Y., Shinoda, K. and Oka, Y. (2001) 'WFS1 (Wolfram syndrome 1) gene product: predominant subcellular localization to endoplasmic reticulum in cultured cells and neuronal expression in rat brain', *Human Molecular Genetics*, 10(5), pp. 477-484.

Takei, D., Ishihara, H., Yamaguchi, S., Yamada, T., Tamura, A., Katagiri, H., Maruyama, Y. and Oka, Y. (2006) 'WFS1 protein modulates the free Ca2+ concentration in the endoplasmic reticulum', *Febs Letters*, 580(24), pp. 5635-5640.

Tang, S., Le, P.K., Tse, S., Wallace, D.C. and Huang, T.S. (2009) 'Heterozygous Mutation of Opa1 in Drosophila Shortens Lifespan Mediated through Increased Reactive Oxygen Species Production', *Plos One*, 4(2).

Teske, B.F., Fusakio, M.E., Zhou, D., Shan, J., McClintick, J.N., Kilberg, M.S. and Wek, R.C. (2013) 'CHOP induces activating transcription factor 5 (ATF5) to trigger apoptosis in response to perturbations in protein homeostasis', *Molecular Biology of the Cell*, 24(15), pp. 2477-2490.

Tessa, A., Carbone, I., Matteoli, M.C., Bruno, C., Patrono, C., Patera, I.P., De Luca, F., Lorini, R. and Santorelli, F.M. (2001) 'Identification of novel WFS1 mutations in Italian children with Wolfram syndrome', *Human mutation*, 17(4), pp. 348-9.

Thanbichler, M. and Shapiro, L. (2006) 'Chromosome organization and segregation in bacteria', *Journal of Structural Biology*, 156(2), pp. 292-303.

Thauvin-Robinet, C., Auclair, M., Duplomb, L., Caron-Debarle, M., Avila, M., St-Onge, J., Le Merrer, M., Le Luyer, B., Heron, D., Mathieu-Dramard, M., Bitoun, P., Petit, J.-M., Odent, S., Amiel, J., Picot, D., Carmignac, V., Thevenon, J., Callier, P., Laville, M., Reznik, Y., Fagour, C., Nunes, M.-L., Capeau, J., Lascols, O., Huet, F., Faivre, L., Vigouroux, C. and Riviere, J.-B. (2013) 'PIK3R1 Mutations Cause Syndromic Insulin Resistance with Lipoatrophy', *American Journal of Human Genetics*, 93(1), pp. 141-149.

Thiselton, D.L., Alexander, C., Taanman, J.W., Brooks, S., Rosenberg, T., Eiberg, H., Andreasson, S., Van Regemorter, N., Munier, F.L., Moore, A.T., Bhattacharya, S.S. and Votruba, M. (2002) 'A comprehensive survey of mutations in the OPA1 gene in patients with autosomal dominant optic atrophy', *Investigative Ophthalmology & Visual Science*, 43(6), pp. 1715-1724.

Thomas, C., Mackey, M.M., Diaz, A.A. and Cox, D.P. (2009) 'Hydroxyl radical is produced via the Fenton reaction in submitochondrial particles under oxidative stress: implications for

diseases associated with iron accumulation', *Redox Report*, 14(3), pp. 102-108.

Thompson, D.B., Pratley, R. and Ossowski, V. (1996) 'Human primary myoblast cell cultures from non-diabetic insulin resistant subjects retain defects in insulin action', *Journal of Clinical Investigation*, 98(10), pp. 2346-2350.

Thorburn, D.R. (2004) 'Mitochondrial disorders: Prevalence, myths and advances', *Journal of Inherited Metabolic Disease*, 27(3), pp. 349-362.

Tondera, D., Grandemange, S., Jourdain, A., Karbowski, M., Mattenberger, Y., Herzig, S., Da Cruz, S., Clerc, P., Raschke, I., Merkwirth, C., Ehses, S., Krause, F., Chan, D.C., Alexander, C., Bauer, C., Youle, R., Langer, T. and Martinou, J.-C. (2009) 'SLP-2 is required for stress-induced mitochondrial hyperfusion', *Embo Journal*, 28(11), pp. 1589-1600.

Toomes, C., Marchbank, N.J., Mackey, D.A., Craig, J.E., Newbury-Ecob, R.A., Bennett, C.P., Vize, C.J., Desai, S.P., Black, G.C.M., Patel, N., Teimory, M., Markham, A.F., Inglehearn, C.F. and Churchill, A.J. (2001) 'Spectrum, frequency and penetrance of OPA1 mutations in dominant optic atrophy', *Human Molecular Genetics*, 10(13), pp. 1369-1378.

Torres, R., Leroy, E., Hu, X., Katrivanou, A., Gourzis, P., Papachatzopoulou, A., Athanassiadou, A., Beratis, S., Collier, D. and Polymeropoulos, M.H. (2001) 'Mutation screening of the Wolfram syndrome gene in psychiatric patients', *Molecular Psychiatry*, 6(1), pp. 39-43.

Torres-Peraza, J.F., Engel, T., Martin-Ibanez, R., Sanz-Rodriguez, A., Rosario Fernandez-Fernandez, M., Esgleas, M., Canals, J.M., Henshall, D.C. and Lucas, J.J. (2013) 'Protective neuronal induction of ATF5 in endoplasmic reticulum stress induced by status epilepticus', *Brain*, 136, pp. 1161-1176.

Torroni, A. and Wallace, D.C. (1994) 'Mitochondrial-dna variation in human-populations and implications for detection of mitochondrial-dna mutations of pathological significance', *Journal of Bioenergetics and Biomembranes*, 26(3), pp. 261-271.

Traaseth, N., Elfering, S., Solien, J., Haynes, V. and Giulivi, C. (2004) 'Role of calcium signaling in the activation of mitochondrial nitric oxide synthase and citric acid cycle', *Biochimica Et Biophysica Acta-Bioenergetics*, 1658(1-2), pp. 64-71.

Trevelyan, A.J., Kirby, D.M., Smulders-Srinivasan, T.K., Nooteboom, M., Acin-Perez, R., Enriquez, J.A., Whittington, M.A., Lightowlers, R.N. and Turnbull, D.M. (2010) 'Mitochondrial DNA mutations affect calcium handling in differentiated neurons', *Brain*, 133, pp. 787-796.

Tuominen, E.K.J., Wallace, C.J.A. and Kinnunen, P.K.J. (2002) 'Phospholipid-cytochrome c interaction - Evidence for the extended lipid anchorage', *Journal of Biological Chemistry*, 277(11), pp. 8822-8826.

Twig, G. and Shirihai, O.S. (2011) 'The Interplay Between Mitochondrial Dynamics and

Mitophagy', *Antioxidants & Redox Signaling*, 14(10), pp. 1939-1951.

Tyynismaa, H. and Suomalainen, A. (2009) 'Mouse models of mitochondrial DNA defects and their relevance for human disease', *Embo Reports*, 10(2), pp. 137-143.

Uziel, G., Ghezzi, D. and Zeviani, M. (2011) 'Infantile mitochondrial encephalopathy', *Seminars in Fetal & Neonatal Medicine*, 16(4), pp. 205-215.

Valero, R., Bannwarth, S., Roman, S., Paquis-Flucklinger, V. and Vialettes, B. (2008) 'Autosomal dominant transmission of diabetes and congenital hearing impairment secondary to a missense mutation in the WFS1 gene', *Diabetic Medicine*, 25(6), pp. 657-661.

Vielhaber, S., Debska-Vielhaber, G., Peeva, V., Schoeler, S., Kudin, A.P., Minin, I., Schreiber, S., Dengler, R., Kollewe, K., Zuschratter, W., Kornblum, C., Zsurka, G. and Kunz, W.S. (2013) 'Mitofusin 2 mutations affect mitochondrial function by mitochondrial DNA depletion', *Acta Neuropathologica*, 125(2), pp. 245-256.

Vinson, C., Myakishev, M., Acharya, A., Mir, A.A., Moll, J.R. and Bonovich, M. (2002) 'Classification of human B-ZIP proteins based on dimerization properties', *Molecular and Cellular Biology*, 22(18), pp. 6321-6335.

von Ballmoos, C., Wiedenmann, A. and Dimroth, P. (2009) 'Essentials for ATP Synthesis by F1F0 ATP Synthases', *Annual Review of Biochemistry*, 78, pp. 649-672.

Votruba, M., Fitzke, F.W., Holder, G.E., Carter, A., Bhattacharya, S.S. and Moore, A.T. (1998a) 'Clinical features in affected individuals from 21 pedigrees with dominant optic atrophy', *Archives of Ophthalmology*, 116(3), pp. 351-358.

Votruba, M., Moore, A.T. and Bhattacharya, S.S. (1998b) 'Clinical features, molecular genetics, and pathophysiology of dominant optic atrophy', *Journal of Medical Genetics*, 35(10), pp. 793-800.

Wallace, D.C., Singh, G., Lott, M.T., Hodge, J.A., Schurr, T.G., Lezza, A.M.S., Elsas, L.J. and Nikoskelainen, E.K. (1988) 'Mitochondrial-dna mutation associated with lebers hereditary optic neuropathy', *Science*, 242(4884), pp. 1427-1430.

Wallace, D.C. and Chalkia, D. (2013) 'Mitochondrial DNA Genetics and the Heteroplasmy Conundrum in Evolution and Disease', *Cold Spring Harbor Perspectives in Biology*, 5(11).

Wang, K., Li, M. and Hakonarson, H. (2010) 'ANNOVAR: functional annotation of genetic variants from high-throughput sequencing data', *Nucleic Acids Research*, 38(16).

Wang, Y. and Bogenhagen, D.F. (2006) 'Human mitochondrial DNA nucleoids are linked to protein folding machinery and metabolic enzymes at the mitochondrial inner membrane', *Journal*

of Biological Chemistry, 281(35), pp. 25791-25802.

Wanrooij, S. and Falkenberg, M. (2010) 'The human mitochondrial replication fork in health and disease', *Biochimica Et Biophysica Acta-Bioenergetics*, 1797(8), pp. 1378-1388.

Wasson, J. and Permutt, M.A. (2008) 'Candidate gene studies reveal that the WFS1 gene joins the expanding list of novel type 2 diabetes genes', *Diabetologia*, 51(3), pp. 391-393.

Waterham, H.R., Koster, J., van Roermund, C.W.T., Mooyer, P.A.W., Wanders, R.J.A. and Leonard, A.V. (2007) 'A lethal defect of mitochondrial and peroxisomal fission', *New England Journal of Medicine*, 356(17), pp. 1736-1741.

Wells, T., Davies, J.R., Guschina, I.A., Ball, D.J., Davies, J.S., Davies, V.J., Evans, B.A.J. and Votruba, M. (2012) 'Opa3, a novel regulator of mitochondrial function, controls thermogenesis and abdominal fat mass in a mouse model for Costeff syndrome', *Human Molecular Genetics*, 21(22), pp. 4836-4844.

Went, L.N., Devriesdemol, E.C. and Volkerdieben, H.J. (1975) 'Family with apparently sex-linked optic atrophy', *Journal of Medical Genetics*, 12(1), pp. 94-98.

White, K.E., Davies, V.J., Hogan, V.E., Piechota, M.J., Nichols, P.P., Turnbull, D.M. and Votruba, M. (2009) 'OPA1 Deficiency Associated with Increased Autophagy in Retinal Ganglion Cells in a Murine Model of Dominant Optic Atrophy', *Investigative Ophthalmology & Visual Science*, 50(6), pp. 2567-2571.

Wiggs, J.L. (2015) 'Mitochondrial Genetics and Optic Neuropathy', *Annual Review of Vision Science, Vol 1*, 1, pp. 97-124.

Wolfram, DJ. and Wagner, HP. (1938) 'Diabetes Mellitus and Simple Optic Atrophy among Siblings: Report of Four Cases', *Mayo Clin Proc*, 13, pp 715-718.

Wong, T.S., Rajagopalan, S., Freund, S.M., Rutherford, T.J., Andreeva, A., Townsley, F.M., Petrovich, M. and Fersht, A.R. (2009) 'Biophysical characterizations of human mitochondrial transcription factor A and its binding to tumor suppressor p53', *Nucleic Acids Research*, 37(20), pp. 6765-6783.

Xin, H., Woriax, V., Burkhart, W. and Spremulli, L.L. (1995) 'Cloning and expression of mitochondrial translational elongation-factor ts from bovine and human liver', *Journal of Biological Chemistry*, 270(29), pp. 17243-17249.

Yamada, T., Ishihara, H., Tamura, A., Takahashi, R., Yamaguchi, S., Takei, D., Tokita, A., Satake, C., Tashiro, F., Katagiri, H., Aburatani, H., Miyazaki, J. and Oka, Y. (2006) 'WFS1-deficiency increases endoplasmic reticulum stress, impairs cell cycle progression and triggers the apoptotic pathway specifically in pancreatic beta-cells', *Human Molecular Genetics*, 15(10), pp.

1600-1609.

Yamaguchi, R., Lartigue, L., Perkins, G., Scott, R.T., Dixit, A., Kushnareva, Y., Kuwana, T., Ellisman, M.H. and Newmeyer, D.D. (2008) 'Opa1-mediated cristae opening is Bax/Bak and BH3 dependent, required for apoptosis, and independent of Bak oligomerization', *Molecular Cell*, 31(4), pp. 557-569.

Yamaguchi, S., Ishihara, H., Tamura, A., Yamada, T., Takahashi, R., Takei, D., Katagiri, H. and Oka, Y. (2004) 'Endoplasmic reticulum stress and N-glycosylation modulate expression of WFS1 protein', *Biochemical and Biophysical Research Communications*, 325(1), pp. 250-256.

Yan, X.K., Wang, X.J., Wang, Z.M., Sun, S., Chen, G.L., He, Y.Z., Mo, J.Q., Li, R.H., Jiang, P.P., Lin, Q., Sun, M.Z., Li, W., Bai, Y., Zhang, J.N., Zhu, Y., Lu, J.X., Yan, Q.F., Li, H.W. and Guan, M.X. (2011a) 'Maternally transmitted late-onset non-syndromic deafness is associated with the novel heteroplasmic T12201C mutation in the mitochondrial tRNA(His) gene', *Journal of Medical Genetics*, 48(10), pp. 682-690.

Yan, L., Ma, Y., Sun, Y., Gao, J., Chen, X., Liu, J., Wang, C., Rao, Z. and Lou, Z. (2011b) 'Structural basis for mechanochemical role of Arabidopsis thaliana dynamin-related protein in membrane fission', *Journal of Molecular Cell Biology*, 3(6), pp. 378-381.

Yang, J., Yan, R., Roy, A., Xu, D., Poisson, J. and Zhang, Y. (2015) 'The I-TASSER Suite: protein structure and function prediction', *Nature Methods*, 12(1), pp. 7-8.

Yang, Y., Muzny, D.M., Reid, J.G., Bainbridge, M.N., Willis, A., Ward, P.A., Braxton, A., Beuten, J., Xia, F., Niu, Z., Hardison, M., Person, R., Bekheirnia, M.R., Leduc, M.S., Kirby, A., Peter, P., Scull, J., Wang, M., Ding, Y., Plon, S.E., Lupski, J.R., Beaudet, A.L., Gibbs, R.A. and Eng, C.M. (2013) 'Clinical Whole-Exome Sequencing for the Diagnosis of Mendelian Disorders', *New England Journal of Medicine*, 369(16), pp. 1502-1511.

Yang, Y., Muzny, D.M., Xia, F., Niu, Z., Person, R., Ding, Y., Ward, P., Braxton, A., Wang, M., Buhay, C., Veeraraghavan, N., Hawes, A., Chiang, T., Leduc, M., Beuten, J., Zhang, J., He, W., Scull, J., Willis, A., Landsverk, M., Craigen, W.J., Bekheirnia, M.R., Stray-Pedersen, A., Liu, P., Wen, S., Alcaraz, W., Cui, H., Walkiewicz, M., Reid, J., Bainbridge, M., Patel, A., Boerwinkle, E., Beaudet, A.L., Lupski, J.R., Plon, S.E., Gibbs, R.A. and Eng, C.M. (2014) 'Molecular Findings Among Patients Referred for Clinical Whole-Exome Sequencing', *Jama-Journal of the American Medical Association*, 312(18), pp. 1870-1879.

Yarosh, W., Monserrate, J., Tong, J.J., Tse, S., Le, P.K., Nguyen, K., Brachmann, C.B., Wallace, D.C. and Huang, T. (2008) 'The molecular mechanisms of OPA1-mediated optic atrophy in Drosophila model and prospects for antioxidant treatment', *Plos Genetics*, 4(1).

Yasukawa, T., Reyes, A., Cluett, T.J., Yang, M.-Y., Bowmaker, M., Jacobs, H.T. and Holt, I.J. (2006) 'Replication of vertebrate mitochondrial DNA entails transient ribonucleotide incorporation throughout the lagging strand', *Embo Journal*, 25(22), pp. 5358-5371.

Yen, M.Y., Chen, C.S., Wang, A.G. and Wei, Y.H. (2002) 'Increase of mitochondrial DNA in blood cells of patients with Leber's hereditary optic neuropathy with 11778 mutation', *British Journal of Ophthalmology*, 86(9), pp. 1027-1030.

Yin, H., Xue, W., Chen, S., Bogorad, R.L., Benedetti, E., Grompe, M., Koteliansky, V., Sharp, P.A., Jacks, T. and Anderson, D.G. (2014) 'Genome editing with Cas9 in adult mice corrects a disease mutation and phenotype', *Nature Biotechnology*, 32(6), pp. 551-553.

Ylikallio, E., Tyynismaa, H., Tsutsui, H., Ide, T. and Suomalainen, A. (2010) 'High mitochondrial DNA copy number has detrimental effects in mice', *Human Molecular Genetics*, 19(13), pp. 2695-2705.

Yoshida, M., Muneyuki, E. and Hisabori, T. (2001) 'ATP synthase - A marvellous rotary engine of the cell', *Nature Reviews Molecular Cell Biology*, 2(9), pp. 669-677.

Yu, C.A., Tian, H., Zhang, L., Deng, K.P., Shenoy, S.K., Yu, L., Xia, D., Kim, H. and Deisenhofer, J. (1999) 'Structural basis of multifunctional bovine mitochondrial cytochrome bc(1) complex', *Journal of Bioenergetics and Biomembranes*, 31(3), pp. 191-199.

Yu, T.W., Chahrour, M.H., Coulter, M.E., Jiralerspong, S., Okamura-Ikeda, K., Ataman, B., Schmitz-Abe, K., Harmin, D.A., Adli, M., Malik, A.N., D'Gama, A.M., Lim, E.T., Sanders, S.J., Mochida, G.H., Partlow, J.N., Sunu, C.M., Felie, J.M., Rodriguez, J., Nasir, R.H., Ware, J., Joseph, R.M., Hill, R.S., Kwan, B.Y., Al-Saffar, M., Mukaddes, N.M., Hashmi, A., Balkhy, S., Gascon, G.G., Hisama, F.M., LeClair, E., Poduri, A., Oner, O., Al-Saad, S., Al-Awadi, S.A., Bastaki, L., Ben-Omran, T., Teebi, A.S., Al-Gazali, L., Eapen, V., Stevens, C.R., Rappaport, L., Gabriel, S.B., Markianos, K., State, M.W., Greenberg, M.E., Taniguchi, H., Braverman, N.E., Morrow, E.M. and Walsh, C.A. (2013) 'Using Whole-Exome Sequencing to Identify Inherited Causes of Autism', *Neuron*, 77(2), pp. 259-273.

Yu-Wai-Man, P. and Chinnery, P.F. (2012) 'Dysfunctional mitochondrial maintenance: what breaks the circle of life?', *Brain*, 135, pp. 9-11.

Yu-Wai-Man, P. and Chinnery, P.F. (2013) 'Dominant Optic Atrophy: Novel OPA1 Mutations and Revised Prevalence Estimates', *Ophthalmology*, 120(8), pp. 1712-+.

Yu-Wai-Man, P. and Chinnery, P.F. (2015) 'Reply: 'Behr syndrome' with OPA1 compound heterozygote mutations', *Brain*, 138.

Yu-Wai-Man, P., Griffiths, P.G., Burke, A., Sellar, P.W., Clarke, M.P., Gnanaraj, L., Ah-Kine, D., Hudson, G., Czermin, B., Taylor, R.W., Horvath, R. and Chinnery, P.F. (2010a) 'The

Prevalence and Natural History of Dominant Optic Atrophy Due to OPA1 Mutations', *Ophthalmology*, 117(8), pp. 1538-1546.

Yu-Wai-Man, P., Griffiths, P.G. and Chinnery, P.F. (2011a) 'Mitochondrial optic neuropathies - Disease mechanisms and therapeutic strategies', *Progress in Retinal and Eye Research*, 30(2), pp. 81-114.

Yu-Wai-Man, P., Griffiths, P.G., Gorman, G.S., Lourenco, C.M., Wright, A.F., Auer-Grumbach, M., Toscano, A., Musumeci, O., Valentino, M.L., Caporali, L., Lamperti, C., Tallaksen, C.M., Duffey, P., Miller, J., Whittaker, R.G., Baker, M.R., Jackson, M.J., Clarke, M.P., Dhillon, B., Czermin, B., Stewart, J.D., Hudson, G., Reynier, P., Bonneau, D., Marques, W., Lenaers, G., McFarland, R., Taylor, R.W., Turnbull, D.M., Votruba, M., Zeviani, M., Carelli, V., Bindoff, L.A., Horvath, R., Amati-Bonneau, P. and Chinnery, P.F. (2010b) 'Multi-system neurological disease is common in patients with OPA1 mutations', *Brain*, 133, pp. 771-786.

Yu-Wai-Man, P., Griffiths, P.G., Hudson, G. and Chinnery, P.F. (2009) 'Inherited mitochondrial optic neuropathies', *Journal of Medical Genetics*, 46(3), pp. 145-158.

Yu-Wai-Man, P., Shankar, S.P., Biousse, V., Miller, N.R., Bean, L.J.H., Coffee, B., Hegde, M. and Newman, N.J. (2011b) 'Genetic Screening for OPA1 and OPA3 Mutations in Patients with Suspected Inherited Optic Neuropathies', *Ophthalmology*, 118(3), pp. 558-563.

Yu-Wai-Man, P., Votruba, M., Moore, A.T. and Chinnery, P.F. (2014) 'Treatment strategies for inherited optic neuropathies: past, present and future', *Eye*, 28(5), pp. 521-537.

Zalloua, P.A., Azar, S.T., Delepine, M., Makhoul, N.J., Blanc, H., Sanyoura, M., Lavergne, A., Stankov, K., Lemainque, A., Baz, P. and Julier, C. (2008) 'WFS1 mutations are frequent monogenic causes of juvenile-onset diabetes mellitus in Lebanon', *Human Molecular Genetics*, 17(24), pp. 4012-4021.

Zanna, C., Ghelli, A., Porcelli, A.M., Karbowski, M., Youle, R.J., Schimpf, S., Wissinger, B., Pinti, M., Cossarizza, A., Vidoni, S., Valentino, M.L., Rugolo, M. and Carelli, V. (2008) 'OPA1 mutations associated with dominant optic atrophy impair oxidative phosphorylation and mitochondrial fusion', *Brain*, 131, pp. 352-367.

Zatyka, M., Ricketts, C., Xavier, G.d.S., Minton, J., Fenton, S., Hofmann-Thiel, S., Rutter, G.A. and Barrett, T.G. (2008) 'Sodium-potassium ATPase beta 1 subunit is a molecular partner of Wolframin, an endoplasmic reticulum protein involved in ER stress', *Human Molecular Genetics*, 17(2), pp. 190-200.

Zeviani, M. (2008) 'OPA1 mutations and mitochondrial DNA damage: keeping the magic circle in shape', *Brain*, 131, pp. 314-317.

Zhang, X., Jones, D. and Gonzalez-Lima, F. (2002) 'Mouse model of optic neuropathy caused by

mitochondrial complex I dysfunction', *Neuroscience Letters*, 326(2), pp. 97-100.

Zhou, Q., Lee, G.-S., Brady, J., Datta, S., Katan, M., Sheikh, A., Martins, M.S., Bunney, T.D., Santich, B.H., Moir, S., Kuhns, D.B., Priel, D.A.L., Ombrello, A., Stone, D., Ombrello, M.J., Khan, J., Milner, J.D., Kastner, D.L. and Aksentijevich, I. (2012) 'A Hypermorphic Missense Mutation in PLCG2, Encoding Phospholipase C gamma 2, Causes a Dominantly Inherited Autoinflammatory Disease with Immunodeficiency', *American Journal of Human Genetics*, 91(4), pp. 713-720.

Zuchner, S., Mersiyanova, I.V., Muglia, M., Bissar-Tadmouri, N., Rochelle, J., Dadali, E.L., Zappia, M., Nelis, E., Patitucci, A., Senderek, J., Parman, Y., Evgrafov, O., De Jonghe, P., Takahashi, Y., Tsuji, S., Pericak-Vance, M.A., Quattrone, A., Battologlu, E., Polyakov, A.V., Timmerman, V., Schroder, J.M. and Vance, J.M. (2004) 'Mutations in the mitochondrial GTPase mitofusin 2 cause Charcot-Marie-Tooth neuropathy type 2A', *Nature Genetics*, 36(5), pp. 449-451.